Behaviour of Corrosion-Protection Coatings in Light Alloys

A THESIS SUBMITTED FOR THE DEGREE OF DOCTOR OF PHILOSOPHY AT THE UNIVERSITY OF OXFORD

TRINITY TERM 2012

DAVID LEE
CORPUS CHRISTI COLLEGE
UNIVERSITY OF OXFORD

Acknowledgements

I am tremendously grateful to my supervisors, John Sykes and Hazel Assender, for their guidance and supervision. Our regular meetings and discussions taught me so much and were vital to my progress. It is hard to imagine if this project could come to completion without them. Many thanks to John for his dedication and passion in the writing-stages of this thesis, especially when he could have been enjoying his days of well-deserved retirement!

I am thankful to my colleagues, Teresa, Yan and Zalilah, for their company and assistance around the laboratory and also the staff in the Materials department who have helped me during my studies.

My time as a DPhil student has been hugely enjoyable (for the most part) and I would like to thank Airbus, David Dixon, EPSRC and the Department of Materials for the opportunity and financial support during the project.

I have also benefited hugely from the friendships that I made in Oxford and I feel it would be too long to list them out individually, but friends of Corpus, Ebbe's, OUABC and 164 (and a few others), thank you. A special word of thanks goes to my Eleanor for her constant encouragement and being a bright light in those dark dark days of writing.

Finally, I would like to thank my parents for their love and support in my studies and this thesis is dedicated to them.

Preface

The work presented in this thesis was carried out at the University of Oxford, Department of Materials between October 2008 and October 2012, under the supervision of Prof. John Sykes, Dr. Hazel Assender and Dr. David Dixon (AIRBUS). No part of this work has been submitted for a degree at this or any other university. Where the work of others has been included it has been acknowledged and references are given at the end of the thesis.

David Lee

Trinity Term, October 2012

Abstract

David Lee
Corpus Christi College
2012

D. Phil Thesis
Trinity Term

Behaviour of Corrosion-Protection Coatings in Light Alloys

Anionic chromate (VI) compounds are inhibitive pigments and have been effectively incorporated into organic coatings to protect metal surfaces from aggressive ions, but their risk as a human carcinogen and being harmful to the environment has led to the search of suitable alternatives. Aluminium alloy, AA2024-T3, is the substrate metal alloy used in the experiments and can be found in aircraft fuselage structures due to their high strength-to-weight ratio. However, the presence of intermetallic particles increases susceptibility to localised corrosion.

To investigate the protection mechanisms of primers on light alloys, many different factors must be taken into account; from aluminium alloy corrosion processes, the effects of intermetallic additions to coating chemistry, morphology and inhibitive pigments. The chemical environment in which the samples are tested in will also affect the corrosion mechanisms of the alloy as well as the performance of the coatings and release of pigments. It will be important to consider which factors are operating under particular conditions so that experimental results can then be best interpreted.

As part of this project, potentiodynamic polarisation, electrochemical impedance spectroscopy and electrochemical noise analysis have been used to investigate the protective mechanisms in which chromate-based paints protect against corrosion and UV-Visible spectroscopy, scanning acoustic microscopy and optical microscopy have been used to investigate pigment release mechanism to identify what characteristics are important when developing new primers.

Contents

Chapter 1 Literature Review

Introduction

This project focuses on the behaviour of inhibitive pigments in epoxy coatings applied on aluminium alloy substrates. Aluminium alloy 2024-T3 is a high-strength alloy with copper as the main alloying element which has been widely used in aircraft parts, such as fittings, gears, shafts, bolts and hydraulic valve bodies[1]. However, aluminium and its alloys are susceptible to localised corrosion such as stress corrosion cracking, filiform corrosion and pitting corrosion in the presence of aggressive ions, discussed in section 1.1.2. The alloying additions of AA2024-T3 form a complex microstructure that further decrease the corrosion resistance of aluminium because the secondary phases and intermetallic particles often act as nucleation sites for pitting corrosion[2]. This will be further detailed in section 1.1.4.

Anionic chromate (VI) primers contain inhibitive pigments that have been effectively incorporated into organic coatings to protect metal surfaces from aggressive ions, but their risk as a human carcinogen and being harmful to the environment has led to the search for suitable alternatives. As part of this project, a variety of techniques have been used to investigate the protective mechanisms by which chromate-based paints protect against corrosion to identify what characteristics are required in new primers. A rare-earth inhibitive compound has also been studied as an 'environmentally-friendly' alternative in chapter 6.

Ordinary use of aircraft will result in damage to paint on the aircraft exterior. This exposes the bare metal, making it susceptible to corrosive attack, particularly in aggressive halide environments. However, corrosion-protective pigments can then leach out of the paint to protect the exposed surface. The 'in-service performance' of the inhibitors is investigated by creating an artificial defect in a paint coating to expose the metal surface below. The corrosion protection by and paint additives are discussed in section 1.2.

1.1 Corrosion of Aluminium Alloys

1.1.1 Electrochemical Processes of Aluminium Corrosion

By understanding the reactions that are involved in the corrosion of aluminium, the protection provided by the inhibitors can be better understood. The corrosion processes can be represented by anodic and cathodic chemical equations. The anodic oxidation of aluminium is represented by metallic aluminium, with oxidation state 0, becoming a trivalent cation after losing three electrons[3]:

$$Al \rightarrow Al^{3+} + 3e^{-} \qquad [1.1]$$

This metal dissolution reaction is balanced by the cathodic reduction of other species in the solution, which can be the evolution of hydrogen (hydrogen reduction) from water:

$$3H^{+} + 3e^{-} \rightarrow {}^{3}/_{2}\, H_2 \qquad [1.2]$$

or the reduction of oxygen, where in acidic solutions:

$$O_2 + 4\, H^{+} + 4e^{-} \rightarrow 2\, H_2O \qquad [1.3]$$

and in alkaline or neutral solutions:

$$O_2 + 2\, H_2O + 4e^{-} \rightarrow 4\, OH^{-} \qquad [1.4]$$

By combining the oxidation and reduction processes, the overall reactions are given by:

In acidic solutions:

$$Al + 3H^{+} \rightarrow Al^{3+} + {}^{3}/_{2}\, H_2 \qquad [1.5]$$

In neutral solutions:

$$Al + ¾\, O_2 + {}^{3}/_{2}\, H_2O \rightarrow Al(OH)_3 \qquad [1.6]$$

Aluminium hydroxide, $Al(OH)_3$, is a white insoluble compound that precipitates in the form of gelatinous flakes. The formation of these flakes does not protect the aluminium surface from

further attack as it does not adhere to the metal. In alkaline solutions, alumina dissolves into $Al(OH)_4^-$ ions so that the gel does not form. It is the formation of aluminium oxide, Al_2O_3, which provides aluminium and its alloys corrosion protection. Further information will be given in section 1.1.3.

The domains of stability for aluminium species can be illustrated by use of a Pourbaix diagram where the species present, and possible reactions that are occurring, are expressed as a function of potential and pH[4]. The diagram in figure 1.1 represents the stable species within the three domains: corrosion, passivation and immunity. Corrosion is defined as when a soluble corrosion product of a concentration of at least 10^{-6}M exists. Passivation occurs when an insoluble oxide or hydroxide forms across the metal surface, and immunity is when the concentration of relevant ions, e.g. relating to aluminium, is less than 10^{-6}M, and metallic aluminium is stable. Figure 1.1 shows that aluminium corrodes in both acidic and alkaline media, illustrating its amphoteric nature.

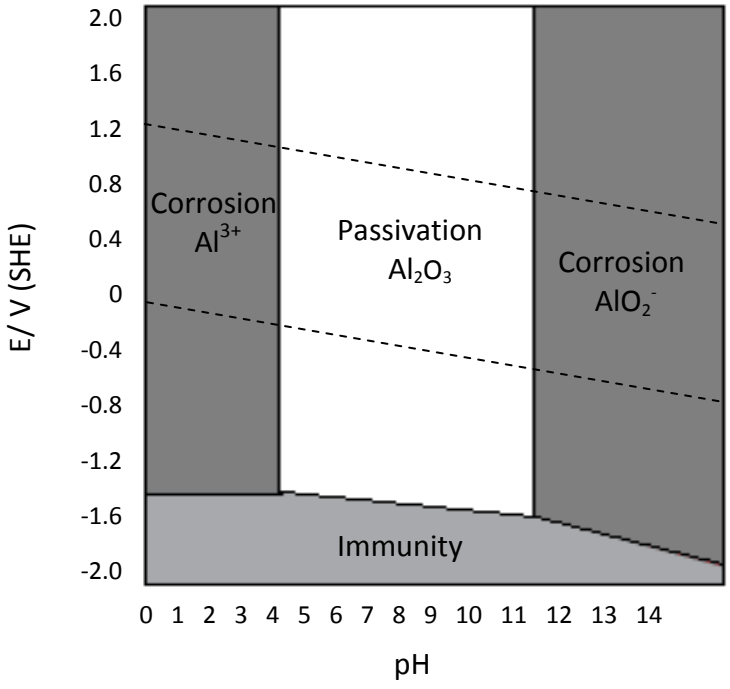

Figure 1.1 – Pourbaix diagram E-pH of aluminium in water at 25°C[5]

It should be noted that Pourbaix diagrams give a limited indication of stability, neglecting metastable phases, because they typically refer to a pure metal in an ideal liquid at a constant temperature. Effects of alloying additions and also the effects of the presence of aggressive ions to initiate localised corrosion cannot be accounted for using E-pH graphs. This is because a Pourbaix diagram is plotted using thermodynamic data, without taking into account the kinetics of a system[6].

1.1.2 Localised Corrosion and Pitting Corrosion

Aluminium and aluminium alloy systems have a protective oxide on their surface which retards general corrosion. However, in the presence of aggressive ions, such as chlorides, aluminium alloys corrode in localised regions where certain parts of a metal surface corrode at a significantly higher rate compared to the rest of the substrate[7]. Pitting corrosion is the most common type of localised corrosion to which aluminium alloys are susceptible to aggressive ions causing localised breakdown and penetration of the oxide film[6, 8]. Pitting occurs more commonly on passive alloys due to the fact that a thin oxide film layer usually provides protection across most of the surface and it is only where the film breaks down at certain points that corrosive attack is allowed to occur.

In this project, the propagation of stable pits, will be taken as the failure point of coating/inhibitor protection. The initiation of pits or metastable pitting has been explained by several theories, with a few main theories described as follows[2]:

1. The **adsorption theory** is an old theory proposed by Uhlig based on the adsorption of oxygen on the surface of aluminium metal, leading to passivation of the surface[2, 9]. Pit initiation occurs when chloride ions are adsorbed unto the surface in preference to

oxygen. This competitive adsorption was largely disproved because it does not take into account the passive oxide layer already found on the metal surface.

2. The **film-breaking model** proposes a continuous breakdown and rebuilding of the passive oxide film where pores or defects in the film cause mechanical stresses, leading to localised breakdown. When the passive layer is repaired, the local environment will determine the likelihood of pit initiation where the presence of aggressive ions could come into direct contact with the metal surface[10].
3. The **penetration model** suggests that anions can penetrate through the passive oxide layer to the metal-oxide interface, leading to the breakdown of passivity[11]. This model assumes the oxide film to be an amorphous crystalline structure containing dislocations whereby the small physical size of anions can diffuse along these dislocations to the interface[12].
4. The **point-defect model**, similar to the penetration model, involves charge-transport through the oxide film to the metal-oxide interface. Chao, Macdonald et al.[13] assumed the oxide film to be a crystalline material that contains point defects, e.g. oxygen anions, electrons and holes.

Pitting corrosion is believed to initiate when aggressive ions come into direct contact with the metal surface, stable pitting does not always propagate as small pits can repassivate. Despite being able to recognise the onset and propagation of pitting corrosion, the mechanisms of pitting have yet to be fully understood but nevertheless cause both safety and aesthetic concerns in engineering applications because heavily pitted sites can lead to perforation or act as initiation sites for cracks.

Environmental factors such as chloride concentration, potential and pH, affect the stability of the oxide film and pitting corrosion can be regarded as a competitive process involving passivation and activation[14]. Any additions of inhibitors will also affect the pitting potential, described further in section 1.1.2.1, where the presence of inhibitive ions will retard the anodic or cathodic reactions. Böhni and Uhlig investigated the effect of inhibitors in chloride solution on the critical pitting potential of aluminium, after Kaesche studied the effect on steel, and found that the potential becomes more active (more negative) with increasing NaCl concentration[15, 16]. Equations representing inhibiting activities of the anion species are as follows[16]:

$$\log C_i = K \log C_a + \text{constant} \qquad [1.7]$$

where K is related to the valencies of the respective ions, and C_i and C_a are the concentrations of the inhibitor and aggressive ion respectively.

$$\log (Cl^-) = 0.65 \log (\text{nitrate}^-) - 0.78 \qquad (1)$$

$$\log (Cl^-) = 0.56 \log (\text{chromate}^{2-}) - 1.11 \qquad (2)$$

$$\log (Cl^-) = 0.41 \log (\text{acetate}^-) - 1.50 \qquad (3)$$

$$\log (Cl^-) = 0.30 \log (\text{benzoate}^-) - 1.80 \qquad (4)$$

$$\log (Cl^-) = 0.31 \log (\text{sulphate}^{2-}) - 2.19 \qquad (5)$$

The pitting potential became more noble (more positive) when inhibitors were added, with effectiveness in the following order (from highest to lowest): nitrate > chromate > acetate > benzoate > sulphate. They suggested that the mechanism of pitting is associated with the competitive adsorption between chloride and oxygen on the metal surface and the addition of inhibitors limited pitting by raising the pitting potential. Böhni and Uhlig also reported that dissolved heavy metal ions in solution, such as copper and iron, can be deposited on the aluminium surface and act as efficient cathodes for reduction of dissolved oxygen or other

reducible species in solution. This, in effect, polarises the aluminium to the potential where pitting or anodic reactions occur.

Rudd and Scully also investigated the effect of inhibitors on the pitting potential and repassivation process of aluminium in $3x10^{-3}$ppm chloride solution and inhibitors of the concentration 0.08 to 0.32M over a pH range to 4-9, and found current transients decayed exponentially to the equation[17]:

$$i = i_o \exp(-\beta t)) \qquad [1.8]$$

where i_o is the initial maximum current, i is the current after time t and β is a constant, $5x10^{-3}$ s^{-1}

They found that inhibitors were effective in raising the pitting potential in the following order (from highest to lowest): nitrate >> phosphate > citrate = tartrate > benzoate > acetate. They suggest that pit initiation is associated with the repassivation rate of the metal and when an aluminium surface is first exposed to an aggressive solution, corrosion occurs at a high density of sites and that stable pit propagation only occurs when the inhibitive species and/or corrosion product does not seal the active sites on the metal surface, i.e. the rate of repassivation is lower than the rate of corrosion[17]. The effect of alloying additions will be discussed further in section 1.1.4.

1.1.3 Aluminium Oxide Films

Aluminium typically passivates when exposed to natural or some corrosive environments to form a transparent aluminium oxide film that covers the exposed metal surface. This oxide film is composed of two superimposed layers; an inner Al_2O_3 layer and an outer AlO(OH) layer[7]. Further investigation by Barr found that the aluminium oxide layer consisted of a composite of $Al(OH)_3$, AlO(OH) and Al_2O_3, with the inner layer predominantly composed of Al_2O_3 and the outer layer AlO(OH)[18]. These different hydrated states of aluminium oxide were studied by Lee and Pyun, who reported that those films with a greater proportion of AlO(OH) demonstrated the best corrosion protection and related it to having a higher ionic and electronic resistance[19].

The compact amorphous layer in contact with the metal, called the barrier layer, has low electronic conductivity and gives rise to dielectric properties. Investigations found that the maximum thickness of the barrier layer is in the order of 4nm on bare aluminium and forms within a matter of milliseconds. The second layer grows on top of the barrier layer, a porous crystalline film. It is an exchange layer that reacts with the external environment and can reach ~100µm under certain conditions. The thickness is dependent on the humidity of the surrounding environment, although techniques such as anodising may be used to thicken the film and enhance the corrosion resistance of the material[20].

The passivity of aluminium oxide films and inhibitive additions to solution or coatings are often used as corrosion protection methods. Inhibitors can be added to promote passive film growth by modifying the local media or reacting with the metal to form an additional oxide layer. Further information on inhibitors will be detailed later in section 1.2.3. However if the film is damaged, corrosion of the substrate can be very severe. The damage could be simply due to mechanical removal of the layer, e.g. physical abrasion, or the passive film could breakdown via localised corrosion, e.g. the formation of pits.

1.1.3.1 Corrosion of Aluminium Oxide Films

Metallic aluminium oxidises when exposed to air to form aluminium oxide:

$$2\ Al + {}^{3}/_{2}\ O_2 \rightarrow Al_2O_3 \qquad [1.9]$$

When exposed to neutral aqueous solutions, the formation of an oxide layer limits aluminium dissolution:

$$2\ Al + 3\ H_2O \rightarrow Al_2O_3 + 6H^+ + 6e^- \qquad [1.10]$$

Figure 1.2 shows a schematic polarisation curve of an aluminium system where the aluminium system exhibits passivity when an increase in potential leads to minimal or no current density increase. This is when the oxide layer acts as a passive layer that acts as a barrier to corrosion. Two cathodic curves are drawn on the diagram to demonstrate when the passivity can be broken down; the breakdown potential, E_{bd}, is the potential at which the passive layer breaks down and can lead to the onset of general localised corrosion. When the cathodic curve intersects the anodic curve the breakdown potential, the corrosion potential, E_{corr}, lies above E_{bd} and breakdown of passivity is initiated (often by pit initiation). Intersection of the cathodic curve at a potential within the passive region does not cause breakdown of passivity.

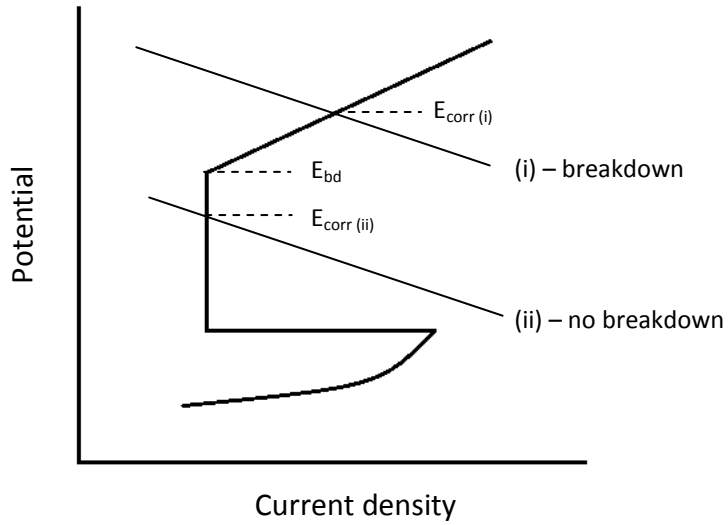

Figure 1.2 – Schematic anodic polarisation curve for a metallic system exhibiting passivity and breaking down after surpassing breakdown potential, E_{bd} [6]

The breakdown of passivity or protection from the oxide layer does not only occur when the critical anodic potential exceeds E_{bd}[21]. In the presence of aggressive ions, such as chloride, the aggressive species can cause localised corrosion of aluminium metal which can lead to stable pit propagation. Localised corrosion is most commonly associated with the formation of unstable or metastable corrosion pits which then develop into stable pits and the mechanisms of localised corrosion have been described in section 1.1.2.

1.1.4 – Effect of Alloying Additions

Pure aluminium is known for its good corrosion resistance, but its relatively low strength and hardness means that alloy elements must be added to enhance its mechanical properties. AA2024-T3 and other 2000 series alloy have copper as the main alloying element and are among the least resistant aluminium alloys to corrosion. Buchheit et al. reported that the intermetallics found in AA2024-T3 are predominantly Al_2CuMg, S-phase, with the remaining particles some composition of AlCuFeMn[22]. Boag et al. used EDX and WDX in scanning electron microscopy to examine the microstructure and found an array of multiphase particles, periphery phases surrounding composite particles and also clustering[23]. This complicated microstructure is difficult to fully characterise due to uncertainties in classification of particles and technique resolutions. The elemental composition of the alloy is presented in table 1.1 below.

Element	Al	Cu	Mg	Mn	Fe	Si	Zn	Ti	Cr
Wt%	90.7-94.7	3.8-4.9	1.2-1.8	0.3-0.9	<0.5	<0.5	<0.25	<0.15	<0.1

Table 1.1 – Elemental composition of AA2024-T3 [23, 24]

The complex microstructure and the presence of intermetallic particles and phases cause the alloy to exhibit different electrochemical characteristics on a more localised scale, for example the susceptibility to corrosion over an intermetallic compared to the bulk matrix [5, 25]. Copper

additions, found in 2000 series alloys, have been reported to be especially detrimental to the corrosion resistance of aluminium, as the copper is more noble than aluminium and acts as cathode sites, whilst the bulk matrix surrounding the secondary phases become anodic [2, 26]. Schmutz et al. used Volta potential mapping to study the localised corrosion of aluminium alloys and found that the copper-rich intermetallics affected the corrosion resistance of the metal surface[27], although there is still debate about the role of the intermetallic particles in the corrosion of aluminium alloys. Zhu and Van Ooij suggest that in AA2024-T3, the Al_2CuMg particles de-alloy, with the loss of aluminium and magnesium, during immersion in chloride solutions and there is a simultaneous dissolution of the bulk aluminium matrix surrounding the intermetallics[28]. Buchheit et al. considered the corrosion to be a selective dissolution of the intermetallics that leave a porous copper-rich layer and which can then be redistributed across the area surrounding the particles[22].

1.2 Paints on Aluminium Alloys

1.2.1 – Paint-protection against Corrosion

Coatings applied on aluminium substrates tend to maintain good resistance because of the relatively good corrosion resistance of the base metal itself, in that the passive oxide film will also provide protection so that paint degradation by corrosion products will be limited. However, this requires that the coating remains intact and suffers no physical or mechanical damage in which the metal is exposed. If the coating is damaged, the corrosive environment, e.g. chloride ions, has direct access to the metal and the protection provided by the paint will be diminished. Modern primers have been designed to contain inhibitive pigments that can be released so that the exposed metal will still receive protection[29].

Organic coatings can be broken down into four main components, which can be then be categorised as continuous and discontinuous phases[30, 31]. The continuous phase consists of a binder and a solvent, and the discontinuous phase comprises of additives and pigments. Each component will be described briefly below:

Binder – This is essentially the base component that acts like a glue, holding everything together. In most cases, the binder is an organic compound consisting of natural resins or polymers. It will largely determine the physical properties of the coating, e.g. mechanical properties, and chemical resistance. Examples include epoxy-amide, resin and polyurethane.

Solvent – Solvents are typically added to dissolve the binder, modify the viscosity and adjust the curing of paints before application on a substrate. Most of the solvent is evaporated off and lost on drying, sometimes leaving some residue. Some paints are water-based, where the solvent used is water, although organic, volatile solvents are more commonly found. Examples include xylol, oxy-ethanol and butanol.

Pigments – Organic pigments are seldom used in primers and are predominantly used for colour, whilst inorganic pigments are used for colour, physical properties and corrosion resistance. Inhibitors can be incorporated as pigments, and some can be dissolved into the binder. Examples include strontium chromate, titanium dioxide and iron oxide.

Additives – Additives are a wide range of chemicals that are added to affect the properties of a coating. These include catalysts, driers, surfactants, dispersing agents, coalescing agents and others. Examples include stearic acid or cobalt and manganese napthenates.

There are a number of ways in which paints can protect metals against corrosion, from physical isolation to galvanic protection and electrical insulation. The barrier protection mainly works by limiting the transport of moisture, ionic and gaseous species between the surrounding environment and bare surface. However, Guruviah and Funke respectively found that the amount of water and oxygen that permeates through coating films on bare steel was much higher than the quantity required for the steel to corrode under various conditions[32]. Therefore, it was unlikely that controlling the diffusion of oxygen through paint coatings plays a significant role in corrosion protection. Current understanding of intact coating corrosion protection is primarily based on two main theories; the ionic barrier mechanism and the adhesion mechanism.

Ionic barrier mechanism – Mayne postulated that the key factor is the resistance against the flow of ionic charge [33] (Figure 1.3). This 'resistance inhibition' hinders the corrosion current between the anode and cathode sites on the metal surface and thus limits the corrosive attack. This means that the sites on the metal where the anodic and cathodic half-reactions take place require a corrosion current that passes between the two sites and the presence of a coating will retard the current flow. A coating does not have to include inhibitive pigments for such an ionic

resistance to be available, and Mayne also showed that the rates of diffusion of water and oxygen within a coating are fast enough to allow cathodic reduction.

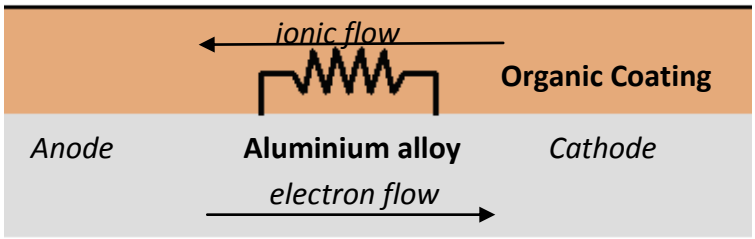

Figure 1.3: Schematic of an organic coating providing 'resistance inhibition', impeding flow of eelectrons between anode and cathode[33]

Adhesion mechanism – The other theory proposed by Funke, relates to the adhesion between the coating and the substrate [30]. Funke's main argument is that if a coating can maintain a good contact with the metal substrate under environments of high humidity, then corrosion would not occur. This 'wet adhesion' takes into account the permeability of a paint film to water and oxygen, but as long as adhesion remained intact between the coating and the substrate, water cannot accumulate at the interface and hence there would be no corrosive attack. However, most organic coatings cannot form strong enough bonds with the oxide surface to prevent water molecules displacing the relatively weak hydrogen bonds between the functional groups and the oxide. Whether Funke's theory of 'perfect' wet adhesion completely eliminating corrosion is correct or not, the question is still investigated today. Van de Brand et al. experimented on epoxy-coated aluminium under different exposure conditions to water[31]. They conclude that the epoxy coating may lose initial adhesion to the substrate, but in fact the water at the interface causes the formation of an oxyhydroxide layer which after some time actually leads to recovery and improvement of adhesion.

Epoxy resins have been commonly used as the binder in industrial applications, and have been regarded to give a good combination of corrosion resistance and mechanical properties[6]. However, when a coating is damaged, the protection that can be provided by the binder component is severely limited, as an aggressive solution would have direct contact with the metal substrate. The paint surrounding the defect could contain inhibitors that can be released into the exposed area so that inhibitive pigments can continue to protect the metal from corrosion.

1.2.2 – Failure of Paints

There are a number of ways in which an organic coating can fail and some industries remove and reapply paints after the lifetime of a coating. Although this project will primarily investigate the behaviour of corrosion-protection pigments after physical damage, such as abrasion or cracks in the coating, it is useful to consider some contributing factors to the failure of paint.

Blisters form when water permeates through the paint film, and salt solutions, which can be formed from soluble corrosion products or components within the paint, accumulate at areas where there is poor adhesion between the coating and the substrate[3, 34]. If the salt solution is of a higher concentration than that of the surrounding aqueous environment, then osmotic processes cause water to pass through the paint film to dilute the solution[31]. This leads to an increasing volume of solution beneath the paint film and further increases the area of delamination at the metal/paint interface. Schneider and Kelly conducted a series of experiments on coating blisters on AA2024-T3 and discussed a number of aspects regarding epoxy-coating failure and corrosion in AA2024-T3[35]. They observed that although for acidic pH solutions, blister formation and growth are both very fast, blister growth is a relatively slow

process in neutral pH conditions and the anodic and cathodic reactions are confined within the blister. Active blisters were red in colour which were thought to be related to copper replating, and areas where the coating is intact showed less corrosive attack. However, as more oxygen passes through the coating to the metal surface, its reduction causes a local increase in pH (becoming more alkaline) which leads to further degradation of the coating[35].

Another form of under-film corrosion that is prevalent in aluminium alloys is filiform corrosion. The term was first used by Sharman to describe filamentary trails of corrosion product on the surface of organic-coated metals[36]. Filiform corrosion is more predominant in humid air with the presence of aggressive ions, such as chlorides[37]. Further research revealed that the heads of the filaments contained electrolyte with metal cations and aggressive anions that usually exhibit a low pH[38], whilst the tails of the filaments consist of dry, porous corrosion products. However, improved coating adhesion can hinder the propagation of filiform corrosion and McMurray et al. studied the inhibition of filiform corrosion by strontium chromate from a polyvinyl butyral-*co*-vinyl alcohol-*co*-vinyl acetate (PVB) using scanning Kelvin probe, SKP, potentiometry[37]. The SKP works by measuring the electrochemical potential of a substrate and mapping out a potential map of the surface. They found that chromate ions were released into the electrolyte beneath the delaminated organic coating and inhibited further delamination of the PVB film by reducing the rate of filiform corrosion propagation. However, for the regions where the coating was still intact, the chromate does not act to inhibit oxygen reduction (as it did for the delaminated areas), and so McMurray et al. concluded that in areas of intact coating, the chromate acts indirectly to inhibit the anodic dissolution of the metal by preventing the coating-substrate interface from becoming a low-pH, high-chloride ion environment by pH buffering.

Another form of paint failure is cathodic delamination, which is prevalent in corrosion of ferrous alloys and is generally regarded to be of little importance in aluminium alloys[35]. As the majority of cathodic reactions on AA2024-T3 would take place on the intermetallic particles, it is expected that the spacing between the intermetallic particles is too large, greater than the width of the delamination zone[39], to have sufficient influence to drive cathodic delamination.

1.2.3 – Pigments for Inhibitive Protection

Inhibitive pigments are dispersed across the coating matrix and when water passes through the matrix, pigments dissolve to release inhibitor. The released inhibitive ions can then react with the aqueous environment or the metallic substrate to inhibit corrosion processes. The two main forms of inhibition are cathodic and anodic. Usually, cathodic inhibitors retard reduction reactions such as the oxygen reduction reaction, whilst anodic inhibitors tend to promote passivation or to selectively cover anodic sites on the metal surface. However, although cathodic inhibitors are used satisfactorily in many applications by inhibiting corrosion, anodic inhibitors, are able to achieve complete protection, provided adequate concentrations are used, depending on chloride concentration[40]. What one must often consider is the composition of the liquid environment, as the ionic composition, arising from the dissolved salts and gases, influences the performance of the inhibitive ions.

Bohni and Uhlig studied the action of mixtures of inhibitive anions and aggressive chloride ions on aluminium[15], using a quantitative relationship between the concentration of inhibitors and aggressive ions that had been derived from tests on mild steel to show that:

$$\log C_i = K \log C_a + \text{constant} \qquad [1.7]$$

where K is related to the valencies of the respective ions, and C_i and C_a are the concentrations of the inhibitor and aggressive ion respectively [40].

It should also be noted that cathodic and anodic inhibitors are not mutually exclusive and inhibitors can fall into multiple classifications. Inhibitors can be 'oxidising' or 'non-oxidising', and are characterised by the ability of the inhibitor to passivate the metal (anodic passivation). They can also be classified as 'safe' or 'dangerous' by considering levels below the minimum concentration for the inhibitor to provide effective corrosion protection, whereby for a 'safe' inhibitor, concentrations below the threshold value would only permit the corrosion rate to be no greater than that of an uninhibited and for a 'dangerous' inhibitor, lead to enhanced localised attack[40]. The pH and the temperature of the system are also factors that affect the performance of the inhibitive ions, which usually have a range in which they are most effective. However, the main emphasis of this literature review will be inhibitive pigments, which are typically inorganic salts[41].

Commonly, the more important inhibitive species for anodic inhibitors are the anionic constituents, which influence the rate of corrosion. Chromates, molybdates, tungstates, phosphates and vanadates are examples of anions that provide corrosion inhibition, whereas anions such as chlorides and sulphates are known to promote corrosion. Cationic constituents are usually selected due to their effect on other properties, physical or chemical, of the compound. This can be solubility, pH and toxicity of the species. However, saying that, there are also cations that also provide cathodic inhibition, such as Zn(II) [41] and there is a lot of work on the inhibition of AA2024-T3 corrosion using rare earth metal cations[42-46].

Chromate-based species have been the most widely and effectively used inhibitors in industrial applications and strontium chromate in particular is found in high performance aircraft primers. The following section will explore the mechanisms of corrosion protection for strontium chromate.

1.2.3.1 Strontium Chromate as an Active Pigment

In 1998, the National Defence Centre for Environmental Excellence supported a study to compare seventeen substitute coatings, in which the outcome showed that chromate-based formulae were the most effective (NDCEE, 1998)[47]. S. Zein El Abedin also used polarisation measurements to compare the effect of chromate, molybdate and tungstate anions on the pitting potential of aluminium[48]. From his investigation, chromate appeared to be the most powerful inhibitor that can exhibit a large passivating influence on aluminium, causing it to form a stable oxide barrier. Chromates are highly effective corrosion inhibitors for not only iron and aluminium, but also zinc and copper. In 2003, Kendig and Buchheit compiled a detailed critical review on the current consensus of the main protective mechanisms by which hexavalent chromium compounds, present in organic coatings or in chromate conversion coatings, inhibit corrosion on aluminium alloys[24].

When strontium chromate is dissolved into an aqueous medium, the following dissolution takes place:

$$SrCrO_4 \rightarrow Sr^{2+} + CrO_4^{2-} \qquad [1.11]$$

After dissolution, the CrO_4^{2-} ions, Cr(VI), react with the surrounding environment in a number of reactions. Cr(VI) ions are a powerful oxidising agent, although more so in acidic environments than alkaline. So it is observed that chromates can to protect in pH 5- 11[49].

The Cr(VI) oxyanions can be characterised by the following equations in aqueous solutions[24]:

$$H_2CrO_4 \leftrightarrow H^+ + HCrO_4^- \qquad K_1 = 0.18 \qquad [1.12]$$

$$HCrO_4^- \leftrightarrow H^+ + CrO_4^{2-} \qquad K_2 = 3.2 \times 10^{-7} \qquad [1.13]$$

$$2HCrO_4^- \leftrightarrow Cr_2O_7^{2-} + H_2O \qquad K_d = 98 \qquad [1.14]$$

where K_1, K_2 and K_d are the respective equilibrium constants and the values obtained at high ionic strength. The equations show that bichromate ($HCrO_4^-$) and dichromate ($Cr_2O_7^{2-}$) are the dominant species in lower pH conditions, between 1 and 6, and that chromate (CrO_4^{2-}) exists predominantly at pH ≥ 7[24].

Strontium chromate has been favoured because of the low solubility of the compound. The amount of pigment added into a primer are often at concentrations beyond the expected solubility limit in water, 6.3mM, so it is assumed that strontium chromate will remain as an undissolved solid within the organic coating, acting as a reserve that will later be able to provide a release of chromate ions for a longer amount of time[41, 50].

The pH of the solution also affects the dissolution and saturation concentration of strontium chromate[51], which means that the distribution of Cr(VI) between the different anionic states varies, and the release of chromate will not only be impacted by the pH of the bulk solution but also the local areas around electrode sites[24]. Figure 1.3 shows the calculated concentrations from Raman spectroscopic experiments of the Cr(VI) oxyanion species in different pH conditions [24, 52].

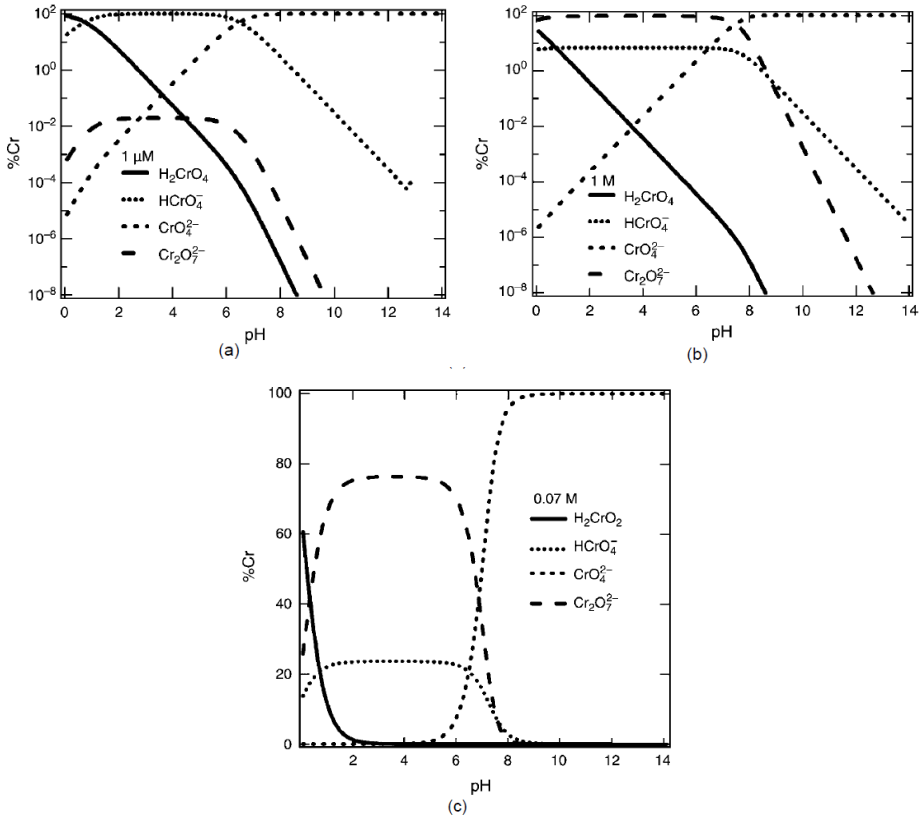

Figure 1.3 – Relative concentration of Cr(VI) oxyanions as a function of pH and total Cr(VI) concentration for: (a) 10^{-6}M, (b) 1M, and (c) 0.070M, a typical concentration for a chromate conversion coating *(Taken from Kendig and Buchheit [24])*

Inhibitor release from within the binder is an important consideration when formulating paints in order that a continuous or on-demand supply of inhibitor can be provided when needed. This is further expanded in section 1.2.4.

Below is a summary on the suggested protection mechanisms provided by chromate anions:

The anodic dissolution of aluminium is inhibited at the cathode by the formation of an Al^{III}/Cr^{III} surface oxide. It is suggested that Cr^{VI} oxyanions are reduced at the cathode to Cr^{III} instead of the dissolution of the anode, aluminium metal, which then combine with the already dissolved Al^{III} ions (from aluminium hydroxide) to produce an Al^{III}/Cr^{III} complex. This stable complex provides protection against further attack.

The above postulation does not include the contest between the chromate anions and the chloride anions, and so it was also suggested that the non-faradaic adsorption of Cr(VI) ions onto the surface of the aluminium oxide surface then modifies the surface charge to coulombically favour chromate oxyanion adsorption, thus disfavouring chloride ions. Chidambaram et al. showed that the interaction of the aluminium hydroxide, $Al(OH)_3$, with CrO_4^{2-} and Cl^- led to the deprotonation of $Al(OH)_3$ to form either a protective aluminium oxide film with chromate or aluminium hydroxychloride or a non-protective lamellar pseudoboehmite structure (that cannot protect against the development of pitting in the presence of aggressive ions) [46]. This preferential adsorption then led to inhibition of the oxygen reduction reaction, ORR, where rapid reduction of the Cr(VI) ions onto the aluminium oxide surface, forming the Al^{3+}/Cr^{3+} hydroxide complex that might contain co-adsorbed Cr(VI) ions, so that a bipolar barrier would be formed that would inhibit further electron transfer[24, 53].

Ilevbare and Scully considered the effect of chromate from chromate conversion coatings on the oxygen reduction reaction and postulate that chromates form a Cr^{III} oxide film that can serve as a barrier to the diffusion of oxygen[54]. Zhao et al. also reported that chromate is an effective cathodic inhibitor and causes inhibition of the cathodic O_2 reduction on copper-rich intermetallics produced by de-alloying processes[55]. Chromate compounds have also been shown to be effective cathodic inhibitors of iron at low concentrations (0.1mM) where Cr(VI) was found to be reduced to Cr(III) although it should also be noted that at even lower concentrations, Cr(VI) has been found to promote iron corrosion[41].

Not only does chromate protect the aluminium substrate, but because it is a strong oxidising agent for other elements, such as iron, copper and zinc, another protection mechanism is the passivation of S-phase ($CuMgAl_2$) intermetallics in AA2024-T3 to protect against de-alloying. Kolics et al. observed that in acidic NaCl solutions, AA2024-T3 undergoes severe bulk de-alloying through the preferential dissolution of magnesium and aluminium, leaving copper in the bulk matrix[56]. They found that addition of chromate strongly prevents the corrosion of magnesium and retards the copper-enrichment of S-phase particles because of a non-uniform chromium-rich film that is formed across the entire metal surface. Using scanning electron microscopy, energy-dispersive X-ray analysis, Auger electron spectroscopy and X-ray photoelectron spectroscopy, they observed that the chromium-rich film was thicker above the S-phase particles than the rest of the bulk matrix.

Whilst chromate species strongly inhibit the cathodic reactions, chromate compounds in sufficient concentrations also provide anodic protection, passivation, which suggests that chromate protection is independent of the dissolved oxygen in the surrounding environment.

However, Kendig and Buchheit noted that the anodic inhibition by chromates is 'modest' and unlike the cathodic inhibition, the anodic inhibition is more affected by environmental factors, such as pH, chloride to chromate ratio and degree of aeration[24, 48]. Anodic inhibition also varies with alloy substrate chemistry and temper. The mechanism of anodic inhibition is not certain, but Kendig et al. suggested, with piezoelectrokinetic, PEK, measurements, that the adsorption of chromate species onto the oxide surface is involved. Cartledge found in 1966, that Cr(VI) anions would inhibit corrosion on stainless steel surfaces without being dependent on the cathodic reactions such as ORR. By performing experiments in aerated and deaerated conditions, he found that the formation of a passive film is not dependent on the presence of an inhibitor, although the inhibitor reduces the minimum current density and the charge required for passivation, but that that no charge transfer from the inhibitive species were necessarily needed [57].

As mentioned earlier, the presence of intermetallic copper-rich particles greatly reduce the corrosion resistance of aluminium, and it is expected that chromate species acts as a cathodic inhibitor by adsorbing onto the alloy surface and becoming reduced to form a passive film. However, it was found that the AlCuFeMn intermetallic phases are more noble compared to the bulk matrix which was linked to the increased chromate reduction around the area [58].

The cationic component, strontium, causes the chromate compound to have a low solubility product[41]. In Sinko's paper, the blistering time of chromate-based coatings on aluminium and plated steel with different cationic constituents was compared, and strontium and barium showed the slowest release of chromate and the coating took the longest times for the onset of blistering. Calcium had leaching times an order of magnitude greater, and sodium exhibited the most severe blistering that further led to delamination. This is due to the local changes in pH

when oxygen reduction causes the local environment to have an increase in hydroxide ions and a mobile cation, such as sodium, will cause the pH to become more alkaline and lead to coating degradation. Whilst the inclusion of strontium in the pigment proves to be beneficial in the limiting of blistering in coatings, Baghni et al. studied the individual effects of strontium and chromate ions on the inhibition of zinc[59]. By using equimolar solutions of strontium chromate, strontium chloride and sodium chromate, the polarisation curves were compared. They found that the cationic component, sodium or strontium, does not greatly affect the cathodic branch of the curve, where chromate provides strong cathodic inhibition. However, the anodic branches of the strontium chromate and sodium chromate differed substantially. Sodium chromate additions exhibited a lower anodic current close to the corrosion potential, whereas strontium chromate additions reveal an extended passive region and a raised pitting potential. Strontium chloride compared against strontium chromate showed an increased oxygen diffusion cathodic current (which proves the cathodic inhibition by chromate)[59]. X-ray photo-electron spectroscopy was also used to examine the zinc surface and found that Cr^{III} ions (not Cr^{VI}) existed in the surface film. Significantly, no strontium was detected in the XPS spectra, which shows that strontium remains in the solution.

Kendig, Davenport et al. used X-ray absorption near edge spectroscopy (XANES) on chromate conversion coatings on AA2024-T3 and found that 20% of the hexavalent chromate remained in the coatings, meaning that the conversion coating could act as an 'active' coating that will provide a source of inhibitor to repair defects. The Cr(VI) that did reduce to hydrated Cr(III) oxide appears to reach a limit after five minutes of processing and the conversion occurred at the substrate/coating interface in the earliest stages of film formation[45]. However, tests on chromate conversion coatings have shown that Cr(VI) oxyanion release decreases significantly

over time, so chromate conversion coatings usually need to be paired with another protective coating. It is generally accepted that the main form of chromate release comes from primer pigments[24, 41, 60].

Jakab and Scully did work on amorphous Al-Co-Ce alloys to investigate how metallic coatings compare with the 'triggered' or 'on-demand' release of inhibitive species that can be achieved with chromate-based systems[61]. This 'active corrosion inhibition' is highly desirable for replacement of protective species and thus the compatibility with the organic coating is important as well as, for example, the water permeability of the paint to allow the delivery of inhibitor.

1.2.4 Inhibitive Pigment Release from Paint

The previous section discussed protection mechanisms of strontium chromate in both solution and in coatings, and this section will explore the complexities of the leaching and release of pigment from the coating.

Prosek and Thierry investigated the release of chromate from organic coatings and noticed that the water permeability of the polyester isocyanate coating affected the action of the strontium chromate [60]. They broke the leaching process down into three stages: (i) rapid release from the surface of the coating, (ii) water penetration through the pores of the coatings and finally (iii) water reaching the substrate/coating interface. It was also expected that by the third stage, all of the chromate available within the coating will affect the leach rate. The amount of chromate released from the coating changes with the amount of strontium chromate in contact with solution and the amount of diffusion of chromate ions through the coating matrix. They believed

that the capabilities of acting as a barrier to water and aggressive ions were antagonistic to an 'on-demand' release of inhibitors, so a primer design needs to balance between the two mechanisms. However, they also noted that the leach rate did not follow an Arrhenius-type relation, where rate increases with temperature. Instead, the optimum leaching rate was at 20°C in a temperature range of 3-60°C and both an increase or decrease in temperature led to a lower rate of chromate release. They postulated that another process must be limiting the inhibitor release such as a modification of the strontium chromate particle/organic matrix interface, possibly the oxidation of the organic matter, restricting pigment diffusion. Prosek and Thierry used ion chromatography analysis to quantify the concentration of chromate ions in aqueous solutions, and were able to determine the concentrations of CrO_4^{2-} anions to a sensitivity of approximately 30ppb with no observable effect from the chloride ions[60].

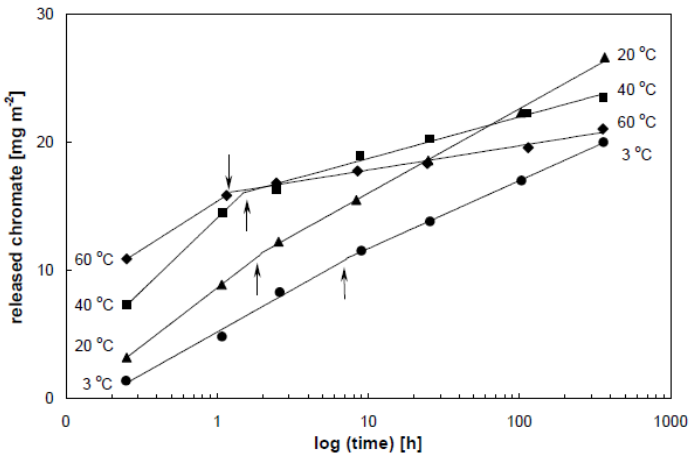

Figure 1.4 – Time dependencies of released chromate from polyester coating in 10mM NaCl at pH 7 at various temperatures. Arrows mark slope changes *(Taken from Prosek andThierry[60])*

They also studied the effect of pH in the solution and found that it had a relatively small effect on the leaching rate, and concluded that the permeability of the coating played a major role and that the rate-controlling step was likely to be related to the release at the pigment particle/coating matrix interface.

The degree to which pigment leaches into solution can also be a factor in paint failure. Howard, Zin, Scantlebury and Lau studied the solubility and leaching of inhibitor ions at cut-edges on galvanised steel and coating defect areas, using inductively coupled plasma emission spectroscopy (ICPES) and found that the leaching rate plays a more important role in the controlling of available inhibitor for corrosion protection[62]. Contrary to Prosek and Thierry, they found that the leaching of pigment was mainly restricted by the polyester binder.

In some cases, inappropriate inhibitors may cause the acceleration of blistering in organic coatings [41, 63]. Excessively soluble pigments can allow too much water to permeate through the coating and cause excessive osmotic pressure so that water passes through the coating to dilute the inhibitor solutions, and through the swelling lead to blister formation and growth[29, 34]. A "permanent primer", which in the aerospace industry is classed as a corrosion resistant coating that can last for over a 30 year period, can only be accomplished if there is a good balance between the mobility, diffusivity and efficiency of the inhibitive species[64]. Osborne et al. worked on non-chromated coatings for aerospace applications and stated that it was unlikely non-chromate inhibitors will be developed that can imitate the overall functionality of hexavalent chromium inhibitors[64]. To retard blister formation, the inhibitor mobility through the coating can be increased or the water permeability of the coating decreased, however, this will either reduce the lifetime of the paint coating or limit the release/supply rate and thus the protection provided by inhibitors.

As somewhat expected from what can be seen on the effect on blister formation, the effectiveness of a pigment within is also dependent on the mobility and solubility of the species within the organic coating (to opposite effect). Sufficient inhibitor needs to be available to protect the metal from corrosive attack. If the solubility of the pigment is too low or if transport

is too slow, then inhibitor release will not be sufficiently rapid to reach the area of attack and conversely, if excessive pigment dissolves in solution, then the protective lifetime of the coating will be relatively shorter because of the wasted leached pigment[31].

Furman, Scholes, Hughes and Lau also investigated chromate leaching from epoxyamide primers under different pH conditions and found that in general, amount released from the primer increased with decreasing pH and increased immersion times until it reaches an equilibrium for all pH values after 30 days[65]

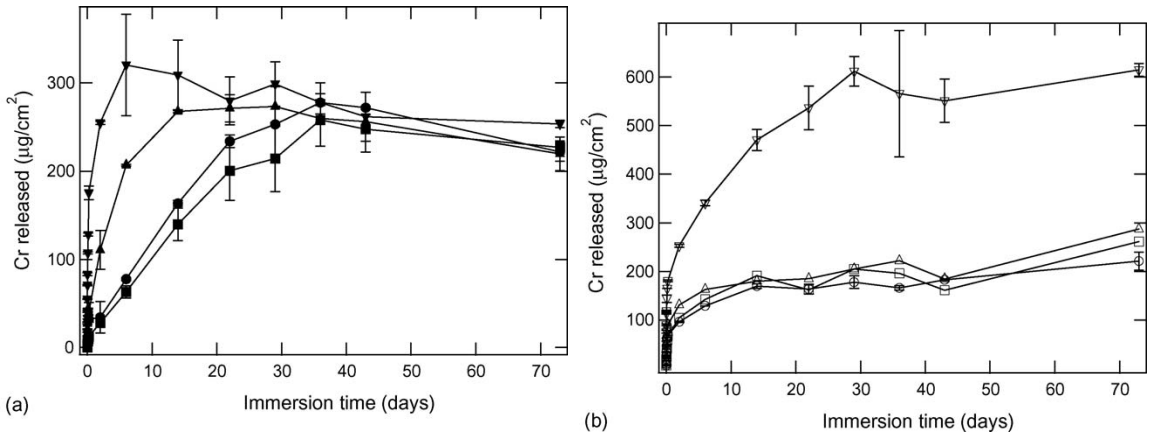

Figure 1.5 – Chromium released (per unit area of coating) into immersion solutions over time for:
a) PR143 primer (pH 1 = ▼ , pH 3 =▲, pH 5 =■, pH 7 = ●)
b) Anzol primer (pH 1 = ▽, pH 3 =△, pH 5 = □, pH 7 = ○) [65]

From figure 1.5, it can be seen that the release of chromium differs greatly between primers in addition to pH and immersion time. The Anzol primer in figure 1.5b exhibited a rapid release in the first 5 days where the majority of released Cr(VI) is leached out and a fraction is released over the course of the next 30 days of immersion. Furman et al. then modelled the release and concluded that the release of pigment is not solely diffusion controlled and in fact $t^{0.25}$ behaviour only fits a part of the release and the early rapid release and the slowing down of diffusion at longer immersion times.

1.3 Alternative Protection Systems

1.3.1 Ion-exchange coatings

To address the problem of blistering, research has been done on the application of ion exchange compounds or 'smart-release' pigments, first addressed by Goldie in the 1980s[66]. These compounds, such as bentonite or hydrotalcite, and can used to store an inhibitive anionic or cationic species, such as vanadates or cerium, that require a form of equivalent exchange to be released into the surrounding environment[67]. This different concept utilises the insolubility of the ion exchange compound to store and bind an active inhibitive species, such that it will only release the inhibitor when anions are supplied for exchange to occur. This could be an environment of aggressive species that surrounds the coating and triggers the discharge of inhibitive ions. It does so by having the ion-exchange compounds existing as positively charged layers in which metal cations, e.g. Al^{3+} or Fe^{3+} occupy the octahedral sites. Layers of anions and water electrostatically bind the different layers together. When in contact with an alkaline salt solution, the inhibitive ions are released and form a thin inorganic coating on the alloy surface and the aggressive Cl^- ions are immobilised. Ion exchange protection is therefore not governed by the solubility of the inhibitor and will not be susceptible to blistering, as the concentration of ions in the coating will remain constant, due to the bound inhibitive ions being replaced with the potentially aggressive ions.

Bohm et al. investigated cerium bentonite as an insoluble cation exchange pigment that will not dissolve and has superior delamination inhibition properties to strontium chromate, thus greatly reducing the probability of osmotic blistering or excessive/insufficient inhibitor leaching[68]. Buchheit et al. also looked at vanadium species containing anion-exchanging hydrotalcite with similar interest[69]. Hydrotalcites are layered clay materials that can be synthesised with

vanadates to provide corrosion protection, and Buchheit demonstrated the use of Al-Zn-decavanadate hydrotalcite pigments to provide corrosion inhibition. By making use of the hydrotalcite basal plane spacing, corrosion sensing can also be achieved via the observation of the X-ray diffraction change in the basal plane when inhibitor ions are released and exchanged with chlorides or sulphates[69].

1.3.2 Alternative Corrosion Inhibitors

In 2001, Sinko compared a number of different inhibitive species, including chromate (CrO_4^{2-}), phosphate (PO_4^{3-}), molybdate (MoO_4^{2-}), silicate (SiO_3^{2-}), cyanamide (NCN^{2-}) and borate (BO_2^-), considering a few mechanisms that explained the '*significant performance "gap"*' compared to strontium chromate [41]. However, anionic inhibitors can sometimes be a double-edged sword, as some anions that can reduce or prevent corrosion for some metals can also be considered as aggressive towards other metals[40]. By promoting the formation of a passivating film, inhibitive anions can effectively repair weak points present in an oxide film. Such a mechanism was first put forward by Stern in 1958, who worked with iron and its oxide film[70]. He proposed that the formation of a passivating oxide was aided by the presence of certain anions, due to an increase in the rate of cathodic processes, (i.e. the reduction of an oxidising anion or the acceleration of oxygen reduction) leading to an increase in the available equivalent anodic current, which can then exceed the critical current density for passivation. He also postulated that anions could possibly facilitate anodic passivation by reducing the magnitude of the critical current density, and subsequent work showed that passivating inhibitors mainly affect the anodic process[40].

When aluminium is immersed in water, the oxide film thickens, and Lorking and Mayne found that in near-neutral and de-aerated solutions, the aluminium oxide film remained stable and protective in both distilled water and chloride solutions, as well as in solutions of inhibitive

ions[71]. Thus they concluded that the inhibition of aluminium differs from iron in that the stabilisation of the oxide film is not dependent on the presence of dissolved oxygen in the solution. They also observed that the inhibition of aluminium occurred only when the initial rate of aluminium oxide dissolution in solutions of anions was less than a critical value.

The Fontana Corrosion Center and Ohio State University have studied the corrosion inhibition of AA2024-T3 by vanadates[72]. The vanadium species can have a number of different oxidation states, from +2 through to +5, and different combinations of the oxidation states prove to provide different corrosion inhibition[73]. For example, Iannuzzi et al. found that the electrochemical behaviour of a clear solution of metavanadates containing monovanadates without decavanadates is distinctively different to an orange solution of decavanadates without monovanadates[72]. The vanadium species present in a solution would depend on the pH, concentration and ionic strength of the solution[73]. Iannuzzi et al. also observed that metavanadates and monovanadates significantly reduced the rate of the oxygen reduction reaction, comparable to that of chromates, although the presence of decavanadates had little effect on the reduction rate, indicating they are a poor cathodic inhibitor[72].

1.3.3 Rare-earth Inhibitive Pigments

Studies have shown that cerium is an effective cationic corrosion inhibitor that can be used on aluminium alloys. Hinton suggested the use of cerium as a non-toxic alternative to chromate-protection coatings due to its formation of an insoluble hydroxide [73]. Research on aluminium alloy AA7075-T6 in aqueous environments showed that 100ppm of cerium chloride in 0.1M sodium chloride reduces the corrosion current by an order of magnitude, but the main problem it faced was the time required for a protective cerium oxide to deposit, requiring in excess of 100hrs to provide significant protection. Aldykewicz et al. worked on AA2024-T3 and using X-ray Absorption Near-edge Spectroscopy found that a cerium-rich insoluble film develops at cathodic sites, namely copper-containing intermetallics[44]. This demonstrated the effect of cerium as a cathodic inhibitor, and Auger electron spectroscopy studies revealed that the film was composed mainly of cerium oxide[43]. Aldykewicz et al. also go on to say that the formation rate of the cerium-rich film is dependent on the reduction kinetics of oxygen and concludes that the aeration of the environment determines whether the cerium ions form a thinner trivalent or a thicker tetravalent film (in de-aerated and aerated conditions respectively)[44].

Smith et al. compared epoxy coatings containing cerium- glycollate, tartrate, chloride and iodate pigments and concluded that there were insufficient cerium cations available to provide adequate protection[74]. Therefore, cerium salts as an inhibitor pigment were not deemed successful until relatively recently, when in 2001, Bohm et al. used calcium- and cerium-exchanged bentonite in a polymer-resin based primer on galvanised steel[68].

More recently, Markley, Forsyth and Hughes performed work on the protection of AA2024-T3 using rare-earth diphenyl phosphates, namely cerium and mischmetal, and used cyclic

potentiodynamic polarisation as one of their techniques to characterise the anodic and cathodic current densities, the free corrosion potential and the breakdown potentials of the alloy after different periods of immersion[75]. From these experiments, they concluded that the rare-earth diphenyl phosphates display cathodic inhibition that decreases the cathodic current density during polarisation tests and Raman spectroscopy also showed that mischmetal diphenyl phosphates can also inhibit pit initiation. These findings show promising potential for both cerium and phosphates as a replacement for existing chromate inhibitors, although such tests were performed in ionic solutions without any organic coatings, and therefore have not yet been able to address the efficiency of the species as an inhibitive pigment.

Chapter 2 Materials and Experimental Techniques

This chapter describes sample preparation and compositional information of the substrate and coatings. The experimental techniques used are described, which include direct current potentiodynamic polarisation, electrochemical impedance spectroscopy (EIS), electrochemical noise analysis (ECN), UV-Visible spectroscopy, scanning acoustic microscopy (SAM), optical microscopy and MicroXAM. By combining the results and analyses from these methods, the protection of inhibited coatings at a defect will be better understood.

2.1 Materials Data

2.1.1 Aluminium Alloy 2024-T3

The aluminium alloy under investigation is AA2024-T3. The 2000 series are particularly high-strength aluminium alloys with copper as the main alloying element, which produces an age-hardening effect[5]. 'T3' indicates the process by which the alloy was prepared, which means that it was solution-quenched, aged and annealed at ambient temperatures[6]. AA2024-T3 also has good machinability and surface finishing capabilities. Its composition mainly consists of aluminium, copper and magnesium. Table 2.1 shows the typical elemental composition of the alloy. T3 indicates the temper designation of the alloy, and is thermo-mechanically processed by solution heat-treatment, cold working followed by naturally aging to a stable condition. Coarse intermetallic particles and secondary phases are formed during solidification due to the elements' low solubility limit in aluminium.

Element	Al	Cu	Mg	Mn	Fe	Si	Zn	Ti	Cr
Wt%	90.7-94.7	3.8-4.9	1.2-1.8	0.3-0.9	<0.5	<0.5	<0.25	<0.15	<0.1

Table 2.1 – Elemental composition of AA2024-T3

2.1.2 Paint Compositions

The paint coatings used in this study are all epoxy resin coatings with different pigments. Airbus supplied the chromate (VI) inhibited and non-inhibitive paint through an external paint company, Mankiewicz. An alternative inhibitive pigmented epoxy paint with cerium diphenylphosphate, was pre-coated onto AA2024-T3 panels and supplied by Monash University. Paint compositions are given in tables 2.2.

2.1.2.1 Non-Inhibitive Control Paint and Chromate (VI) Pigmented Paint 113-22

The paint composition for the chromate (VI) 113-22 paint is listed in table 2.2 below. Mankiewicz were not prepared to disclose greater detail the composition used in a commercial product, and it is uncertain whether the amount of strontium and barium chromate (highlighted in red) are independent of each other or whether typically the combined weight percentage of chromate must lie within a specified range, e.g. 6-17.5wt% for total CrO_4^- species (sum of two minima as lower boundary and two maxima as upper boundary) or 10-13.5wt% for combined CrO_4^- species (sum of minima and maxima as upper and lower boundaries).

Component	Weight Percentage
Bisphenol-A epoxy resin	12.5 – 20%
Naptha	5 – 12.5%
Xylol	5 – 12.5%
2-butoxy-ethanol	5 – 12.5%
Strontium chromate	5 – 12.5%
Barium chromate	1 – 5%
Kerosin	1 – 5%
1-methoxy-2-propanol	1 – 5%
N-Butylacetate	1 – 5%
Butan-1-ol	1 – 5%
4-hydroxy-4-methy-2-pentanone	1 – 5%

Table 2.2 – Paint composition for 113-22 epoxy resin

The non-inhibitive control paint also supplied by Airbus has an identical epoxy composition as the 113-22, but does not contain any chromate (VI) inhibitor nor any other inhibitive components. Again, it is not known what pigments were used as replacement for the inhibitors.

2.1.2.2 Cerium Diphenylphosphate Pigmented Paint

Cerium diphenylphosphate $Ce(dpp)_3$ has been of recent interest because of its anti-corrosive properties and is one possible alternative to chromate (VI) pigments. Monash University stated that it was difficult to mix the inhibitor well into an epoxy coating (Epigen) so that paint application was uneven and thicknesses were extremely high, ranging between 300 - 500μm. The basic composition of the coatings were 20wt% $Ce(dpp)_3$ and 80wt% Epigen epoxy polyamide binder.

2.2 Sample Preparation

AA2024-T3 was received in the form of rolled plates of approximate size, 69mm x 48mm x 2mm. These were cut in half using a heavy circular saw. The surface was washed with acetone and ethanol to remove any oil, rinsed with deionised water and dried.

Organic coatings were prepared by mixing the two-component primer, essentially binder and hardener, using the mixing ratio, 10 parts to 3 parts by weight, provided by Mankiewicz. After adding the two parts together, primers were stirred and left for approximately 30 minutes as a pre-reaction time before application.

To coat a sample, pieces of insulation tape were stuck along both sides of the aluminium sheet. These acted as spacers that provide height for the pull-down method; paint was poured on the upper edge of the sample and a glass rod, of approximate diameter 7mm, was then used to

apply the coating by the pull-down method. The freshly coated samples were then left to dry away from dust and to cure at ambient temperature, in accordance to the paint information data sheets supplied.

Paint application in industry is often done by high pressure spraying that can achieve thicknesses of 20 - 25μm. This technique was not available in our laboratory and the pull-down method limited the minimum thickness achieved to approximately 50±10 μm. The $Ce(dpp)_3$ coated samples from Monash University had thicknesses of 300 - 500μm. The large difference in thickness means a larger reserve of inhibitive pigment would be within the coating layer.

Electrochemical tests were performed in 0.5M and mostly 2M sodium chloride (analytical grade, 99.5% purity) solution, made in de-ionised water. For small-volume tests, an agar gel of 1wt% was made using the 2M NaCl solution. The high concentration of 2M sodium chloride was used, after initial trials, to counteract innate anti-corrosive properties of the AA2024-T3 substrate (seen in succinct, short-term exposure to 0.5M NaCl with no spontaneous pitting) and to focus on the inhibitive pigments. It also serves to simulate high concentrations of salt that could be found on aircraft surfaces as moisture evaporates.

Most tests were performed on coated samples with a defect, some on fully-intact coated samples and also some on bare alloy. Defects were made using a 1mm-width steel tool or a narrow scribe line was made using a steel scalpel, to investigate the effects of defect width.

2.2.1 Experimental Setups

2.2.1.1 Testing in Bulk Solution (Large Volume Test)

Testing in a 0.5litre electrochemical cell was initially used for direct current potentiodynamic polarisation tests and intact coating tests. It was especially useful in that the sample is clamped against one side of the electrochemical cell with a hole of size 1cm^2 to expose a controlled area of the reaction surface. A schematic diagram is shown in figure 2.1 below:

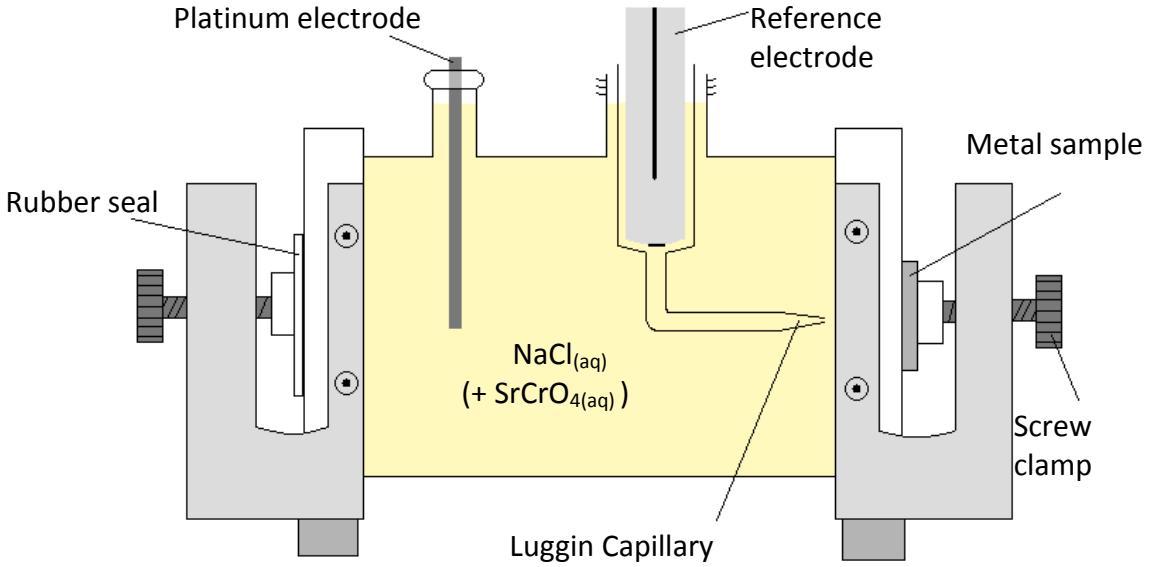

Figure 2.1: Schematic of cell used for large volume electrochemical testing

A Teflon O-ring was used to seal the sample to the cell and eliminate crevice corrosion and prevent leaking. A saturated calomel reference electrode (SCE) was used to measure potential and a luggin capillary is brought close to the sample surface to reduce any Ohmic potential drop that may occur due to distance of the reference electrode from the surface. A platinised titanium counter-electrode was used.

2.2.1.2 No Stirring Testing (Agar gel test)

A smaller volume electrochemical cell was devised where solution is on thin filter paper and agar gel, to reduce convection, connected to electrodes. Inhibitor released from the coating would diffuse more slowly into the surrounding medium and retain a higher concentration close to the test surface. A 27mm x 27mm piece of filter paper was placed above the defect and a Perspex cell was placed on top. The edges of the Perspex cell were sealed with a hot 4:1 beeswax/colophony mixture to avoid any leaking. The Perspex cell has a platinum wire counter electrode that threads out of the top, and a hole for a rubber bung in which a standard calomel electrode was placed to prevent drying out of the gel. The 2M NaCl agar gel is pipetted into the space above the filter paper and the reference electrode bung is placed on top. A schematic diagram is shown below:

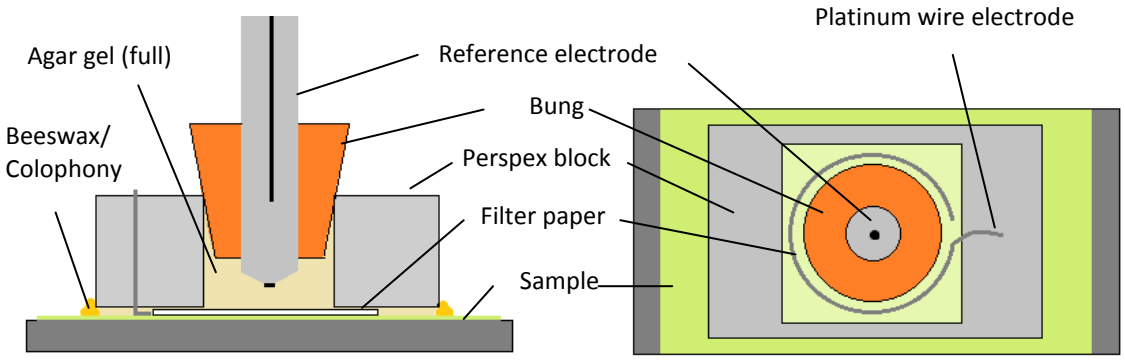

Figure 2.2: Schematic of cell used for small volume electrochemical testing

The small volume cell was used to perform electrochemical impedance and noise tests on coated samples with defects using a Gill AC Potentiostat.

2.3 Testing Techniques

2.3.1 Direct Current Potentiodynamic Polarisation

The corrosion behaviour of a metal is commonly characterised by the polarisation curve of a sample. The metal sample will find an equilibrium potential in its surrounding environment and a polarisation curve is measured by taking the metal across a potential range. The difference between the metal electrode potential and the equilibrium potential is known as the polarisation (also known as the overvoltage or overpotential). Ideally, the potential-current curve would represent the behaviour of the sample at near steady-state condition, in that the current recorded at a certain potential would be of similar value after a longer period of constant potential. However, in practice this isn't really possible because a sample that is corroding will be changing significantly with time, which means that a steady state is not feasible. Sweeping the potential also processes a changing current because of the electrode capacitance.

Before polarisation tests were performed, the free corrosion potential of the system was logged using a PicoLog ADC-16 connected to a PC using the Pico Technology data acquisition software. These produced potential versus time plots which showed how the alloy's corrosion potential changed after immersion into the aggressive ion test solution.

The rest potential was recorded each time before a sample was polarised. Polarisation curves were then performed starting from the rest potential using the ACM Instruments AutoTafel potentiostat connected to a PC with AutoTafel software. It was important to start polarisation tests from the rest potential so that a more accurate anodic or cathodic curve for the immersed sample can be taken. For example, when measuring the anodic curve of the alloy, starting below the corrosion potential, E_{corr}, will initially drive the cathodic half reaction, e.g. oxygen reduction, before the anodic reactions. This would affect the pitting potential of the alloy, as cathodically polarising the sample before anodic polarisation could raise the local pH, thicken the passive

film across the alloy surface and therefore increase the passive region of the alloy - raising the pitting potential.

Potential sweeps were performed at a rate of 10mV/min. The potentiodynamic nature of the experiment means that the system will never be in a steady state condition, however, the lower scan rate will hope to achieve a quasi-potentiostatic system, i.e. a electrochemical system that is not under a large potential bias that could alter the behaviour of the metal.

Polarisation curves were plotted as potential versus log current density. A schematic anodic polarisation curve of a pitting metal is shown in figure 2.3 below.

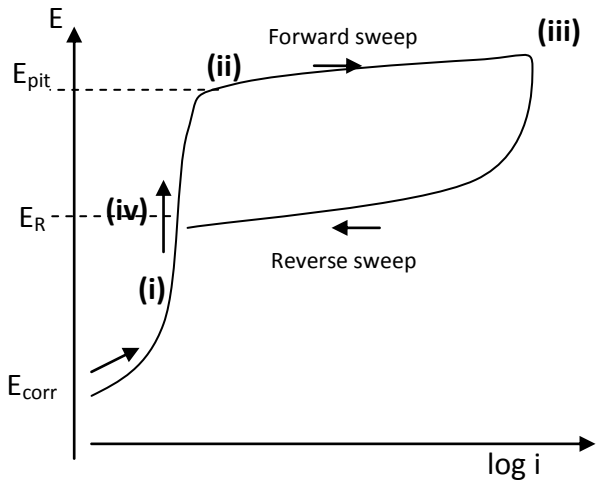

Figure 2.3 – (i) voltage sweep from free corrosion potential, E_{corr}, enters passive region as potential is increased; (ii) sample reaches pitting potential and current density starts in increase dramatically; (iii) potential sweep is reversed; (iv) some samples will have the ability to repassivate, otherwise the downwards sweep will bring the sample through to cathodic polarisation

2.3.2 Electrochemical Impedance Spectroscopy

Impedance is equivalent to direct current (DC) resistance for an alternating current (AC), and is the complex resistance exhibited when current flows through a circuit composed of resistors, capacitors or inductors or a combination of these. When it is measured as a function of the frequency of an AC source, the technique is known as Electrochemical Impedance Spectroscopy (EIS). EIS uses a small sinusoidal signal that reveals a system's resistance, i.e. impedance, and because of small signals, the non-linear response of an electrode can be regarded as linear. These small signals are also commonly regarded to be non-destructive for the metal-solution interface and thus allows for extended investigation as well as introducing the possibility to study intact paint coatings, with low conductivity.

Electrochemical impedance measurements were made using a Gill AC Potentiostat with the standard three electrode cell configurations found in figure 2.1 and 2.2. The typical frequency range measured was from 30kHz to 0.1Hz, with an amplitude of 10mV and 25 readings per test. A few tests were taken down to a lower frequency (>0.01Hz), although lower frequency data points require a longer recording time and concerns arose regarding the possible electrochemical changes of the sample when held potentiostatically for extended periods of time. This is because the corrosion potential of a metal naturally fluctuates in solution and by keeping the potential static, it is possible that pitting events can lead to accelerated corrosion. EIS data can be analysed roughly using the 'Circle Fit' program within the ACM software. More accurate analyses were made using the ZSimpWin 3.22 to perform regression fitting of the component values from pre-selected equivalent electrical circuit models.

2.3.2.1 Data Representation and Equivalent Electrical Circuits

The most common approach in interpreting EIS measurements is by using electrical equivalent circuits that have similar electrical characteristics to the sample to model the behaviour.

The table below shows how the impedance of individual circuit elements can be expressed as real or imaginary numbers.

Circuit Element	Current – Voltage	Impedance	Phase Shift φ
Resistor	E = I R	Z = R	0
Capacitor	I = C dE/dt	Z = 1/(jωc)	-90°
Inductor	E = L dI/dt	Z = jωL	+90°

For a parallel-plate capacitor, the capacitor C is proportional to the dielectric constant and inversely proportional to the thickness of the dielectric layer d:

$C = \varepsilon_0 \varepsilon_r A/d$

where ε_0 and ε_r are the permittivity of free space and relative permittivity of the dielectric, and A is the test surface area

A Constant Phase Element (CPE) is used to model non-ideal capacitors where

$Z = (\frac{1}{j\omega c})^{\alpha}$

where α is an exponent from 0 to 1. When α = 1, it describes an ideal capacitor and when α = 0.5, it describes a Warburg element (when semi-infinite linear diffusion is occurring). A non-ideal capacitor has a α value between 0.5 and 1, usually closer to 1.

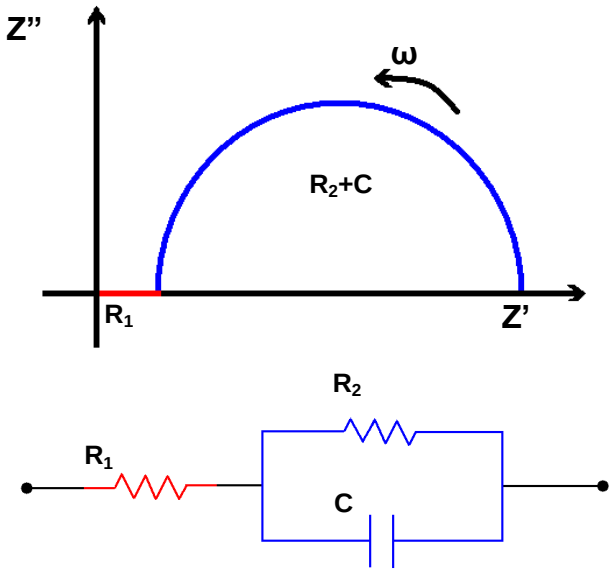

Figure 2.4 – Nyquist plot and Randles equivalent circuit

The Nyquist plot, also known as a Cole-Cole plot or a complex impedance plane plot, as shown in figure 2.4, plots the frequency response in the complex plane of a system on axes of the real and imaginary components of impedance, Z. This plot is often used to compare with a simple equivalent circuit, known as the Randles equivalent circuit, so that impedance responses can be associated with electrical behaviour. The Randles circuit consists of three components: R1 is the solution resistance, R2 is the polarisation resistance and C is the double-layer capacitance of the metal solution interface. Resistive and capacitive components in parallel are used to represent a time constant response, such as interfacial charge transfer, and appear as a semicircle in a Nyquist plot. Real systems often involve more than one semicircle and other contributing components.

Another form of data representation is the Bode plot. The Bode plot shows the frequency-dependent behaviour for the electrochemical system. This means that the frequency break points associated with each rate-determining step in the electrochemical process can be easily

distinguished. For a Randles circuit, as seen in figure 8, a resistor would produce a horizontal line on the amplitude plot and a constant phase of zero on the phase plot. The RC parallel combination produces a gradient of -1 as the frequency increases (as the amplitude of the impedance is $1/(2\pi fC)$, where f is the frequency and C the capacitance). A schematic representation for Bode plot analysis is shown in figure 2.5 below:

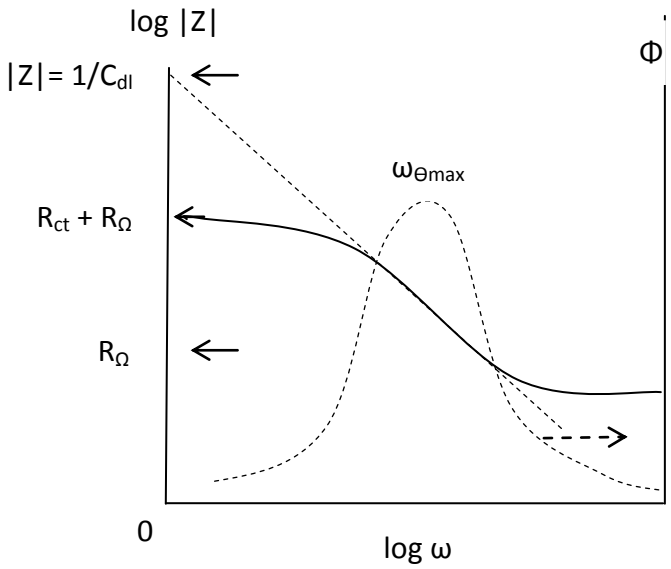

Figure 2.5: Representative Bode plot for simple electrochemical system[6]

For an intact coating system, a second parallel resistor and capacitor combination needs to be added, with the resistor corresponding to the resistance to ionic current passing through the paint and the capacitor corresponding to the capacitance of the paint film (acting as the dielectric in a parallel-plate capacitor).

For a system with a defect, it is expected that the current will mainly flow through the defect and largely 'ignore' the paint film (with a much smaller flow though). However, aluminium also forms an oxide layer which will also affect the impedance response. It should be noted that it is

good practice to derive an equivalent circuit first based on possible physical processes and later modify the circuit to fit the features of the impedance data.

The proposed equivalent electrical circuit for the system in this project is shown below:

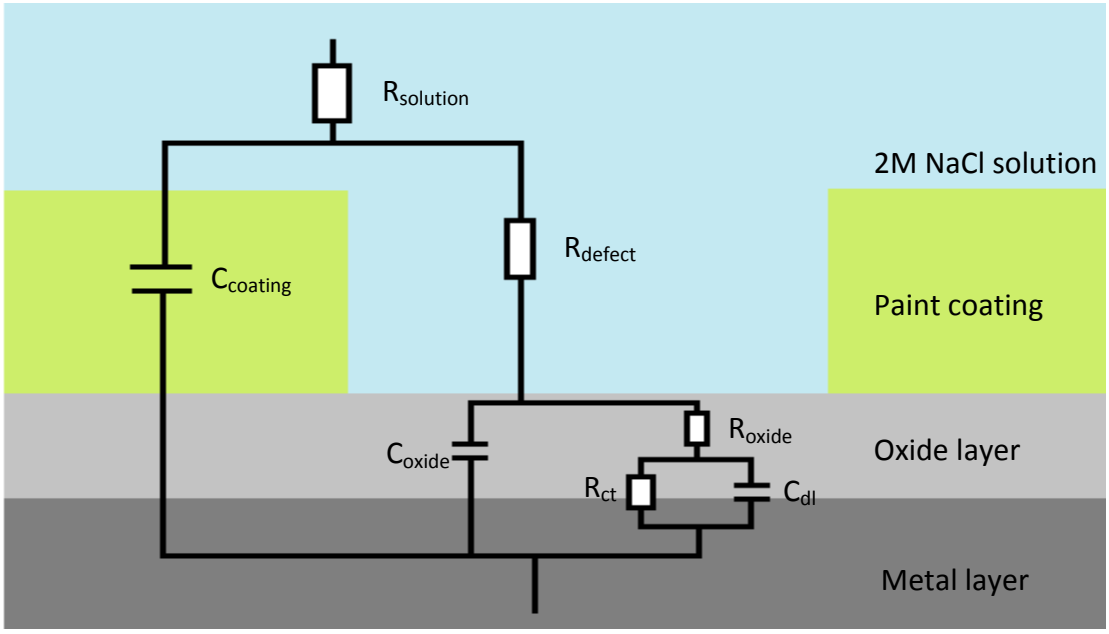

Figure 2.5: Schematic of model circuit of system under investigation

In practice, it was often difficult to accurately fit impedance data. If elements have a similar time constant, electrical responses overlap with each other and the exact number of contributing elements cannot be determined. On a Nyquist plot, a simple Randles circuit would show a perfect semicircle (for an ideal capacitor), but if there were more elements with similar time constants in the circuit, the semicircle will appear horizontally elongated. Figure 2.5 shows a model circuit for the system under investigation. It is expected that the current will mainly flow through the defect in the coating and subsequently through any defects in the oxide layer.

2.3.3 Electrochemical Noise Analysis

Research in electrochemical noise (ECN) has increased substantially in recent years and ECN is now widely used by engineers in monitoring of corrosion-susceptible systems. Electrochemical noise monitors the naturally occurring potential or current fluctuations of a system (without any external bias), and can pick up stochastic events that can be generated by a number of different processes, such as metal dissolution, pit initiation, gaseous evolutions or paint film cracking. Potential noise records sample potential against a reference electrode and current noise is recorded between two identical samples.

Electrochemical noise measurements were also made using a Gill AC Potentiostat with a three electrode cell, two working electrodes and one standard calomel electrode. A defect was made in the coating on both samples and the coating edges were sealed with beeswax/colophony. The small volume electrochemical cell was placed on top between the two samples over both defects. Recordings were taken every 0.5 seconds for a period of 30 minutes every 6 hours for the first 24 hours, then every 12 hours for up to one week.

2.3.4 UV-Visible Spectroscopy

Ultraviolet-Visible Spectroscopy (UV/VIS) makes measurements of light absorption of specified wavelengths by comparing a sample against a reference solution. UV/VIS can be used to perform quantitative analysis on solutions containing transition metal ions and highly conjugated organic compounds. The technique is based upon the Beer-Lambert law that states that '*the absorbance of a solution is directly proportional to the concentration of the absorbing species in the solution and the path length',* so for a given path length, UV/VIS can determine the concentration of absorbing species in a solution.

$$A = \alpha l \qquad [2.1]$$

where A is absorbance, α is the absorption coefficient and l is the path length.

A range of different wavelengths of light is directed through a cell containing the solution and then passes through another reference cell without the absorbing species under investigation, before reaching a detector. Species are characterised by the wavelengths at which absorption occurs, and the collected data is then compared against a standard with known concentrations and the concentration of the investigated species can then be calculated. Chromate species absorb light at a wavelength of approximately 374nm, so a as the light passes through, a peak on the absorbance versus wavelength graph will be observed.

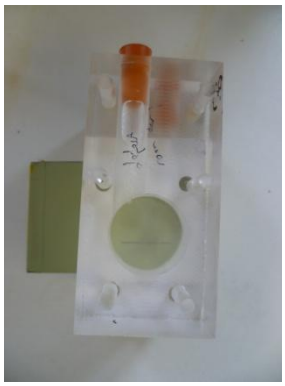

Figure 2.6 – Photograph of cell used for paint immersion

Pigment release was measured by clamping a coated panel to a cell with a known area of the coating is in contact with a fixed volume of the test solution (20cm^3), 2M sodium chloride solution. Fully intact coatings and coatings with defects were tested at room temperature and 30°C. A JASCO V-570 UV-VIS-NIS spectrophotometer was used to perform tests, where a glass pipette was used to transfer a sample of the test solution from the cell to a cuvette. The second cuvette is used as a reference and filled with 2M NaCl solution. After testing, as much of the sample solution is returned to the cell as possible by pipette. Tests were performed at regular intervals over the course of a week.

2.3.5 Scanning Acoustic Microscopy

The scanning acoustic microscope (SAM) directs focused sound from a transducer unto the surface of the material under investigation. The sample is immersed in water as a medium to transmit the sound waves, and on striking the surface of the coated sample, the waves are absorbed, reflected, transmitted or scattered. A SAM graph is then generated by processing the collected sound reflections. The SAM technique has not been widely used in corrosion studies, but has been used as a complementary method to electrochemical impedance spectroscopy to provide insight into processes at the metal-coating interface[76]. It has been effectively utilised alongside techniques such as the scanning Kelvin probe (SKP) to reveal coating deterioration or the onset of corrosion[77], where Reddy. Doherty and Sykes combined SAM and SKP to detect coating disbonding and blistering underneath optically opaque organic coatings and to track the anodic and cathodic behaviour of the sample[78]. They could reveal the development of blisters and the relocations of the anode and later on, Sykes and Doherty included electrochemical impedance spectroscopy to provide polarisation resistance values of the corroding sample against the SKP and SAM data[78].

Figure 2.7 shows SAM A-scans and C-scans, explained below, from a $Ce(dpp)_3$ Epigen coated AA2024-T3 panel from experiments and will be analysed and discussed later in chapter 6.

An A-scan shows the amplitude of a reflected signal as a function of time on one particular point of the sample. The signal can be interpreted to identify the different mediums (e.g. water, coating, pigment or metal) across the sample depth and an example is shown in figure 2.7b. Peaks correspond to reflections from particular interfaces. When the waves travel from slower medium to a faster medium, e.g. from water to the epoxy coating, or from the coating to the metal, the amplitude of the sinusoidal wave goes from positive to negative and the wave would be inverted when the media are reversed, i.e. travelling from a faster medium to a slower medium.

From figure 2.7b, it can be seen that there are two major 1.5 sine waves, going from a slower medium to a faster medium. This is interpreted as the sound waves travelling between the water/coating interface for the first sine wave and between the coating/metal interface for the second. The smaller inflections within the sinusoidal waves are likely from inhomogeneities within the coating or substrate, but at distances too close for the SAM to separate.

A C-scan is created by setting the gate width from an A-scan, i.e. the time parameters at which reflected signals/peaks are collected (depicted by the bold red horizontal line on the A-scan), and then combining the signals across the surface area to form an image of the sample at the set depth.

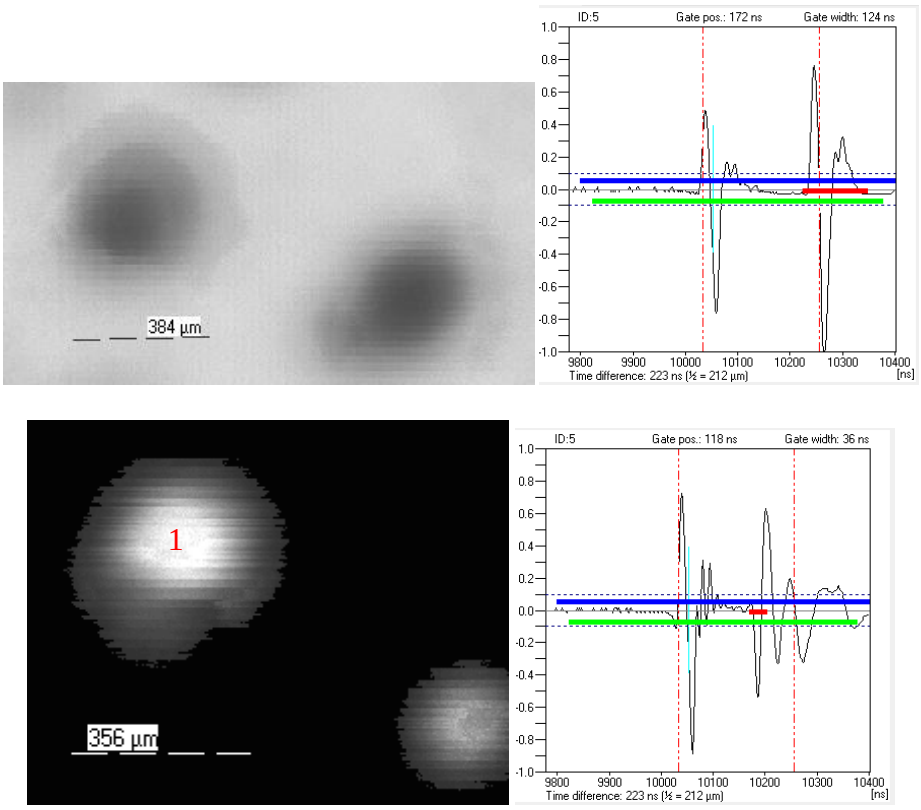

Figures 2.7 a-d – a) C-scan of $Ce(dpp)_3$ coating , gate set at centre of image at coating-metal interface, b) A-scan of image 2.7a, c) C-scan of image 2.7a, gate set at point 1 (in red), e) A-scan of image 2.7d

SAM images were taken using an 80MHz transducer and the A-scans of a sample, shown in figure 2.7b and d, are used to set the gate width for the associated C-scans. The red, dashed vertical lines on the A-scans are line markers which help indicate the time differences between peaks. It should be noted that the times include the passages of waves both in and out of the material, so a time difference that states 200ns would be 100ns one-way.

SAM images were taken on tested and untested coated samples to investigate the coating and coating/metal interface.

2.3.6 Optical Microscopy and MicroXAM

Some surface microscopy was performed on untested and EIS tested coatings using a Zeiss Axioskop 2 MAT optical microscope with an Axiocam digital colour camera. The $Ce(dpp)_3$ Epigen coated panels were also cut and mounted to examine the cross-section. Acrylic resin, ClaroFast Struers, was used in a Struers LaboPress-3 at 180°C for 9 minutes, followed by a 6 minute cooling period. The mounted samples were then ground with silicon carbide papers of 1600 and 3200 grades followed by polishing with 3 micron and then 1micron diamond solution.

MicroXAM is a non-contact phase shift profiler used to map the surface/topography of a coating. The device is placed under the lens and the phase-shift lines found. The magnification is then increased and an image is taken between the phase-shift lines. Position of lens is adjusted between measurements to achieve maximum contrast and detail. The lens is higher when measuring contact thickness and morphology, but lower when measuring polymer contact and morphology.

Chapter 3 Corrosion Behaviour of Bare AA2024-T3

3.1 Introduction

A brief study to characterise the corrosion behaviour of bare AA2024-T3 using direct current polarisation techniques and electrochemical impedance spectroscopy is described in this chapter. By better understanding the uncoated system, the innate corrosion resistance of the alloy and the effects of inhibitive species can be determined as a baseline for comparison with coated system and at defects in coatings, so that the protection provided by coatings can be clearly identified.

Figure 3.1 shows multiple polarisation curves of AA2024-T3 in 0.5M sodium chloride solution, tested after one day of immersion. It can be seen that the alloy sits at a rest potential below the pitting potential, -680mV, -750mV and -780mV for the blue, red and green curves respectively. The pitting potential for all three tests lie at a similar value of approximately -600mV, which means that in 0.5M NaCl solution, a passive region of 80 to 180mV can be exhibited in the aluminium alloy.

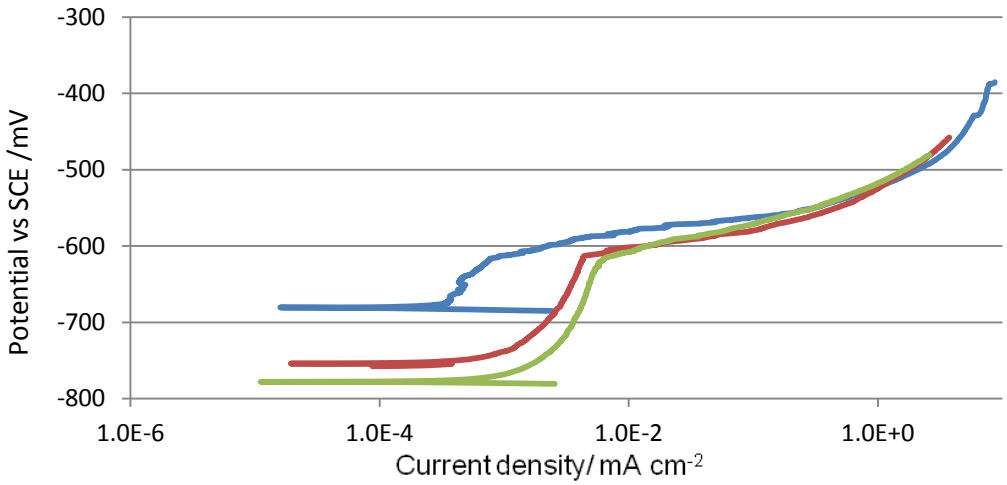

Figure 3.1 – DC Polarisation curves of AA2024-T3 in 0.5M NaCl solution

Most experiments in this project were performed in 2M sodium chloride solution, which is higher than typical testing condition, e.g. salt spray tests. The reason behind this is to ensure breakdown of the unprotected aluminium alloy in chloride conditions so that the protection of chromate inhibitors can be more clearly identified.

3.2 Effect of Strontium Chromate in Aggressive Solution

Before each electrochemical test was performed, the sample was immersed in 2M sodium chloride solution and the free corrosion potential was monitored. It was observed that the free corrosion potential, E_{corr}, of the system changes randomly with no general trend observed. To allow electrochemical stabilisation of the alloy after immersion into the test solution, the samples were immersed for 24 hours before the polarisation tests were started.

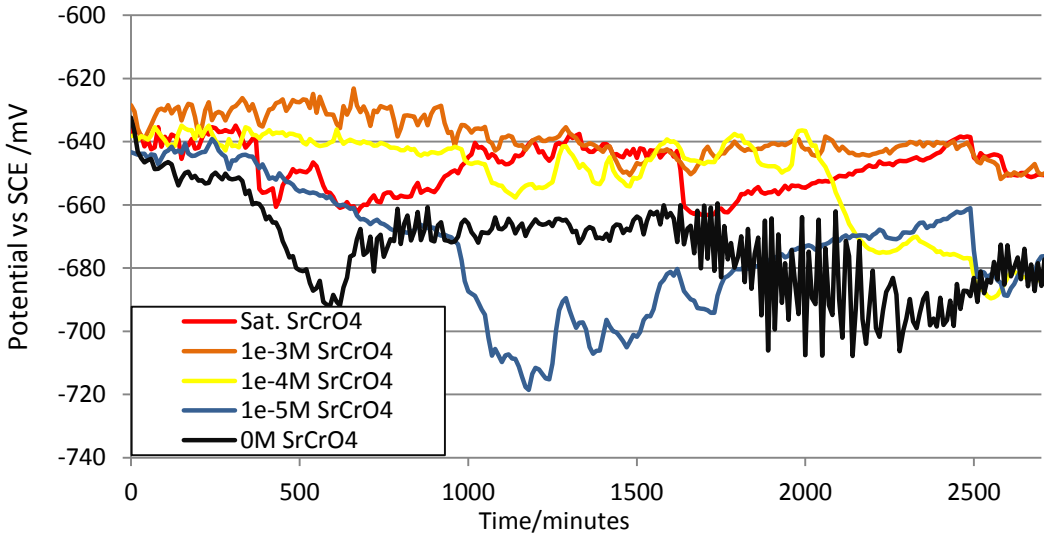

Figure 3.2 – Free corrosion potential of AA2024-T3 in 2M NaCl w/ varying concentrations of $SrCrO_4$

Figure 3.2 shows the free corrosion potential against time graph for the samples before the direct current polarisation tests were performed. It can be seen that for a system without strontium chromate, shown by the black line, the free corrosion potential became a lot noisier

after 1500 minutes. The free corrosion potential was slowly decreasing, but with potential jumps of ~50mV, between -660mV and -710mV. This is more likely to be due to metastable pitting events occurring, with pitting corrosion and passivation of pits continuously taking place[17]. After 40 hours of immersion, the free corrosion potential of the AA2024-T3 sample without strontium chromate drops from an initial value of -632mV to -680mV. For experiments with solutions containing strontium chromate, the free corrosion potential behaved differently. The general trend is that the higher the concentration of strontium chromate, the higher the free corrosion potential. High concentrations of strontium chromate, $1x10^{-3}$M and a saturated solution indicated by the orange and red lines, show free corrosion potentials starting at around -630mV and after 2500 minutes, the AA2024-T3 sample in $1x10^{-3}$M strontium chromate and the sample in a saturated solution have a free corrosion potential of approximately -650mV. The free corrosion potentials of the alloy in $1x10^{-4}$M and $1x10^{-5}$M strontium chromate after 40 hours of immersion were both approximately -680mV.

It can be seen that the free corrosion potential of the alloy fluctuates over time and there are general patterns of higher free corrosion potentials with increasing concentrations of strontium chromate. However, even after 40 hours, no consistent reproducible condition was attained and an arbitrary choice of 24 hours pre-exposure was made.

3.2.1 Strontium Chromate Concentration versus Pitting Potential

Direct current polarisation tests were first performed in the large volume test cell. The samples were anodically polarised from the rest potential at a sweep rate of 10mVmin^{-1} described in section 2.3.

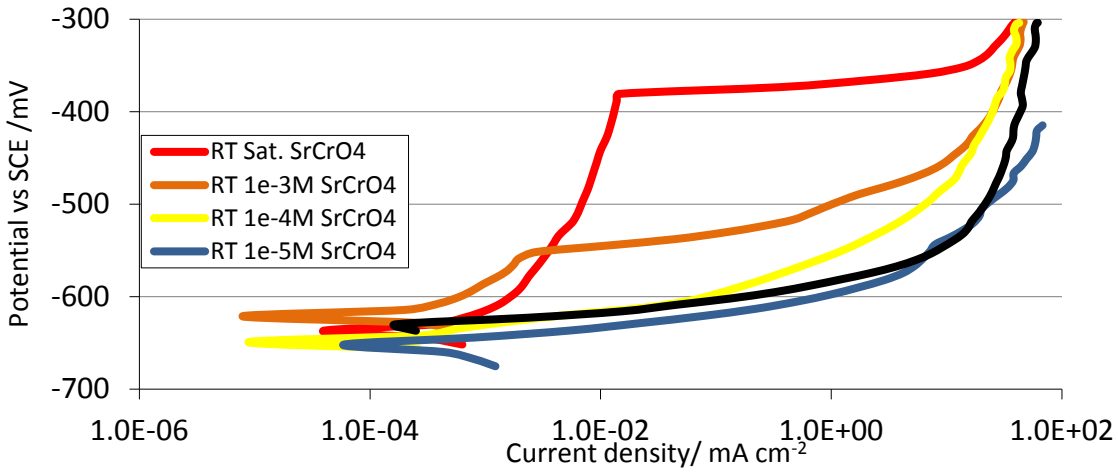

Figure 3.3 – DC Polarisation curves of AA2024-T3 in 2M NaCl solution

Figure 3.3 shows the curves for AA2024-T3 tested in 2M sodium chloride with varying concentrations of strontium chromate in solution. Localised corrosion begins once the anodic current density increases significantly, and the pitting potential is identified as the potential at which stable pits initiate. From the polarisation curves, it can be seen that for concentrations of chromate from 0M to 1x10^{-4}M when the alloy is anodically polarised, corrosion current increases steadily and the alloy is corroding. There is no passive region between the rest potential and the pitting potential. This suggests that there is little anodic inhibition from low concentrations of strontium chromate. However, when the concentration is increased to 1x10^{-3}M and higher, a clear region of passivity develops where there is little current increase with increasing potential until the onset of pitting at a higher potential. A concentration of 1x10^{-3}M strontium chromate gave the alloy a pitting potential of approximately -550mV and a saturated

solution of strontium chromate pushed the pitting potential up to approximately -380mV. If we take the rest potential of AA2024-T3 to be approximately -650mV, it means that for stable pits to occur in the high concentrations of strontium chromate, a potential barrier of 100 – 270mV must first be overcome. In high concentrations of strontium chromate, the corrosion protection is apparent at ambient temperature, but salt spray tests in industry are usually performed at an elevated temperature of 30°C, so the protective effects were investigated again at 30°C in the next section. The free corrosion potentials after 24 hours are broadly similar.

3.2.2 – Effect of Temperature and Inhibitor Concentration

A thermostatically-controlled box was set up to test the protective abilities of strontium chromate at different temperatures. Most experiments in this project were conducted at ambient temperature, which is ~20°C, but direct current polarisation experiments in this section were conducted at room temperature, 25°C and 30°C.

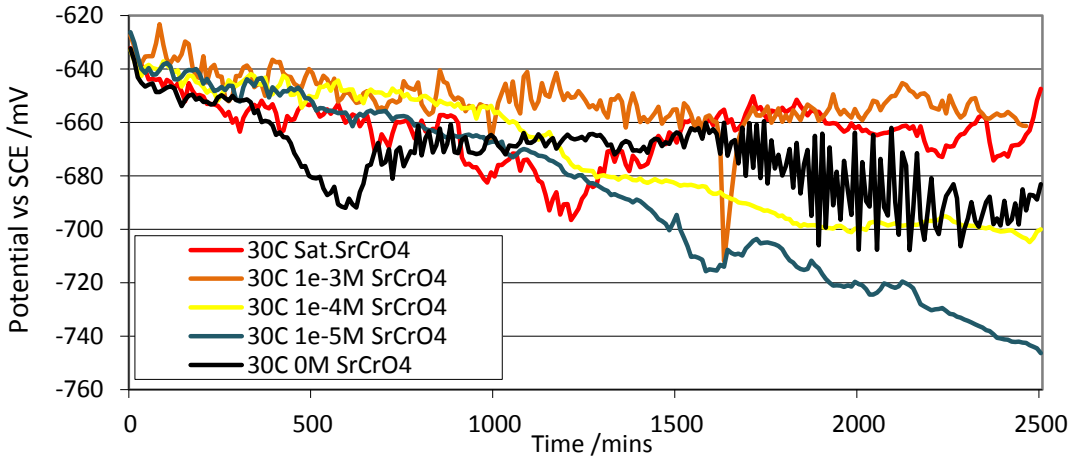

Figure 3.4 – Free corrosion potential of AA2024-T3 in 2M NaCl w/ varying concentrations of $SrCrO_4$ at 30°C

Figure 3.4 shows that the potential of AA2024-T3 started at around -630mV to -640mV, similar to the potential logs at room temperature, but as time progressed, the potential fell further. After 2500 minutes of immersion, the free corrosion potential of AA2024-T3 with no strontium

chromate dropped from an initial value of approximately -630mV to -690mV. Experiments containing strontium chromate, behaved quite similarly to the room temperature tests. The alloy tested in the lowest concentration of strontium chromate, $1x10^{-5}$M, had its potential drop over 100mV from approximately -630mV to -740mV giving the lower final temperature. Alloys immersed in higher concentrations of strontium chromate also had a potential drop. The general trend is again that with increasing concentrations of strontium chromate, the higher the free corrosion potential after immersion. The free corrosion potentials of the alloy in $1x10^{-4}$M, $1x10^{-3}$M and a saturated solution strontium chromate after 40 hours of immersion were -703mV, -661mV and -651mV respectively. Direct current polarisation tests were performed after potential logging.

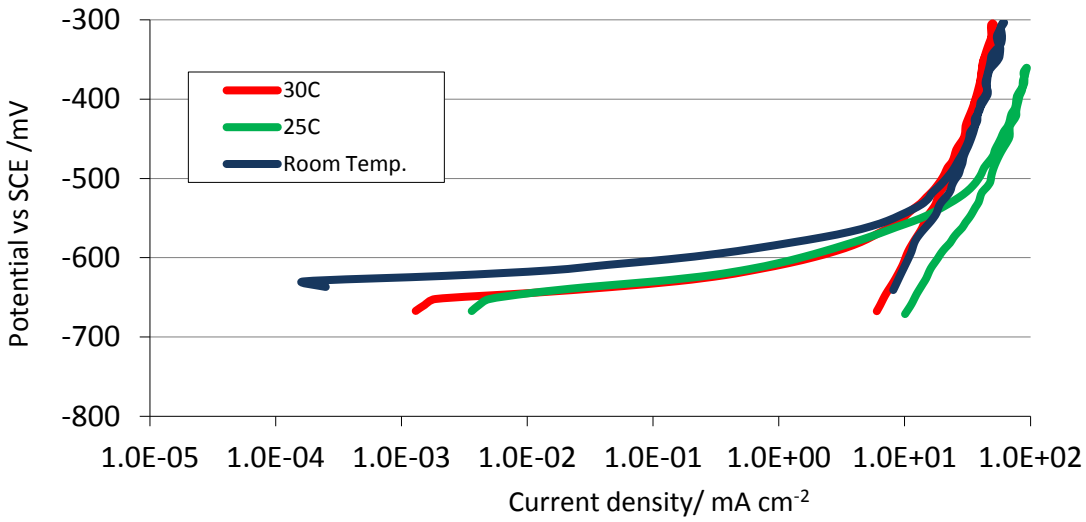

Figure 3.5 – DC Polarisation curves of Bare AA2024-T3 in 2M NaCl w/ 0M $SrCrO_4$

Figure 3.5 shows the anodic polarisation curves for AA2024-T3 in 2M sodium chloride solution performed at the three different temperatures. The rest potential for all three temperatures lies just on or slightly below the pitting potential, so that when the potential is increased, the corrosion current increases almost instantly. The rest potential for the 30°C test is

approximately -670mV, 40mV lower than the rest potential at room temperature, -630mV. The rest and pitting potentials at 25°C lie at approximately -670mV, which are both similar to the potentials recorded at 30°C. Apart from the slightly lower rest/pitting potentials of AA2024-T3 at 30°C, the anodic behaviour of the alloy without chromate remains the same. Figures 3.6 to 3.9 show the anodic polarisations of the alloy tested at different temperatures in 2M sodium chloride solution with different concentrations of strontium chromate.

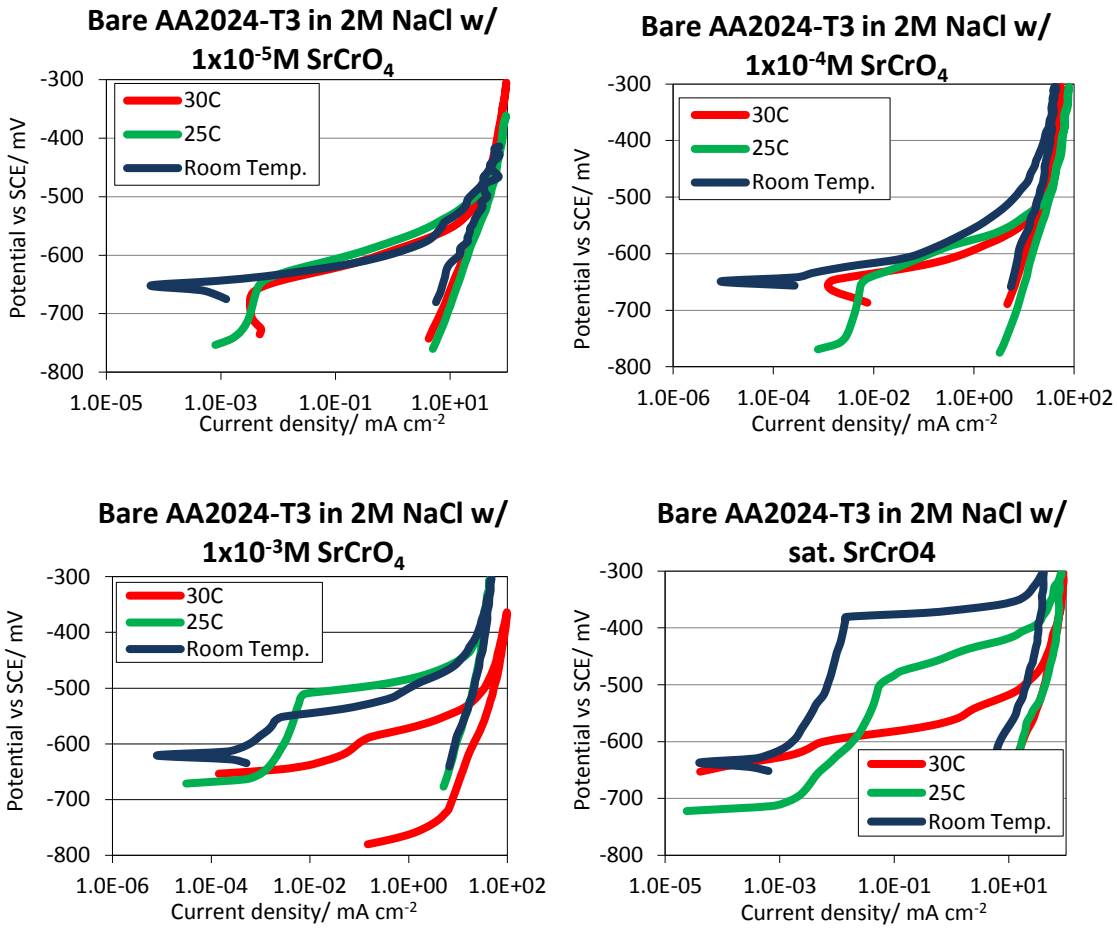

Figures 3.6-3.9 – DC Polarisation curves of AA2024-T3in 2M sodium chloride solution w/ different concentrations of strontium chromate

Moving within a relatively small temperature range of 10°C greatly affects the electrochemical behaviour of the alloy in solution. For ambient temperature experiments, the pitting potential of the alloy is only significantly affected when concentrations of strontium chromate are $1x10^{-3}$M and above. When the temperature of the experiment is raised to 30°C, the passivity that strontium chromate provides is greatly reduced, and the pitting potential lies much closer to the rest potential. However, the rest potential is also significantly affected by temperature with strontium chromate. At lower concentrations of strontium chromate, $1x10^{-4}$M and below, the rest potential of the alloy is significantly lowered to approximately -750mV at 30°C. Therefore, rather than raising the pitting potential to create a potential barrier, the rest potential of the alloy falls to create a passive region.

3.2.3 Effect of Strontium Chromate Concentration: EIS

EIS experiments were first performed in the large volume test cell, as described in section 2.4. Figures 3.11 to 3.14 show Bode plots of bare AA2024-T3 with varying concentrations of strontium chromate tested after 24 and 72 hours of immersion respectively. Figures 3.14 to 3.17 show the corresponding Nyquist plots.

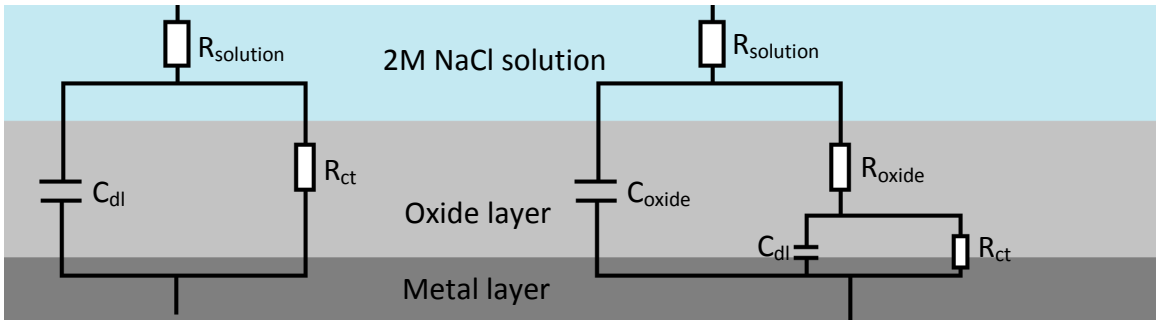

Figure 3.10 – (a) R(QR) model circuit for one time constant response, (b) R(Q(R(QR))) model circuit for two time constant response

The Nyquist plots were fitted with the ZSimpWin software to the model circuit, R(Q(R(QR))), seen in figure 3.10b, or in some cases R(QR), figure 3.10a, if two semicircles could not be clearly defined. Nyquist plots that show two semicircles for an uncoated alloy indicate that there is a passive layer that results in a second time constant. This has been observed for aluminium systems by several authors[14, 80]. The first semicircle is related to the oxide layer on the surface of the alloy, where R_{oxide} and C_{oxide} are the resistance and capacitance of the oxide. The second semicircle can be defined as the charge transfer resistance, R_{ct}, and double layer capacitance, C_{dl}, of the anode and cathode sites, which are related to corrosion processes. Calculated parameters from equivalent circuit fits are presented in table 3.1.

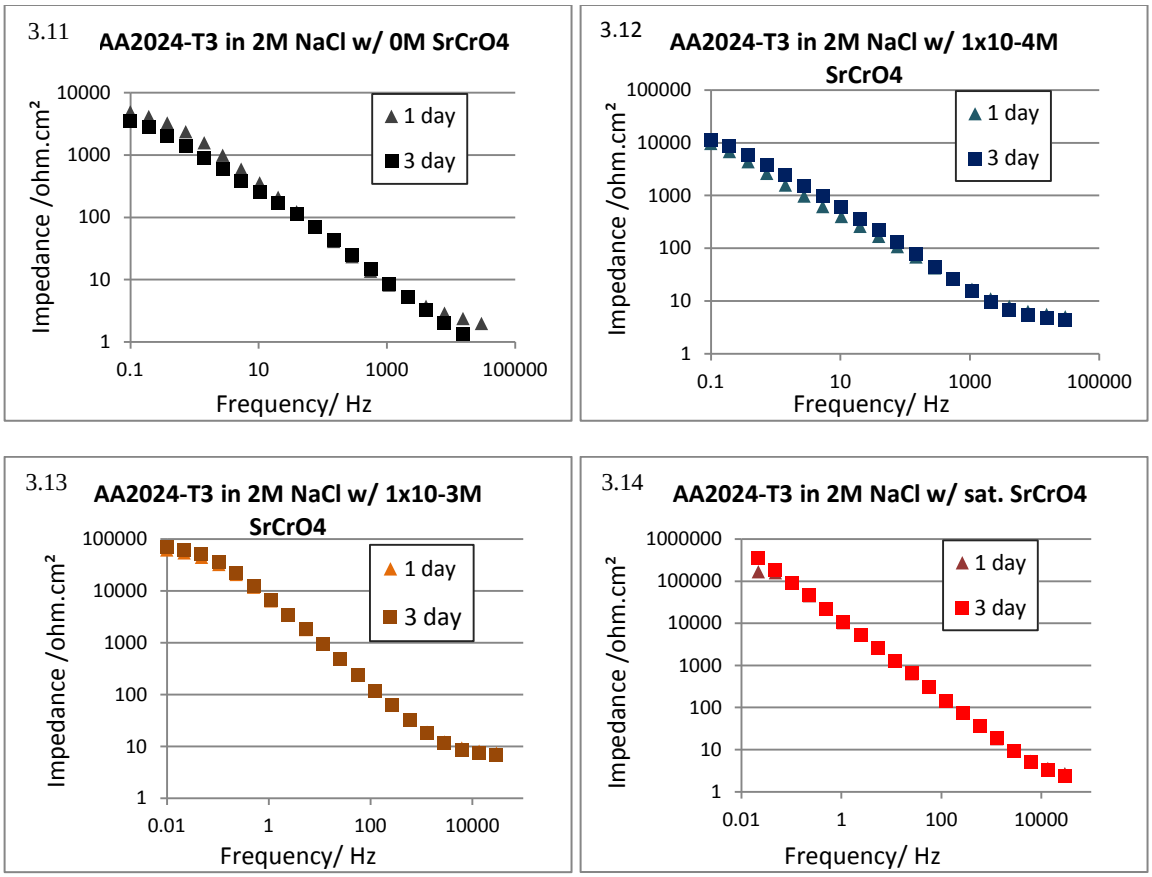

Figure 3.11 – 3.14 – Bode plots after 24hours and 72hours of immersion respectively

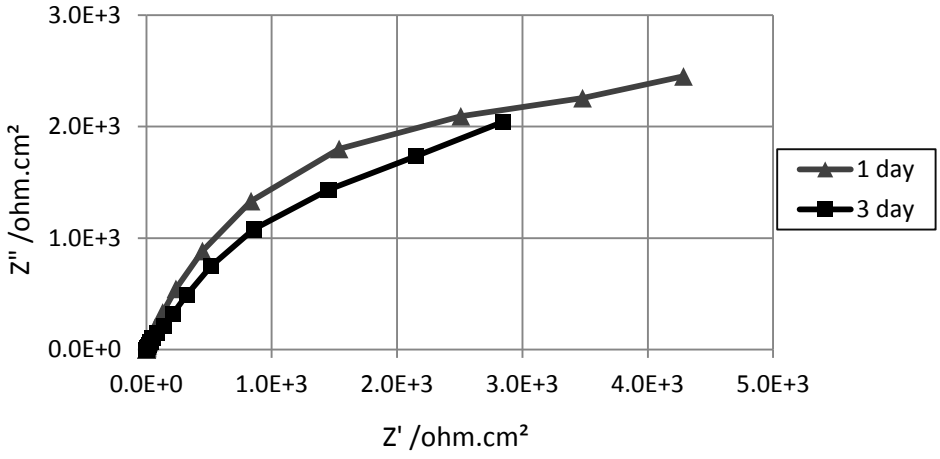

Figure 3.15 – Nyquist plots of AA2024-T3 in 2M NaCl w/ 0M $SrCrO_4$ after 24hours and 72hours of immersion respectively

From figure 3.15, we see that the size of the semicircles of the Nyquist plot decreases slightly between the 1 day and 3 day measurement. The calculated model circuit parameters show that the charge transfer resistance, in fact, does decrease with time as well as the double layer capacitance. This suggests that the system is suffering an increased level of corrosion attack. The Bode plot, shown in figure 3.11, reveals that the low frequency impedance of the system decreases only slightly with time as protection from the oxide becomes less effective. However, the response from the oxide film is not apparent in these results, possibly being short-circuited at the corrosion sites.

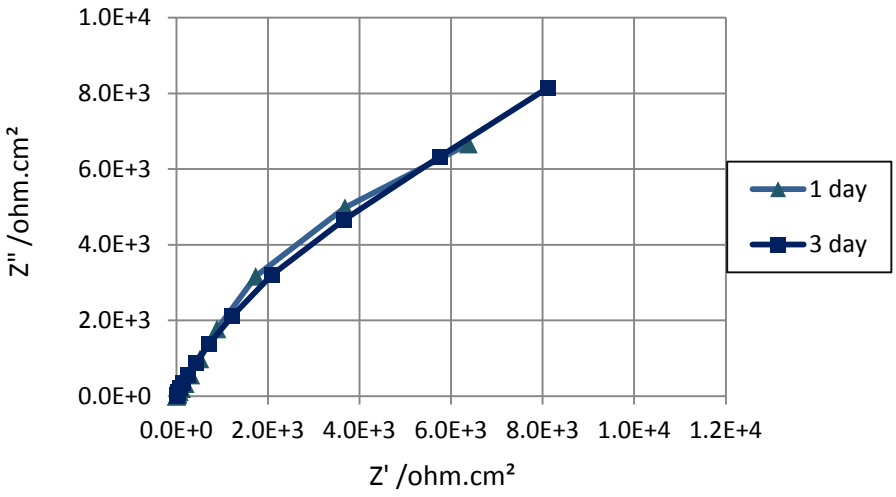

Figure 3.16 – Nyquist plot AA2024-T3 in 2M NaCl w/ $1x10^{-4}$M $SrCrO_4$ after 24hours and 72hours of immersion respectively

The Bode plot and Nyquist plots in figure 3.12 and 3.16 reveal however that even with only $1x10^{-4}$M strontium chromate added into 2M sodium chloride solution, the lower frequency behaviour shows an increase in impedance over time rather than a decrease. Calculated model circuit parameters, seen in table 3.1, show that the charge transfer resistance increased from $2.33x10^4$ to $7.21x10^4 \Omega cm^2$.

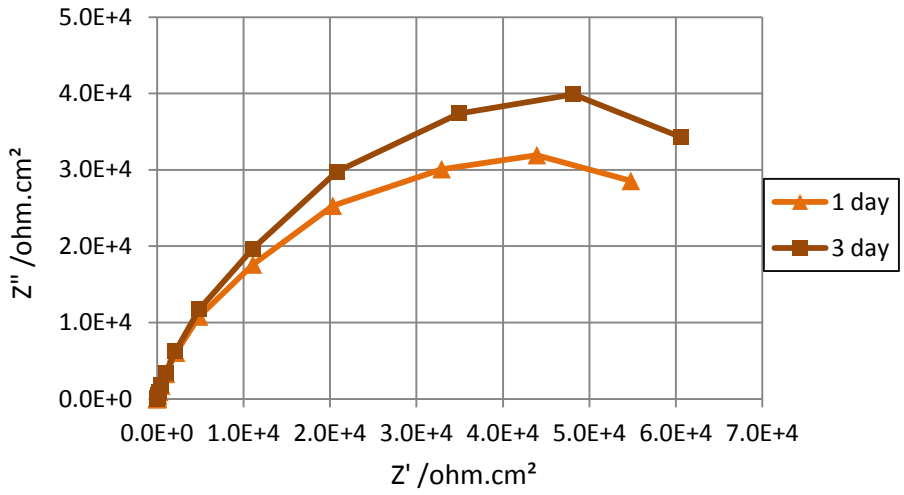

Figure 3.17 – Nyquist plot AA2024-T3 in 2M NaCl w/ $1x10^{-3}$M $SrCrO_4$ after 24hours and 72hours of immersion respectively

Figure 3.13 and 3.17 show the Bode and Nyquist plots for AA2024-T3 immersed in 2M sodium chloride solution with $1x10^{-3}$M strontium chromate. Little difference can be seen between the two curves on the Bode plot, although the Nyquist plot shows that with longer immersion, the size of the semicircle increases. Fitting program, ZSimpWin, could not easily identify two time constants from the data so a simpler R(QR) model circuit was used. The parameters are shown in table 3.1. The total resistance of the R(QR) circuit, increased from $7.36x10^4$ to $8.94x10^4 \Omega cm^2$.

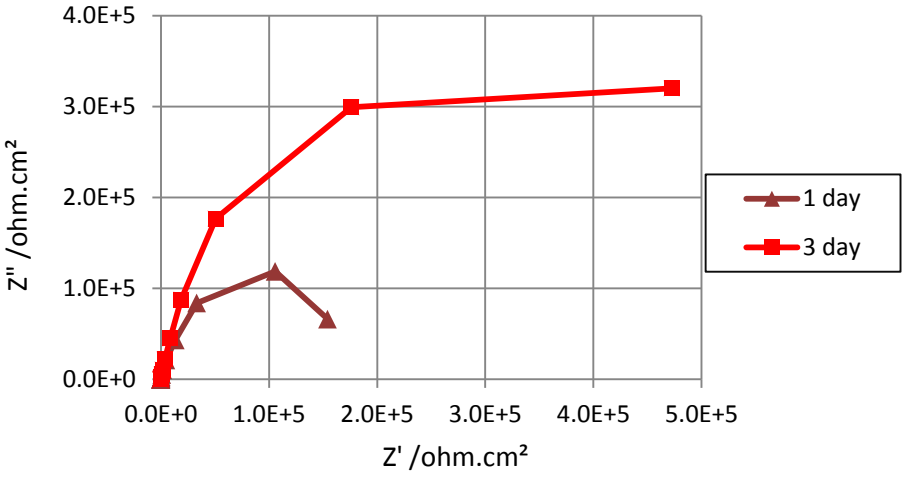

Figure 3.18 – Nyquist plot AA2024-T3 in 2M NaCl w/ sat. $SrCrO_4$ after 24hours and 72hours of immersion respectively

Figure 3.14 and 3.18 show the Bode and Nyquist plots for AA2024-T3 immersed in2M sodium chloride solution with saturated strontium chromate. Similar to the test in $1x10^{-3}$M strontium chromate, little change with time is seen between the two curves on the Bode plot, except in the lower frequency measurements. This suggests that the main change over time is related to the charge transfer processes between the anode and cathode. The Nyquist plot exhibits a more obvious change in the size of the semicircle in the lower frequency measurements. After three days, the size of the semicircle increases significantly although the last data point for the 3 day fit extends out further beyond the first semicircle. The simpler R(QR) model circuit was also used to fit the data. The parameters are shown in table 3.1. The total resistance increased from $3.14x10^5$ to $8.51x10^5 \Omega cm^2$.

Time (hrs)	Equivalent Circuit Model	$SrCrO_4$ Concentration (M)	CPE ($x10^{-5}$ $S \cdot s^{-n} cm^{-2}$) C_{oxide}	Freq. Power (n)	Resistance (Ωcm^2) $R_{oxide/ct}$	CPE ($x10^{-5}$ $S \cdot s^{-n} cm^{-2}$) C_{dl}	Freq. Power (n)	Resistance ($x10^4$ Ωcm^2) R_{ct}	Chi-squared ($x10^{-3}$)
24	R(Q(R(QR)))	0	9.3	0.82	5400	90.5	0.90	0.8	7.7
24	R(Q(R(QR)))	$1x10^{-4}$	0.04	1	4.8	1.3	0.71	5.7	7.4
24	R(QR)	$1x10^{-3}$	-	-	-	3.2	0.84	7.4	18.1
24	R(QR)	$6.3x10^{-3}$	-	-	-	1.6	0.91	31.4	8.0
72	R(Q(R(QR)))	0	7.9	0.83	330	17.0	0.65	0.6	21.4
72	R(Q(R(QR)))	$1x10^{-4}$	5.7	0.80	5000	7.1	0.44	7.2	17.4
72	R(QR)	$1x10^{-3}$	-	-	-	3.0	0.85	8.9	19.9
72	R(QR)	$6.3x10^{-3}$	-	-	-	1.6	0.91	85.1	8.3

Table 3.1 – Parameters of fitted Nyquist plots for AA2024-T3 in 2M sodium chloride solution

From table 3.1, it is noticed that the capacitance of the first semicircle for the $1x10^{-4}$M strontium chromate test, highlighted in red, was significantly smaller than the other capacitances calculated. This could indicate that the active area was much smaller from C_{dl}, or the oxide layer

was much thicker, from C_{oxide}. However, after 72 hours, the capacitance became comparable with the calculated values of other samples.

The resistances highlighted in green on table 3.1 were taken to be the charge transfer resistances and figure 3.18 shows the plotted resistances against time. It can be seen that with increasing concentrations of strontium chromate, charge transfer resistances also increase. The experiments with strontium chromate added have resistances increasing with time, but the experiment with no added strontium chromate exhibits a small decrease in resistance over time.

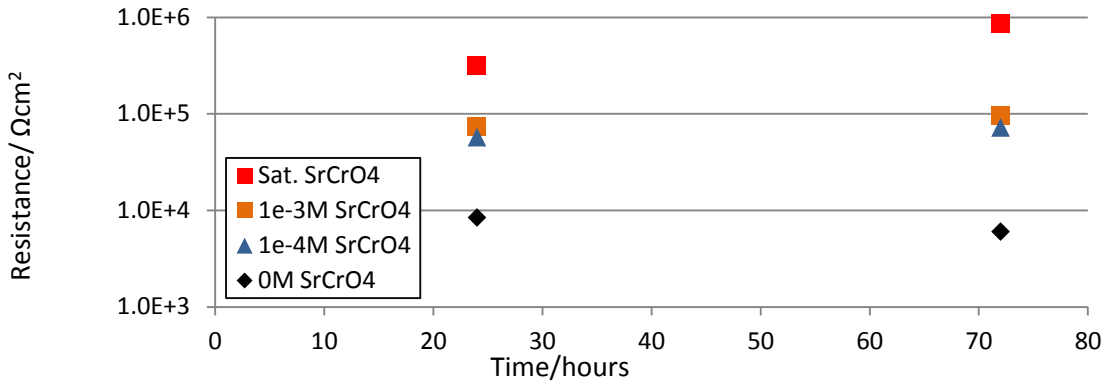

Figure 3.19 – EIS-calculated charge transfer resistance against time for varying concentrations of strontium chromate in 2M sodium chloride solution

The increase in resistance with increasing concentrations of strontium chromate indicates that the rate of corrosion decreases with increasing levels of chromate and extended immersion. It is likely that when aluminium oxide layer is penetrated by the pitting events, the chromate (VI) ions are reduced to chromate (III) to form an oxide Al-Cr complex on the surface of the alloy[24]. Anodic attack of aluminium within the pits, i.e. metal dissolution, leads to faster reduction of Cr(VI) ions. If the reduction of chromate can inhibit anodic or cathodic corrosion reactions, then the charge transfer resistance will fall. The decrease in charge transfer resistance with time for the system with no strontium chromate indicates that the rate of corrosion has increased.

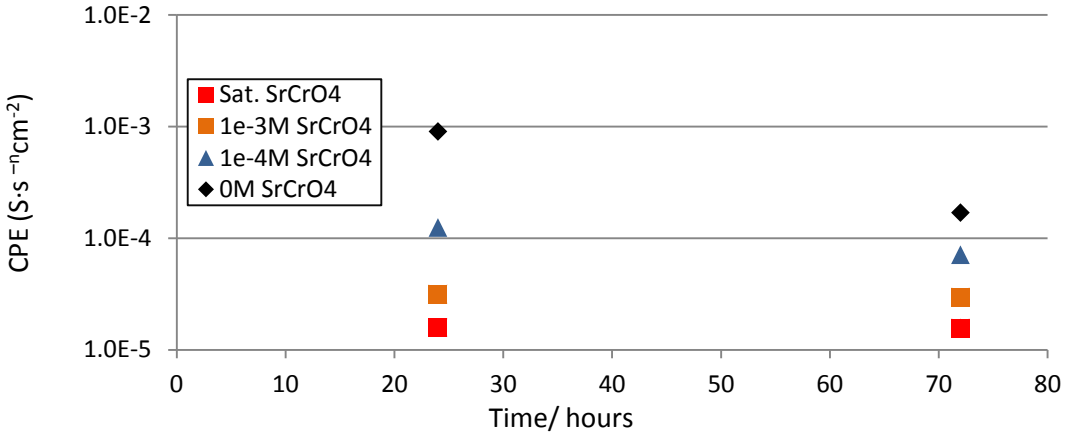

Figure 3.20 – EIS-calculated double layer capacitance against time for varying concentrations of strontium chromate in 2M sodium chloride solution

The CPEs highlighted in blue on table 3.1 were taken to be the double layer capacitances and figure 3.19 shows the plotted capacitances against time. It can be seen that with increasing concentrations of strontium chromate, double layer capacitances decrease. The double layer capacitance values are related to the active area of the anode and cathode sites, and a larger value indicates a larger active area. Therefore, for higher concentrations of strontium chromate, the active areas of the electrode sites become smaller.

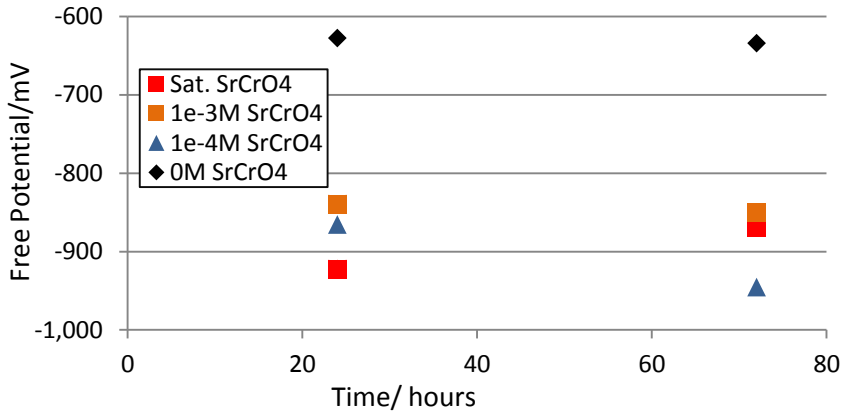

Figure 3.21 – Free corrosion potential against time for varying concentrations of strontium chromate in 2M sodium chloride solution (measured before EIS tests)

Figure 3.21 shows free corrosion potential behaviour significantly different to the free corrosion potential logs in section 3.2, but by combining the potential data with the EIS calculated resistances, we can explain the potential behaviour of the alloy. The test with no chromate shows the alloy sitting close to the pitting potential as expected, and after 72 hours falls slightly. Experiments with additions of chromate exhibit free corrosion potentials that have decreased significantly away from the pitting potential (of approximately -630mV) in the region of -850 to -950mV.

As seen in the polarisation curves in section 3.2.2, the addition of chromate inhibitive species can lower the free corrosion potential of the system to create a passive region (potential barrier), although the lowering of potential can also be the result of the breakdown of passivity. The schematic Tafel plots in figure 3.22 will explain the two situations of a decreasing potential:

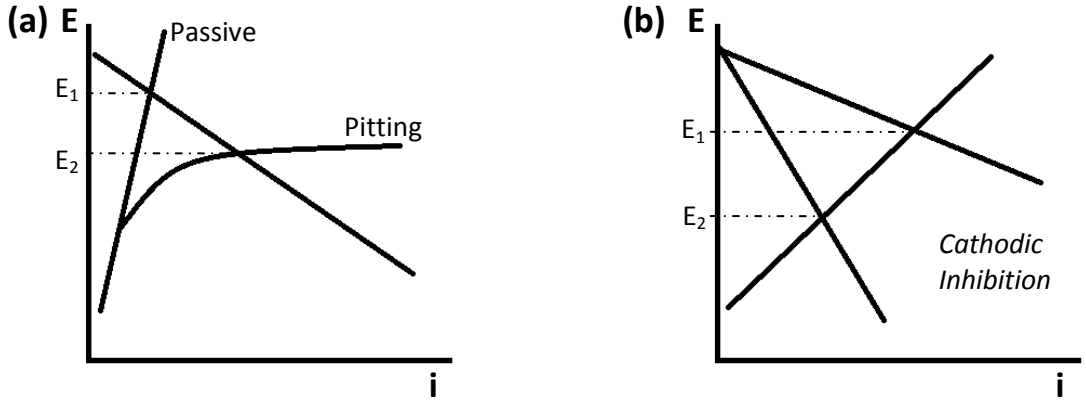

Figure 3.22 – Schematic Tafel plots of: a) breakdown of passivity, b) cathodic inhibition

Figure 3.22a shows how the alloy can experience a breakdown of passivity when the potential of the system decreases. The anodic line of the Tafel plot changes from a line in the passive region of the metal to a region in the curve where pitting takes place. The potential then moves down the cathodic line and the current density of the system would increase. Figure 3.22b demonstrates how cathodic inhibition of the system would also decrease the potential. If the cathodic reaction is inhibited, the gradient of the cathodic line decreases, and the potential

would subsequently decrease and move down the anodic line of the Tafel plot. The current density would also decrease along with the potential. Therefore, the low potentials exhibited by the EIS tests with chromate additions are likely due to cathodic inhibition of the alloy, as the calculated charge transfer resistances indicate that increased additions of strontium chromate lead to lower corrosion rates.

3.3 Discussion

The protective effect of strontium chromate is clearly apparent from the direct current polarisation for an uncoated sample of AA2024-T3. Increased additions of the inhibitor cause an extended passive region for the alloy, which indicates that strontium chromate effectively prevents stable pit initiation. Baghni et al. tested equimolar sodium chromate, strontium chloride and strontium chromate (0.236mM) on zinc in acid rain conditions (pH 4.5) and found that the cathodic branches solutions with strontium chloride of the polarisation curve were very similar, where the corrosion potential is shifted 300mV in the negative direction because it is believed that the anionic component, CrO_4^{2-}, provides cathodic inhibition[59]. DC polarisation tests in this chapter agree with Baghni's work in that the free corrosion potential was also shifted in the negative direction, but only by 100mV. This is could be related to the high concentration of aggressive ions, whereby the 2M NaCl concentration caused the alloy to sit at a free corrosion potential closer to the pitting potential or even a potential where only metastable pitting can occur.

Baghni also investigated the effect of the cationic species of the inhibitors by comparing the anodic branches of the polarisation curves of the different solutions and revealed that the sodium chromate solution showed lower anodic corrosion current nearer the corrosion

potential but above 0.88V SCE the strontium chromate solution demonstrated an extended passive region and a higher pitting potential. It was not determined how strontium affected the system, but it was noted that solution analysis and an XPS scan showed that the concentration of strontium (0.236mM) in solution did not change before and after immersion, and that no strontium was detected on the metal surface. Whilst no experiments were performed in this investigation on any possible inhibition mechanisms of strontium, it is generally accepted that strontium chromate is widely used as the inhibitor because of its low solubility, so that the protective chromate species do not get rapidly depleted.

Similar experiments conducted by Zein El Abedin on aluminium[48], at a concentration of $1x10^{-4}M$ CrO_4^{2-}, in this case as sodium chromate, only slightly raised the pitting potential. According to the review compiled by Kendig and Buchheit[24], the anodic inhibition provided by chromate ions is modest, and depends upon the chloride:chromate ratio, where the pitting potential is ennobled if the ratio is lower, between 10:1 to 1:1. However, it was observed here that for ambient temperature, even in extremely high concentrations of sodium chloride (2M), tests with higher concentrations (2000:1) of the inhibitive species, of over $1x10^{-3}M$, still demonstrated an extended passive region with the pitting potential of the alloy raised to over 200mV above the rest potential. The review by Kendig and Buchheit also states that the mechanism by which chromate ions raises the pitting potential and provide anodic inhibition is unclear. An early suggestion by Cartledge in 1966[57] was that chromate (VI) ions can adsorb onto the oxide layer without being reduced and consequently discourage the adsorption of aggressive chloride ions. This preferential adsorption theory has been supported more recently by McCafferty et al. for chromate (VI) ions as well as other inhibiting oxoanions[81].

Little previous work has been reported that a small temperature increase of 10°C greatly affect the protective qualities of strontium chromate. Lowering of the rest potential with additions of chromate was apparent at ambient temperature conditions after prolonged immersion, but when the test temperature was raised by 5 or 10°C, the additions of strontium chromate caused a more rapid lowering of the corrosion potential. However, at higher temperatures (30°C), the anodic protection becomes reduced. This behaviour at 30°C, where the inhibitor shows little protection against pitting raises a question in the effectiveness of the inhibitive qualities of strontium chromate under fully immersed conditions.

EIS demonstrated the protective qualities of strontium chromate in aggressive solution and show an obvious increase in charge transfer resistance even at lower concentrations of strontium chromate ($1x10^{-4}$M). The potentiostatic EIS measurements ideally will not initiate corrosion processes unlike the initiation of pitting in direct current polarisation tests. It also revealed that as time progressed, the systems that had additions of strontium chromate had increased resistances as well as decreased capacitances. These results also suggest that the chromate is inhibiting corrosion processes by limiting reactions such as oxygen reduction or metal dissolution and the decreasing capacitance can also support the theory that chromate ions adsorb unto the oxide layer reducing the active area of the cathode.

Electrochemical impedance tests exhibited two semicircles, which are RC parallel loops, one at high frequencies and the other at lower frequencies. This is in agreement with work done by Lee and Pyun[19] as well as Martin et al.[80], who also reported two capacitive loops. The model circuit used in their work was also R(Q(R(QR))) although Lee suggested that the two capacitances were both caused by capacitance in the oxide layer, but changing the passive layer to a chloride ion-

containing outer film and a fresh inner oxide film. Martin suggested that the two constant phase elements were caused by the oxide layer and the Helmholtz double layer.

3.4 Conclusions

Chapter 3 investigated the electrochemical behaviour of bare AA2024-T3 in sodium chloride solution using potentiodynamic polarisation and electrochemical impedance spectroscopy. The majority of electrochemical experiments were performed in 2M sodium chloride solution so that any innate passive behaviour of the aluminium was eliminated.

In the potentiodynamic polarisation tests, it was found that lower concentrations of strontium chromate (0M to $1x10^{-4}$M) did not affect the anodic polarization curve, i.e. no passive region introduced between the rest potential and pitting potential, although at concentrations above$1x10^{-3}$M, a region of passivity developed. This indicates that strontium chromate does not provide much anodic inhibition unless at high concentrations. The potential barrier between the free corrosion potential and the pitting potential was between 100 – 270mV increasing with chromate concentration.

As salt spray tests in industry are performed at 30°C (10°C higher than ambient tests in these experiments), further tests were performed at 25°C and 30°C, and the small change in temperature greatly affected the electrochemical behaviour AA2024-T3. Increasing the test temperature lowered the rest potential of the alloy, more than raising the pitting potential. This suggested that the cathodic inhibition of inhibitive chromate affected by temperature, and whilst prolonged immersion lowered the rest at ambient temperature conditions, when the test temperature was raised by 5 or 10°C, the free corrosion potential dropped more rapidly.

However, the pitting potential at raised temperature conditions was less apparent and much closer to the rest potential; passivity was still exhibited at higher temperatures but was noticeably reduced.

Electrochemical impedance spectroscopy demonstrated that the charge transfer resistance increases with strontium chromate concentration in 2M sodium chloride solution. As time progressed, the alloy exhibited increased resistances and decreased capacitances. The results suggest that the chromate inhibits corrosion processes (increased charge transfer resistance), and is likely due to limiting reactions such as oxygen reduction or metal dissolution and the decreasing capacitance suggests that chromate ions adsorb unto the oxide layer reducing the active area of the cathode.

Chapter 4 Corrosion Behaviour with Intact Coatings

4.1 Introduction

This chapter describes the investigation of fully-coated systems, where the paint coating on the aluminium substrate is intact with no defects. Chromate-pigmented epoxy coated systems have been well-documented for their good corrosion protection, so this chapter will mainly focus on the additional protection that the inhibitive pigments provide compared to an organic coating of similar chemical composition without inhibitors. Electrochemical impedance spectroscopy was used to study the deterioration of intact coatings. UV-Visible spectroscopy was used to investigate the release of inhibitor from the chromate-pigmented coating.

4.2 Corrosion Behaviour with Intact Coatings: EIS

Initially, EIS experiments were performed in the large volume test cell with the EIS method, as described in section 2.4. The equivalent circuit shown in figure 4.1 was chosen to model the intact coating system is R(Q(R(QR). With the bare alloy system, it was possible to separate the R_{oxide} and R_{ct}, but only a two time constant response was seen in the coated sample results so the individual effects are indistinguishable. From the circuit values, it could be concluded that the 'fast' response was linked to the coating. The two resistances, R_{oxide} and R_{ct}, are therefore combined and presented together as the polarisation resistance, R_{pol}.

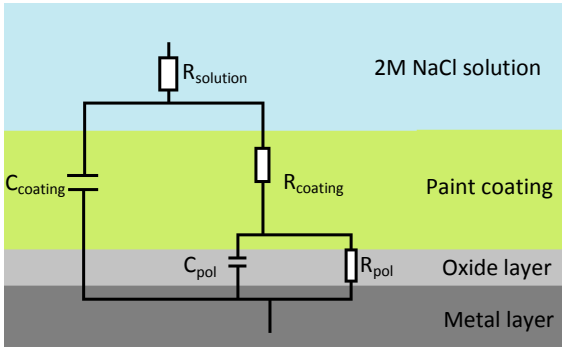

Figure 4.1 – Schematic of model circuit, R(Q(R(QR))), under investigation

Various authors have used the R(Q(R(QR))) model where R_1 is the solution resistance, R_2 is the pore resistance where the coating is least resistant, also known as the coating resistance and R_3 is the polarisation resistance, $R_{pol.}$ Two constant phase elements (CPE) were used instead of ideal capacitors because it was found to give a better fit. $C_{coating}$ represents the capacitance of the paint coating, and C_{pol} is the polarisation capacitance. R_{pol} and C_{pol} represent corrosion processes at the metal-paint interface and including contributions from the oxide layer. The same model circuit, R(Q(R(QR), was used as the bare alloy system in terms of mathematical function, but the circuit elements in this intact coated system are different to uncoated system as described in section 3.2.1. This is because the high frequency response is picked up in the coating and the low frequency response of the oxide and corrosion cannot be clearly separated.

4.2.1 Non-Inhibitive Control Coating

Before the coatings with inhibitive pigments were investigated, the control coating was tested.

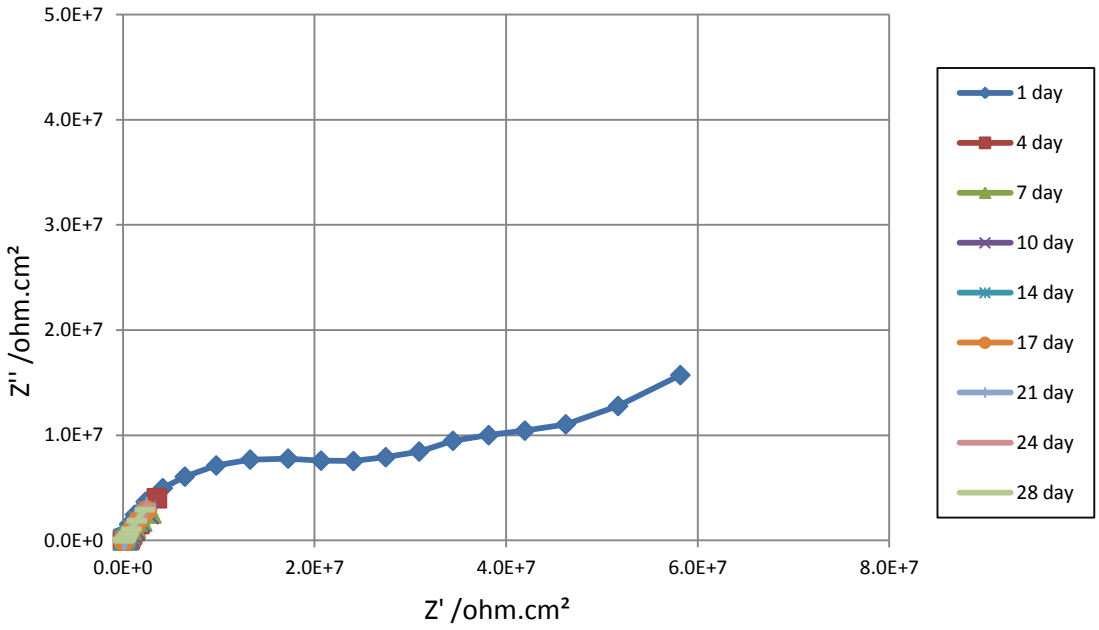

Figure 4.2 –Nyquist plots of control paint over 28 days

Figure 4.2 shows the Nyquist plots for the non-inhibited control paint over the course of four weeks. A close-up of the high-frequency measurements is shown in figure 4.3. The 1 day measurement, shown by the blue line with diamond markers, is significantly larger than the subsequent measurements for the same range of frequencies, 30000 to 0.1Hz. The parameters for the equivalent circuit fits are shown in table 4.1. By looking more closely at the high frequency measurements, shown on figure 4.3, the coating resistance, given by the high frequency semicircle, drops by two orders of magnitude in the 1st week from 10^7 to $10^5 \Omega cm^2$ and halves again between the first and second weeks of immersion.

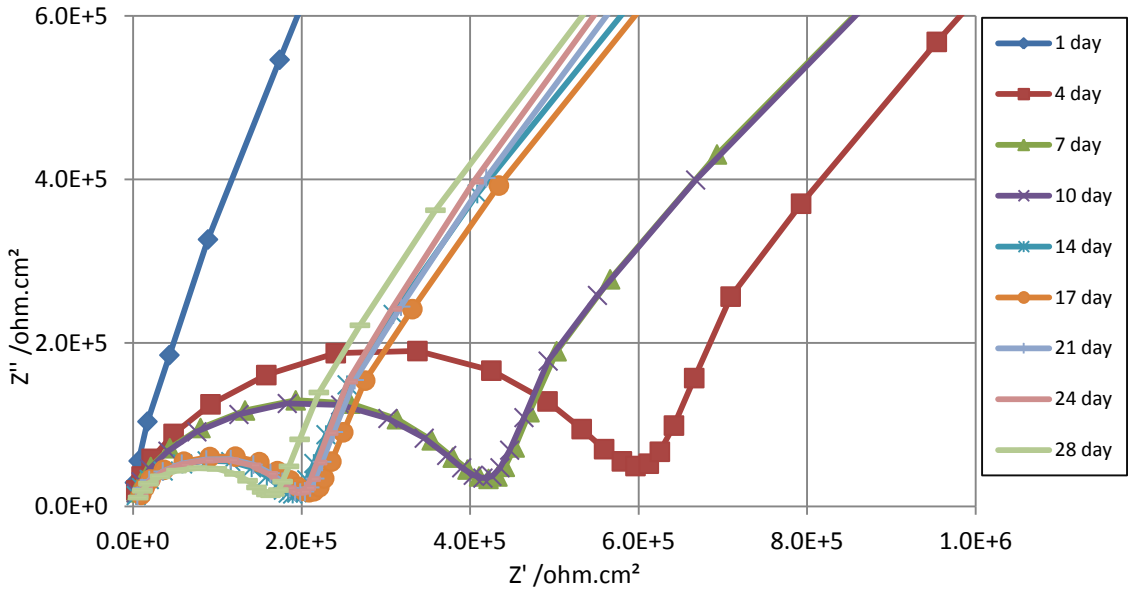

Figure 4.3 – High-frequency section of Nyquist plots of control paint

Figure 4.3 shows the high-frequency section of the Nyquist plots and a set of distinct depressed first 'semicircles' are seen. This indicates that CPEs are recorded rather than ideal capacitances. Table 4.1 shows a sharp drop in coating resistance after day 1. Subsequent decrease in resistance changes more slowly and is likely to be related to the deterioration of the coating

which could be linked to corrosion processes, e.g. blistering, change in pH. Coating resistances of the order of $10^5\Omega$ are regarded as a low resistance. The polarisation resistance, R_{pol}, is much higher than the coating resistance which suggests that the protection now comes mostly from the passive oxide layer.

Time (days)	Equivalent Circuit Model	CPE ($x10^{-9}$ $S{\cdot}s^{-n}cm^{-2}$) $C_{coating}$	Freq. Power (n)	Resistance ($x10^5\Omega cm^2$) $R_{coating}$	CPE ($x10^{-6}$ $S{\cdot}s^{-n}cm^{-2}$) C_{pol}	Freq. Power (n)	Resistance ($x10^7\Omega cm^2$) R_{pol}	Chi-squared ($x10^{-3}$)
1	R(Q(R(QR)))	1.1	0.84	190	420	0.70	4.0	21.7
4	R(Q(R(QR)))	2.9	0.80	5.8	2.3	0.72	2.0	8.2
7	R(Q(R(QR)))	4.0	0.78	4.1	3.1	0.74	0.8	8.3
10	R(Q(R(QR)))	4.4	0.78	4.1	3.3	0.73	0.8	8.8
14	R(Q(R(QR)))	6.3	0.76	1.9	3.8	0.78	0.9	11.2
17	R(Q(R(QR)))	12.3	0.69	2.2	3.8	0.79	0.9	6.4
21	R(Q(R(QR)))	8.4	0.74	2.0	3.8	0.79	1.1	8.8
24	R(Q(R(QR)))	7.6	0.74	2.6	3.6	0.79	1.4	8.5
28	R(Q(R(QR)))	8.9	0.73	2.7	3.8	0.79	1.2	7.5

Table 4.1 – Model Parameters for non-inhibitive control coating for 28days

The polarisation resistance, R_{pol}, decreases fairly rapidly in the first week from approximately 40MΩ to 10MΩ. Because the coating is intact, it is likely that R_{pol} is associated with the corrosion current passing through a smaller area than the $1cm^2$ being tested. The drop in resistance means that the rate of corrosion attack or the area being attacked increases and this could be due to ions passing through the coating so that the increase of chloride ions at the oxide surface leads to more pitting. The polarisation resistance then remains at around $10M\Omega cm^2$ which indicates the rate of corrosion has steadied. Figure 4.4 shows the Nyquist plots for a second sample, focusing on the second semicircle where R_{pol} and C_{pol} are calculated.

Comparing the EIS values between the intact control coating after 28days and the uncoated bare alloy after 72hours in 2M NaCl without strontium chromate, the polarisation resistance calculated for the coated sample is 3-4 orders of magnitude greater than the bare alloy, yet the capacitances relating to polarisation are only a magnitude of order greater for the bare alloy, C_{dl}, compared to the intact coating, C_{pol}.

Intact coated sample (28days):

$C_{coating} = 1.13nS.s^{-n}cm^{-2}$

$R_{coating} = 18M\Omega cm^2$

$C_{pol} = 3.8\mu S.s^{-n}cm^{-2}$

$R_{pol} = 12M\Omega cm^2$

Bare alloy sample (72hours):

$C_{oxide} = 0.79\mu S.s^{-n}cm^{-2}$

$R_{oxide} = 330\Omega cm^2$

$C_{dl} = 1.7mS.s^{-n}cm^{-2}$

$R_{ct} = 6k\Omega cm^2$

The increased polarisation resistance indicates a very much lower corrosion rate and can be explained using the Stern Geary equation:

$R_{pol} = B/i_{corr}$ where B is the proportionality constant and i_{corr} is the corrosion current

The corrosion current could be limited by the extra epoxy layer coating providing both an additional barrier to ionic transport which could lead to a limited extent of pitting which would be supported by the change in capacitance, suggesting that the coating layer reduces the number of active corrosion sites across the alloy surface, although rate is slower from resistance values so it's not solely controlled by area.

Along with the EIS results earlier in this section, the SAM images suggest that the control coating does not provide protection and pitting corrosion occurs and propagates. Repeat tests also showed similar behaviour where the coating resistance dropped sharply after the first day and the charge transfer resistance was higher than the coating resistance.

Figure 4.4a shows a digital photograph and figures 4.5b and c shows a SAM C and A-scan of a dried unpigmented control coating after four weeks of immersion in 2M sodium chloride solution and EIS testing.

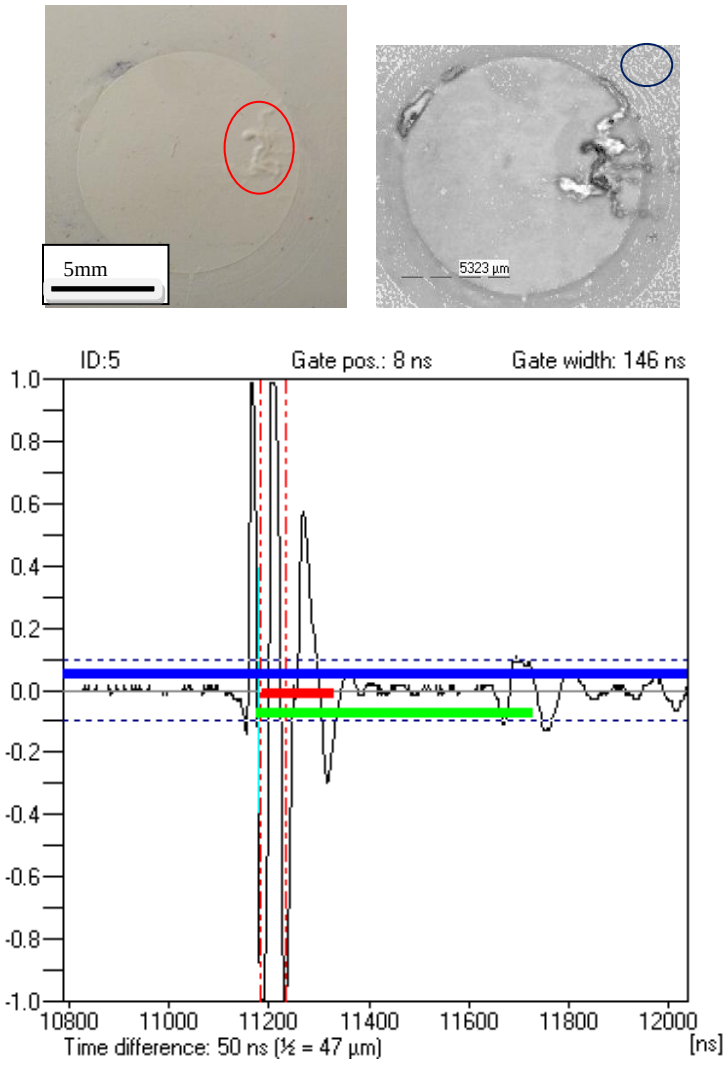

Figures 4.4 a) Digital photograph of top surface of intact white coating, b) Scanning acoustic micrograph of sample across coating, c) A-scan of figure 4.5b

From figure 4.4a, blisters can be seen across the top surface of the sample (circled in red). SAM micrographs revealed that filiform corrosion had been propagating across the surface of the

alloy and a large pit had formed underneath the coating. Blister can occur due to the build-up of corrosion product or change in chemical environment, such as pH. Chloride ions that diffuse through the coating break down the alloy oxide to create pits on the surface. The reduction of oxygen at cathode sites produces an alkaline hydroxide environment which typically reduces coating adhesion, weakening the alloy-coating interface. This consequently allows further accumulation of hydroxide ions. The breakdown of the passive oxide also allows metal dissolution. A combination of corrosion by-products and water osmosis could cause volume expansion underneath the coating and the formation of blisters[34]. The presence of filiform corrosion is unusual in immersion conditions as filiform corrosion would be a cathodic disbondment process which does not typically occur on aluminium. Disbondment of aluminium is usually via anodic under-cutting.

Optical microscopy performed on the surface of the coating did not show any distinct features. Figure 4.5 shows two optical images of the coating before and after testing in sodium chloride solution.

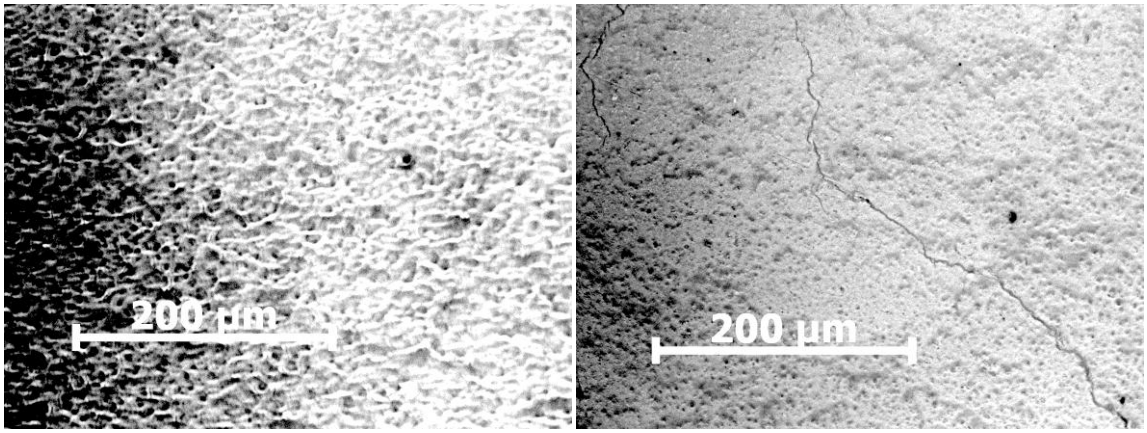

Figure 4.5 – Optical microscope images of a) untested b) tested and dried control paint surfaces

A dimpled effect can be seen across the surface of the coating, although at higher magnifications, images were more difficult to take on the rough surface. The main difference after testing and drying was that cracks could be seen across the coating surface. This indicates that the epoxy coating does not maintain good structural integrity.

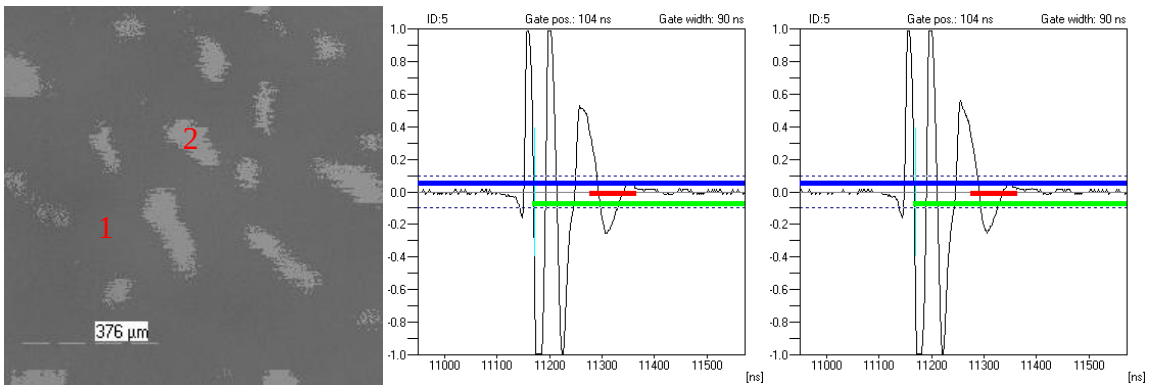

Figure 4.6 a-c – a) C-scan of untested area of control paint, gate set at coating-metal interface, b) A-scan of image 4.7a with transducer centred at red point labelled 1 away from artefact, c) A-scan of red point 2 in white artefact region

White specks were seen across the untested sample in SAM images, highlighted by the blue circle in figure 4.4b. Figure 4.6 shows a SAM A-scan analysis of the artefacts, where the transducer was focused on points 1 and 2 on the C scan, figure 4.6a, and the corresponding A-scans are shown in figures 4.6b and 4.6c respectively. The scale bar on the C-scan shows that the artefacts were around 100-300µm, but there is no obvious difference in the A-scans, indicating that the artefacts are not likely due to adhesion loss as there is no separation between the coating and the substrate.

It is uncertain what the white specks in the coating represent, but the above SAM analysis on the control coating has been included in this study as background to the SAM investigation of the $Ce(dpp)_3$ Epigen coating found later in chapter 6.

4.2.2 Chromate-pigmented 113-22 Coating

The same experiments were performed on chromate-pigmented 113-22 coated samples of AA2024-T3.

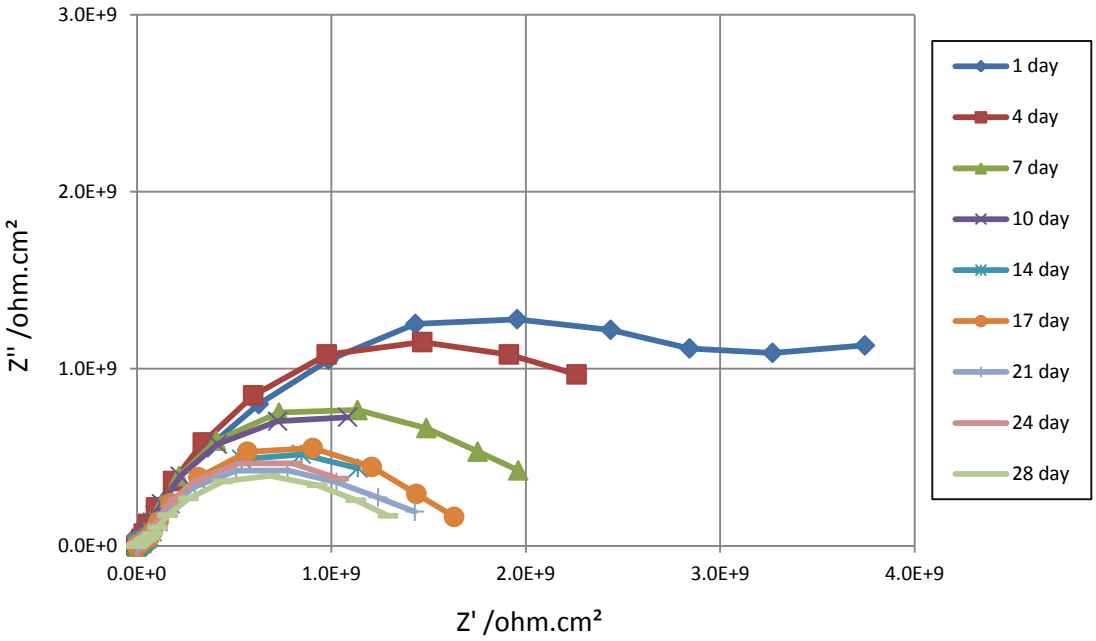

Figure 4.7 – Nyquist plots of 113-22 coated AA2024-T3 in 2M NaCl solution over 28 days

From figure 4.7, it can be seen that there is again a two time constant response in the impedance data for the 113-22 coated samples. The impedances are all very large, greater than $10^9 \Omega cm^2$. Surprisingly, the high frequency semicircle, representing the coating resistance and capacitance, is actually smallest on the first day, the opposite of the control coated sample. Figure 4.8 shows the high frequency semicircle more clearly for the day 1 measurement and figure 4.9 shows the subsequent high frequency data.

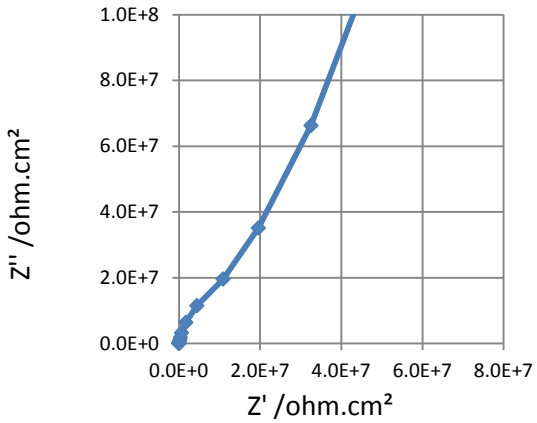

Figure 4.8 – High-frequency section of Nyquist plot of 113-22 coated sample on day 1

Despite having the lowest resistance, table 4.3 shows that the coating resistance on day one is 8MΩ, which is comparable to the control coated tests. Interestingly, the day 1 impedance measurement reveals impedance data beyond the second semicircle for the two lowest frequencies, suggesting that the electrochemical system is more complex than the equivalent circuit so far used to fit the data.

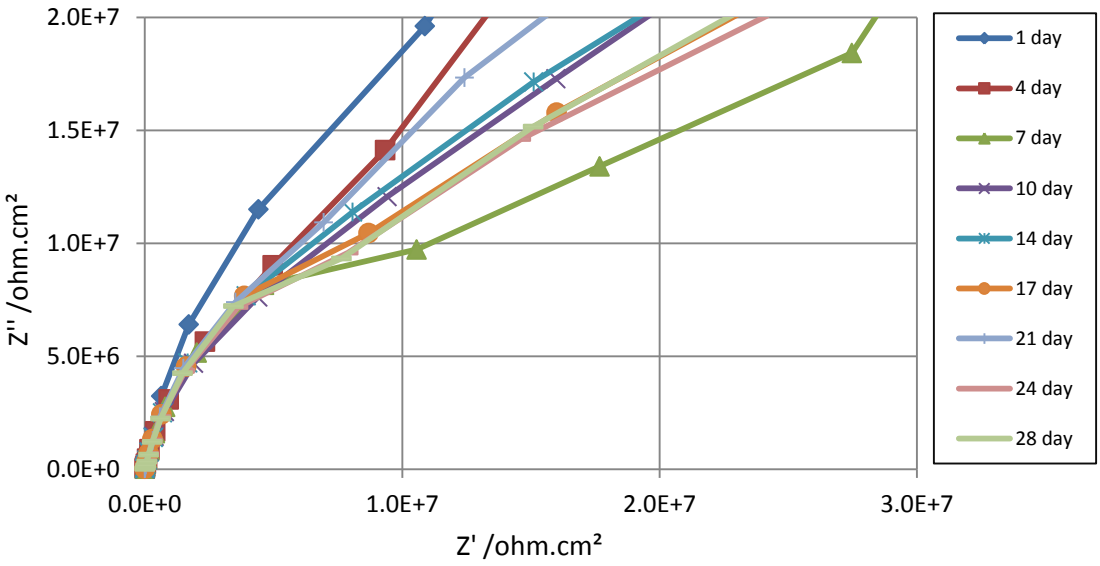

Figure 4.9 – High-frequency section of Nyquist plots of 113-22 coated sample over 28 days

It can be seen from figure 4.9 that the first semicircle merges into the second semicircle before taking a clear shape, but data-fitting software is able to distinguish the two semicircles using the equivalent circuit shown in figure 4.1. Compared to the control coating, the 113-22 coating resistance remains relatively unchanged at ~$10^7\Omega$. This maintained high resistance is likely due to a lessened deterioration of the coating, where the presence of soluble pigment is expected to lessen the barrier or because the inhibitive pigments have reduced the amount of corrosion which means that less corrosion product, such as hydroxide ions, will have been formed.

This is still a relatively low resistance for corrosion-protective coatings and again it is the low frequency measurements that show high resistances, but now significantly greater than the control paint-coated test, shown in table 4.2.

Time (days)	Equivalent Circuit Model	CPE ($x10^{-10}$ $S{\cdot}s^{-n}cm^{-2}$) $C_{coating}$	Freq. Power (n)	Resistance ($x10^7\Omega cm^2$) $R_{coating}$	CPE ($x10^{-9}$ $S{\cdot}s^{-n}cm^{-2}$) C_{pol}	Freq. Power (n)	Resistance ($x10^9\Omega cm^2$) R_{pol}	Chi-squared ($x10^{-2}$)
1	R(Q(R(QR)))	2.8	0.95	0.8	0.7	0.57	4.4	2.0
4	R(Q(R(QR)))	3.1	0.95	1.7	1.3	0.71	3.3	1.4
7	R(Q(R(QR)))	4.5	0.92	3.1	3.7	0.76	2.2	1.6
10	R(Q(R(QR)))	5.5	0.91	3.5	3.6	0.76	2.2	1.0
14	R(Q(R(QR)))	6.7	0.89	5.0	5.6	0.77	1.5	1.2
17	R(Q(R(QR)))	6.4	0.90	4.7	5.3	0.76	1.7	1.5
21	R(Q(R(QR)))	2.8	0.95	0.8	0.7	0.57	4.4	2.0
24	R(Q(R(QR)))	3.1	0.95	1.7	1.3	0.71	3.3	1.4
28	R(Q(R(QR)))	4.5	0.92	3.1	3.7	0.76	2.2	1.6

Table 4.2 – Model Parameters for 113-22 chromate-pigmented coating for 28days

The polarisation resistance of the 113-22 coated sample decreases slowly over time, but remains at values >10^9 Ωcm^{-2}. These values are two orders of magnitude greater than the

control coated sample and four orders of magnitude greater than the bare alloy tests. The high R_{pol} values indicate that the corrosion rate of the 113-22 coated sample is low and that the coating and pigments are inhibiting the corrosion processes. The difference between the composition of the control and 113-22 coatings is the pigment, one non-inhibitive and the other chromate-based. As the coating resistance for both the control and 113-22 paints are relatively low, this suggests that the chromate pigments play the major role in protecting against corrosion. The bare metal tests showed that strontium chromate can provide anodic inhibition at high concentrations (greater than 1mM) by elevating the pitting potential and lowering the corrosion potential so that a passive region is exhibited. Lower concentrations of strontium chromate on bare metal tests do not reveal significant anodic inhibition which suggests than the corrosion protection is not limited to anodic passivation. The control paint-coated EIS tests reveal that when water and aggressive ions penetrate the organic coating, the corrosion protection comes mainly from the passive oxide layer on the surface of the metal, but filiform attack can be initiated by the ingress of chloride ions through the oxide. Therefore, the chromate pigment in the 113-22 coating is likely preventing the breakdown of passivity at local active sites so that filiform or pitting corrosion does not propagate.

Figure 4.10 shows a digital photograph and scanning acoustic micrographs of the 113-22 coating after four weeks of immersion in 2M sodium chloride solution and EIS testing.

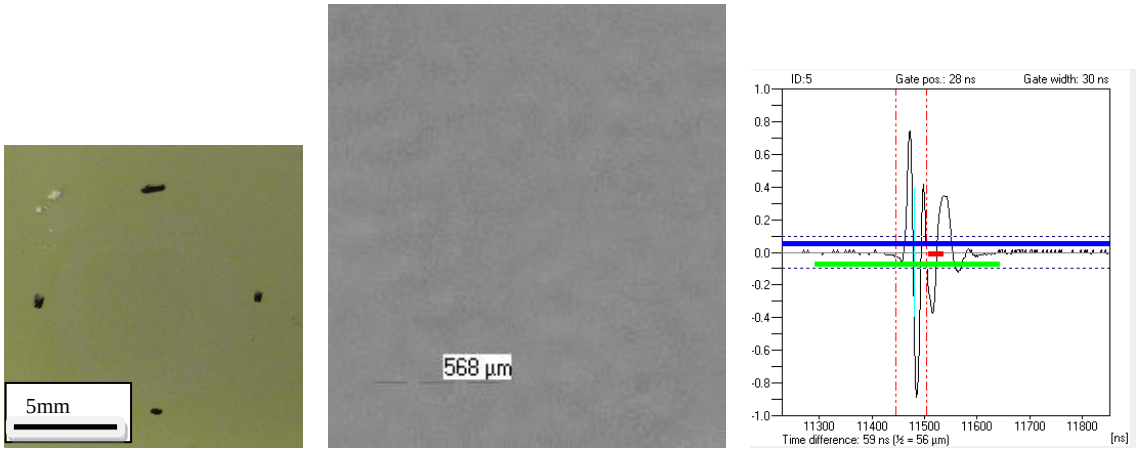

Figures 4.10 a) Digital photograph of top surface of intact 113-22 coating, b) Scanning acoustic micrograph of sample across coating, c) A-scan of figure 4.11b

From figure 4.10a, there are no visible defects on the top surface of the paint coating. There is, however, slight discolouration of the test area where the yellow-green paint is paler in colour. The white specks seen on the untested control coating are a lot finer on the 113-22 coating. It is uncertain what these are, and it may be clusters of chromate pigment that have been distributed evenly across the epoxy coating. Also, the area of immersion is not distinguishable from the unexposed areas from the SAM image, unlike the control coating. No visible corrosion attack can be seen on the alloy surface underneath the coating. The microscopy on the control coating showed that water and aggressive ions can still penetrate the epoxy and corrosion activity can still occur. No corrosive attack was detected for the 113-22 coated sample which confirms that for intact coatings the chromate pigments prevented breakdown of passivity in the oxide layer.

Optical microscopy performed on the surface of the coating did not show any distinct characteristics. Figure 4.11, on the following page, shows two optical images of the coating before and after testing in sodium chloride solution.

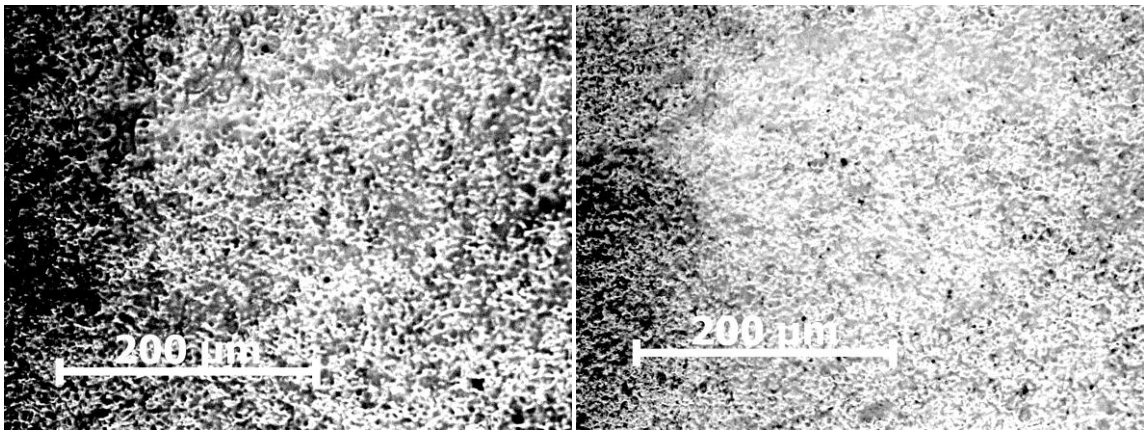

Figure 4.11 – Optical microscope images of a) untested b) tested and dried 113-22 paint surfaces

Similar to the control coating optical images in figure 4.11, a dimpled effect can be seen across the surface of the coating. No obvious difference can be seen between the untested and tested samples and the cracks seen in the control coating after drying were not seen in the 113-22 samples.

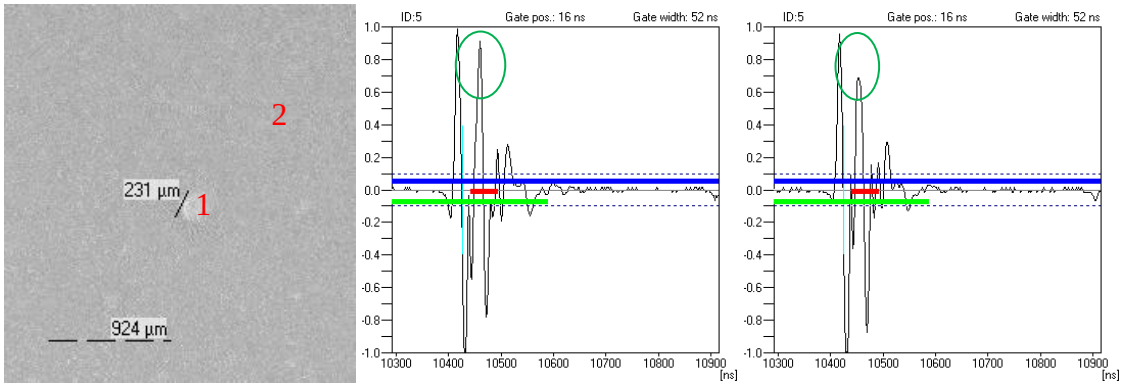

Figures 4.12a-c – a a) C-scan of untested area of control paint, gate set within coating, b) A-scan of image 4.12a with transducer centred at red point labelled 1, c) A-scan of red point 2

A-scans of the fine array of white specks were compared, where the transducer was focused on points 1 and 2 on the C scan, figure 4.12a, and the corresponding A-scans are shown in figures 4.12b and 4.12c respectively. The scale bar on the C-scan shows that that a cluster of artefacts are of similar size to the specks seen on the control coating (100-300μm). The A-scans show a shorter peak within the coating, highlighted by the green circles in figures 4.12b and 4.12c. This indicates that there is a stronger signal at point 1 where the cluster is. The signal appears from within the bulk of the coating, but it is uncertain what the white specks in the coating represent.

4.3 Release of Inhibitive Pigments

UV-Visible spectroscopy was used to quantify the inhibitive pigment release of the 113-22 paint coating. A number of solutions of known concentration of strontium chromate were prepared to calibrate the method. Control solutions of 100, 500 and 1000 times dilution of saturated strontium chromate were made. Test cells holding 20-25ml of 2M sodium chloride solution were clamped against a 113-22 painted sample so that the top surface area of approximately 8cm^2 of the paint was exposed to the solution. A smaller volume test cell held 3-4ml of sodium chloride solution against the same surface area of coating. The small volume tests were performed to investigate whether the amount of pigment released from the coating is a fixed quantity. In other words, if the volume of sodium chloride solution was reduced, would the amount of chromate leached out into the solution be increased? The method was described in more detail in section 2.3.4.

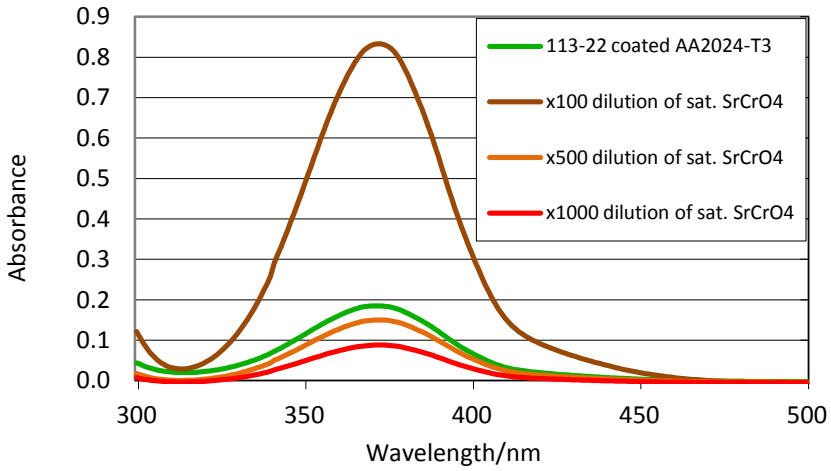

Figure 4.13 – UV-Vis spectrum of 113-22 coated sample and standard solutions of $SrCrO_4$

Figure 4.13 shows the absorbance spectrum of the chromate-pigmented 113-22 coating on AA2024-T3 after being immersed in 2M sodium chloride solution for three days. The calibration standards, of known concentrations, reveal that the amount of inhibitive pigment released from the 113-22 coating was comparable to a 500x diluted solution of saturated strontium chromate.

The Beer-Lambert law states that there is a linear dependence between absorbance and concentration so a more precise estimate of the pigment release can be made. Figure 4.14 shows a calibration graph where known concentrations of 100x, 500x and 1000x the dilution of a saturated strontium chromate solution are plotted.

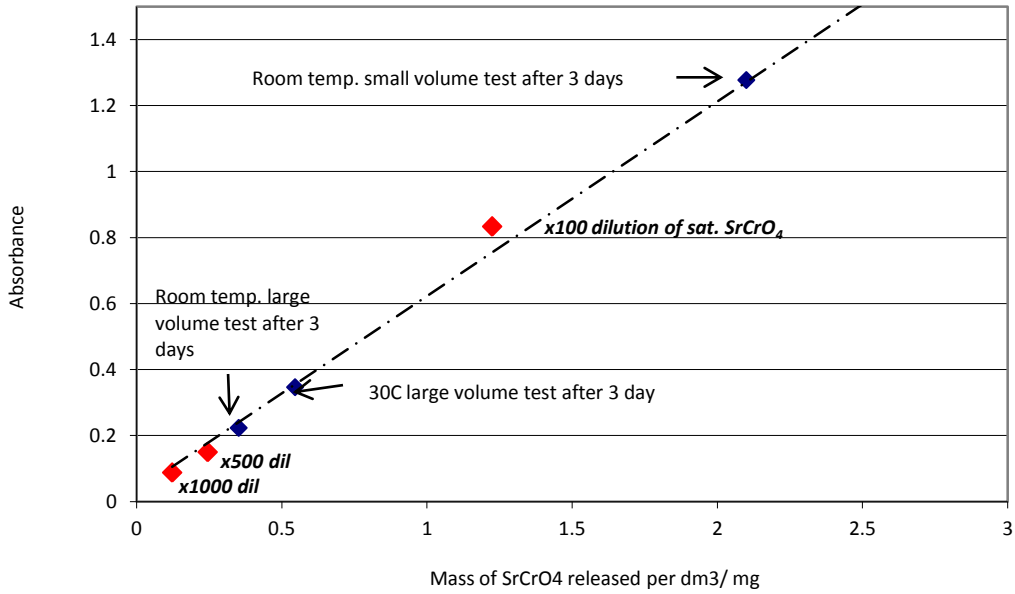

Figure 4.14 – Absorbance vs. mass graph showing linear dependence

Figure 4.14 also shows the results for pigment release test performed at 30°C. It shows that at the higher temperature, a higher absorbance is recorded indicating that more pigment is released. The test at 30°C was not performed for the smaller volume test cell because the higher temperature caused too much solution to evaporate from the cell and affecting the reliability of the absorbance data. The method described in section 2.6 had limited accuracy. It was difficult to retain all the test solution when transferring between test cells, glass pipettes and UV-Vis cuvettes due to residue solution being left on surfaces and being unable to wash the residue solution back into the cell (as that would change the test volume). When sodium chloride solution containing released chromate is not replaced back into the cell, if the paint is still releasing pigment, the measured concentrations would increase.

Figure 4.15 shows the change in mass of pigment against root time (so that the initial measurements, where rapid release takes place can be seen clearly) for the both the small and large volume tests. The large volume tests were performed to measure long-term pigment release but the small volume tests investigated short-term release. Although concentrations are different for the two volumes, the mass of chromate released was plotted to normalise for volume. It can be seen that the mass released from the small volume tests superimpose onto the long-term tests and indicate that the rate and total amount of pigment released into the bulk solution is the same for both volumes of test solution. Figure 4.15 also show that after approximately three days, the concentration of inhibitor in the bulk solution begins to level off and even after extended immersion times (four weeks); the concentration does not increase further. It should be noted that the concentrations in both cases is well below saturation.

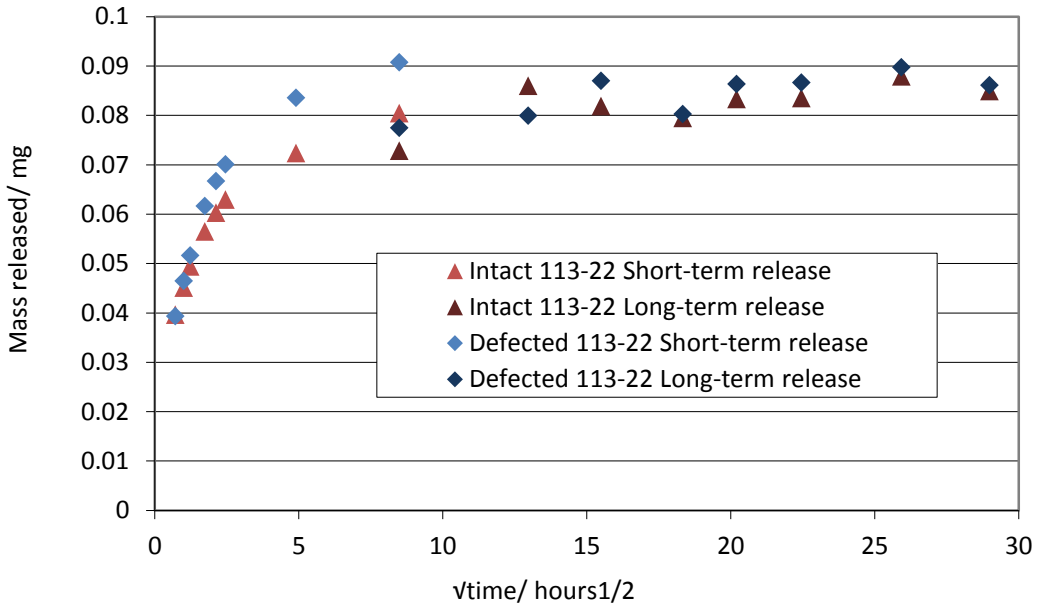

Figure 4.15 –Mass released vs. root time graph for 113-22 coatings on AA2024-T3 tested at room temperature

Tests were also performed with coatings that had a 1x30mm sized defect, exposing the cut-edges of the coating to the salt solution. This checks whether the release of pigmented is augmented at a cut edge compared to the surface, i.e. the surface of the coating may be less permeable, providing more information relevant to damaged coatings. The graph in figure 4.16 indicates that the presence of a defect does not significantly change the amount of pigment released and variation in UV-Vis tests. The concentrations measured were used to quantify the mass of pigment released from the paint and to calculate what proportion of pigment within the coating is released into the bulk solution.

4.3.1 Mass of pigment in paint coating

The mass of chromate released into the bulk solution from the 113-22 paint is calculated from UV-Visible spectroscopy experiments. Bare alloy tests described in chapter 3 and the standard solutions made for the UV-Vis experiments use only strontium chromate, whilst the 113-22 paint contains both strontium chromate and barium chromate as the effective inhibitive species. However, as the UV-Vis technique is detecting the yellow colour of the chromate (VI) ions, the addition of barium chromate should not affect the analysis.

Unfortunately, the compositional data from Mankiewicz only states that:

Concentration of strontium chromate in wet paint: 5 – 12.5%wt

Concentration of barium chromate in wet paint: 1 – 5%wt

Dry film weight: 47g m^{-2} @ 25µm thickness

For coatings of an average thickness of 50µm, the dry film weight will be 9.4 mg cm^{-2} @ 50µm

Weight of solid content = 54% -> Weight of wet paint (of dry thickness 50µm) = 17.4mg cm^{-2}

Therefore, the mass of chromate per square centimetre will be:

- ⇨ 0.87 – 2.18 mg cm^{-2} of $SrCrO_4$

  -> 0.50 – 1.24 mg cm^{-2} of CrO_4^{2-}

- ⇨ 0.17 – 0.87 mg cm^{-2} of $BaCrO_4$

  -> 0.099 – 0.50 mg cm^{-2} of CrO_4^{2-}

- ⇨ 0.59 – 1.73mg cm^{-2} of CrO_4^{2-}

The surface area of coating in UV-Vis experiments is 7.8cm^2, so that the theoretical mass of chromate available in a test sample is:

- ⇨ 4.6 – 13.5 mg of CrO_4^{2-}

Using the concentrations derived from the UV-Vis experiments and taking the molar mass of chromate, CrO_4^{2-}, to be 116g/mol, we can calculate the mass of chromate released into the bulk solution (unaffected by volume of test solution).

Absorbance (fig4.20)	Concentration/µM	Mass of CrO_4^{2-}/mg
0.22 @ RT	17.2	0.050
0.35 @ 30°C	26.8	0.078

Table 4.3 – Table of absorbance and equivalent chromate concentration and mass

For room temperature tests, only 0.4 to 1.1% of the theoretical value of chromate in the coating has been released. This percentage is increased to 0.6 to 1.7% in 30°C temperature tests.

The calculated percentages of released pigment are surprisingly low. This suggests that the majority of chromate species in the coating is not freely available and does not rapidly diffuse into the bulk solution. The small percentage of inhibitor that does leach into the bulk solution can be the pigment that is exposed at the surface of the coating or becomes accessible as pigment dissolves and that chromate buried within the coating's polymer matrix does not get released until a new surface of coating is revealed. When new surfaces result from physical damage to the coating, this reveals fresh surfaces for the pigment to dissolve into the bulk solution.

4.4 Discussion

Under the conditions of these tests, inhibitive pigments incorporated into a paint are extremely important in protecting against corrosion, even when the coatings are fully-intact and have no physical defects. Coated samples of AA2024-T3 were tested in high concentrations of chloride for a period of one month. The equivalent circuit used to model the EIS data has been used by other authors[82], although the Warburg element added to the model[64] to model reaction-diffusion processes at the metal interface and characterised by a 45°straight line in the low frequency region of Nyquist plots was not necessary.

Both organic coatings used in these tests demonstrated relatively low coating resistances which suggest that main mechanism of corrosion protection is inhibition by chromate. It was observed with the use of electrochemical impedance spectroscopy techniques that the coating without inhibitive pigments provides little corrosion protection and scanning acoustic microscopy revealed that AA2024-T3 coated with the control coating is susceptible to filiform corrosion propagating and forming pits across the alloy surface as well as blisters forming beneath the paint. Cracks were also seen in the control coating after testing. The presence of inhibitive species led to polarisation resistances of $>10^9\Omega$ over the course of a month and SAM and optical microscopy showed that there was no visible corrosion attack on the alloy and the physical integrity of the coating was maintained.

UV-Visible spectroscopy experiments concluded that only a small fraction, 1-6%, of the available inhibitor within the paint is actually released into the bulk solution. The inhibitor released from the epoxy coating is probably from a surface layer that is in contact with the bulk solution and despite water and aggressive ions being able to penetrate the polymer matrix, the bulkier

inhibitive species are locked within the coating. However, if water reaches the metal-coating interface, any chromate particles exposed at that interface will provide a source of inhibitive chromate. It is only when fresh surfaces to the bulk solution are formed, such as via physical damage, that further inhibitor can be released into the solution. UV-Vis experiments at higher temperatures (30°C) also revealed that, the amount of inhibitor released is increased. It was seen in chapter 3 that a small temperature increment could noticeably affect the inhibitive properties of strontium chromate on bare AA2024-T3 and again, in UV-Vis tests, a temperature difference of 10°C affects the amount of pigment release. Prosek and Thierry found that chromate leached with a logarithmic dependence with time from a polyester isocyanate coating[60]. They noticed a temperature dependence on pigment release, but found that the optimum release temperature was 20°C and that rate of release did not follow an Arrhenius relation (where increase in temperature would increase rate of release). They suggested that increasing temperatures affected the chromate-polymer interface with possible oxidation of the organic matter. UV-Vis experiments in the current study revealed that at 30°C, release was initially faster but did not greatly affect the longer term amount.

Howard, Zin, Scantlebury and Lyon investigated the leach rates of different pigments from a polyester primer on zinc and found that the polymer layer significantly slowed down the release of inhibitors[62]. They noticed, however, that the leaching behaviour of chromate inhibitor was different to the other pigments and concluded that it was caused by a chemical interaction between the inhibitor and the substrate.

Previous research has suggested that the leach rate of chromate inhibitors is heavily dependent on pH, with more acidic conditions allowing greater pigment release[83]. Furman also observed

that the abrasion of a primer surface would increase pigment release by over threefold, which can be explained by the increase of surface area in contact with solution. Furman's investigation also used EPMA and Raman mapping to determine depletion depth. He suggested that water passes through an epoxy primer rapidly, and that water uptake into the primer predominantly controls pigment release (therefore only being released from coating surfaces in contact with solution).

Experiments in this study do not agree with Furman or Prosek and Thierry[60], where water uptake into the primer creates a network of pores and channels that then play an important role in the degree of dissolved chromate. UV-Vis experiments in this investigation showed extremely limited release of chromate into the bulk solution and it is likely due to the bulkier ions being restricted within the polymer binder. These results are more in agreement with the investigation by Howard et al. where release was limited by the polymer layer. The ability of the binder to resist the leaching of soluble factions would support the primer requirements of releasing inhibitive pigments only when the coating is damaged. However, this raises the question that if the amount of pigment released is restricted to the top surface of a coating (in contact with solvent), would the amount of inhibitor be enough to provide corrosion protection to the exposed alloy? The next chapter will move on to examine the protection provided by chromate-inhibited epoxy paint when a coating is damaged and the bare alloy is revealed.

4.5 Conclusions

Chapter 4 investigated the corrosion behaviour of fully-intact coated AA2024-T3 using the non-inhibitive control coating and the chromate-pigmented 113-22 coating. Electrochemical impedance spectroscopy was the main method to investigate the electrochemical behaviour

and test data revealed a two time-constant response which was attributed to the coating response and the polarisation response.

Despite no physical damage to the coating, the polarisation resistance of the sample coating with non-inhibitive control paint coated samples still decreased over the course of one week of immersion in 2M NaCl solution. This indicated that the rate of corrosion attack or the area being attacked increases and showed that water and ions were able to pass through the coating and cause corrosion events.

The polarisation resistance of the chromate-pigmented 113-22 coated sample decreased less significantly over time and after a week of testing was still two orders of magnitude greater than the control coated sample and four orders of magnitude greater than the bare alloy tests. This indicated that the presence of inhibitive pigments in the coating caused corrosion inhibition for a fully-intact coated sample, even though the control tests showed that water and aggressive ions could still penetrate the coating layer.

UV-Visible spectroscopy experiments were performed to investigate the release of pigment from the 113-22 coating and it was concluded that only a small fraction of the inhibitor in the coating is released into the bulk solution. It is likely that the pigment release came from the surface layers in contact with the test solution as the majority of inhibitor was released in the first 2-3 days of immersion, and extended immersion did not release much more pigment. Further experiments conducted at 30°C showed a faster initial pigment release but did not greatly affect the overall longer term amount.

Chapter 5 Corrosion Behaviour of Coated Systems with a Defect

5.1 Introduction

The previous two chapters have demonstrated how chromate species can decrease the corrosion rate of AA2024-T3 both in solution at low levels and when incorporated into an epoxy coating. The investigation moves onto painted aluminium alloy systems that have a defect in the coating. Such defects will be caused by everyday use where paint is removed via abrasion so in this chapter, narrow scribe line defects were made using a scalpel and a wider 1mm defect was made using a steel chisel-edge tool to simulate different types of damage. Electrochemical impedance spectroscopy, direct current polarisation and electrochemical noise were used to investigate the corrosion protection. Chapter 4 showed that pigment is released from the surface of the coating, but inhibitors encapsulated deep within the polymer matrix do not readily pass into the bulk solution. Inhibitive pigment on the underside of the coating, at the metal-coating interface, is likely to be dissolved in water that passes through the coating and will be available at the alloy surface to passivate any corrosion reactions. At a damage site, chromate pigment will be released locally at the cut edges and diffuse away. Chromate will also be available from the free surface, but bulk levels are still unlikely to be high enough to provide protection; the mass of released chromate measured in section 4.2.2 is markedly less than the concentrations of chromate required in chapter 3 to cause significant corrosion protection on the bare alloy.

5.2 Potentiodynamic Corrosion Behaviour of Coated Samples with a Defect

As the defect exposes the bare alloy surface to the sodium chloride solution, direct current polarisation testing could be used and was performed in the large volume test cell, as described in section 2.2.1.1. Tests were performed both at ambient temperature and at 30°C.

5.2.1 Non-inhibitive Control Coating

A defect was made on a sample with control paint and results were compared against the uncoated and fully-intact coated systems. This is to investigate what influence the coating has on corrosion behaviour at the defect.

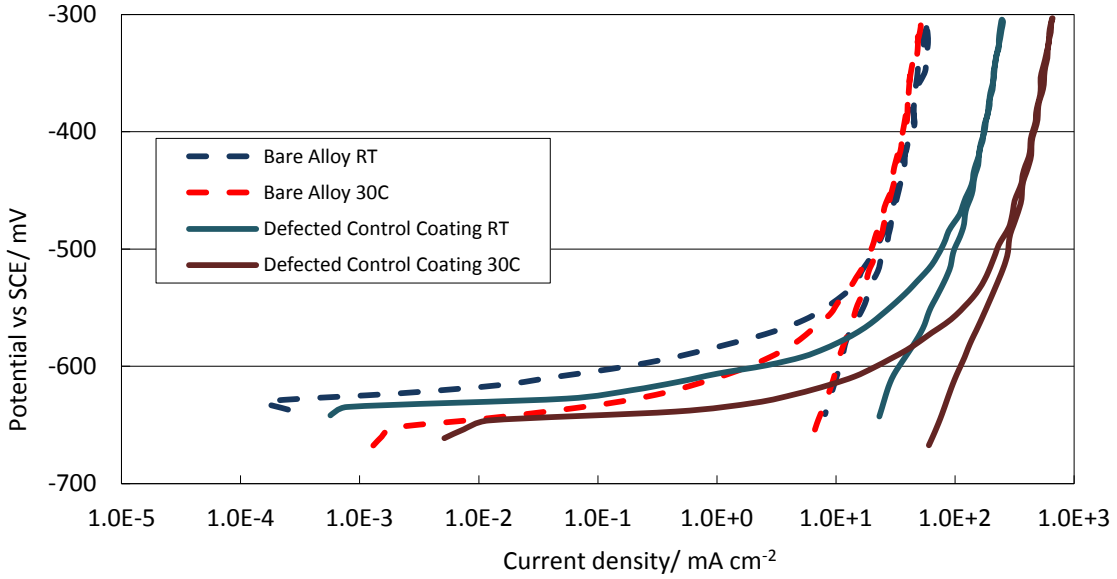

Figure 5.1 – Area-normalised DC Polarisation curves of bare and Control-paint coated AA2024-T3 with a chisel-edge defect in 2M NaCl

Figure 5.1 shows anodic polarisation curves for bare AA2024-T3 tested in 2M sodium chloride as a dashed line and the defected control-coated samples as a solid line. The DC polarisation was performed after 48 hours of immersion. The current density data is area-corrected to the size of the defect, 1mm x 10mm. The anodic behaviour for both defected-coated tests, at room temperature and 30°C, are quite similar to the bare metal tests. The rest potential for the room temperature test is -634mV (compared to -636mV for the bare metal test) and the rest potential for the 30°C test is -661mV (-667mV for bare test). When the potential is increased, the

corrosion current increases almost at once. This indicates that the alloy is sitting at or just below the pitting potential.

The higher current densities observed at high potentials in the defected coated sample tests are likely related to the geometry of the test area. Both the bare alloy and coated sample experiments test are normalised to a surface area of $1cm^2$, but the narrow defect in the coating will give a higher current density because of the low solution resistance with a radial spreading of the current at the defect.

5.2.2 Chromate-pigmented 113-22 Paint Coating

The control coating tests show that without inhibitor the coating provides no protection to the exposed metal at the defect. This section will compare a defected chromate 113-22 coated AA2024-T3 sample with a fully intact coating and the bare alloy tests.

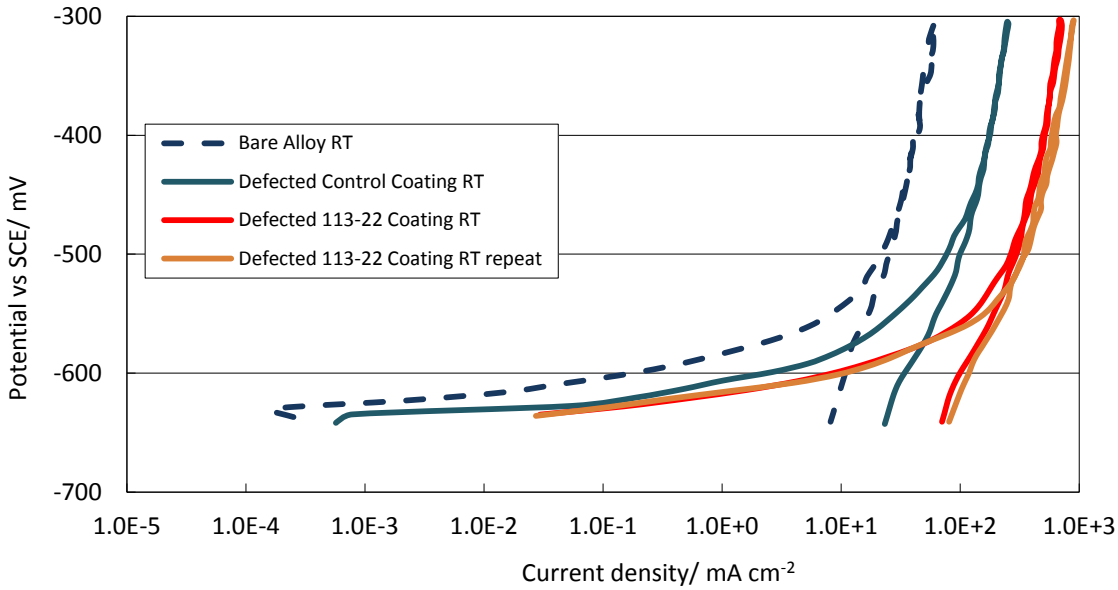

Figure 5.2 – Area-normalised DC Polarisation curves of bare and coated AA2024-T3 with a chisel-edge defect in 2M NaCl at room temperature

Figure 5.2 shows the anodic polarisation curves for bare AA2024-T3 tested in 2M sodium chloride at room temperature as a dashed line and the defected (1mm x 10mm) coated samples as solid lines. As before, the DC polarisation was performed after 48 hours of immersion. The current density data is area-corrected to the size of the defect. The anodic behaviour for both defected paint coating tests are very similar to the bare metal tests. The rest potential for the room temperature 113-22 coated test is -628mV compared to rest potentials of -634mV and 636mV for the control coated and bare metal tests respectively. When the potential is increased, the corrosion current increases at once. This again indicates that the alloy is sitting on or just below the pitting potential. This indicates that the presence of inhibitive pigments in the paint does not show any significant improvement in potentiodynamic polarisation tests. From bare metal DC polarisation tests in section 3.2.1 and the pigment release test in section 4.2.2, it is expected that the amount of chromate released from the 113-22 paint is significantly less than the concentrations of strontium chromate needed to cause anodic inhibition and as expected the pitting potential has not been shifted. However, it was noted in section 4.2.2, that more chromate was released from the paint at 30°C compared to room temperature, so DC polarisation tests on defected 113-22 coated samples were performed at 30°C and again compared with the control coated tests and bare alloy tests.

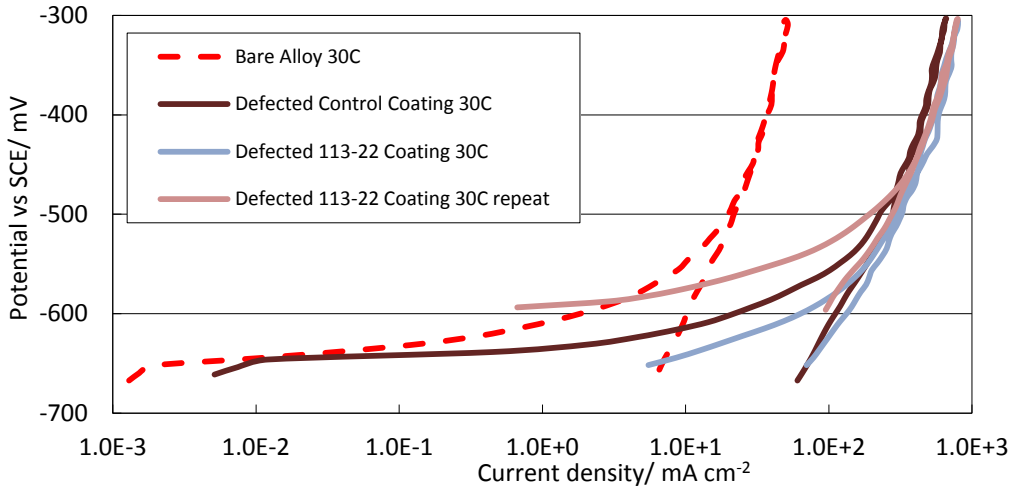

Figure 5.3 – DC Polarisation curves of bare and coated AA2024-T3 with a defect in 2M NaCl at 30°C

Figure 5.3 shows the anodic polarisation curves for bare AA2024-T3 tested in 2M sodium chloride at 30°C as a dashed line and the defected coated samples as solid lines. The DC polarisation was performed after 48 hours of immersion. The current density data is area-corrected to the size of the defect, 1mm x 10mm. The anodic behaviour for both defected paint coating tests at 30°C show some differences to the bare metal tests. The rest potentials for two 113-22 coated tests were different, one lying at -651mV (which is close to the control and bare metal tests) but the repeat test was raised to -587mV. Despite one rest potential being 60mV higher than the other, the corrosion current increases instantly with potential for both tests, indicating that the alloy is again sitting on or just below the pitting potential. The repeat experiment shows an upwards shift in E_{corr} and E_{pit}, suggesting that there is some anodic inhibition, possibly by a smaller corrosion current, i_{corr}, shifts the potential up the cathode line. UV-Vis spectroscopy tests, in section 4.2.2, indicated that the majority of pigment release from a fresh surface occurs in the first 72 hours of immersion. Therefore, as current tests were performed after 48 hours, new tests were performed after one week to allow more inhibitive species to be released from the coating and interact with the bare alloy surface.

5.2.2.1 Extended Immersion of Defected 113-22 Coated Sample

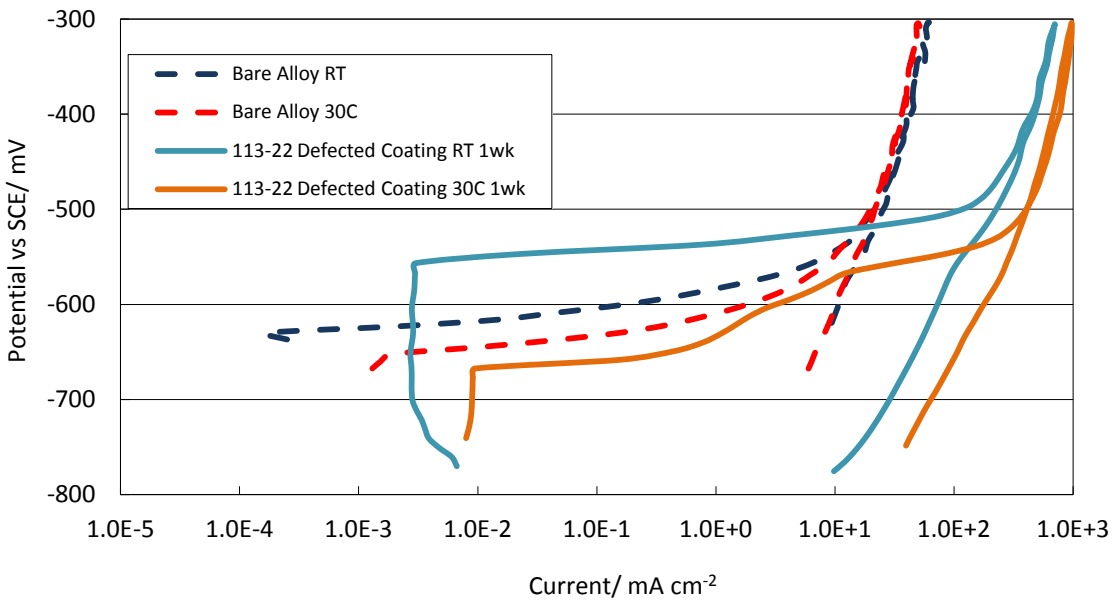

Figure 5.4 – DC Polarisation curves of bare and 113-22 coated AA2024-T3 with a defect in 2M NaCl

Pre-exposure of the coated samples in 2M sodium chloride solution for one week instead of 48 hours caused significant changes in the potentiodynamic corrosion behaviour. Figure 5.4 again shows the anodic polarisation curves for bare AA2024-T3 tested in 2M sodium chloride large cell at room temperature and 30°C as dashed lines and the defected 113-22coated samples as solid lines. The rest potential for the defected 113-22 coated sample at room temperature after one week decreased to -760mV but the pitting potential was raised to -556mV, creating a passive potential range of almost 200mV. A similar raising of the pitting potential was exhibited in the bare metal tests, in section 3.2.2, for strontium chromate concentrations greater than $1x10^{-3}$M, although bare metal tests were performed after 48 hours of immersion whilst the polarisation tests in this section required a week of immersion to exhibit anodic inhibition. The lowering of the rest potential was also exhibited in the bare metal tests, although more markedly at higher

temperatures (e.g. 25°C and 30°C) rather than at room temperature. This would suggest that the protection provided by chromate species is time-dependent.

For the 30°C test, the rest potential fell to -731mV, but the pitting potential did not change significantly at -667mV. The lowering of the rest potential on bare metal tests at 30°C was seen at lower concentrations of strontium chromate ($1x10^{-5}$M and $1x10^{-4}$M) but was not seen at higher concentrations. However, lower concentrations of strontium chromate did not affect the pitting potential of the alloy, although higher concentrations (>$1x10^{-3}$M) showed a stepped anodic line. A second 'inflection'/increase was observed on the anodic line of the defected coated sample where the corrosion current increased more slowly with potential up to approximately -576mV, although the corrosion current was already fairly high at 1mA cm^{-2} before the inflection began. It is uncertain what these 'inflections' correspond to (possibly a second breakdown).

It can be seen in this section that the inhibitive species in the 113-22 epoxy paint can show corrosion protection in potentiodynamic polarisation tests if the sample is pre-immersed in solution for enough time. However, increasing the temperature of the system by a relatively small increment of 10°C significantly affects the behaviour of the inhibitive pigments. Direct current polarisation tests performed after 48 hours in defected 113-22 coated samples showed no effect of the inhibitor yet did demonstrate protective qualities when the sample is immersed for seven days. The downwards shift is likely to be cathodic inhibition due to deposition of Cr_2O_3. This hold at low potential, where pitting is not possible, may mean that pit initiation is delayed when the sweep is run. These studies show the importance of not relying simply on short-term tests. The next section will use EIS on defected coated samples to investigate the effect of inhibitive pigments in paint.

5.3 Electrochemical Impedance Spectroscopy on Defected Coated AA2024-T3

5.3.1 Equivalent circuit

The equivalent circuit shown in figure 5.5, as used in section 2.4.3, can be used to represent the entire electrochemical system, which will give a response with three separate time constants. However, R_{defect} is now much smaller than $R_{coating}$ so that the response for the parallel combination of $C_{coating}$ and R_{defect} will be too fast to see.

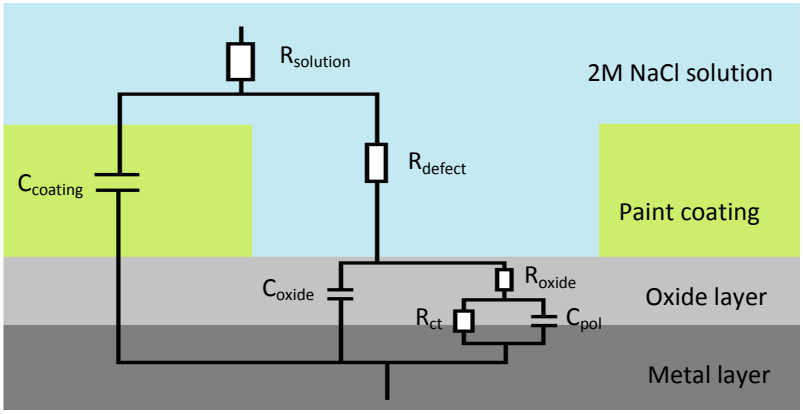

Figure 5.5 – Schematic of model circuit of system under investigation

Real EIS data collected in the experiments could not distinguish three time constant response but only two time constant response. Accordingly, figure 5.6 shows the equivalent circuits used to model the EIS data. The models shown are the same as the models used in chapter 3, section 3.2.3, as the investigated system is expected to be the exposed bare metal at the defect.

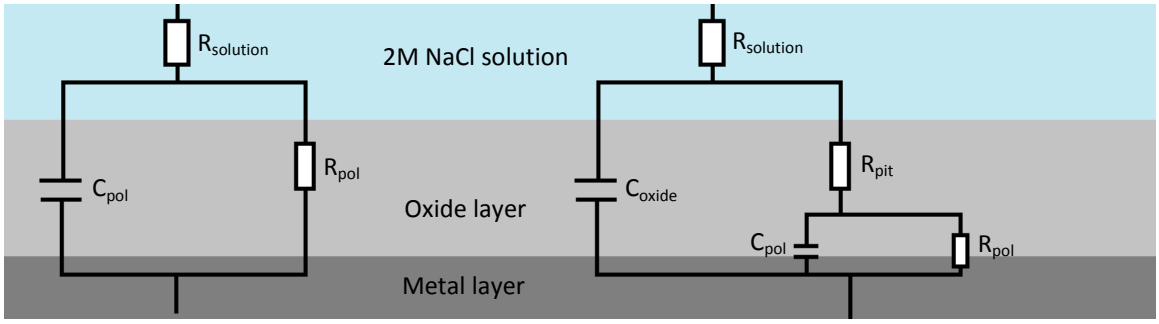

Figure 5.6 – (a) R(QR) model circuit for one time constant response, (b) R(Q(R(QR))) model circuit for two time constant response

The R(Q(R(QR))) model shows R_1 as the solution resistance, R_2 as the oxide or pit resistance and R_3 as the polarisation resistance, R_{pol}. C_{oxide} represents the capacitance of the oxide and C_{pol} is the polarisation capacitance. R_{pol} and C_{pol} represent corrosion processes at the sample-solution interface. The simpler R(QR) model is used when it could not be distinguished two time constants from the EIS data. R_{pit} and C_{pit} are combined with R_{pol} and C_{pol} to represent the total electrochemical response with a single time constant.

5.3.2 Preliminary EIS Testing in Large Volume Cell

Initially, EIS measurements were continued in a large volume cell, results are shown below for a 113-22 coating that performs effectively in industry. Defects in the coating were made using a 1mm width tool. The EIS data shown in figures 5.6 and 5.7 are from an experiment on a defected 113-22 coated sample tested over 28 days. The DC polarisation tests above have revealed that the protection provided by chromate is time dependent and so the coated sample was tested for an extended time.

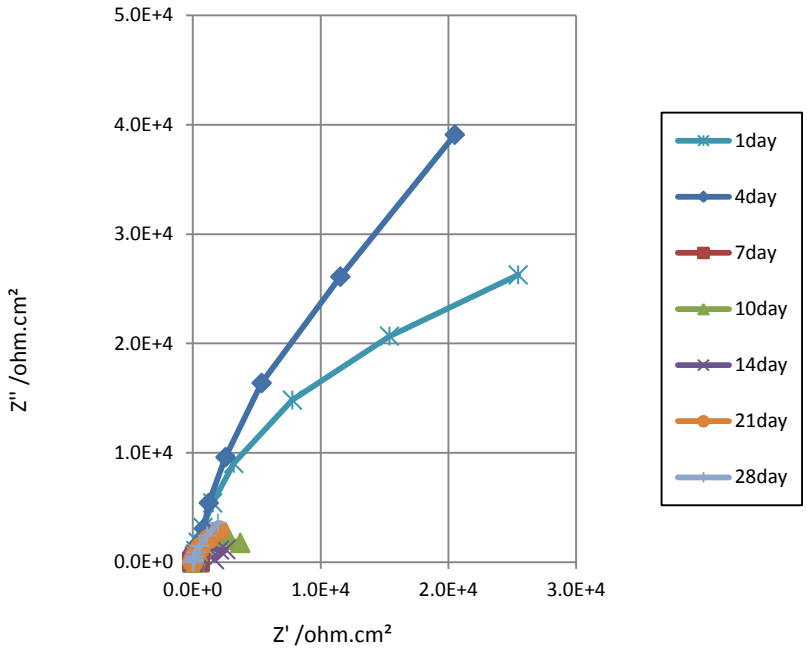

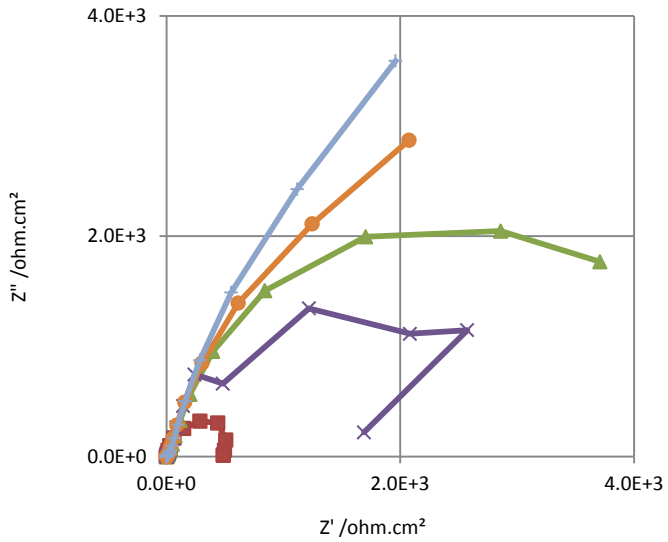

Figure 5.7 – a) Nyquist plots of defected 113-22 coated AA2024-T3 in 2M NaCl over 28days,

b) Nyquist plots for 7-28 days

From figure 5.7, it can be seen that the size of the semicircles in the Nyquist plots increase from day 1 to day 4, but then decrease rapidly after the day 4 measurement. After the drop in day 4, the size of the semicircle does not recover to its initial size and the 'collapsed semicircle' shapes seen on day 7 and day 14 of figure 5.8b suggest that the alloy is pitting. Resistance falls rapidly during the test. The Bode plot, shown in figure 5.9, also shows the decrease in impedance in the mid to low frequency measurements from day 7 and beyond. Calculated parameters from equivalent circuit fits are presented in table 5.1.

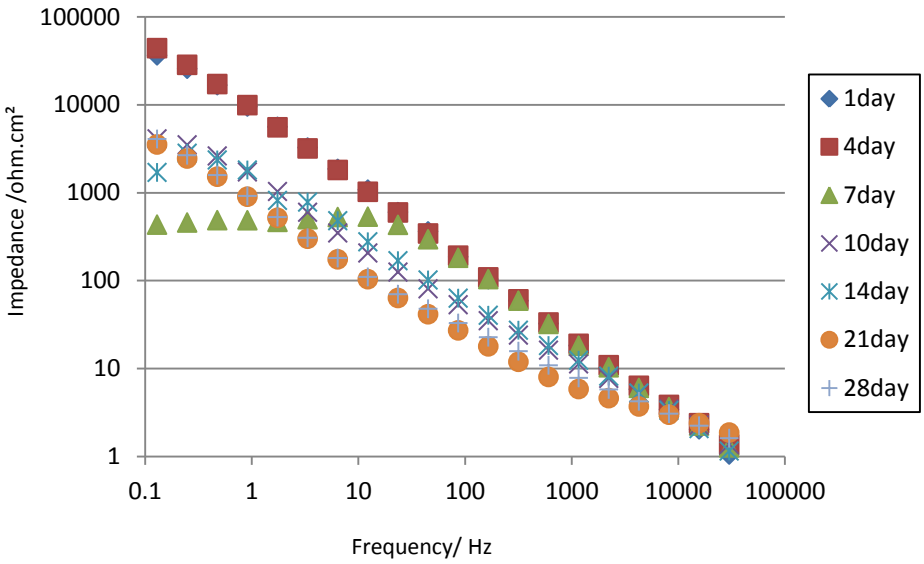

Figure 5.8 – Bode plots of defected 113-22 coated AA2024-T3 in 2M NaCl over 28days

Time (days)	Equivalent Circuit Model	CPE ($x10^{-5}$ $S{\cdot}s^{-n}cm^{-2}$) C_{oxide}	Freq. Power (n)	Resistance ($x10^{3}\Omega cm^{2}$) R_{oxide}	CPE ($x10^{-5}$ $S{\cdot}s^{-n}cm^{-2}$) C_{pol}	Freq. Power (n)	Resistance ($x10^{4}\Omega cm^{2}$) R_{pol}	Chi-squared ($x10^{-2}$)
1	R(Q(R(QR)))	2.0	0.89	5.0	6.3	0.68	50.5	$5.10x10^{-3}$
4	R(Q(R(QR)))	2.5	0.86	16.4	3.0	0.53	78.4	$3.76x10^{-2}$
7	R(QR)	1.6	0.92	0.5	-	-	-	$1.51x10^{-1}$
10	R(Q(R(QR)))	11.9	0.85	5.2	35.6	1	1.1	$5.70x10^{-3}$
14	R(QR)	13.0	0.73	3.2	-	-	-	$2.56x10^{-1}$

Table 5.1 – Parameters of fitted EIS data for defected control-coated AA2024-T3 in 2M NaCl

The area-corrected polarisation resistance, R_{pol}, is in the region of $10^{5}\Omega$ for the first 4 days, which is similar to the R_{pol} measurements for a bare alloy in high concentrations (>1mM) of strontium chromate (and 2M sodium chloride), seen in section 3.2.1.. So in first two measurements indicate that the inhibitive pigment is providing extra corrosion protection, but from day 7, R_{pol} falls dramatically and reverts to values similar to a bare alloy in 2M sodium

chloride solution with no strontium chromate ($1x10^{3-4}\Omega$). The capacitance value also increases significantly and could be because the active area increases. From SAM microscopy, in figure 5.9, we can identify corrosion undercutting the coating. From 7 days to 14days, R_{pol} recovers slightly but is still very low. This suggests that the inhibitor released from the paint coating can provide some protection when samples are first immersed into aggressive solution, but the protection falls away rapidly after one week.

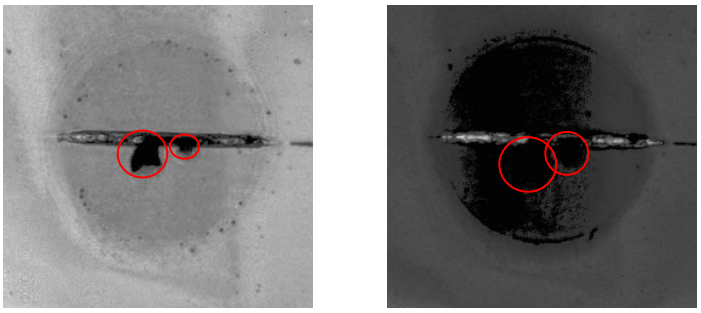

Figure 5.9 – a) Scanning acoustic micrograph at 113-22 underneath coating, b) SAM micrograph close to surface of metal

Scanning acoustic microscopy was used to examine the samples under the surface of the coating after 28 days of EIS testing in full immersion of 2M NaCl solution. This was performed by setting the width of the receiving 'gate' so that micrograph shows the reflected sound waves of a particular depth. Figure 5.9 reveals pits that have also formed alongside the defect beneath the coating (circled in red), and figure 5.9b shows that at a lower depth, at the coating-metal interface, the pits are very large. Unlike the fully-intact coating tests, no filiform corrosion is seen and pits appear to initiate from the defect. The pits grow away from the defect, rather than centred on the defect.

5.3.3 Use of small volume test cell for EIS measurements

The small volume test cell, shown in figure 5.10 below and found in section 2.2.1.2, was used to record the majority of the EIS data. Filter paper will suppress convection so that chromate disperses by diffusion so that in principle, the surface of the paint could be at or close to saturation (if diffusion of chromate away from the surface is slow enough). However, chromate will still need to diffuse to the bare metal to protect the exposed surface.

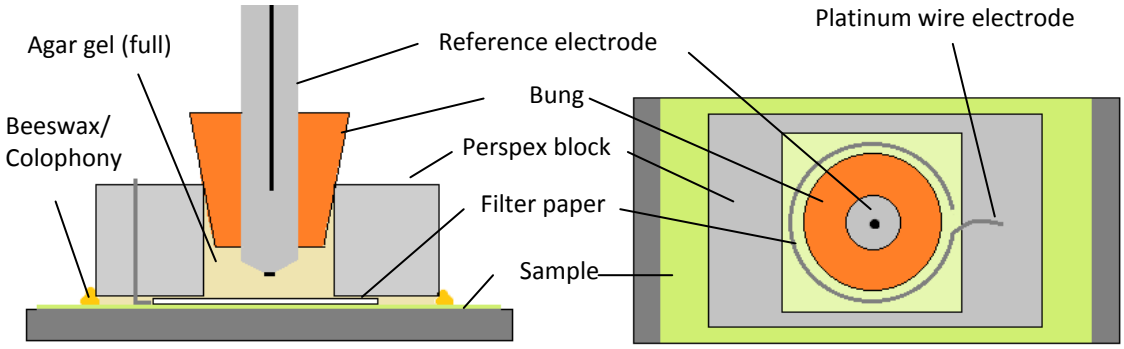

Figure 5.10 – Schematic of cell used for small volume electrochemical testing

EIS experiments initially performed in the large volume test cell found that chromate pigment only had limited benefit. The small volume test cell reduced the volume of aggressive solution and prevented convective stirring so that a concentration gradient is established while chromate is released. This better emulates real situations where an aircraft will be exposed to smaller volumes of solution, e.g. condensation, rainfall with high concentrations of salt (aircrafts are not expected to survive immersion in salty water!).

5.4 Electrochemical Impedance Spectroscopy Testing in Small Volume Cell

5.4.1 Non-inhibitive Pigmented Control Coating

For EIS experiments performed in the small volume cell, as described in section 2.3.2, with a narrow scalpel sized defect were fitted to the same model circuits as bare metal (fig5.6).

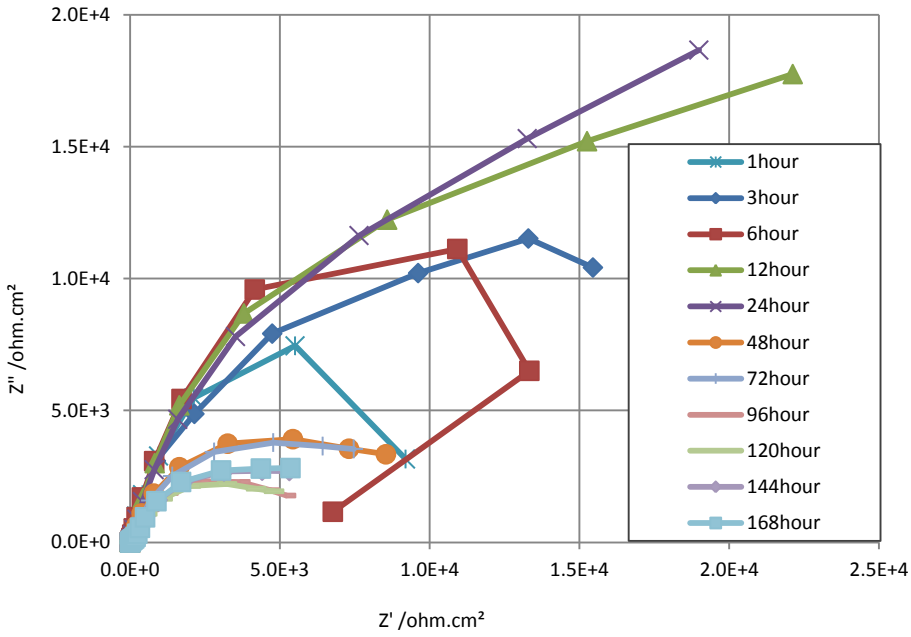

Figure 5.11 – Nyquist plots of control coated AA2024-T3 with scalpel defect in 2M NaCl over 168hours

In figure 5.11, it can be seen for the control coating that the size of the semicircles in the Nyquist plots increase during the first 24 hours of measurements, but decrease rapidly after 24 hours. Calculated parameters from equivalent circuit fits are presented in table 5.2. From the Nyquist and Bode plots in figures 5.12 and 5.13, it can be seen that the low frequency measurements exhibit a sharp drop in impedance for the first three measurements, 1-6 hours. This was also seen in repeat experiments. Such a shape can result from inductive behaviour, but further investigation described later in section 5.4, suggests that it is the low frequency Nyquist semicircle collapsing with time and the EIS equipment measuring a smaller semicircle. This

would be related to changes in the sample whilst EIS measurements are taking place and electrochemical processes, such as metastable/stable pitting corrosion, would cause decreases in impedance. It is likely that this behaviour tends to appear in the initial hours of immersion due to the sample being introduced into a high chloride environment.

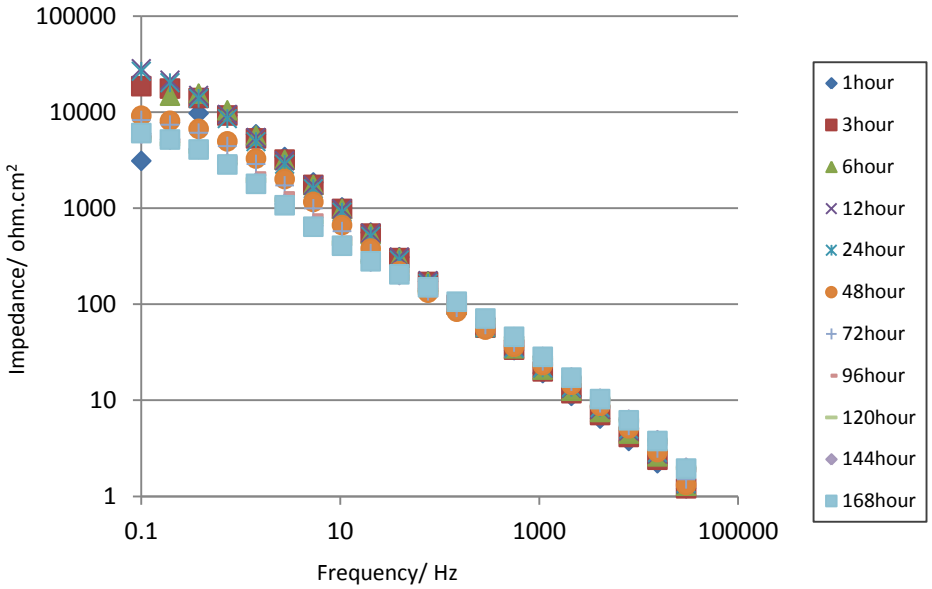

Figure 5.12 – Bode plots of control coated AA2024-T3 with scalpel defect in 2M NaCl over 168hours

Time (hours)	Equivalent Circuit Model	CPE ($x10^{-5}$ $S{\cdot}s^{-n}cm^{-2}$) C_{oxide}	Freq. Power (n)	Resistance ($x10^{1}\Omega cm^{2}$) R_{oxide}	CPE ($x10^{-5}$ $S{\cdot}s^{-n}cm^{-2}$) C_{pol}	Freq. Power (n)	Resistance ($x10^{4}\Omega cm^{2}$) R_{pol}	Chi-squared ($x10^{-2}$)
1	R(Q(R(QR)))	1.3	0.2	7.1	0.6	0.95	1.2	9.8
3	R(Q(R(QR)))	1.2	0.92	3.4	1.6	0.82	2.7	8.4
6	R(Q(R(QR)))	1.3	0.91	8.2	0.9	0.91	2.0	5.5
12	R(Q(R(QR)))	1.5	0.88	5.0	1.2	0.84	4.1	0.3
24	R(Q(R(QR)))	0.9	0.92	3.2	2.3	0.81	4.5	0.4
48	R(Q(R(QR)))	2.7	0.82	11.2	1.7	0.88	1.0	0.2
72	R(Q(R(QR)))	3.6	0.79	22.4	1.8	0.90	1.0	0.4
96	R(Q(R(QR)))	4.8	0.75	24.5	1.9	0.95	0.6	0.2
120	R(Q(R(QR)))	5.5	0.77	10.4	7.6	0.84	0.6	0.4
144	R(Q(R(QR)))	4.3	0.76	32.3	4.5	0.88	0.7	0.3
168	R(Q(R(QR)))	4.6	0.75	36.0	4.6	0.89	0.7	0.3

Table 5.2 – Parameters of fitted EIS data for control-coated AA2024-T3 with scalpel defect in 2M NaCl

Looking at the polarisation resistance, R_{pol}, in table 5.2, we see that the resistance increases more or less continuously from 10kΩ to 45kΩ. Comparing to the bare alloy values in section 3.2.1, the polarisation resistance after 24 hours is higher than at 72 hours, which is the same as the results seen here. The increase in resistance over the initial 24 hours is not recorded in chapter 3, but a repeat of the test shows a similar trend.

Despite the high concentration of chloride present and absence of inhibitive ions, R_{pol} increases at first indicating a decrease in the corrosion rate in the first 24 hours. A graph showing the corrosion resistance against time can be found later in figure 5.13.

This behaviour was seen in a study by Martin et al.; they suggest that the presence of chloride ions decreased the density of oxygen vacancies in the oxide layer and subsequently reduced the charge transport and thus corrosion rate. Another possible explanation could be the increase in oxide layer thickness due to the exposed metal, i.e. exposing defect sodium chloride solution[80]. However, after 24 hours, R_{pol} drops sharply and continues to decrease to $<1x10^4$ Ω and this is can most likely be related to the breakdown of the passive layer and the onset of pitting corrosion.

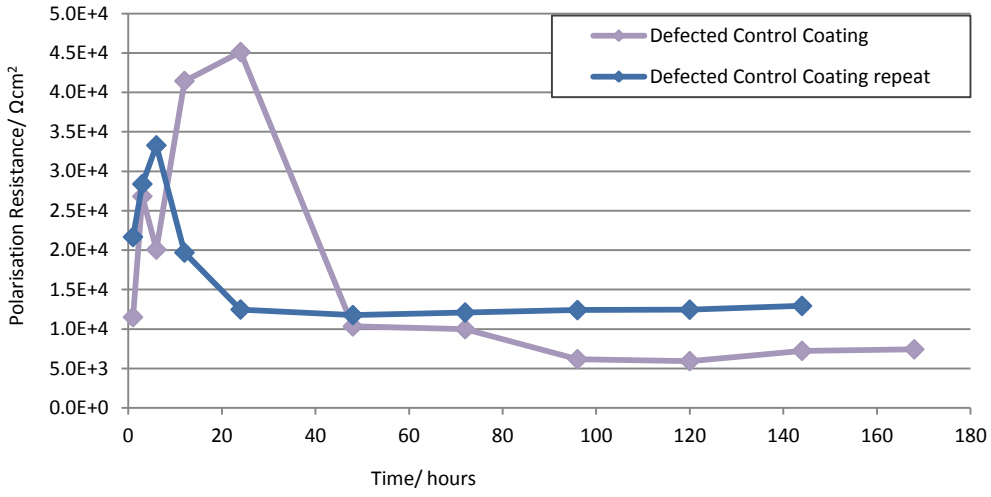

Figure 5.13 – Polarisation resistance against time for control coated sample with scalpel defect

Figure 5.13 shows the polarisation resistance against time for the control coated with scalpel defect samples. The resistance increases during the first 24 hours of immersion before sharply dropping to a value around 10kΩcm^2. The repeat test also shows similar behaviour in the initial increase followed by a rapid decrease.

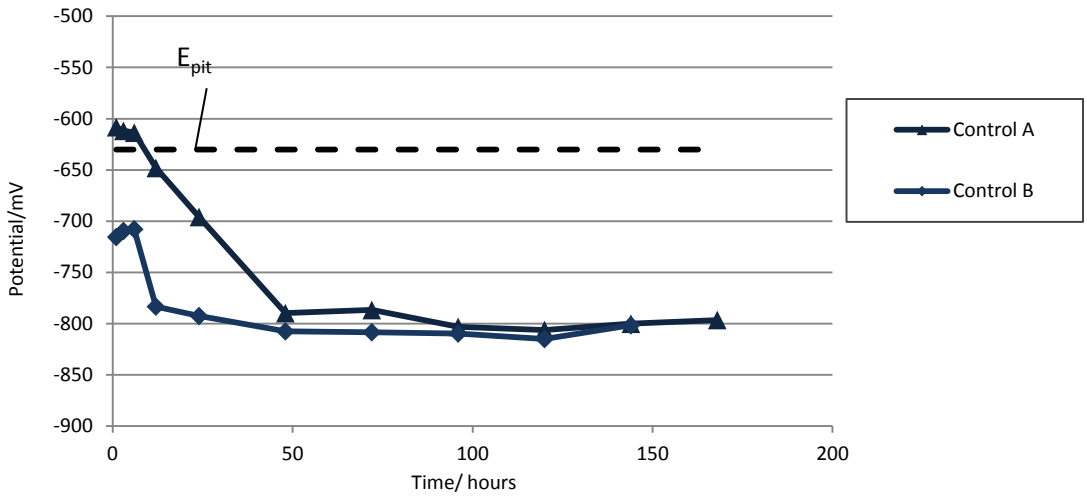

Figure 5.14 – Rest potential of defected coated AA2024-T3 samples before EIS tests

Figure 5.14 shows the free corrosion potential of the sample against time before the impedance measurements were performed. The pitting potential, E_{pit}, is marked by the black dashed line at approximately -630mV (taken from bare alloy measurements in chapter 3). It can be seen that the potential of the control-coated alloy decreased over time, and by 48hours, the potential drops to approximately -800mV and remains there. This is likely to be the onset of stable pitting corrosion.

5.4.2 Chromate-pigmented 113-22 Paint Coating

The same experiments were performed on chromate-pigmented 113-22 coated samples of AA2024-T3 with a scalpel sized defect. This narrow defect was selected to give best access of chromate from the primer to the exposed alloy.

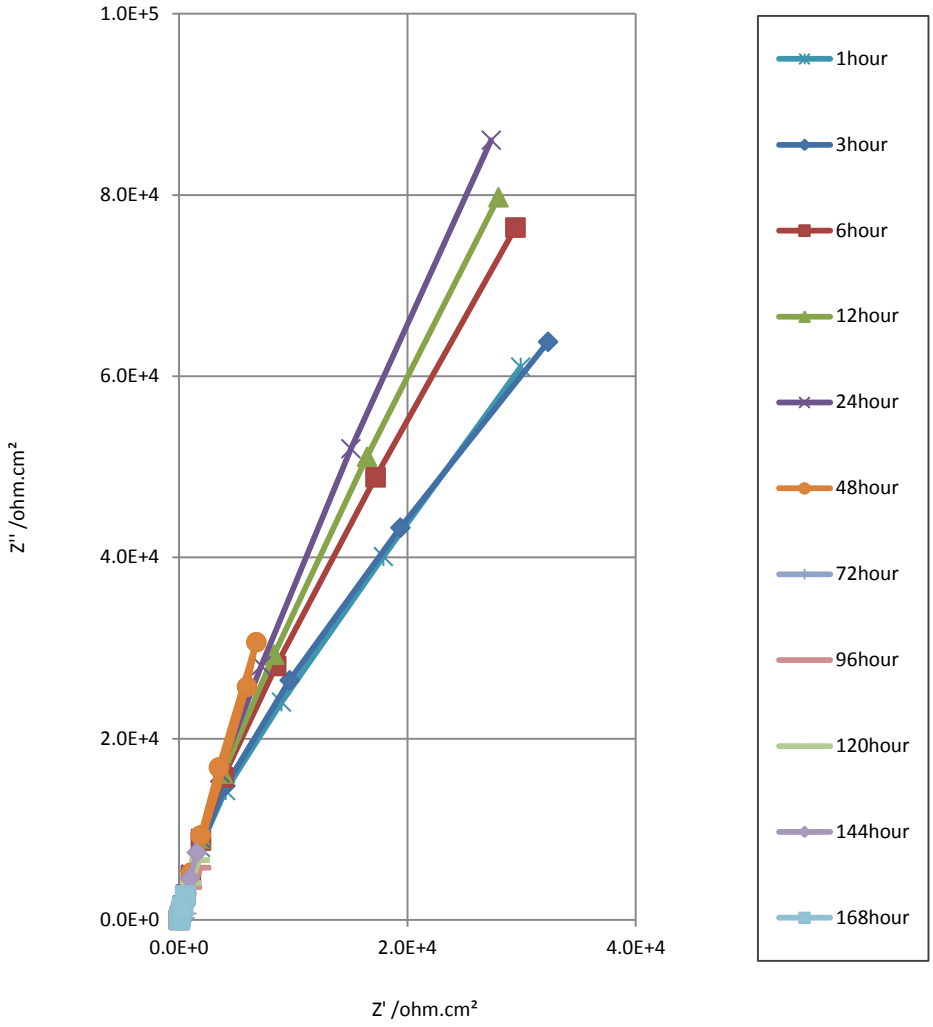

Figure 5.15 – a) Nyquist plots of 113-22 coated AA2024-T3 in 2M NaCl solution over 168 hours,

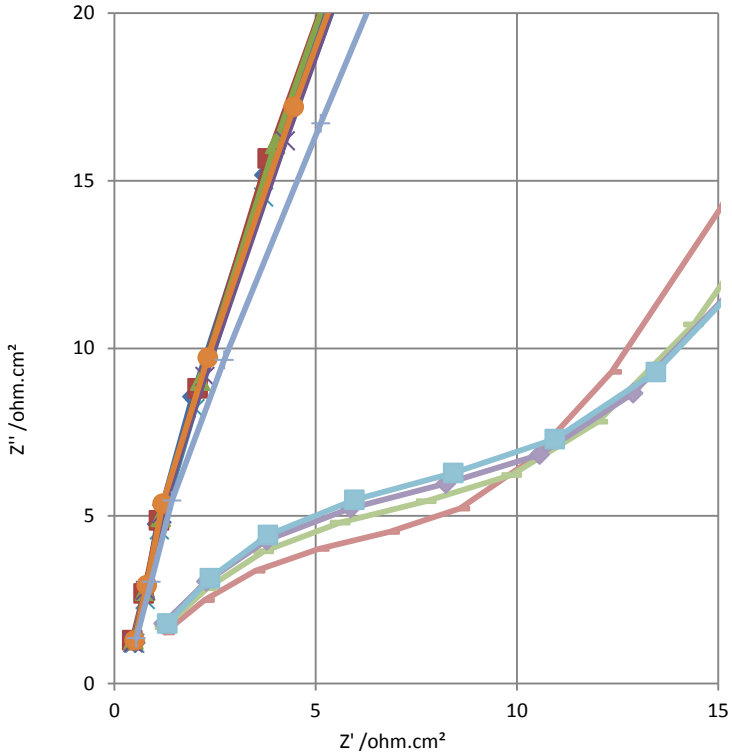

Figure 5.15 – b) High frequency measurements for Nyquist plots of 113-22 coated AA2024-T3 in 2M NaCl solution over 168 hours

From figure 5.15a, only one time constant response can be seen, but on closer inspection of the high frequency region on figure 5.15b, a small second semicircle can be seen to develop as time progresses. Calculated parameters from fitting to the model circuit in table 5.3 show the first semicircle to be very small. Mid to low frequency measurements in figure 5.15a show that a large semicircle can be extrapolated and its size calculated from equivalent circuit models. The size of the semicircles in the Nyquist plots increase in the first 24-48 hours of measurements, but decrease rapidly after 48 hours.

It can be seen more clearly on the Bode plot in figure 5.16 that the low frequency (0.1Hz) measurements for the 48 and 72 hour tests exhibit a smaller portion of the Nyquist circle.

Subsequent measurements show that the impedance of the system recovers, suggesting that the corrosion event occurring during the 72 hour measurement has not continued into stable pitting corrosion.

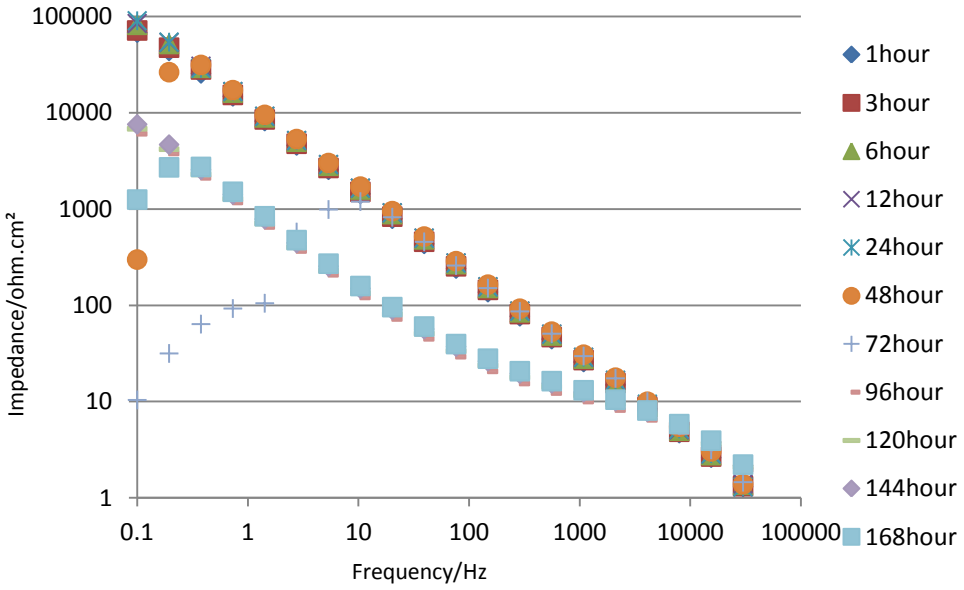

Figure 5.16 – Bode plots of 113-22 coated AA2024-T3 in 2M NaCl solution over 168 hours

Time (hours)	Equivalent Circuit Model	CPE ($x10^{-5}$ $S \cdot s^{-n} cm^{-2}$) C_{oxide}	Freq. Power (n)	Resistance ($x10^{1} \Omega cm^{2}$) R_{oxide}	CPE ($x10^{-5}$ $S \cdot s^{-n} cm^{-2}$) C_{pol}	Freq. Power (n)	Resistance ($x10^{5} \Omega cm^{2}$) R_{pol}	Chi-squared ($x10^{-3}$)
1	R(Q(R(QR)))	0.5	0.99	5.2	1.4	0.81	2.5	1.4
3	R(Q(R(QR)))	0.6	0.96	7.0	1.1	0.81	2.5	1.6
6	R(Q(R(QR)))	0.6	0.96	7.2	1.1	0.80	4.8	1.0
12	R(Q(R(QR)))	0.5	0.97	7.8	1.1	0.80	6.5	1.1
24	R(Q(R(QR)))	0.7	0.95	9.8	0.9	0.80	8.7	6.8
48	R(QR)(QR)	2.9	1	0.7	1.5	0.89	4.3	4.7
72	R(QR)(QR)	2.2	1	0.8	1.9	0.87	0.1	11.6
96	R(QR)(QR)	19.0	0.64	1.3	23.4	0.86	0.7	4.0
120	R(QR)(QR)	13.6	0.66	1.6	21.5	0.85	7.0	4.4
144	R(QR)(QR)	425	0.32	5.1	18.8	0.88	5.7	1.6
168	R(QR)(QR)	516	0.31	9.7	17.2	0.89	1.2	1.1

Table 5.3 – Parameters of fitted EIS data for 113-22-coated AA2024-T3 with scalpel defect in 2M NaCl

From the model parameters in table 5.3, the polarisation resistance, R_{pol}, increases steadily from 0.3MΩ to 0.9MΩ over the first 24 hours. After 24 hours, R_{pol} is higher for the defect than a bare alloy surface in saturated strontium chromate after the same amount of time. However, similar to the control coating, R_{pol} falls after 24 hours and at 72 hours, the resistance fell to 13kΩ, a value close to the tests with no chromate. This suggests that aggressive ions are still able to penetrate the oxide and cause corrosive attack. However, unlike the non-inhibited system, R_{pol} subsequently rises to $7x10^5Ω$. The inhibitive pigment can therefore be preventing the propagation of stable pitting. The polarisation resistance increased a second time after 72hours, but fell away after 120 hours. This cyclic build up and breakdown of resistance was seen in repeats of the test and shown in figure 5.17.

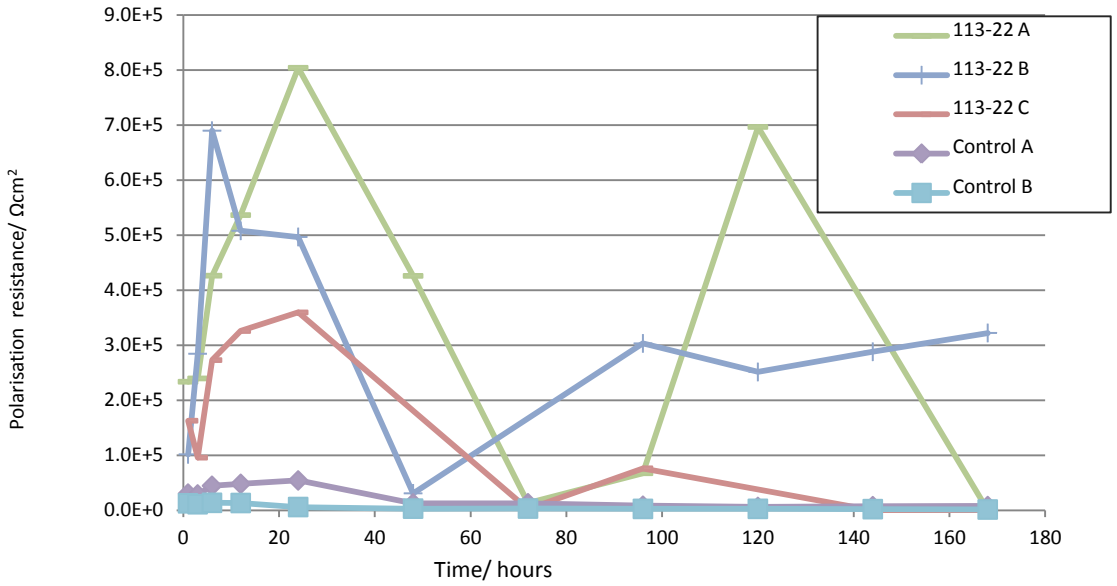

Figure 5.17 – Polarisation resistance against time for 113-22 and control coated samples w/ scalpel defect

Even under these conditions, it appears that stable passivity does not result at a defect from addition of chromate to the primer. However, it can be seen clearly in figure 5.17 that the corrosion protection provided by the inhibitor is significantly greater than the control-coated samples (effectively bare metal with the inclusion of a defect).

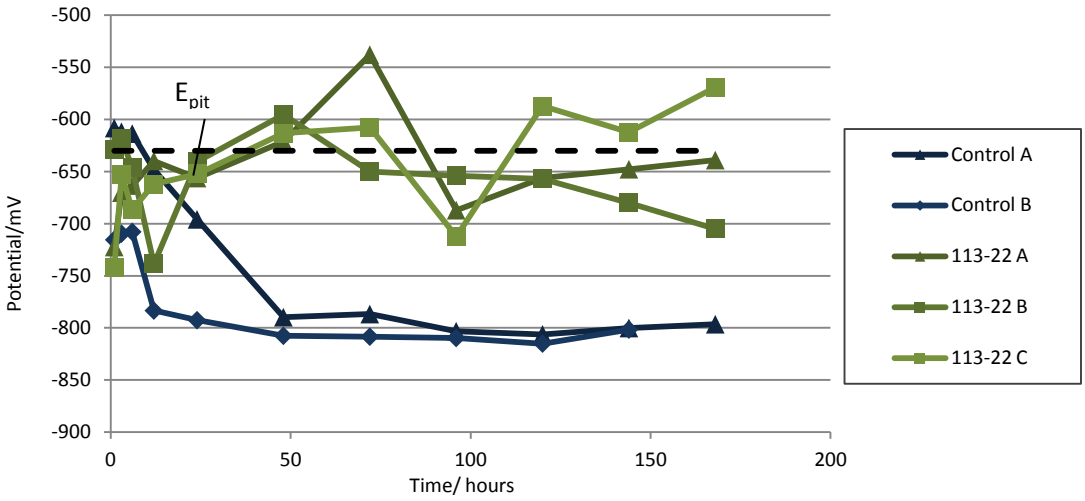

Figure 5.18 – Rest potential of defected coated AA2024-T3 samples before EIS tests

Figure 5.18 shows the free corrosion potentials of the control coated and 113-22 coated samples with a scalpel defect before EIS tests were performed. The potentials of the 113-22 coated samples start off lower than the pitting potential, suggesting rapid cathodic inhibition, but as time progressed, the potential moves towards the pitting potential and above it. The cyclic rise and fall of the potential is similar to the build up and breakdown of polarisation resistance. This would suggest that when the corrosion rate is low (high polarisation resistance), the potential of the sample is below the pitting potential and cathodic inhibition is provided, and when the corrosion rate is high, the sample is pitting and the potential is above the pitting potential.

5.4.3 Different Conditions of Testing

It has been shown in the previous section that although the 113-22 paint does not produce stable passivity, it does retard the rate of corrosion, indicated from the polarisation resistances of the system. Section 4.2.2 revealed that the epoxy paint releases only a limited amount of pigment over a certain period and the majority of the pigment remains isolated within the coating. It is likely that if fresh surfaces in the 113-22 are exposed to solution, further inhibitor

will be released into the system. Sections 5.3.4.3.1 and 5.3.4.3.2 will investigate the corrosion protection of the defected coating when the pigment on the top surface of the paint is washed off before the test or covered with a topcoat so that chromate is only released locally at the damage site. Section 5.3.4.3.3 will study the 113-22 coated system with a defect using a lower concentration of sodium chloride solution, 0.5M NaCl. The tests were performed in the small volume electrochemical cell with agar gel and filter paper.

5.4.3.1 Pre-washed 113-22 Coating with defect

The uncoated edges of 113-22 coated AA2024-T3 panels were sealed with beeswax-colophony, exposing only the 113-22 coating. The panels were then immersed in a large volume of distilled water for one week. After one week, the samples were taken out of the water and air-dried before a scalpel defect was made and tested in 2M NaCl using electrochemical impedance spectroscopy. Under these conditions, no further release of inhibitor should take place from the free surface, but it is expected that there will be local release at the freshly cut edge.

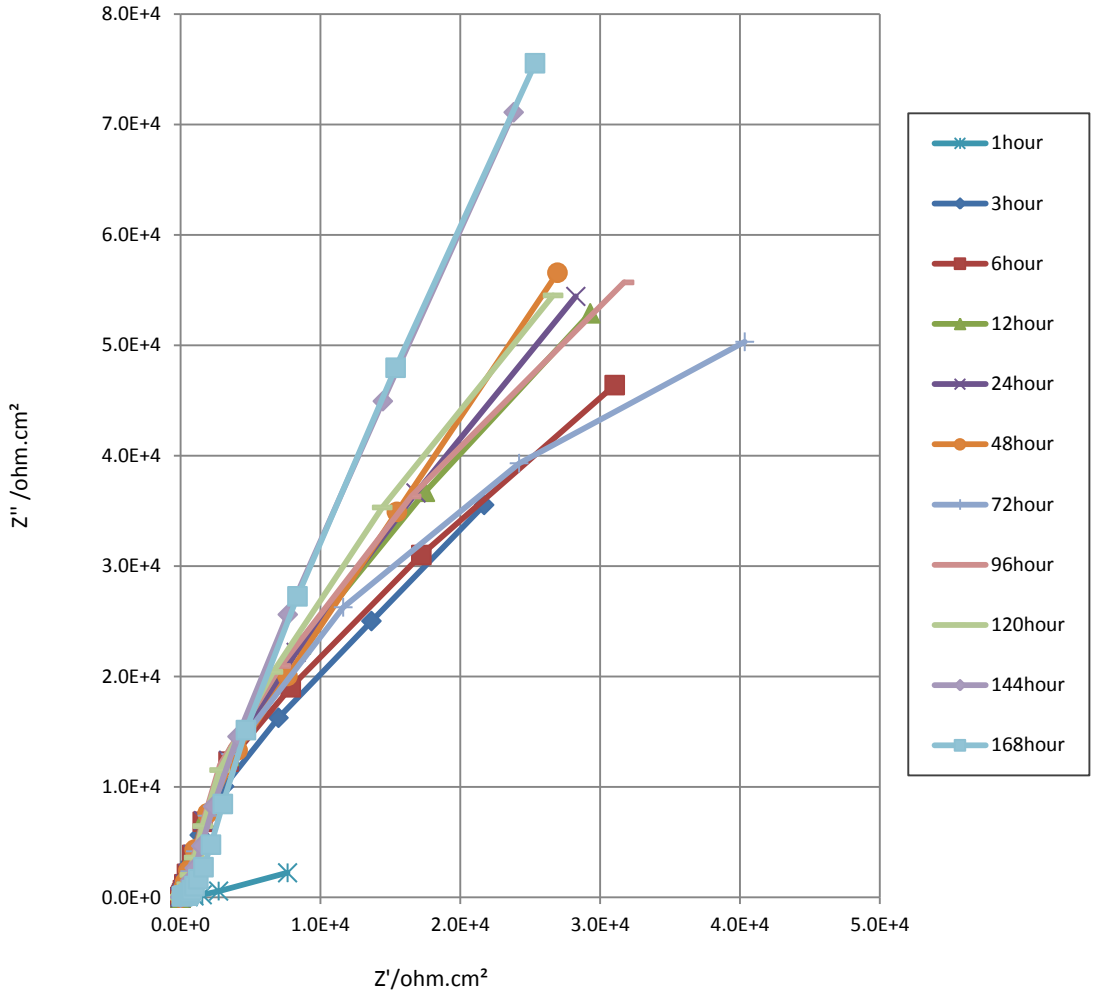

Figure 5.19 – Nyquist plots of 113-22 coated AA2024-T3 with scalpel defect in 2M NaCl over 168 hours

From figure 5.19, a large semicircle can be fitted to the Nyquist plots. The measurement at 1 hour shows the impedance dropping at low frequencies, seen more clearly in the Bode plot on figure 5.20. As time progresses, the size of the semicircle in the Nyquist plot and the impedance seen in the Bode plots increase. EIS data is fitted to the model circuits shown in figures 5.6 and calculated parameters are shown in table 5.4.

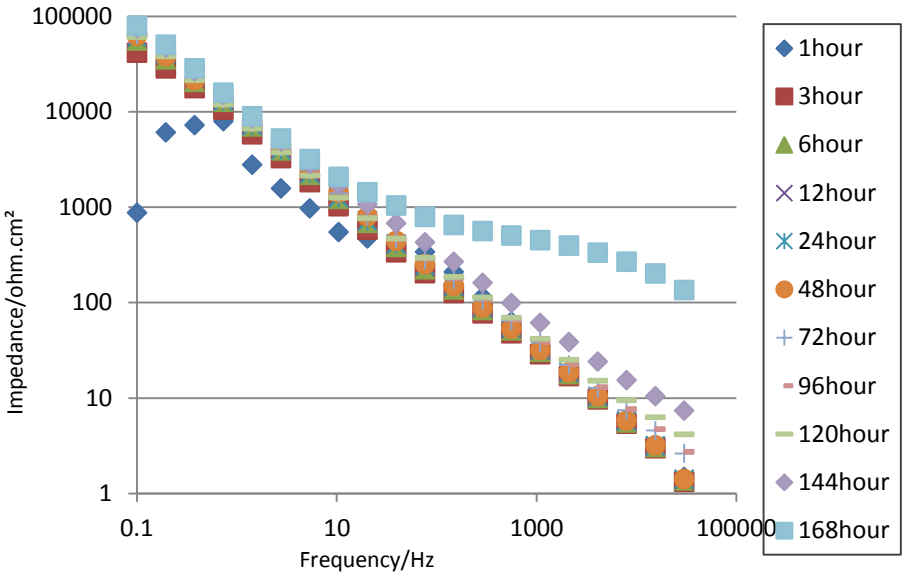

Figure 5.20 – Bode plots of 113-22 coated AA2024-T3 with scalpel defect in 2M NaCl over 168 hours

Time (hours)	Equivalent Circuit Model	CPE ($x10^{-6}$ $S \cdot s^{-n} cm^{-2}$) C_{oxide}	Freq. Power (n)	Resistance ($x10^{2} \Omega cm^{2}$) R_{oxide}	CPE ($x10^{-6}$ $S \cdot s^{-n} cm^{-2}$) C_{pol}	Freq. Power (n)	Resistance ($x10^{5} \Omega cm^{2}$) R_{pol}	Chi-squared ($x10^{-3}$)
1	R(Q(R(QR)))	6.6	0.95	12.1	18.0	1	0.05	336
3	R(Q(R(QR)))	8.6	0.93	1.3	18.4	0.82	1.2	5.8
6	R(Q(R(QR)))	8.2	0.93	1.5	27.0	0.86	1.7	3.8
12	R(Q(R(QR)))	18.5	0.84	7.2	2.3	1	2.1	1.8
24	R(Q(R(QR)))	17.1	0.85	6.2	4.2	0.92	2.3	1.4
48	R(Q(R(QR)))	4.7	1	1.3	16.6	0.78	3.1	2.6
72	R(Q(R(QR)))	9.1	0.92	5.7	8.1	0.88	1.2	8.4
96	R(Q(R(QR)))	11.2	0.90	9.3	9.4	0.88	1.8	2.0
120	R(Q(R(QR)))	12.5	0.89	11.8	9.4	0.87	2.1	1.9
144	R(Q(R(QR)))	16.1	0.82	60.0	2.4	1	9.4	2.6
168	R(Q(R(QR)))	14.8	0.82	74.1	2.7	1	8.9	4.0

Table 5.4 – Parameters of fitted EIS data for 113-22-coated AA2024-T3 with scalpel defect in 2M NaCl

Looking at the polarisation resistance, R_{pol}, in table 5.4, we see that the resistance of the first hour measurement is very low and it is likely that the sample is pitting. At 1hour immersion, there will be little chromate released. However, R_{pol} increases over time and a graph is plotted in figure 5.21.

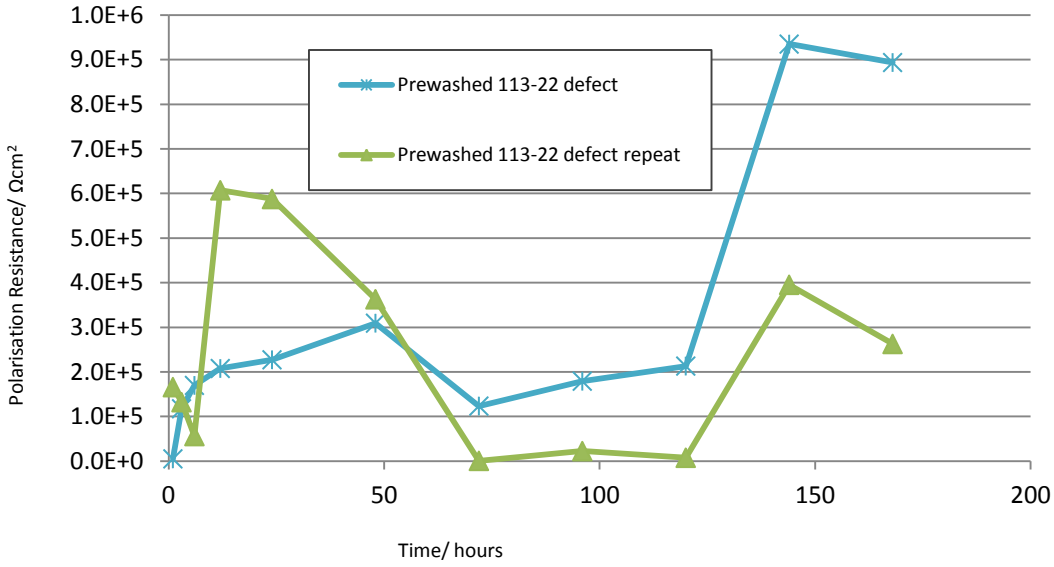

Figure 5.21 – Polarisation resistance against time for prewashed 113-22 coated samples

The prewashed samples still exhibit a higher polarisation resistance compared to the control paint system in section 5.4.3.1 and despite there being only limited release of inhibitor from the fresh cut surfaces, R_{pol} values reach maxima of 0.9MΩ and 0.6MΩ for the two samples, which are comparable to an unwashed 113-22 coated sample. The prewashed 113-22 coated samples also exhibit the cyclic build up and breakdown of resistance. This comparison tells us that the 113-22 coating continues to provide corrosion protection after the inhibitor has been leached out of the top surface and the sample is exposed to a fresh chloride solution with only the fresh-cut edge able to release chromate. Results indicate that inhibitor is released from the fresh-cut edge at amounts high enough to provide protection.

5.4.3.2 Topcoated 113-22 Coating with defect

External parts of an aircraft have an additional topcoat over the 113-22 coating. This will also block inhibitor release from the free top surface, so EIS experiments were also performed on a topcoated 113-22 coated sample with a scalpel defect through both paint layers to expose the metal alloy, to further explore how local chromate release at a damage site might control corrosion.

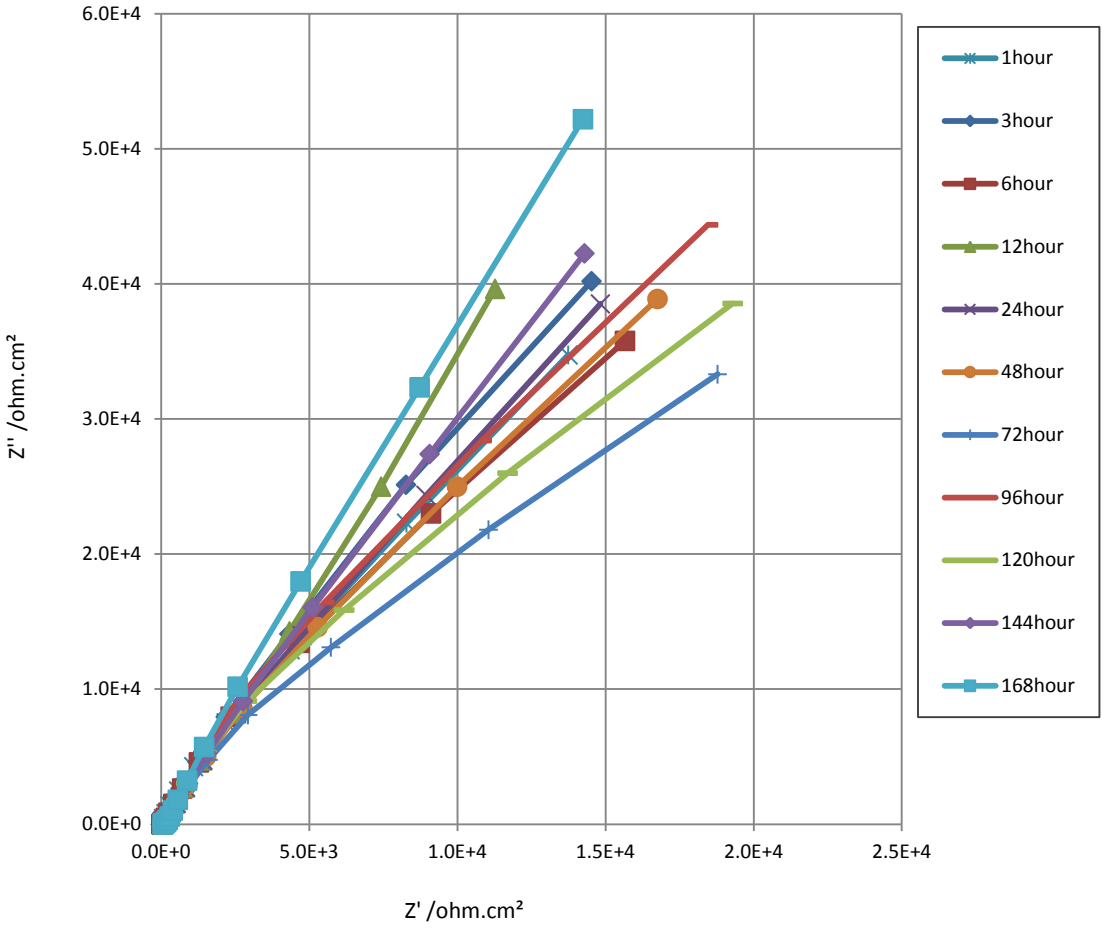

Figure 5.22 – Nyquist plots of 113-22 coated AA2024-T3 with additional topcoat and scalpel defect in 2M NaCl over 168 hours

Figure 5.22 shows a large semicircle can again be fitted to the Nyquist plots. The diameter of the semicircle in the Nyquist plot increases as time progresses. The high frequency measurements on the Bode plot in figure 5.23 show an increase in impedance after 3 hours. The impedance increases initially which implies that inhibitor is likely being released as the corrosion resistance of the system increases.

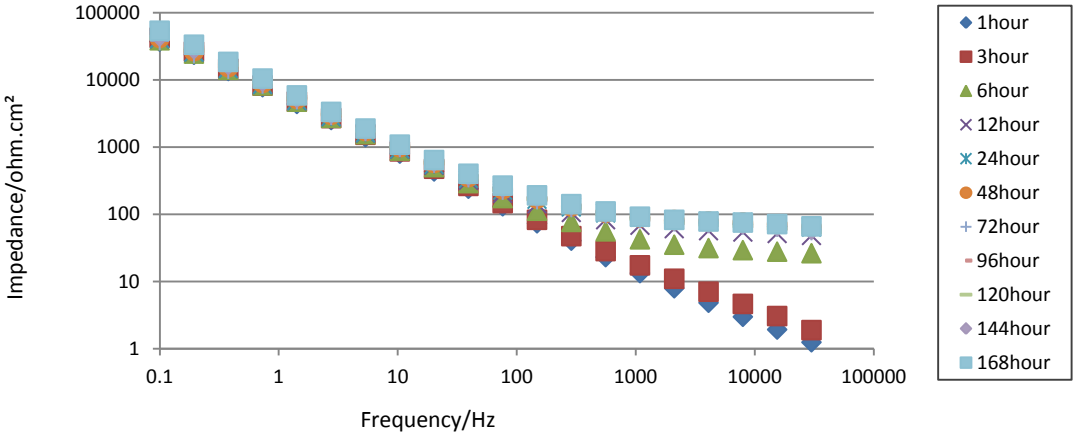

Figure 5.23 – Bode plots of 113-22 coated AA2024-T3 with additional topcoat and scalpel defect in 2M NaCl over 168 hours

Time (hours)	Equivalent Circuit Model	CPE ($x10^{-6}$ $S \cdot s^{-n} cm^{-2}$) C_{oxide}	Freq. Power (n)	Resistance ($x10^{1} \Omega cm^{2}$) R_{oxide}	CPE ($x10^{-5}$ $S \cdot s^{-n} cm^{-2}$) C_{pol}	Freq. Power (n)	Resistance ($x10^{5} \Omega cm^{2}$) R_{pol}	Chi-squared ($x10^{-3}$)
1	R(Q(R(QR)))	4.8	1	0.5	3.0	0.84	1.9	2.5
3	R(Q(R(QR)))	24.9	0.84	2.9	0.7	0.93	2.8	2.6
6	R(Q(R(QR)))	2.7	0.82	1.9	3.2	0.83	2.7	5.6
12	R(Q(R(QR)))	27.4	0.91	2.8	3.3	0.84	7.7	2.1
24	R(Q(R(QR)))	0.5	0.80	8.9	3.4	0.82	5.2	5.8
48	R(Q(R(QR)))	1.1	0.73	8.7	3.2	0.82	3.3	5.6
72	R(Q(R(QR)))	0.7	0.80	8.1	3.4	0.81	1.6	4.9
96	R(Q(R(QR)))	1.4	0.73	8.4	2.8	0.84	3.6	7.4
120	R(Q(R(QR)))	1.9	0.71	8.6	2.8	0.83	2.3	7.6
144	R(Q(R(QR)))	32.3	0.85	5.2	3.0	0.84	4.5	2.2
168	R(Q(R(QR)))	42.5	0.81	8.2	2.6	0.87	7.7	1.5

Table 5.5 – Parameters of fitted EIS data for defected 113-22-coated AA2024-T3 with additional topcoat and scalpel defect in 2M NaCl

Calculated parameters for the EIS data are plotted in table 5.5. The polarisation resistance, R_{pol}, starts at 0.2MΩ and builds steadily to 0.8MΩ before falling, again exhibiting the dynamic buildup and breakdown of resistance. A graph plotting R_{ct} against time is shown below.

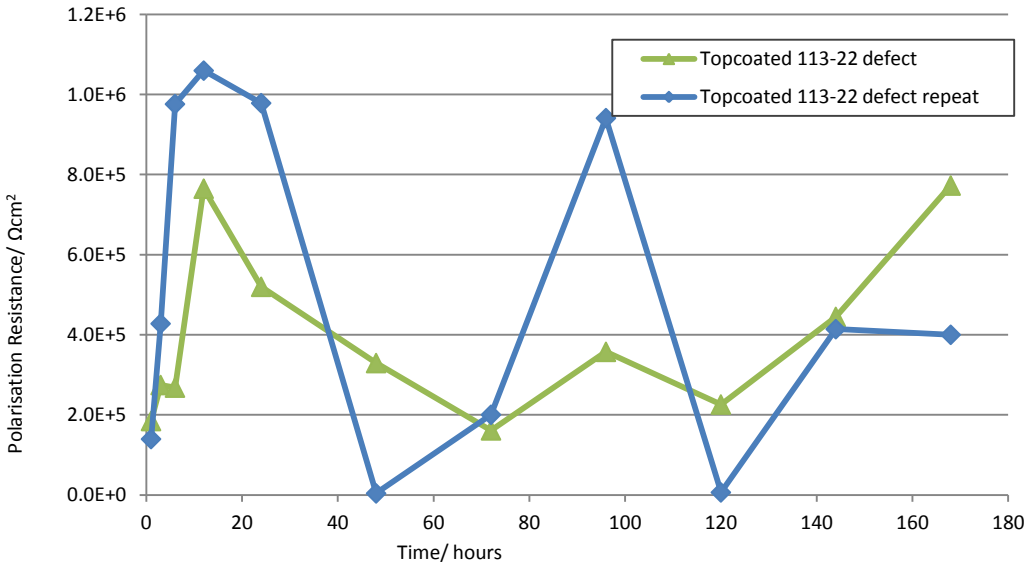

Figure 5.24 – Polarisation resistance against time for topcoated 113-22 coated samples

The additional topcoat layer potentially limits inhibitor release to the defect site with no release into the bulk solution away from the defect. However, whilst high R_{pol} values are recorded, the resistance still breaks down (and later recovers). This comparison tells us that the 113-22 coating provide similar corrosion protection even when the top surface of the 113-22 is covered by a topcoat. Results therefore indicate that enough inhibitor is released from the freshly cut edge to provide protection and that local release at the defect site is the most important cause of inhibition.

5.4.3.3 Lower Concentration of Aggressive Ions

It is widely recognised that the concentration of inhibitor required depends on the level of aggressive ions [15]. Böhni and Uhlig investigated the effects of aggressive ions and inhibitive ions and found that there was a relationship between concentrations of the two species and the pitting potential. The extremely high concentration of sodium chloride (2M) used here could possibly overwhelm the amount of inhibitor available and prevent continuous protection. Therefore, experiments were performed where a lower concentration (0.5M) sodium chloride was used.

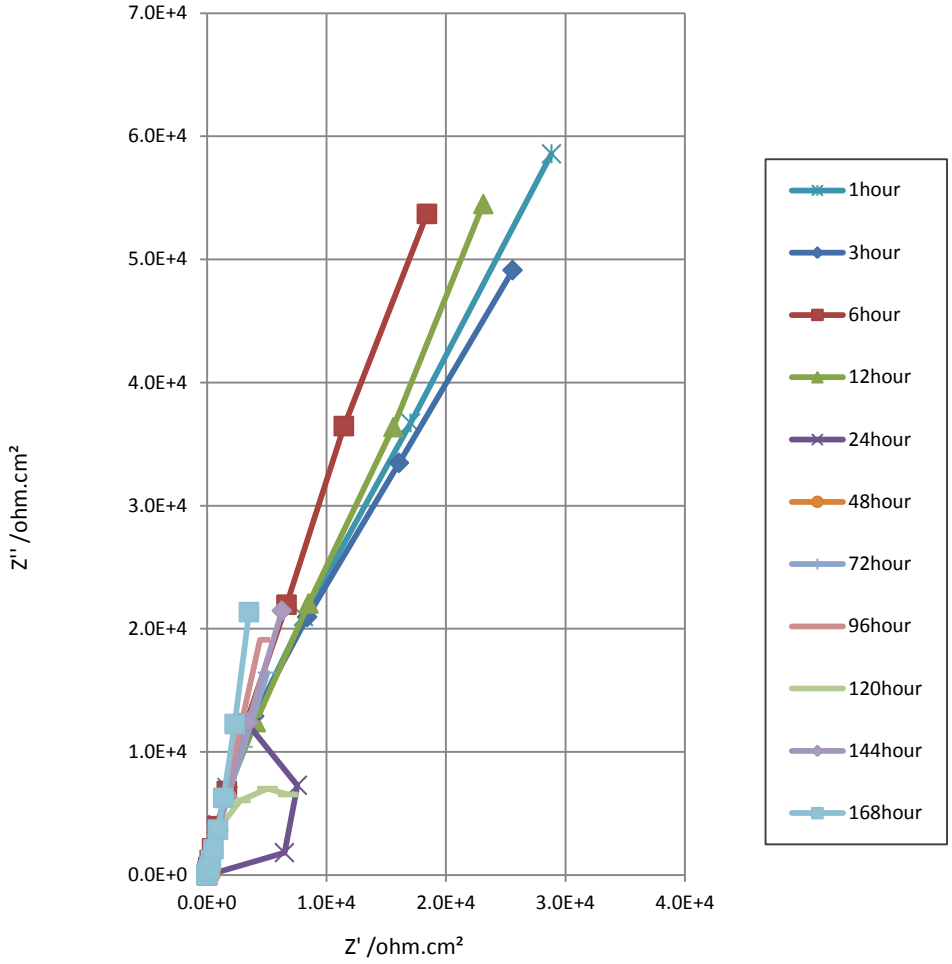

Figure 5.25 – Nyquist plots of 113-22 coated AA2024-T3 with a scalpel defect in 0.5M NaCl over 168 hours

Figure 5.25 show the Nyquist plots for 113-22 coated AA2024-T3 with a scalpel defect. The size of the lower frequencies semicircle is not significantly larger than in the 2M sodium chloride experiments. Similar to the 2M NaCl tests, the semicircle collapses after 24-48 hours. Figure 5.26 shows a sequence of Bode plots.

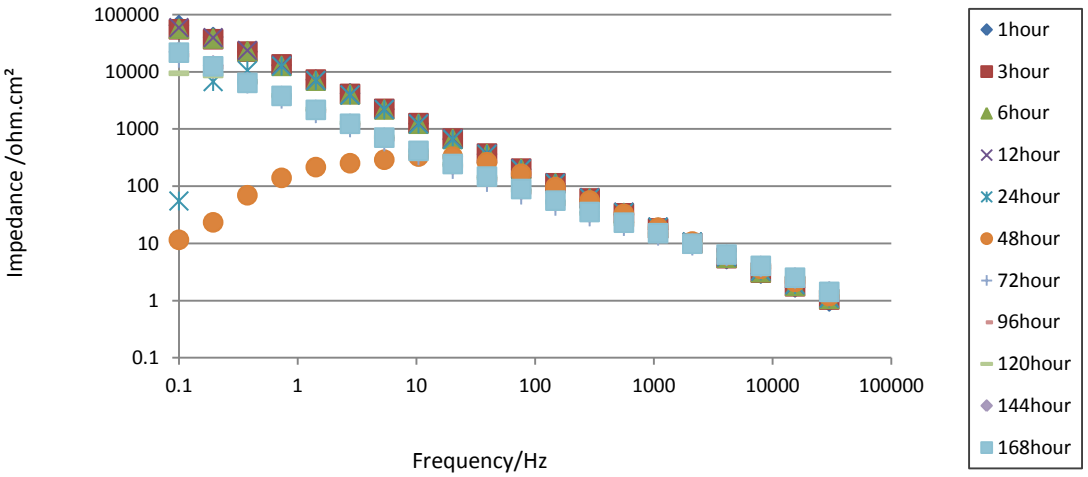

Figure 5.26 – Bode plots of 113-22 coated AA2024-T3 with a scalpel defect in 0.5M NaCl over 168 hours

Time (hours)	Equivalent Circuit Model	CPE ($x10^{-5}$ $S \cdot s^{-n} cm^{-2}$) C_{oxide}	Freq. Power (n)	Resistance ($x10^{1} \Omega cm^{2}$) R_{oxide}	CPE ($x10^{-5}$ $S \cdot s^{-n} cm^{-2}$) C_{pol}	Freq. Power (n)	Resistance ($x10^{5} \Omega cm^{2}$) R_{pol}	Chi-squared ($x10^{-3}$)
1	R(Q(R(QR)))	0.6	1	0.9	1.5	0.81	2.1	2.8
3	R(QR)	-	-	-	1.9	0.90	1.4	5.1
6	R(Q(R(QR)))	0.7	0.98	0.8	1.5	0.80	3.7	2.5
12	R(QR)	-	-	-	2.0	0.89	1.9	4.2
24	R(QR)	-	-	-	1.9	0.90	0.2	11.8
48	R(Q(R(QR)))	0.7	1	8.5	2.1	0.82	0.01	273
72	R(Q(R(QR)))	3.0	0.91	6.2	8.1	0.83	1.8	1.9
96	R(Q(R(QR)))	53.1	0.59	2.7	7.3	0.86	12.9	1.1
120	R(Q(R(QR)))	3.4	0.83	3.8	3.9	0.84	0.2	17.8
144	R(Q(R(QR)))	61.7	0.57	5.0	6.8	0.87	2.4	1.7
168	R(Q(R(QR)))	3.4	0.83	4.6	3.8	0.84	0.5	7.4

Table 5.6 – Parameters of fitted EIS data for 113-22-coated AA2024-T3 with a scalpel defect in 0.5M NaCl

Calculated parameters for the EIS data are plotted in table 5.6. The polarisation resistance, R_{pol}, starts at $2.1x10^5\Omega$ and similar to the 2M NaCl tests shows dynamic buildup and breakdown of resistance. One peak R_{pol} is calculated at $1.3M\Omega cm^2$, which is higher than values calculated for tests performed in 2M NaCl, but the resistance still falls away sharply.

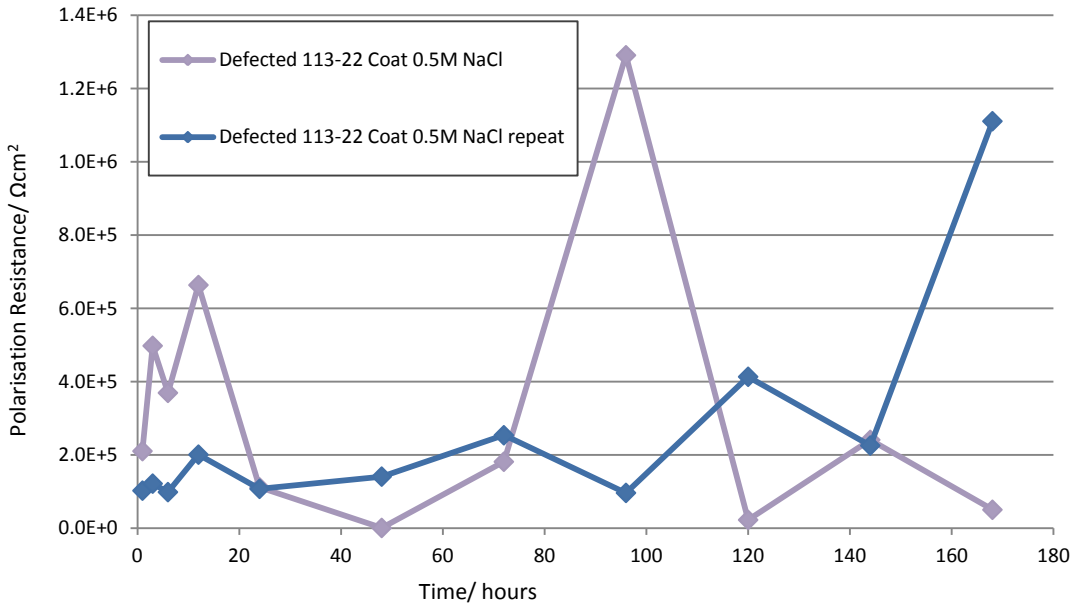

Figure 5.27 – Polarisation resistance against time for 113-22 coated samples with a scalpel defect

In a graph of R_{pol} against time, figure 5.27, apart from a high peak of $1.3M\Omega cm^2$ of resistance, the magnitude and behaviour of R_{pol} is similar in both concentrations of sodium chloride. It indicates that different sites are still susceptible to aggressive ion attack at the lower chloride concentration and levels of chromate are not sufficient to sustain stable passivity.

5.3 Cathodic Polarisation of Coated Samples with Defects

This section will investigate the mechanism of protection during the earlier hours of exposure. EIS experiments in this chapter have indicated that the polarisation resistance usually increases during the first 12-24 hours of immersion, i.e. the corrosion rate falls steadily. As chromate species are known to act as excellent cathodic inhibitors even at low concentrations[24], samples were cathodically polarised -300mV at a scan rate of 10mV per minute from the rest potential, before corrosion had initiated. Tests were performed on both control paint and 113-22 coated samples 18 hours after the start of immersion in 2M sodium chloride solution.

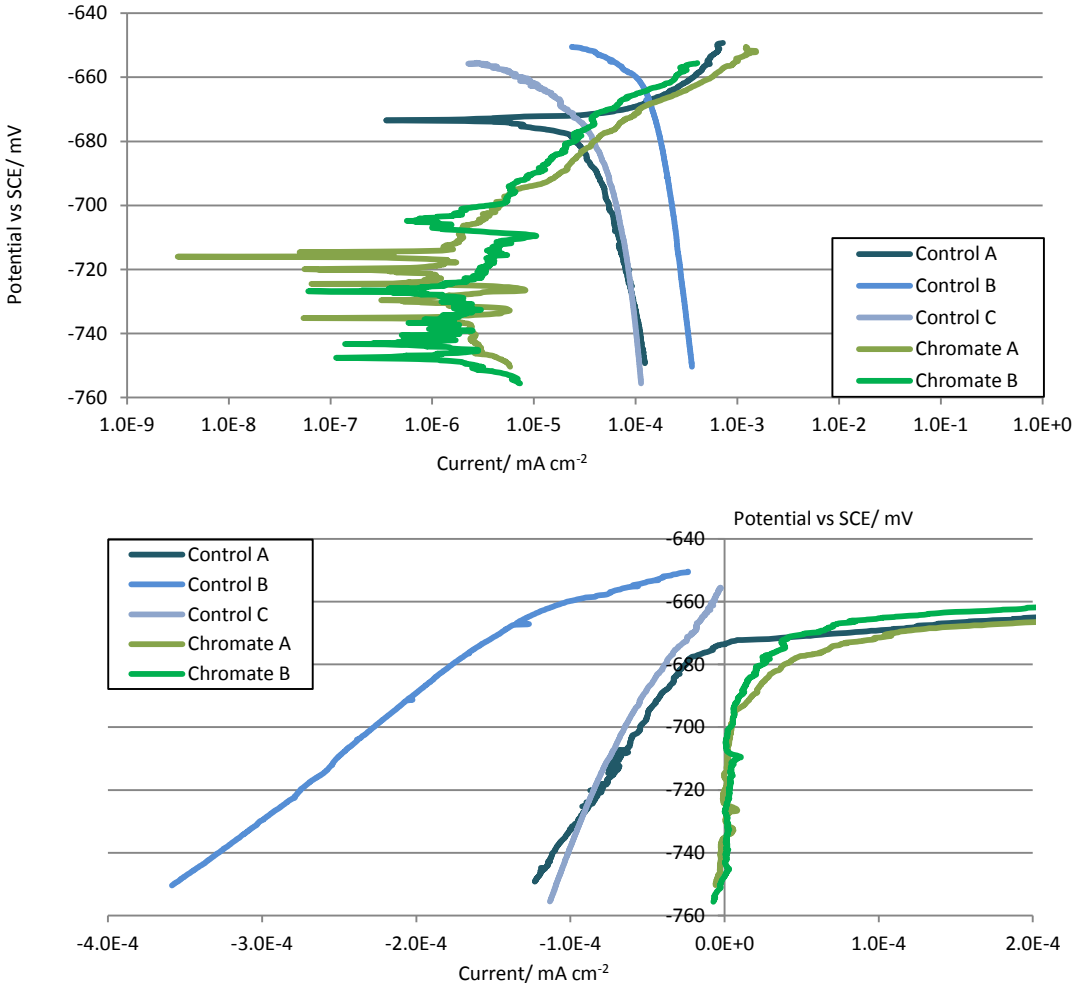

Figure 5.28 – a) Logarithmic cathodic polarisation curves of control and 113-22 coated panels with a defect in 2M NaCl after 18 hours immersion, b) Linear cathodic polarisation curves

Figure 5.28 clearly demonstrates the reduction of the cathodic line gradient due to cathodic inhibition. The 113-22 coated samples both rest at a potential that is slightly along the anodic line above the corrosion potential, $E_{corr,}$ suggesting that the alloy is sitting on a metastable pitting potential. As the sample is cathodically polarised, the anodic current decreases but the cathodic current is strongly inhibited. Below -700mV, a lot of current noise can be observed in the 113-22 coated sample tests. It is likely that as the system moves from the anodic region to the cathodic region, the system passes a counterbalancing region, where both anodic and cathodic reactions are being retarded by the inhibitor and the potential bias.

For the control coated sample tests, the sample sits at a rest potential along the anodic curve. When the potential is lowered, any anodic current is rapidly eliminated and the cathodic current increases steadily. Comparing with the 113-22 coated tests, it can be clearly seen that the presence of inhibitive pigments greatly limit the cathodic reaction, (oxygen reduction). If we look at the currents in figure 5.34b at -760mV, the control coating samples show a large current whereas the coatings with chromate show currents almost too small to measure. This is due to cathodic inhibition by chromate. A consequence is that the corrosion potential is much lower with chromate.

5.6 Possible Limitation to the EIS technique

It is puzzling that coatings that meet the requirements of salt spray tests and perform well in service show fluctuating performance when subjected to EIS testing. A possible explanation of the 'loop' or collapse of the semicircle that has been observed in EIS experiments is that the system begins to pit whilst measurements are being taken. EIS tests in this investigation are, as usual, potentiostatic measurements, meaning that the rest potential of the system is recorded at the start of the test and then held at this potential with a small superimposed sine signal whilst the impedance is measured across different frequencies. Extended periods at a controlled potential will accelerate corrosion damage because if the alloy starts to pit under free corrosion, the potential of the system will drop so maintaining potential at a fixed higher level causes more rapid corrosion development. A single EIS measurement was performed on a defected 113-22 coated sample after 12 hours of pre-immersion to check R_{pol} and then after the test, the potential was held at -637.51mV, the measured free corrosion potential, for one day and the current monitored.

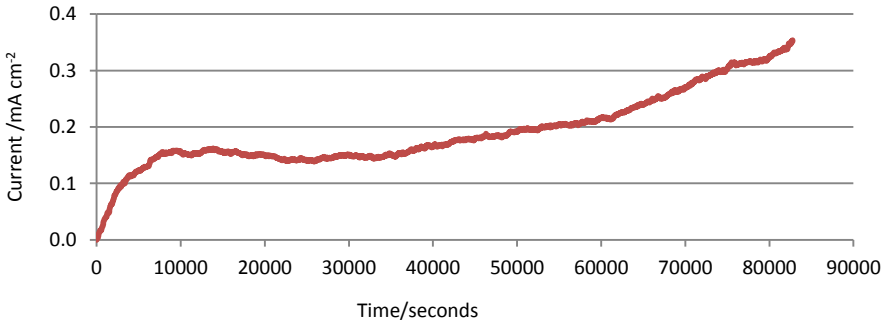

Figure 5.29 – Current versus time under potentiostatic conditions

Figure 5.29 show the measured current against time over the course of one day (86400 seconds), and it can be clearly seen that the current starts at zero but then increases over time. The current reaches approximately 0.1mA after an hour of static potential. EIS measurements take a period of time usually less than 15minutes (depending on frequency) to record the impedance,

and because the potential perturbations about the rest potential are small, EIS is considered to be non-invasive and non-destructive technique. However, we see here that the application of a steady DC potential (initially E_{corr}) for short periods can lead to the passage of significant anodic currents that would not take place in free corrosion.

5.7 Electrochemical Noise Technique

EN analysis was used as a non-destructive technique to compare results with those gathered from EIS experiments. Two coated panels were placed side-by-side and sealed with beeswax-colophony at the interface. A 1cm scalpel defect was made on each panel and a piece of filter paper was placed over the two defects with the small volume electrochemical cell placed on top, as shown in figure 5.30. Control paint and 113-22 coated samples were tested.

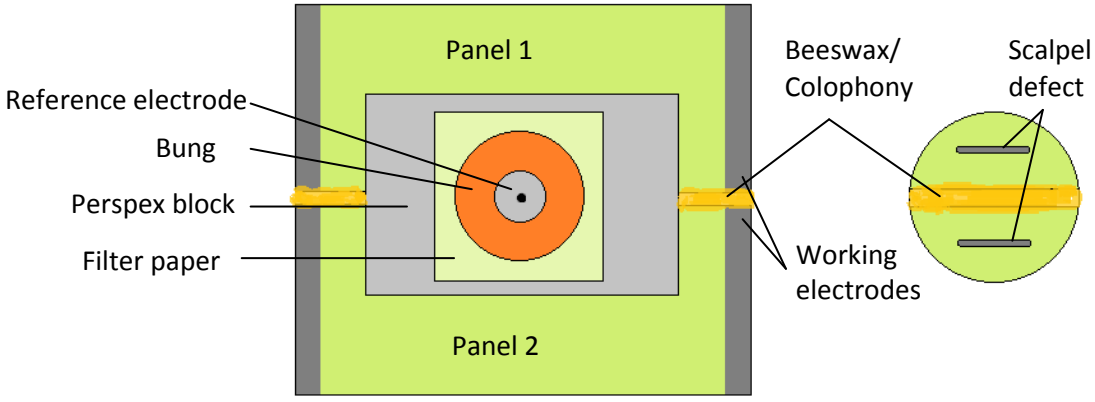

Figure 5.30 – a) Schematic of cell used for electrochemical noise testing, b) Test area beneath bung-filter paper revealing exposed alloy surface

Measurements of the potential and galvanic current between the two samples were recorded at two readings per second for half an hour every six hours on the first day and every 24 hours subsequently up to one week using the Gill AC potentiostat as a ZRA.

The following electrochemical shot noise formulae were used to determine I_{corr} and q, the mean charge per transient event[84,85]:

$$R_{noise} = \sigma_E / \sigma_I \quad [5.1]$$

$$I_{corr} = B / R_{noise} \quad [5.2]$$

$$q = (\sigma_E * \sigma_I)/(Bb) \quad [5.3]$$

$$f_n = I_{corr}/q \quad [5.4]$$

where R_{noise} is electrochemical noise resistance (assumed to be equal to R_{pol}), σ_E and σ_I are the standard deviation for electrochemical potential and current respectively, I_{corr} is the corrosion current, B is the Stern-Geary coefficient, q is the mean charge in the transient events, b is the bandwidth of measurements ($b = 1/2\Delta t$) and f_n is the frequency of events

5.7.1 Electrochemical Noise Resistance

Electrochemical noise resistance was calculated from the standard deviations in current and potential using the equation shown in section 5.5 and resistance-time graphs are shown below:

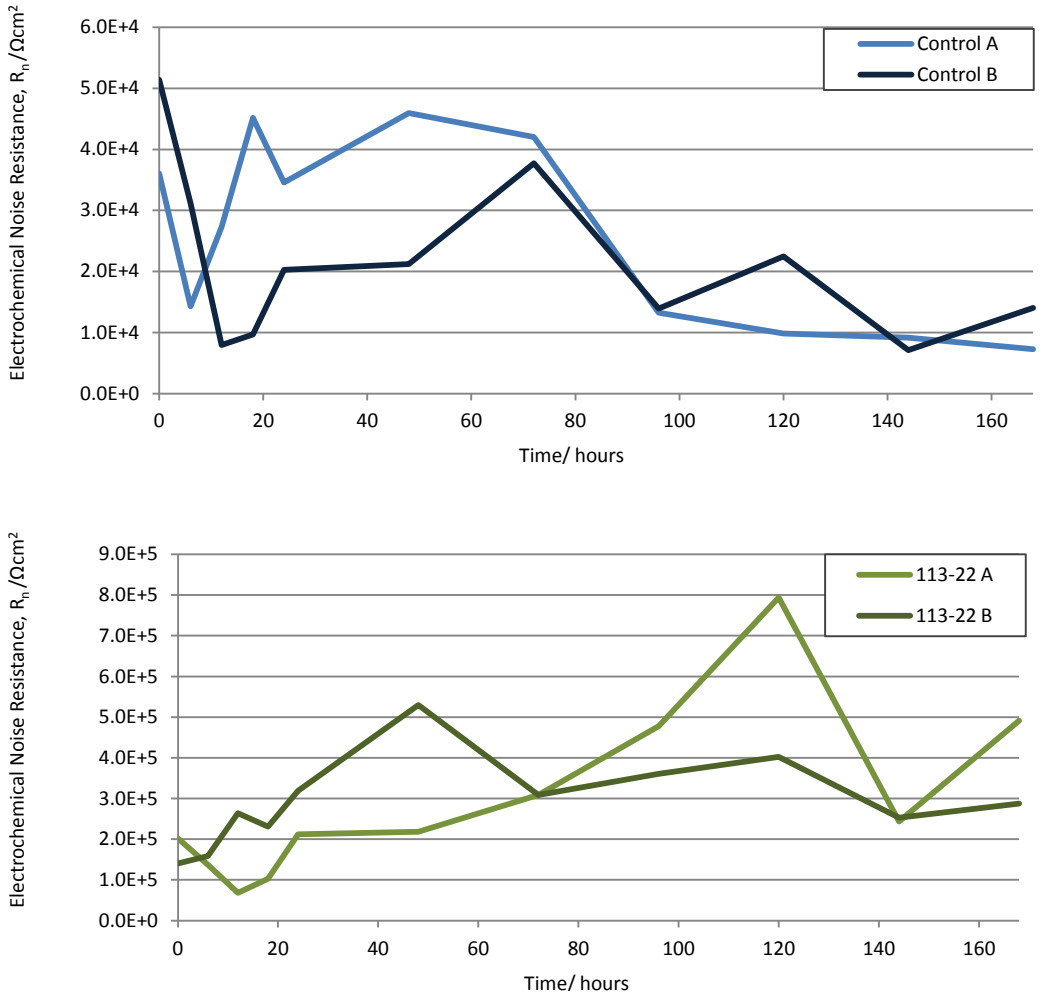

Figure 5.31 – Electrochemical noise resistance against time graph for defected coated panels:

a) control b) 113-22 coated AA2024-T3

Figure 5.31 shows the development of electrochemical noise resistance against time for the pair of defected coated systems. Because the noise technique uses a relatively low sample rate, the information gained will correspond with the low frequency part of the EIS measurements. By comparing the above graphs with the polarisation resistance against time graphs in figures 5.13

and 5.17, similarities can be observed between the two techniques. For the control paint system, figure 5.31a shows a higher resistance in the initial period, in the region of 10 – 50kΩcm^2. The resistance then decreases steadily after approximately 72 hours. The R_{pol}-time graph in figure 5.13 exhibits resistances of similar magnitude and an initial period of higher resistance, followed by a distinct decrease after 24 hours. The times taken for the resistance to fall away for EIS experiments are shorter than those seen in the EN experiments, although the trend and resistance values are essentially the same. For the 113-22 coated samples, figure 5.31b shows both R_n starting off at 0.1-0.2MΩcm^2 and increases over time. R_n dips occasionally, but 113-22A shows the resistance increasing up to 0.8MΩcm^2 with distinct peaks in resistance that are followed by a sharp decrease are again observed. The values of R_n calculated are very similar to the R_{pol} values seen in figure 5.17 and despite EN analysis being carried out at E_{corr} for the coupled pair, increasing resistances followed by distinct drops are seen in R_n-time graphs. The results support that although individual EIS runs may be spoiled by causing pit initiation at a fixed potential, the EIS technique can still provide an accurate picture of the behaviour of an electrochemical system.

5.7.2 Further Electrochemical Noise Analysis

EN was also used to examine how the frequency of events, f, as time progressed as well as the charge in events, q, to indicate the degree of corrosion in the samples. Electrochemical noise formulae stated in section 5.5 were used. The Stern Geary coefficient, B, was approximated to b_a from the anodic curve of the AA2024-T3in 2M NaCl polarisation curve and is measured to be ~2.65, so that bandwidth, b, is 1/(2*180) = 0.0028. Data collection was performed in periods of 30minutes and split into 10 blocks of 3minutes.

Calculated f_n data was arranged from the smallest value to the largest and the cumulative probability is measured as M(N+1), where M is the rank of the ordered frequency data, f_n, and N is the total number of f_n data.

5.7.2.1 Noise Resistance

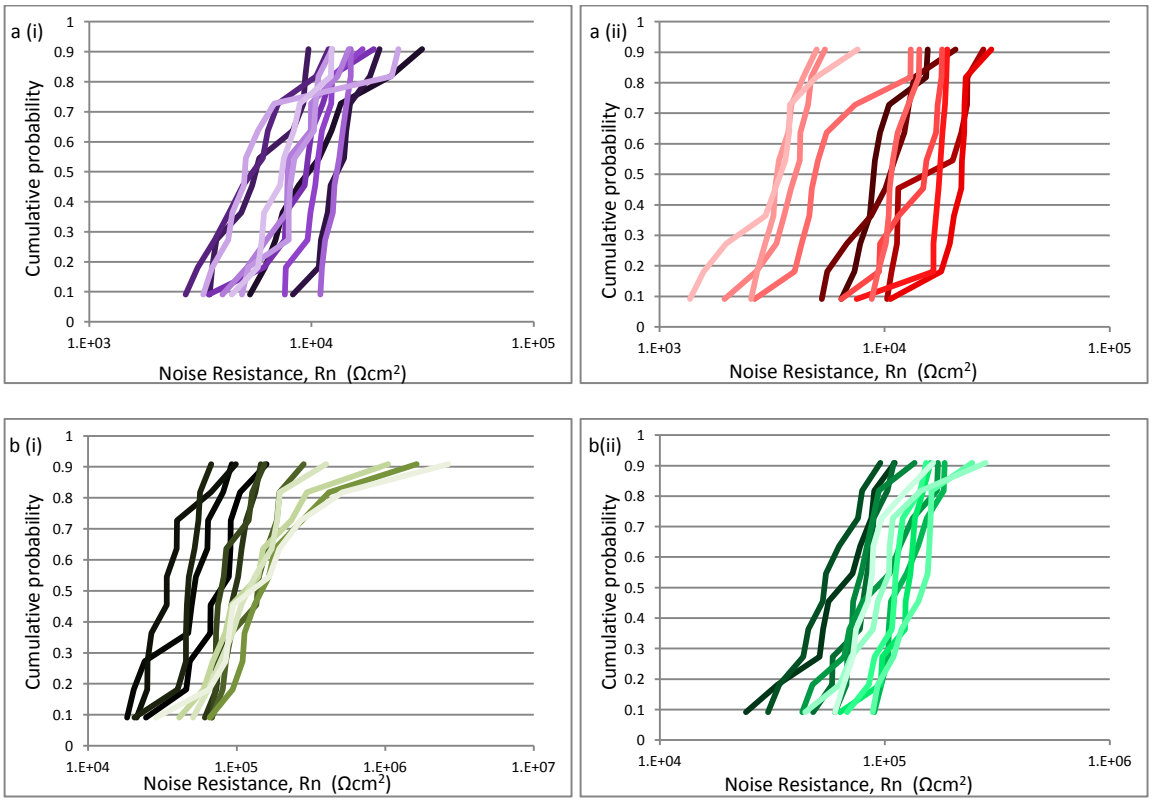

Figure 5.32 – Cumulative probability graphs for electrochemical noise resistance for: a) i) control ii) control repeat b) i) 113-22 ii) 113-22 repeat coated AA2024-T3

Figure 5.32 shows the cumulative probability graphs for the electrochemical noise resistance of the two systems, control and 113-22 coated AA2024-T3. As time progresses, the shade of the line becomes lighter. Figure 5.32a(ii) shows the noise resistance, after an initial shift to the right, shifted to the left over time, meaning that as time progresses, the resistance of the system decreases. For the 113-22 coated system, both figures in 5.32b show the noise resistance shifting gradually to the right over time. This indicates that R_n is increasing and as time progresses, the rate of corrosion falls.

5.7.2.2 Charge

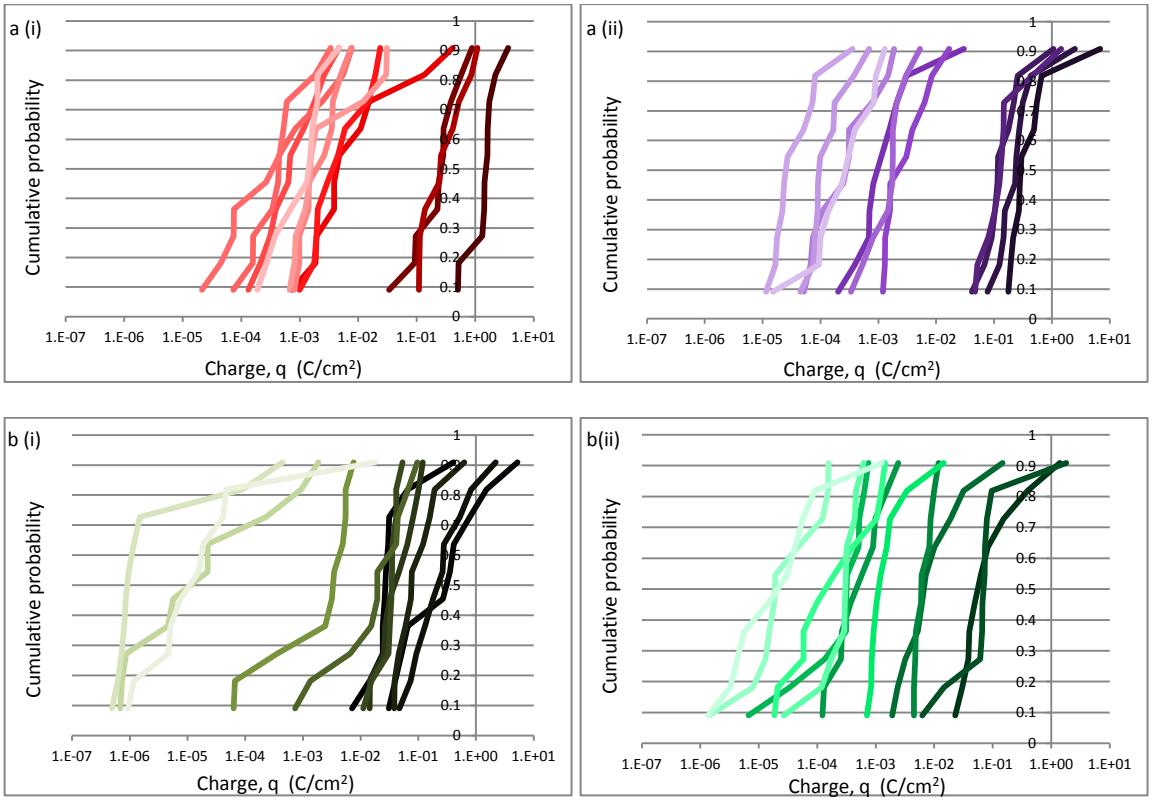

Figure 5.33 – Cumulative probability graphs for electrochemical charge in each event for:
a) i) control ii) control repeat b) i) 113-22 ii) 113-22 repeat coated AA2024-T3

Figure 5.33 shows the cumulative probability graphs for the electrochemical charge in each event the two systems, control and 113-22 coated AA2024-T3. As time progresses, the shade of the line becomes lighter. It can be seen in both systems that as time progresses, the plots shift to the left, indicating that degree of corrosion attack in each event becomes smaller. The mean charge for individual events falls with time, corresponding to smaller metastable pits. Figure 5.33b(i) shows the lowest extended-time q values, but across a wide spread (variation). Most lines for both systems have similar slopes/variation. When figure 5.33 is compared against the cumulative probability of event frequency graphs in figure 5.34, a clearer understanding of the corrosion behaviour can be inferred. With the charge of each event being similar, the degree of corrosion attack can be determined by the frequency of events.

5.7.2.3 Frequency of events

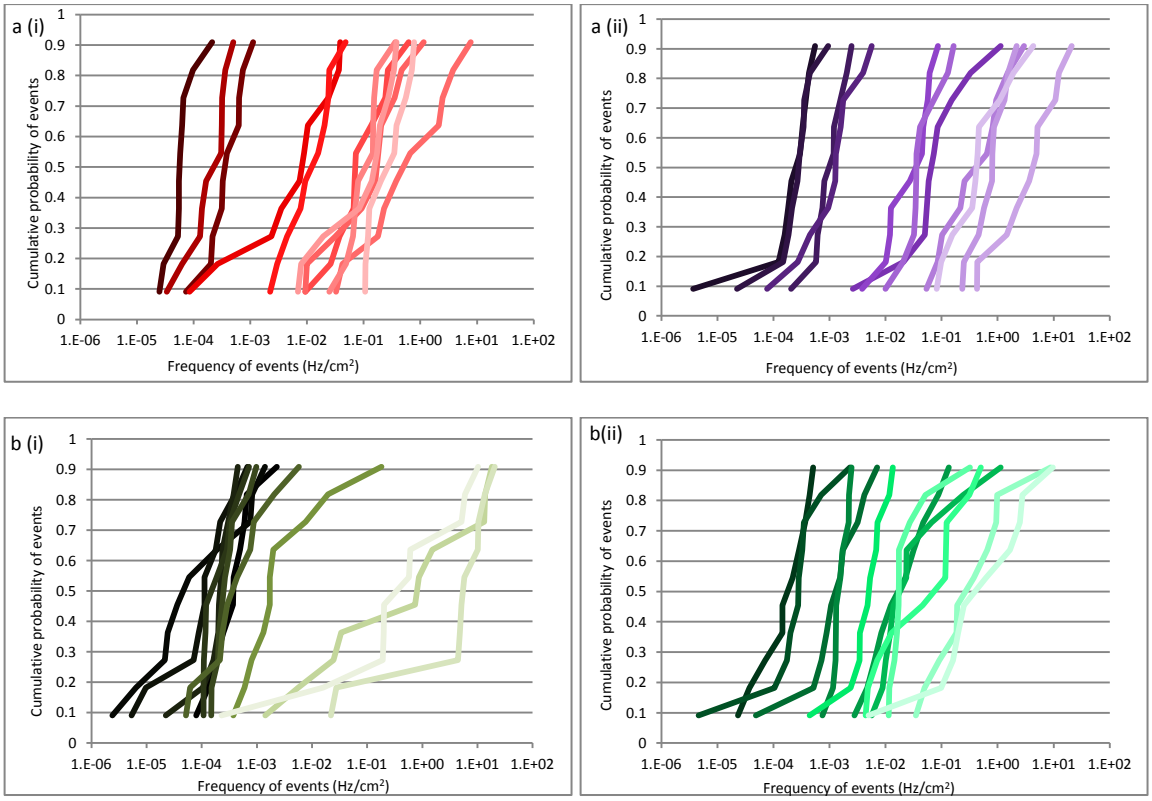

Figure 5.34 – Cumulative probability graphs for frequency of events for:

a i) control ii) control repeat b) i) 113-22 ii) 113-22 repeat coated AA2024-T3

Figure 5.34 shows the cumulative probability graphs for the frequency of events for the two systems, control and 113-22 coated AA2024-T3. As time progresses, the shade of the line becomes lighter. It can be seen in both systems that as time progresses, the plots shift to the right, indicating that pitting events occur more frequently. Both control coatings in figure 5.34a show a steady increase in frequency over time, whilst figure 5.34b(i) shows that the 113-22 coated system reduces the frequency of events for most of the measurement time (4-5 days) before in the end shifting to the right. It is also observed that the width of the distribution of f_n at long time increases with the presence of inhibitor. The lower frequency regions suggest localised corrosion, e.g. pitting, and as it shifts to the higher frequencies a more uniform

corrosion is indicated (from shot-noise theory). It appears that the presence of chromate delays the onset of general attack, although it cannot completely prevent corrosion processes as the frequencies seen in later measurements are similar in both environments.

5.8 Discussion

When a defect was introduced into a coating and tested in bulk solution, the chloride solution has direct contact with the alloy which behaves similarly to uncoated alloy tests. The control coated tests exhibited no protection from the coating and for chromate-inhibited coated samples, the protection provided by the coating and pigments was greatly reduced. Potentiodynamic polarisation tests for defected coated samples showed similar behaviours to a bare AA2024-T3 sample in 2M sodium chloride solution with no chromate inhibitor. This was expected in the sense that the amount of chromate available is limited and the volume of aggressive ion solution is overwhelming (so that concentrations of chromate in solution are minimal). However, when the sample was left in solution for an extended period (seven days), the rest potential of the samples slowly decreased and at room temperature, the pitting potential was raised so that a passive region was observed during the anodic sweep. Similar to the bare alloy experiments in chapter 3, the inhibitive effects of chromate were reduced when the temperature was increased to 30°C.

In EIS experiments, tests performed in large volumes of solution overwhelm the inhibitor protection, because the released pigment is dissolved into the large bulk volume and convection in the fluid environment rapidly prevents any build-up in the concentration gradient (high concentration of chromate closer to cut edge). The small volume cell with 2M NaCl agar allowed the defected 113-22 coatings to provide noticeable polarisation resistances of ~1MΩ. However,

this resistance was not sustained and falls away, and to rise again later. This cyclic buildup and breakdown of resistance is possibly due to the release of chromate pigment from fresh coating surfaces as corrosion propagates. As described in chapter 4, the majority of pigment is encapsulated within the binder matrix and only a limited amount is released when the pigment is in direct contact with the bulk solution. Therefore, the breakdown of resistance is due to the chloride ions attacking the alloy through the oxide layer and this leads to a developing alkaline environment (that forms from hydroxide reacting with the sodium ions), which then causes coating degradation. This degradation will thus release more inhibitive pigment close to the metal surface and the corrosion processes are subsequently inhibited. The trapping of inhibitor within the binder matrix also allows the coating to maintain its structural integrity (and not crack, as seen with the control coating in chapter 3), and so, to some degree, the 113-22 coating achieves an 'on-demand' release of pigment when needed. This would possibly be achieved by the supply of fresh chromate beneath the paint being released when corrosion undercuts beneath the paint.

This proposition was further confirmed by performing EIS tests with pre-washed samples and topcoated samples. Pre-washed samples that were immersed in distilled water for one week had sufficient time for all accessible pigment to be released and yet the resistive behaviour of samples over one week was similar to the unwashed samples. The same was again seen with the topcoated samples, where a topcoat was applied over the 113-22 coating so that pigment release would mainly be at the cut edge. The cyclic breakdown and build up of polarisation resistance apparently cannot be explained by the high concentration of sodium chloride, as experiments performing using 0.5M sodium chloride solution also exhibited this dynamic process.

As mentioned in chapter 4, Howard et al. concluded that the limited release of chromate into the bulk solution compared to other pigments was due to chemical reactions between chromate and the zinc metal substrate[62]. It is likely that the protection mechanism of chromate acts the same way for the AA2024-T3 system. Therefore, due to a preferential adsorption of the inhibitive species (rather than being quickly released into the bulk solution), chromate inhibitor can still provide noticeable protection even with the low amounts that are released from the fresh surfaces of the thin primer layer.

Electrochemical noise analysis on the control and 113-22 coatings showed resistance values that were similar to those fitted in EIS models. To a less obvious extent, the breakdown and buildup of resistance of chromate-inhibited coatings was again seen which means that EIS techniques can effectively take measurements without seriously affecting the electrochemical system (in a way that potentiodynamic polarisation would). Further ECN analysis showed that the frequency of events for the 113-22 coating was lower than for the control coated samples in the first stages of testing although towards the end of the week, frequency of events were similar. The presence of inhibitors did not significantly change the charge of events over time.

Cathodic potentiodynamic polarisation tests were then performed on defected control and 113-22 coated samples showed that the presence of chromate species greatly inhibited the cathodic reaction, e.g. oxygen reduction.

5.9 Conclusions

Chapter 5 investigated the corrosion behaviour of the non-inhibitive control coating and the chromate-pigmented 113-22 coating on AA2024-T3 with a defect introduced in the coating.

Potentiodynamic polarisation tests showed that when a defect is introduced into the coating, the control coating provides no protection at the exposed metal surface and corrosion behaviour is very similar to the bare metal alloy tests.

The chromate-pigmented 113-22 also provides limited corrosion protection when the coating is damaged and the corrosion protection was only observed after a longer pre-exposure before testing.

Polarisation testing was also used to investigate the cathodic inhibition of the coated samples with a defect, and when samples were cathodically polarised, the 113-22 coated samples showed significant cathodic inhibition. When the control coated sample tests were cathodically polarised, the cathodic current increased steadily. The cathodic inhibition by chromate also lowered the free corrosion potential of the alloy.

Electrochemical impedance spectroscopy experiments made use of a small electrochemical cell using filter paper and sodium chloride agar as the test solution. This was to reduce the test solution volume as well as eliminate the convection in the cell so that released inhibitor can remain at higher concentrations around the exposed metal surface.

Both the non-inhibitive control coating and the 113-22 coating exhibited an initial increase in polarisation resistance in the first 12-24 hours of immersion, but subsequent measurements showed the polarisation resistance of the control coating rapidly decreasing. The chromate-

pigmented 113-22 coating exhibited a cyclic behaviour of increasing resistance followed by a sharp drop. EIS results indicated that the chromate prevented the propagation of stable pitting, but did not continuous corrosion protection, suggesting that the inhibitor acts as a reactive response to provide corrosion protection.

Chapter 4 indicated that the majority of inhibitor released came from the free surfaces of coating in direct contact with the test solution. Experiments were performed on pre-washed and top-coated 113-22 samples to remove or restrict the inhibitor on the free surfaces, and a cyclic rise and fall of polarisation resistance was still demonstrated, indicating that the coating still provide corrosion protection.

Electrochemical noise measurements were performed to investigate the two techniques, EIS and ECN, in measuring electrochemical behaviour, and it was found that the ECN resistance results were consistent with the EIS polarisation resistance results. ECN noise resistance results showed a continuous build up and breakdown of resistance, and further ECN analysis also suggested that the chromate provides corrosion protection by reducing the frequency of corrosion events, but the amount of charge of each event was not affected by the presence of inhibitor.

Chapter 6 Investigation of Behaviour of an Alternative Inhibitor

6.1 Introduction

This chapter will focus on the protective qualities of a rare-earth corrosion inhibitor that has been studied as an alternative to chromate-containing inhibitors. A small number of cerium diphenyl-phosphate, $Ce(dpp)_3$, inhibited coated samples were provided by M. Forsyth from Monash University. The Epigen polymer coatings were used because they were epoxy-based like the other paints used in this investigation. Research into the incorporation and use of rare earth inhibitors in organic coatings is very recent and limited; Mardel et al. studied cerium dibutyl-phosphate inhibited epoxy coatings on AA2024-T3 and found that $Ce(dbp)_3$ is rapidly released into the surrounding area at low pH, and effectively inhibit filiform corrosion[86]. They believe that the inhibitor predominantly provides protection via cathodic inhibition by the cerium ions and the dibutyl phosphate acts to modify the aluminium oxide layer to improve coating adhesion.

Rare earth inhibitor research has predominantly been in-solution and studies have shown cerium to be a highly effective corrosion inhibitor, compared against praseodymium, lanthanum and neodymium[46,87]. Combinations of rare earths can also be used together to provide extra protection. Cerium is shown to retard the cathodic processes, particularly oxygen reduction and causing oxide formation on intermetallics (cathode sites) which then retards the cathodic reaction and lowers the free corrosion potential, E_{corr}. Phosphates are anodic inhibitors that react with cations to form an insoluble precipitate to act as a protective barrier on areas of corrosion attack.

Direct current polarisation and electrochemical impedance spectroscopy were used in this study to investigate fully-intact coated and a defected coated $Ce(dpp)_3$ inhibited samples of AA2024-T3. Narrow scribe line defects were made using a scalpel. The coatings on the samples were extremely thick, 300-500µm, six to ten times greater than the control and 113-22 coatings tested in chapters 4 and 5. This was because of difficulties in coating application and poor mixing qualities of the inhibitor into the wet epoxy mixture.

6.2 Corrosion Behaviour of Intact Coatings

EIS experiments were performed in the large volume test cell with the EIS method, as described in section 2.4, over the course of 28 days in 2M sodium chloride solution.

The same equivalent circuit model, figure 6.1, used for the intact coatings in chapter 4 was chosen to model the intact coating system, Nyquist plots for intact coatings usually revealed a two time constant response in the form of two distinct semicircles. The explanation for individual elements can be found in section 4.2.

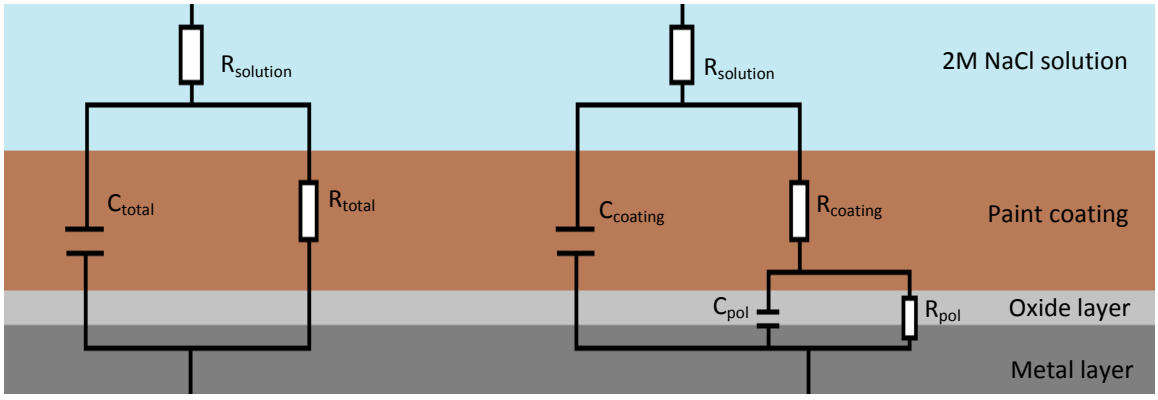

Figure 6.1 – Schematic of model circuits, R(QR) and R(Q(R(QR))), under investigation

The R(Q(R(QR))) model shows the solution resistance, $R_{solution}$ (usually negligible), the coating resistance, $R_{coating}$, and the polarisation resistance, R_{pol}. $C_{coating}$ represents the capacitance of the coating and C_{pol} is the polarisation capacitance. R_{pol} and C_{pol} represent corrosion processes at the metal-solution interface. The simpler R(QR) model was used when it was not possible to distinguish two time constants from the EIS data. $R_{coating}$ and $C_{coating}$ may be thus combined with R_{pol} and C_{dl} to represent a single time constant response that fits the actual electrochemical response, or if the frequency range tested is insufficient to detect the interface response, the 'first' semicircle of the Nyquist plot would represent just the coating.

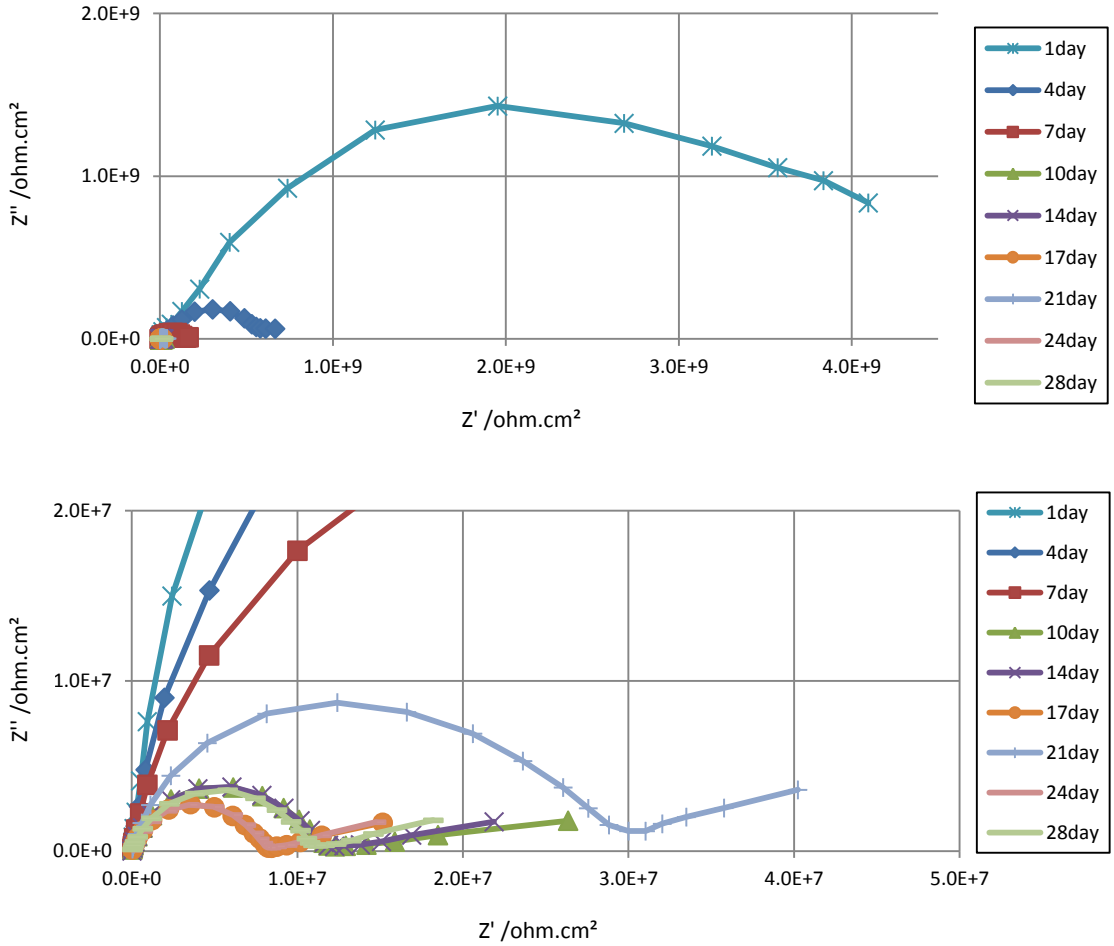

Figure 6.2 – a) Nyquist plots of intact $Ce(dpp)_3$ Epigen coated AA2024-T3 tested over 28 days, b) Nyquist plots focussing on day 10 onwards

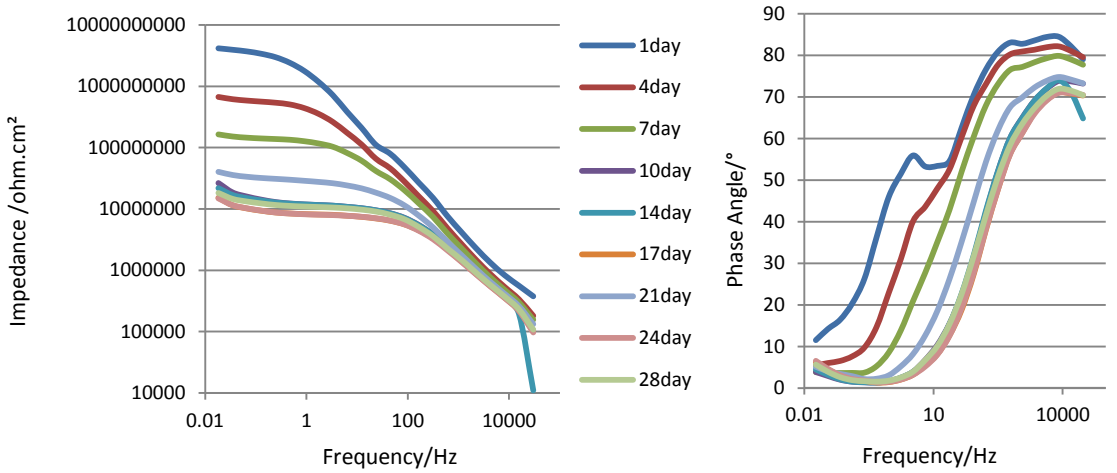

Figure 6.3 – a) Bode impedance plots of intact $Ce(dpp)_3$ Epigen coated AA2024-T3 tested over 28 days, b) Bode phase angle plots focussing on day 10 onwards

Time (days)	Equivalent Circuit Model	CPE $C_{coating}$ ($x10^{-10}$ $S{\cdot}s^{-n}$ cm^{-2})	Freq. Power (n)	Resistance $R_{coating}$ ($x10^{7}\Omega cm^{-2}$)	CPE C_{dl} ($x10^{-9}$ $S{\cdot}s^{-n}$ cm^{-2})	Freq. Power (n)	Resistance R_{ct} ($x10^{7}$ Ω cm^{-2})	Chi-squared ($x10^{-2}$)
1	R(QR)	-	-	-	0.1	0.86	395	4.5
4	R(Q(R(QR)))	1.3	0.89	17.7	0.3	0.81	37.8	1.6
7	R(Q(R(QR)))	1.9	0.86	5.7	1.8	0.51	9.9	0.8
10	R(Q(R(QR)))	1.8	0.86	7.7	1.4	0.67	9.3	0.8
14	R(Q(R(QR)))	2.2	0.85	5.8	2.5	0.55	7.0	0.8
17	R(Q(R(QR)))	2.9	0.82	5.7	3.1	0.64	3.9	0.7
21	R(Q(R(QR)))	2.7	0.83	5.8	1.6	0.70	5.2	0.9
24	R(Q(R(QR)))	2.8	0.83	5.2	4.5	0.62	3.0	0.6
28	R(QR)	-	-	-	0.4	0.79	7.8	1.1

Table 6.1 – Model Parameters for intact $Ce(dpp)_3$ Epigen coated AA2024-T3 for 28days

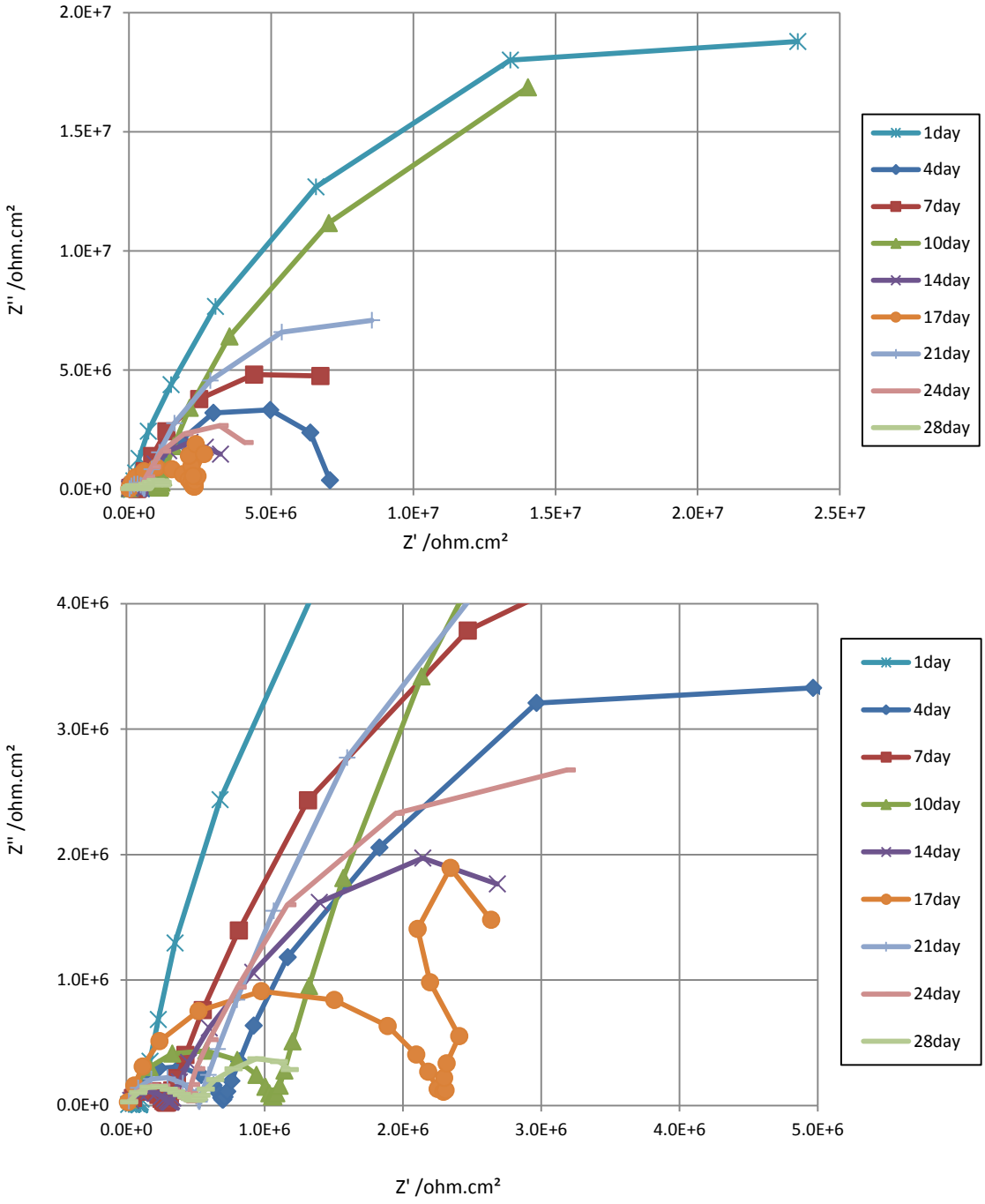

Figure 6.4 – a) Nyquist plots of intact $Ce(dpp)_3$ Epigen coated AA2024-T3 tested over 28 days, b)Expanded Nyquist plots focussing on high frequency from day 10 onwards

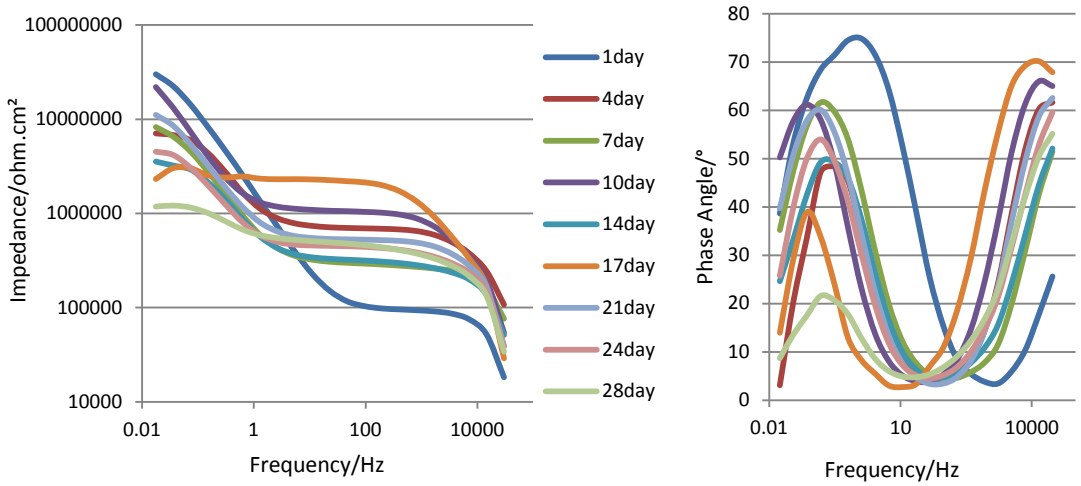

Figure 6.5 – a) Bode impedance plots of intact $Ce(dpp)_3$ samples, b) Bode phase angle plots

Time (days)	Equivalent Circuit Model	CPE $C_{coating}$ ($x10^{-10}$ $S{\cdot}s^{-n}$ cm^{-2})	Freq. Power (n)	Resistance $R_{coating}$ ($x10^{5}$ Ωcm^2)	CPE C_{pol} ($x10^{-7}$ $S{\cdot}s^{-n}$ cm^{-2})	Freq. Power (n)	Resistance R_{ct} ($x10^{7}$ Ωcm^2)	Chi-squared ($x10^{-2}$)
1	R(Q(R(QR)))	2.9	1	0.6	1.3	0.87	4.5	3.1
4	R(Q(R(QR)))	1.3	0.90	6.9	2.2	0.90	0.7	0.7
7	R(Q(R(QR)))	1.4	0.94	2.6	4.0	0.82	1.3	0.8
10	R(Q(R(QR)))	1.6	0.91	1.0	2.8	0.88	4.7	1.7
14	R(Q(R(QR)))	3.8	0.87	2.9	4.5	0.86	0.3	5.0
17	R(Q(R(QR)))	2.3	0.90	21.6	11.9	1	0.1	2.5
21	R(Q(R(QR)))	1.0	0.98	4.9	3.5	0.83	1.9	2.4
24	R(Q(R(QR)))	2.9	0.89	4.1	5.7	0.82	0.8	2.7
28	R(Q(R(QR)))	11.2	0.77	4.7	10.6	0.79	0.1	3.0

Table 6.2 – Model Parameters for intact $Ce(dpp)_3$ Epigen coated AA2024-T3 repeat for 28days

The Nyquist plots for two tests of the intact $Ce(dpp)_3$ Epigen coated AA2024-T3 are shown in figure 6.2 and 6.4. Two semicircles can be distinguished from most Nyquist plots in figure 6.2, after closer inspection of the high frequency measurements in figure 6.2b. A slight inflection can be seen in the high frequency measurements on the Bode phase angle plot in figure 6.3b. A short 'tail' was also seen at the low frequency end of many Nyquist plots. The values were mainly fitted to the R(Q(R(QR))) model when possible but when plots could not be fitted, the simple model circuit of R(QR) was used. Similar to the control and 113-22 coated EIS tests, seen in figures 4.3 and 4.17, a small semicircle can be seen at high frequency measurements on the

repeat test in figure 6.4b. The first semicircles, typically related to coating, show a CPE of 10^{-9} to 10^{-10} $S \cdot s^{-n}$, and the coating resistances shown in table 6.1 are two orders of magnitude greater than those given in table 6.2. Coating resistance values shown in table 6.2 are comparable to the values for the control and 113-22 coatings in chapter 4, which suggests that the epoxy-based coating does not provide good corrosion protection, only exhibiting values $>10^6 \Omega cm^2$, whilst table 6.1 shows coating resistances of magnitudes of $10^7 \Omega cm^{-2}$. Despite being 9-10 times thicker than the control and 113-22 coatings, the resistances of both coatings are fairly low. Therefore, it is expected that the coating will not be a significant barrier to water and aggressive ions and corrosion protection will predominantly rely upon the inhibitors in the coating.

The second resistances, labelled R_{pol}, are of similar orders of magnitude of approximately $10^7 \Omega cm^{-2}$ in both samples, except the initial measurements shown on table 6.1 where the resistance drops from $4G\Omega cm^2$ to $0.4G\Omega cm^2$ to $50\text{-}100M\Omega cm^2$. R_{pol} for the repeat test, in table 6.2, is slightly lower ranging from $10\text{-}50M\Omega cm^{-2}$. From chapter 4, it was found that the control coating provided polarisation resistances, R_{pol}, of $>10M\Omega$ but quickly decreased as filiform and pitting corrosion began. R_{pol} values for the 113-22 coating were consistently over $1G\Omega cm^2$ and no corrosion attack was seen when observed under a scanning acoustic microscope. R_{pol} values for the $Ce(dpp)_3$ Epigen paint were closer to those of the control coating. This suggests that the $Ce(dpp)_3$ inhibitor within the coating is not inhibiting as well as chromate, meaning that the aggressive ions and water could allow pitting corrosion to occur.

6.3 Corrosion Behaviour of Coatings with a Defect

6.3.1 Electrochemical Impedance Spectroscopy

Figure 6.6 shows the equivalent circuits used to model the EIS data. The impedance of the defect will be much smaller than the intact coating and therefore, the investigated system is expected to focus at the exposed bare metal.

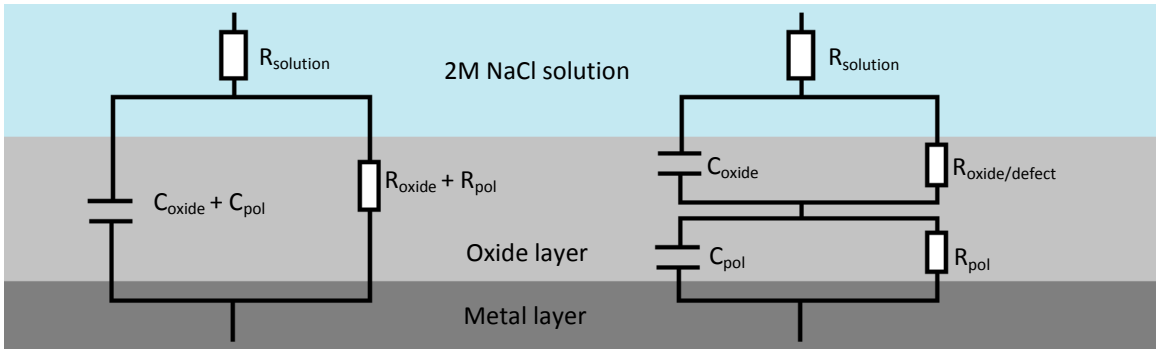

Figure 6.6 – (a) R(QR) model circuit for one time constant response, (b) R(QR)(QR) model circuit for two time constant response

The R(QR)(QR) model is used to fit the following data because the software is able to fit data more consistently using this model (which is mathematically equivalent to the previously used R(Q(R(QR))) model). $R_{solution}$ shows the solution resistance, R_{oxide} the oxide resistance and the polarisation resistance, R_{pol}. R_{oxide} values vary 10^2 to $10^6 \Omega cm^2$ and it is suggested that when R_2 is large, it represents the resistance of the oxide and when R_{oxide} is small, it represents a defect in the oxide layer, such as a pit. C_{oxide} represents the capacitance of the oxide and C_{pol} is the polarisation capacitance. R_{pol} and C_{pol} represent corrosion processes at the metal-solution interface. The simpler R(QR) model is used when it is not possible to distinguish two time constants from the EIS data. R_{oxide} and C_{oxide} are thus combined with R_{pol} and C_{pol} to give a single time constant response that models the actual electrochemical response.

6.3.2 Preliminary EIS Testing in Large Volume Cell

EIS experiments were also performed on $Ce(dpp)_3$ Epigen coated samples with a large defect in the large volume test cell. Figures 6.7 and 6.8 show EIS data from a 28 day test.

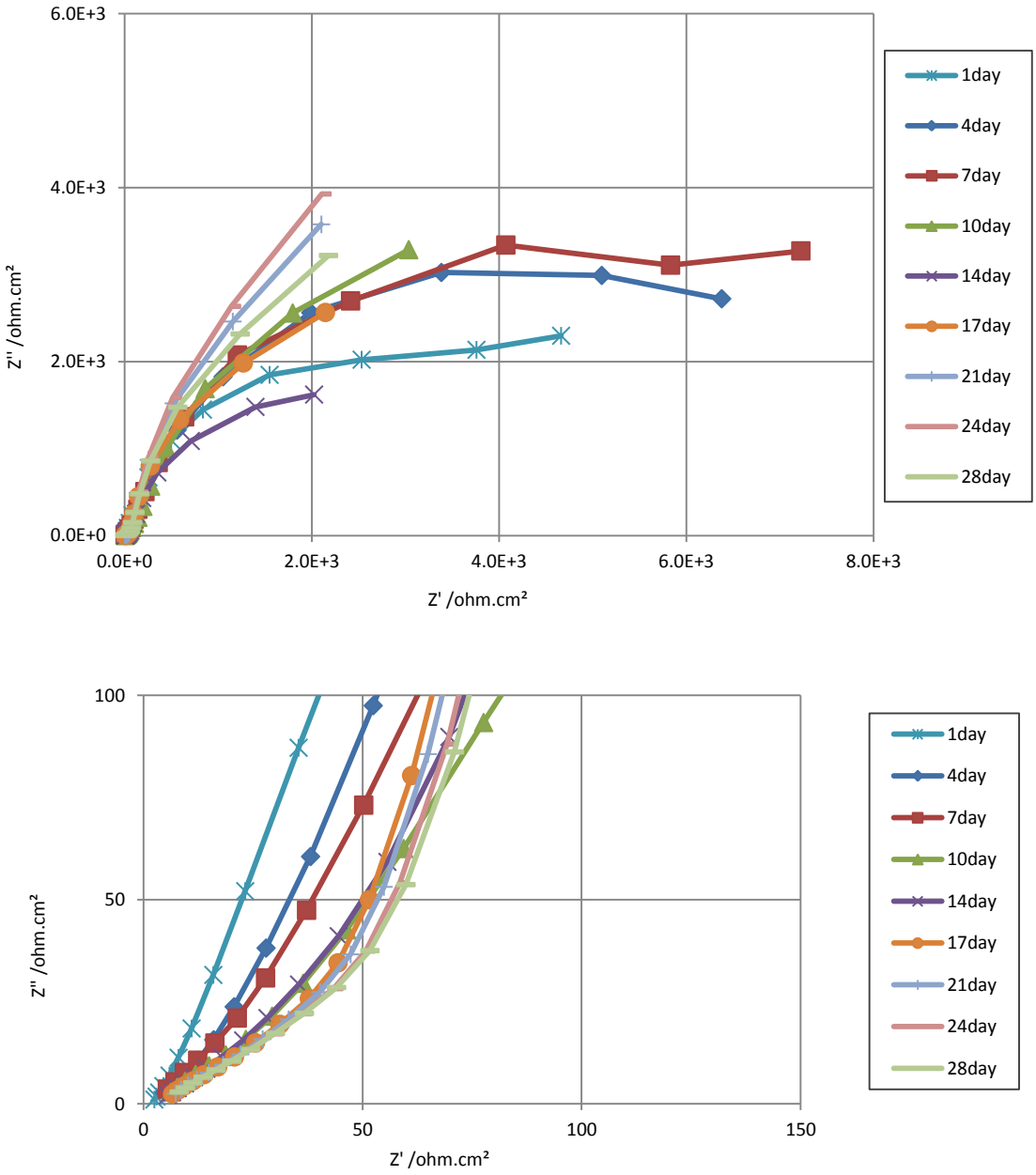

Figure 6.7 – a) Nyquist plots of defected $Ce(dpp)_3$ Epigen coated AA2024-T3 tested over 28 days, b) Expanded Nyquist plots focussing on high frequency measurements

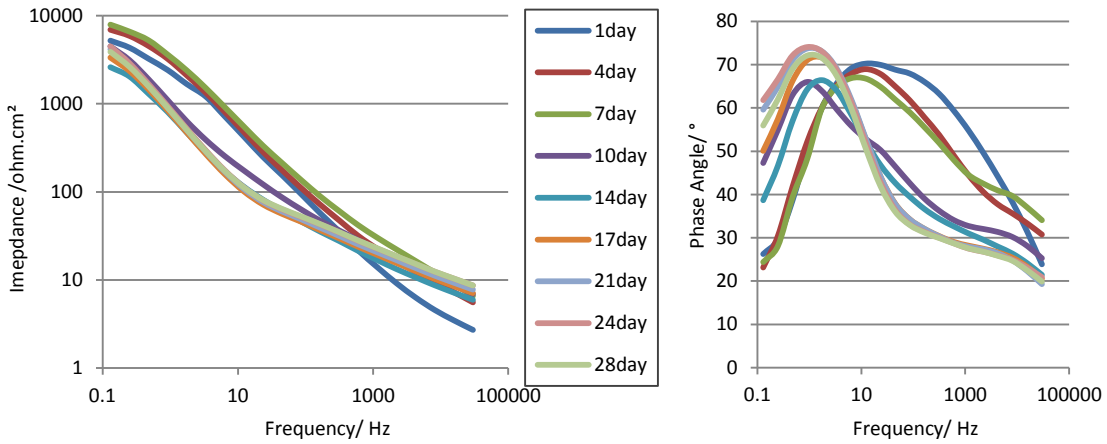

Figure 6.8 – a) Bode impedance plots of defected $Ce(dpp)_3$ samples, b) Bode phase angle plots

Time (days)	Equivalent Circuit Model	CPE C_{oxide} ($x10^{-5}$ $S{\cdot}s^{-n}$ cm^{-2})	Freq. Power (n)	Resistance R_{oxide} (x10 Ωcm^2)	CPE C_{pol} ($x10^{-5}$ $S{\cdot}s^{-n}$ cm^{-2})	Freq. Power (n)	Resistance R_{pol} ($x10^4$ Ωcm^2)	Chi-squared ($x10^{-2}$)
1	R(QR)(QR)	1.6	0.89	1.0	6.3	0.74	0.6	0.6
4	R(QR)(QR)	6.2	0.71	4.1	1.5	0.89	1.1	11.0
7	R(QR)(QR)	5.1	0.69	6.6	1.6	0.86	1.2	0.8
10	R(QR)(QR)	8.9	0.68	5.0	14.9	0.78	1.2	1.4
14	R(QR)(QR)	20.6	0.64	6.1	13.2	0.89	0.5	1.4
17	R(QR)(QR)	25.3	0.60	6.6	9.7	1	1.2	2.0
21	R(QR)(QR)	21.2	0.62	6.8	9.5	1	2.4	1.7
24	R(QR)(QR)	19.4	0.62	7.1	9.7	1	2.9	1.6
28	R(QR)(QR)	22.4	0.60	7.7	9.5	1	1.9	1.6

Table 6.3 – Model Parameters for defected $Ce(dpp)_3$ coated AA2024-T3 for 28days

From the EIS data in figure 6.9, it can be seen that the magnitude of the impedance values are in the range of 10-100kΩcm^2, an order of magnitude lower than measurements in defected chromate coated experiments, in the previous chapter. The calculated model parameters are shown in table 6.3. The polarisation resistance, R_{pol}, is very low, in the region of $10^4\Omega cm^2$ which is similar to the R_{pol} measurements for a defected control coated sample. However, there is no peak in resistance during the first 24hours. The resistance of the oxide is also very low, similar to previous control and 113-22 defected coated samples, which suggests that the oxide has defects that reduce the corrosion protection.

The repeat experiment, shown in figure 6.9 to 6.10, shows EIS data where the readings across the frequencies show low impedances. The sample is believed to be heavily pitting.

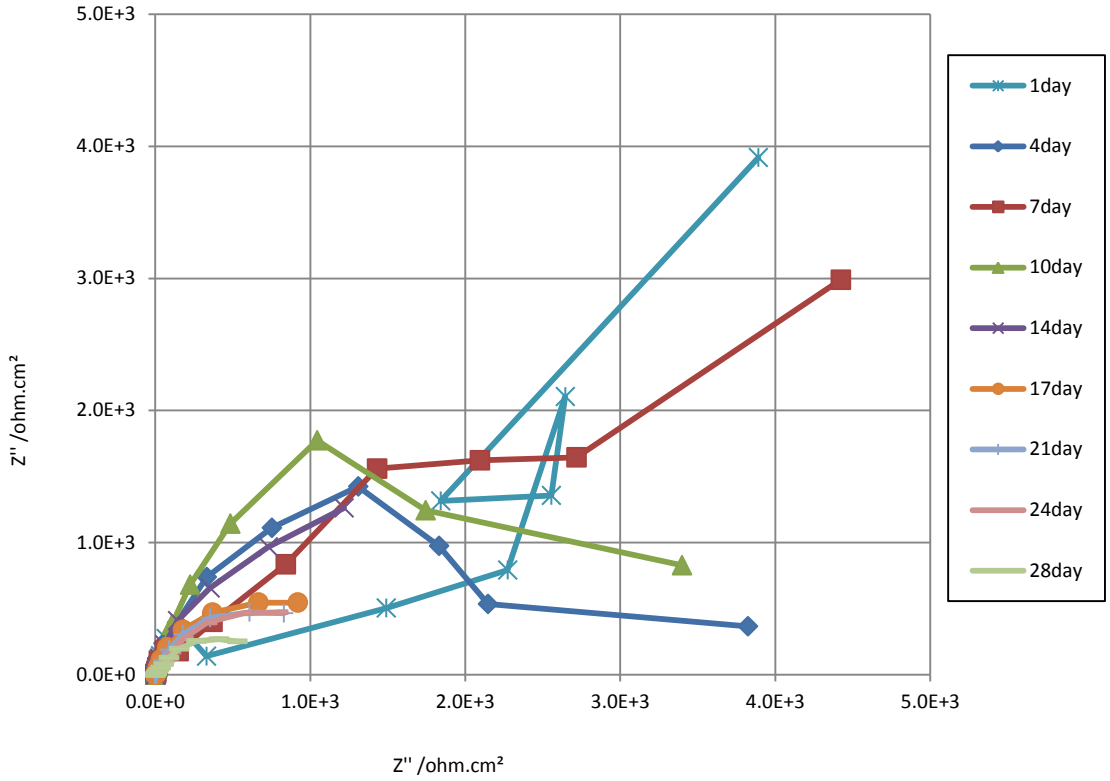

Figure 6.9 – Nyquist plots of defected $Ce(dpp)_3$ Epigen coated AA2024-T3 tested over 28 days,

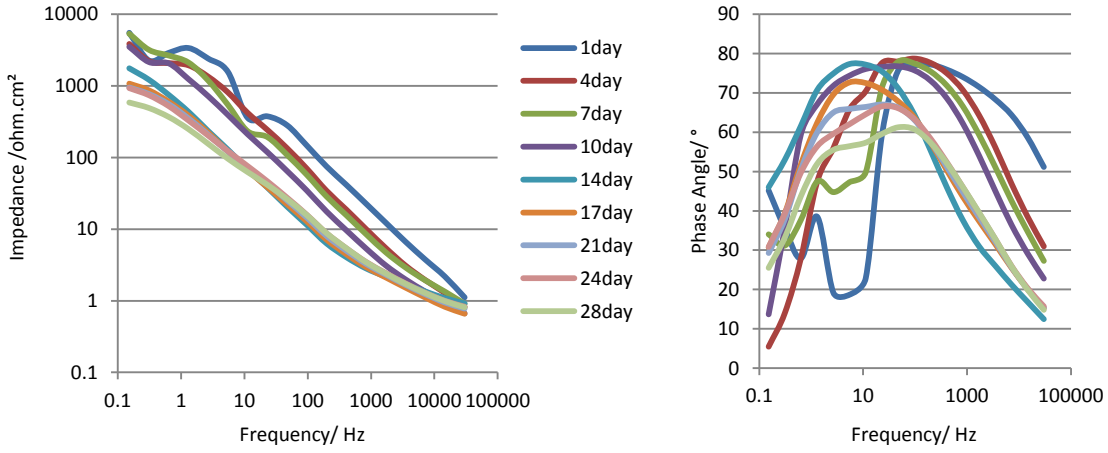

Figure 6.10 – a) Bode impedance plots of defected $Ce(dpp)_3$ samples, b) Bode phase angle plots

6.4 EIS Testing in Small Volume Cell

EIS experiments were performed in the small volume cell, as described in section 2.2.1.2, and a smaller scalpel sized defect was made. The equivalent circuits shown in figure 6.6 were again used to model the defected coating system.

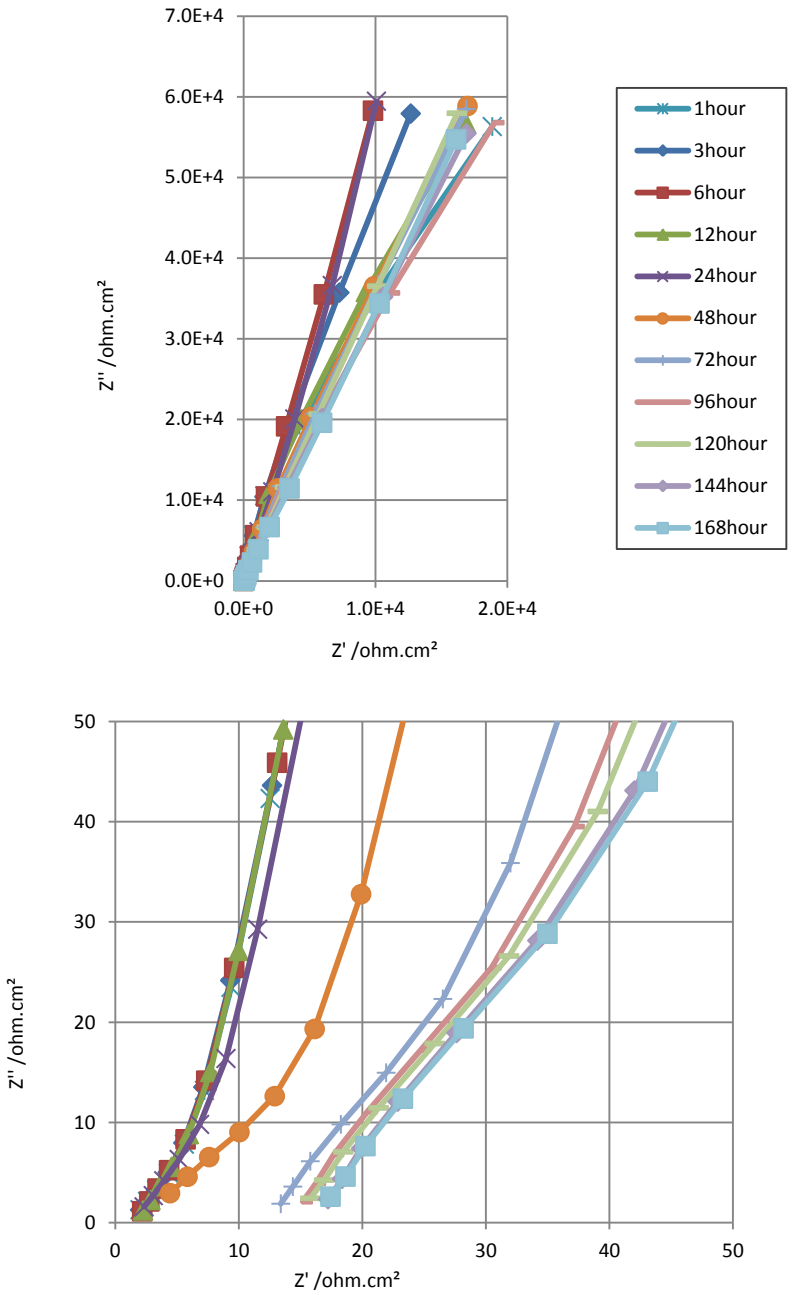

Figure 6.11 – a) Nyquist plots of defected $Ce(dpp)_3$ Epigen coated AA2024-T3 tested over 168 hours, b) Expanded Nyquist plots focussing on high frequency measurements

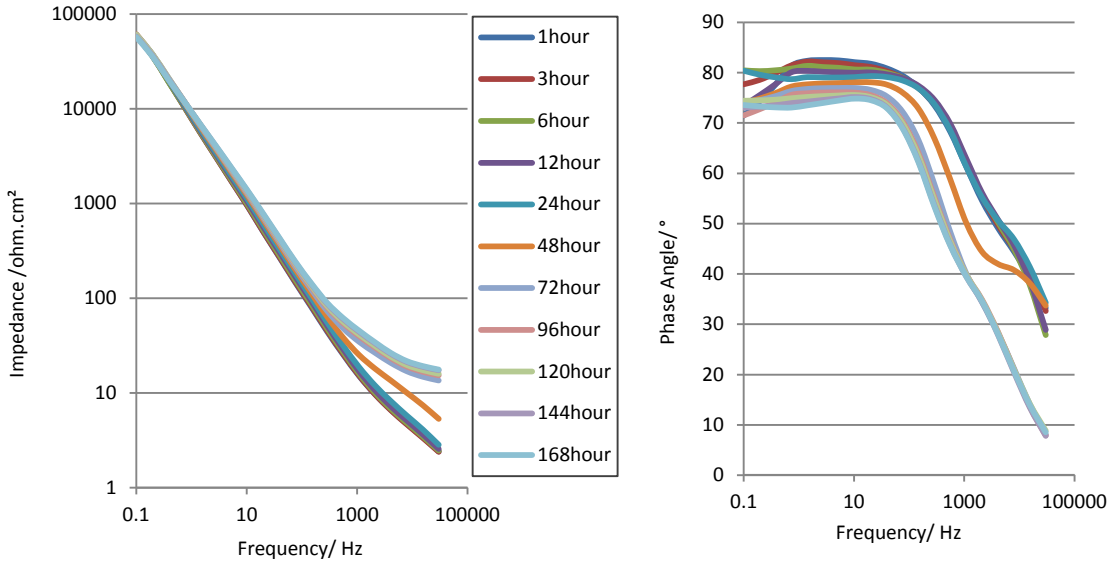

Figure 6.12 – a) Bode impedance plots of defected $Ce(dpp)_3$ samples, b) Bode phase angle plots

Time (hours)	Equivalent Circuit Model	CPE C_{oxide} ($x10^{-6}$ $S{\cdot}s^{-n}$ cm^{-2})	Freq. Power (n)	Resistance R_{oxide} (Ωcm^2)	CPE C_{pol} ($x10^{-5}$ $S{\cdot}s^{-n}$ cm^{-2})	Freq. Power (n)	Resistance R_{pol} ($x10^5$ Ωcm^2)	Chi-squared ($x10^{-3}$)
1	R(QR)(QR)	9.3	0.76	4.6	2.3	0.92	2.7	1.6
3	R(QR)(QR)	11.0	0.76	4.1	2.4	0.92	6.0	1.5
6	R(QR)(QR)	6.1	0.83	3.5	2.4	0.91	10.7	0.7
12	R(QR)(QR)	1.4	0.96	2.7	2.3	0.90	4.0	1.6
24	R(QR)(QR)	1.7	0.91	3.6	2.3	0.89	12.0	1.3
48	R(QR)(QR)	1.3	0.86	9.0	2.2	0.88	5.2	1.9
72	R(QR)(QR)	0.9	0.95	9.9	2.2	0.88	4.1	1.8
96	R(QR)(QR)	0.9	0.95	12.3	2.2	0.86	4.6	2.0
120	R(QR)(QR)	1.0	0.93	12.8	2.2	0.86	8.3	2.4
144	R(QR)(QR)	0.8	0.96	13.0	2.3	0.85	6.6	2.7
168	R(QR)(QR)	0.8	0.95	12.8	2.3	0.84	7.7	3.2

Table 6.4 – Model Parameters for defect $Ce(dpp)_3$ Epigen coated AA2024-T3 for 168 hours

From figure 6.11a, it can be seen that the size of the second semicircles in the Nyquist plots remain large over the course of the week of testing, which is completely different to the tests in bulk solution. The first semicircle merges into the second semicircle, seen in figure 6.11b, and is a lot smaller, only seen at very high frequency measurements. The corresponding Bode plot in

figure 6.12a shows little change in impedance in the low frequency measurements, but as time progressed, the high frequency measurements show increased impedance. Calculated parameters from equivalent circuit fits are presented in table 6.4.

Looking at the polarisation resistance, R_{pol}, in table 6.4, we see that the resistance increases from 0.3 to 1.2MΩcm^2 in the first 24 hours. At 12 and 48hours, R_{pol}, drops from >1MΩcm^2 to 0.5MΩcm^2. However, R_{pol} values remain greater than 0.4MΩcm^{-2}, which are higher than the resistances seen in the 113-22 coated tests in section 5.3.4.2, and a R_{pol} against time graph is plotted in figure 6.14. However, it should be noted that the thickness of the Epigen coating is ten times greater than the 113-22 coating, which means that there is a larger supply of inhibitive pigments in the $Ce(dpp)_3$ Epigen system. The oxide resistance is again very low, suggesting that there is are defects or pits in the oxide layer.

Figure 6.13 and 6.14 shows the Nyquist and Bode plots for a repeat experiment. Calculated parameters from equivalent circuit fits are presented in table 6.5.

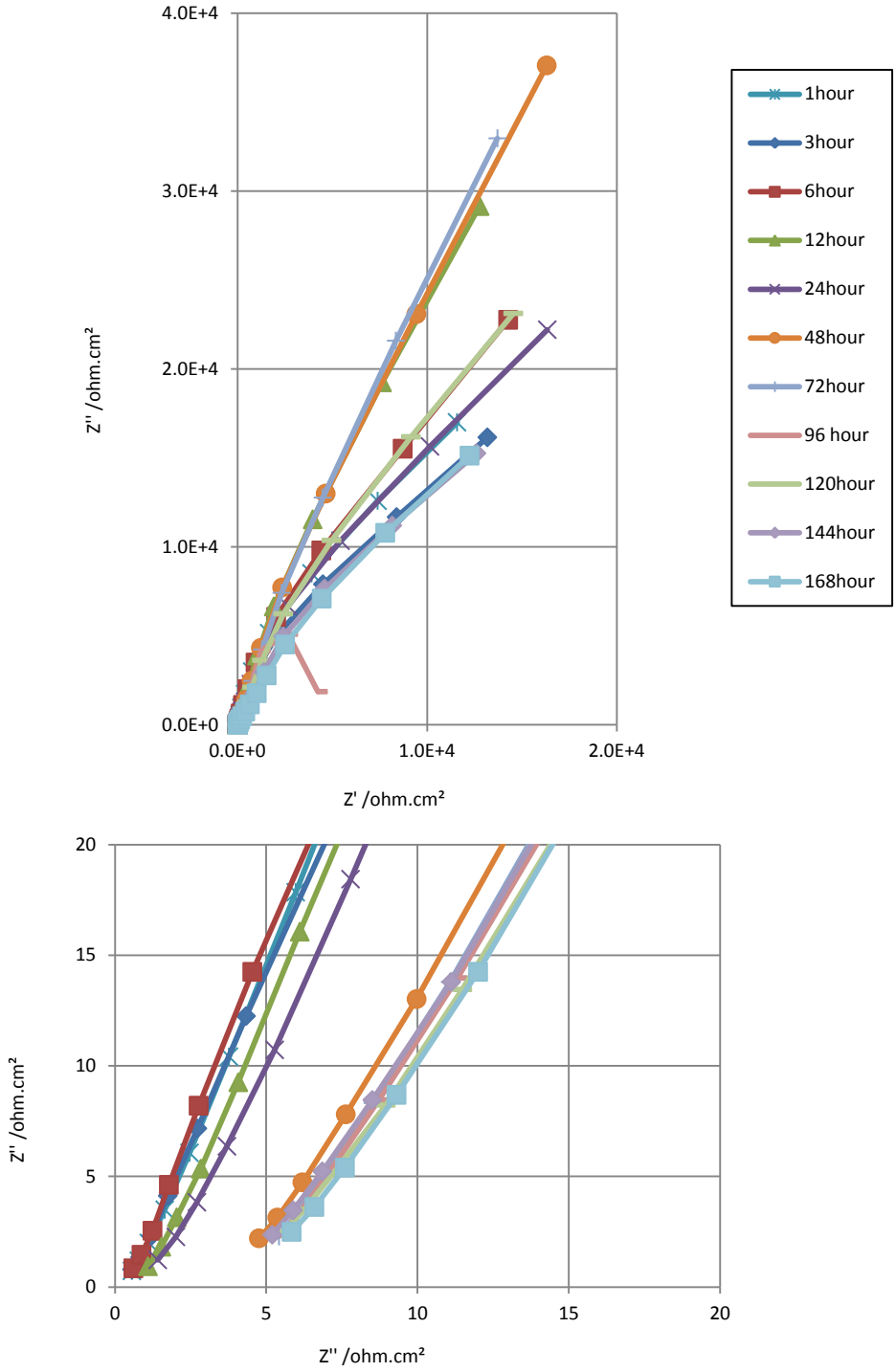

Figure 6.13 – a) Nyquist plots of defected $Ce(dpp)_3$ Epigen coated AA2024-T3 tested over 168 hours, b) Expanded Nyquist plots focussing on high frequency measurements

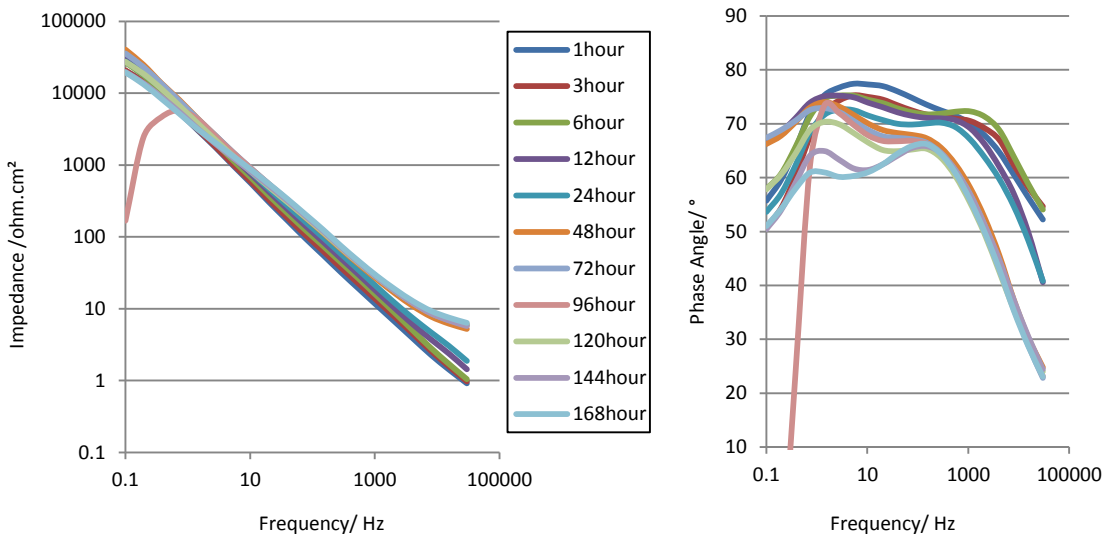

Figure 6.14 – a) Bode impedance plots of defected $Ce(dpp)_3$ samples, b) Bode phase angle plots

Time (hours)	Equivalent Circuit Model	CPE C_{oxide} ($x10^{-4}$ $S{\cdot}s^{-n}$ cm^{-2})	Freq. Power (n)	Resistance R_{oxide} (x10 Ωcm^2)	CPE C_{pol} ($x10^{-5}$ $S{\cdot}s^{-n}$ cm^{-2})	Freq. Power (n)	Resistance R_{pol} ($x10^4$ Ωcm^2)	Chi-squared ($x10^{-3}$)
1	R(QR)	-	-	-	5.3	0.84	5.6	6.5
3	R(QR)	-	-	-	5.3	0.83	4.6	3.9
6	R(QR)	-	-	-	4.5	0.83	8.2	2.9
12	R(QR)	-	-	-	4.2	0.82	23.7	3.4
24	R(QR)	-	-	-	4.2	0.80	7.8	3.5
48	R(QR)(QR)	3.9	0.62	25.2	3.4	0.87	17.3	6.7
72	R(QR)(QR)	3.9	0.65	12.1	3.7	0.83	24.4	1.3
96	R(QR)	-	-	-	4.1	0.78	1.3	146
120	R(QR)	-	-	-	4.8	0.76	15.9	5.1
144	R(QR)(QR)	1.1	1	5.4	5.8	0.74	6.6	3.2
168	R(QR)(QR)	0.8	1	13.3	6.2	0.73	6.7	4.7

Table 6.5 – Model Parameters for defected $Ce(dpp)_3$ Epigen coated AA2024-T3 for 168 hours

The sizes of the second semicircles are smaller than those seen in figure 6.13b and the R(QR) model frequently had to be resorted to calculate the overall polarisation resistance rather than separating the model components. The 96 hour measurements on the two graphs also show the impedance dropping sharply during the low frequency measurements, suggesting that the system is pitting.

Table 6.5 shows the model parameters for a repeat test on the $Ce(dpp)_3$ Epigen coated system and the R_{pol} values are noticeably smaller than those in table 6.4. R_{oxide}, when calculated, is also small, suggesting that there is a pit in the oxide layer. Although lower than the first test, the polarisation resistance (the sum of the calculated resistances) is still comparable to values calculated for the defected 113-22 coated tests, which suggest that the $Ce(dpp)_3$ inhibitor can provide similar protection to chromate-based inhibitors. The polarisation resistance against time graph in figure 6.15 again shows the dynamic build-up and breakdown of protection.

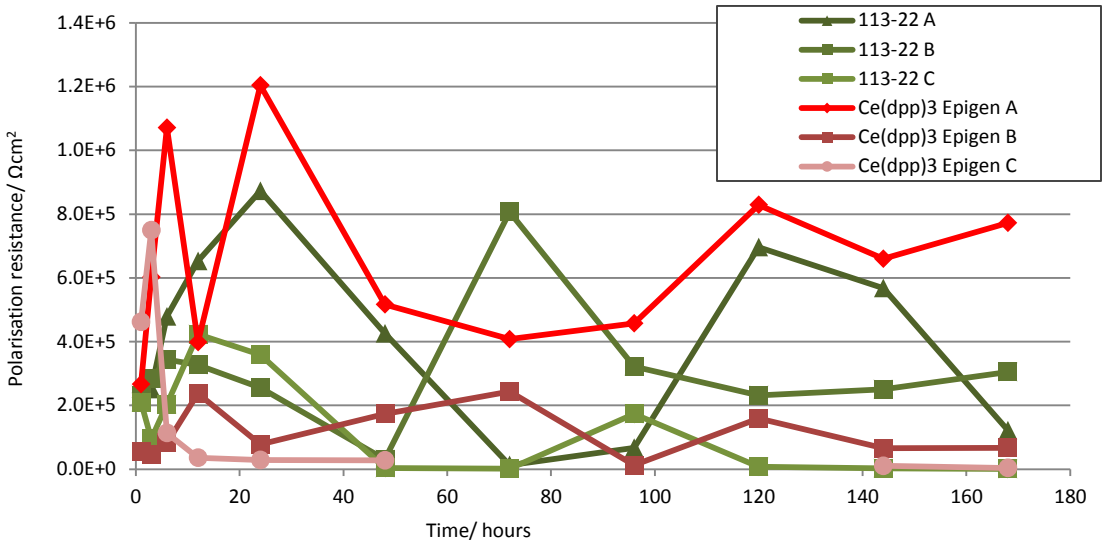

Figure 6.15 – Polarisation resistance against time for defected coated samples

Figures 6.16 - 6.17 and table 6.6 show the EIS data and model parameters for a second repeat test

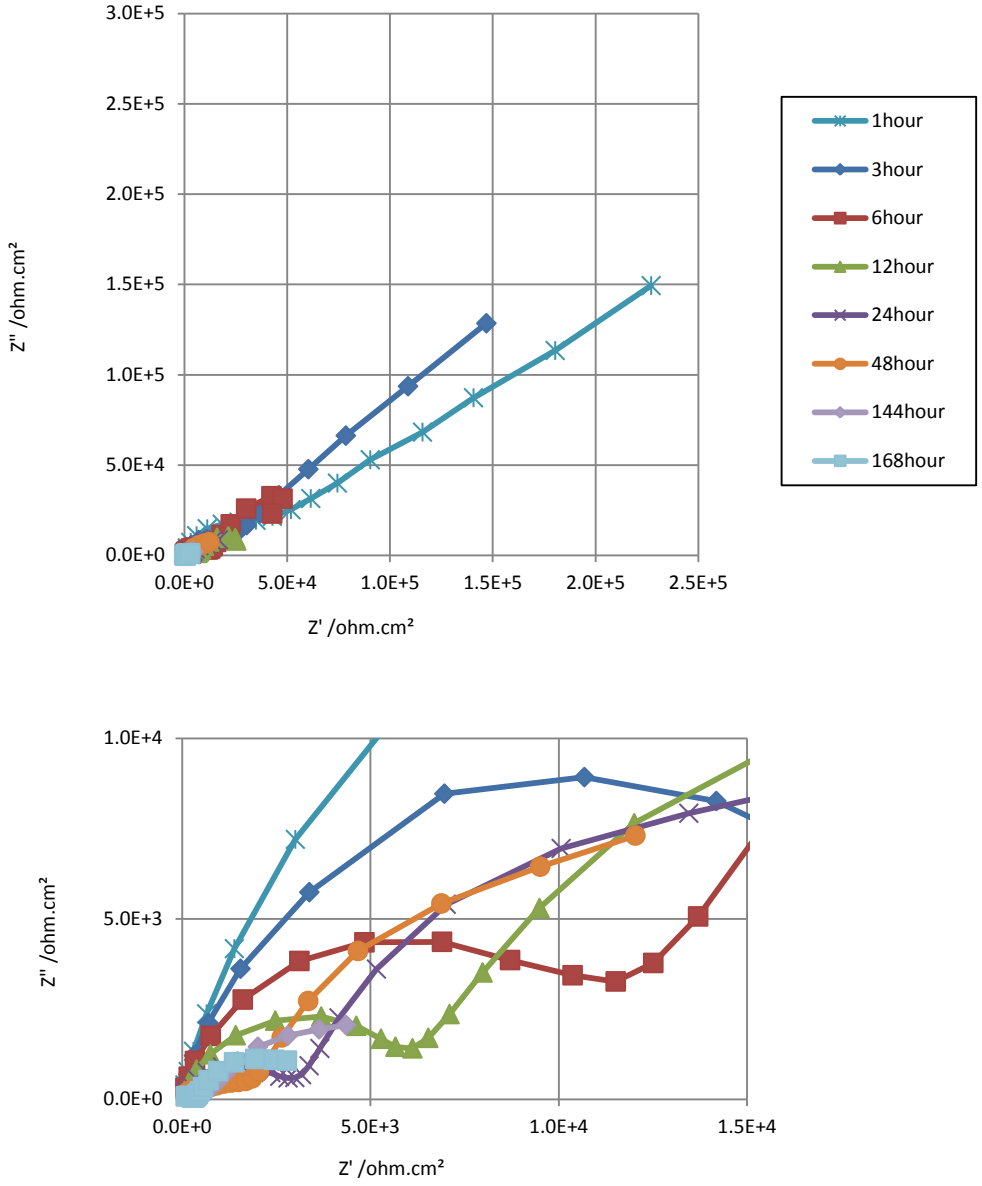

Figure 6.16 – a) Nyquist plots of defected $Ce(dpp)_3$ Epigen coated AA2024-T3 tested over 168 hours,

b) Expanded Nyquist plots focussing on high frequency measurements

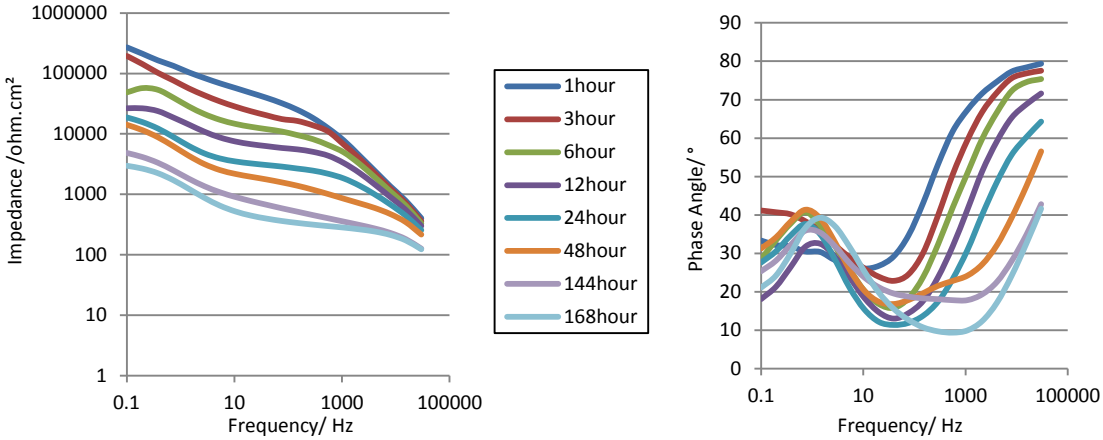

Figure 6.17 – a) Bode impedance plots of defected $Ce(dpp)_3$ samples, b) Bode phase angle plots

Time (hours)	Equivalent Circuit Model	CPE C_{oxide} ($x10^{-7}$ $S{\cdot}s^{-n}$ cm^{-2})	Freq. Power (n)	Resistance R_{oxide} ($x10^{3}$ Ωcm^2)	CPE C_{pol} ($x10^{-5}$ $S{\cdot}s^{-n}$ cm^{-2})	Freq. Power (n)	Resistance R_{pol} ($x10^{4}$ Ωcm^2)	Chi-squared ($x10^{-2}$)
1	R(QR)(QR)	0.6	0.88	38.5	0.3	0.64	42.4	1.3
3	R(QR)(QR)	0.4	0.94	15.9	0.6	0.59	73.4	0.5
6	R(QR)(QR)	0.9	0.86	10.2	1.0	0.66	10.3	1.9
12	R(QR)(QR)	1.6	0.82	5.8	1.8	0.72	3.0	0.3
24	R(QR)(QR)	4.3	0.75	2.9	4.4	0.72	2.6	0.2
48	R(QR)(QR)	35.0	0.58	1.5	6.5	0.66	2.6	1.0
144	R(QR)(QR)	71.7	0.56	0.4	17.9	0.54	1.0	0.5
168	R(QR)(QR)	16.6	0.67	0.3	19.3	0.68	0.4	0.2

Table 6.6 – Model Parameters for defected $Ce(dpp)_3$ Epigen coated AA2024-T3 for 168 hours

The second repeat test shows polarisation resistance rapidly increasing initially but then falls away quickly. The Nyquist plots seen in figure 6.16 show a larger high frequency semicircle compared to those seen in the previously and R_{oxide} values reflect a higher resistance. This could be due to a thickening oxide layer, providing passivity. This anodic inhibition by the diphenylphosphate ions has been suggested by various authors [ref]. Looking at the rest potential against time graph in figure 6.18 $Ce(dpp)_3$ Epigen C, it can also be seen that the rest potential of this test does not start off at a low potential ~-800mV, like the other two tests, but rather at approximately -650mV, further indicating that the corrosion resistance exhibited is

unlikely to be due to cathodic inhibition. However, once the protection falls away, the impedance of the system continues to steadily decrease over time. No cathodic inhibition appears to be exhibited in this repeat test.

6.4.1 Rest Potential against Time from Electrochemical Impedance Spectroscopy Data

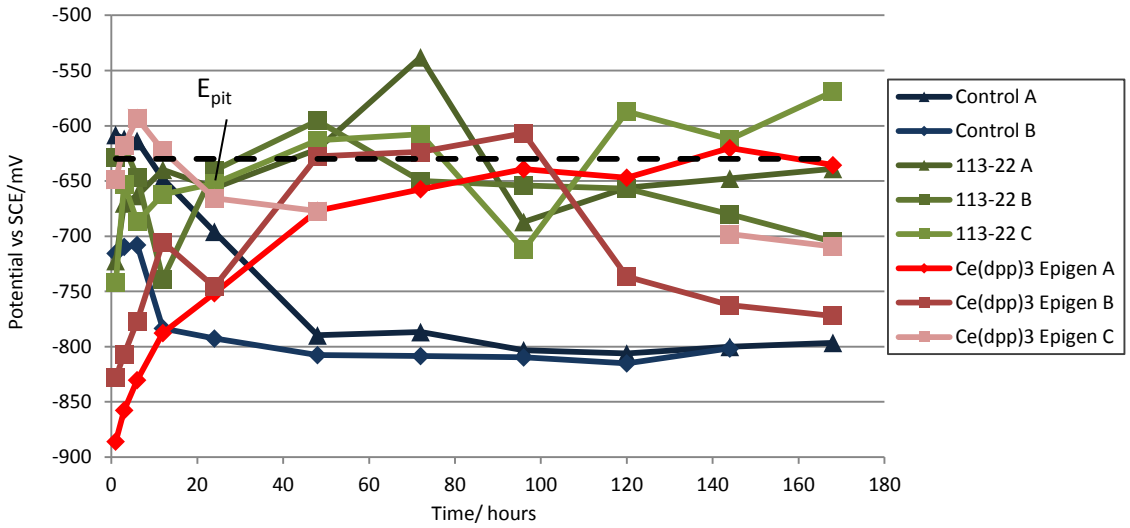

Figure 6.18 – Rest potential of defected coated AA2024-T3 samples before EIS tests

Figure 6.18 shows the rest potentials of the EIS tests before the impedance measurements were performed. The high concentration of aggressive chloride ions means that the alloy is likely to rest close to or on the pitting potential, E_{pit}, which is marked by the black dashed line at approximately -630mV. The control coated samples, displayed on the graph with blue lines, show the potential of the alloy decreasing over time, and by 48hours, the potential drops to approximately -800mV and remains there. This is likely to be the onset of stable pitting corrosion. However, the chromate and cerium inhibitors are known cathodic inhibitors, meaning that the cathodic reaction, e.g. oxygen reduction, is inhibited and the lowering of the rest potential would be related to the suppression of the cathodic reaction so that the corrosion

potential is lowered and a passive region is created. Markley et al. noted that $Ce(dpp)_3$ in solution lowered the corrosion potential of AA2024-T3, into the cathodic region[75].The rest potentials of the $Ce(dpp)_3$ started off the lowest at -830 to -885mV, indicating rapid cathodic inhibition from the inhibitors, but the graph above shows the potential increasing as time progressed. This is could possibly be due to the depletion of available inhibitive cerium ions around the exposed alloy and the alloy moving towards the stable pitting. The lowering of the rest potential for the $Ce(dpp)_3$ Epigen B line from 96hours could be a delayed release of inhibitor, leading to renewed cathodic inhibition, or the development of pitting corrosion. It is not certain what causes the delayed release, but could be related to factors including diffusion of inhibitive ions through the polymer coating, corrosion attack leading to fresh coating surfaces.

6.5 Potentiodynamic Corrosion Behaviour of Coated Samples with a Large Defect

Direct current polarisation testing was performed in the large volume test cell, as described in section 2.3.1. Tests were performed at both ambient temperature and at 30°C and compared with chromate pigmented paint.

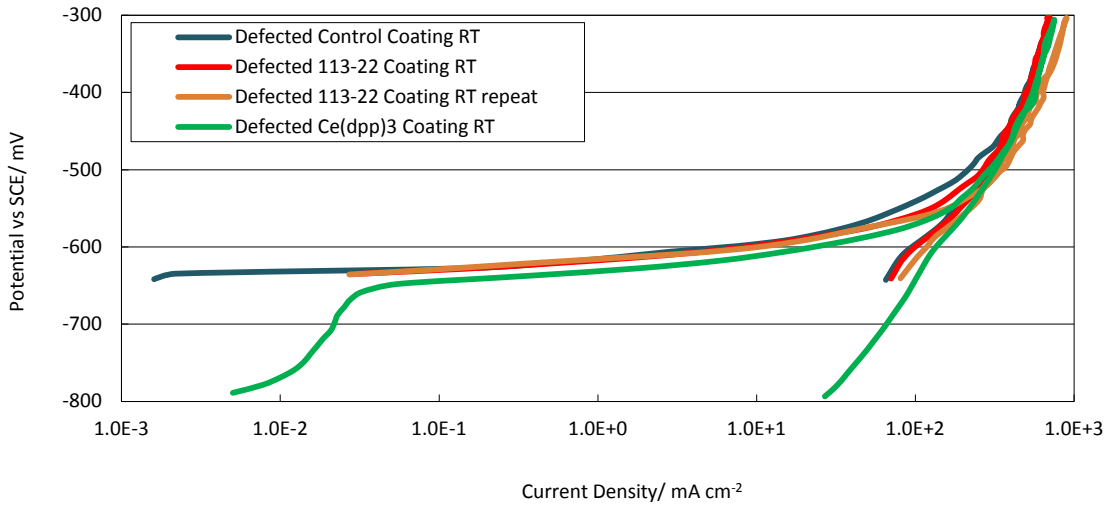

Figure 6.19 – DC Polarisation curves of defected coated AA2024-T3 in 2M NaCl at room temp.

Figure 6.19 shows the anodic polarisation curves for AA2024-T3 coated with the three different epoxy coatings tested after two days at room temperature. The current-density data has been area-corrected to the size of the defect, 1mm x 10mm. The anodic behaviour for two of the coated samples, control and 113-22, showed similar corrosion behaviour to the bare alloy tests, where the rest potential lies at the pitting potential and when the potential is increased, current density increases rapidly.

The rest potential for the room temperature $Ce(dpp)_3$ Epigen coated test has fallen to -778mV, approximately 150mV lower than the two other systems, so when the potential is increased, a passive region is observed, indicating that the presence of inhibitive pigments is providing corrosion protection for the bare surface, even for tests in bulk solution. The pitting potential is reached at -670mV, which means that the passive barrier is approximately 110mV.

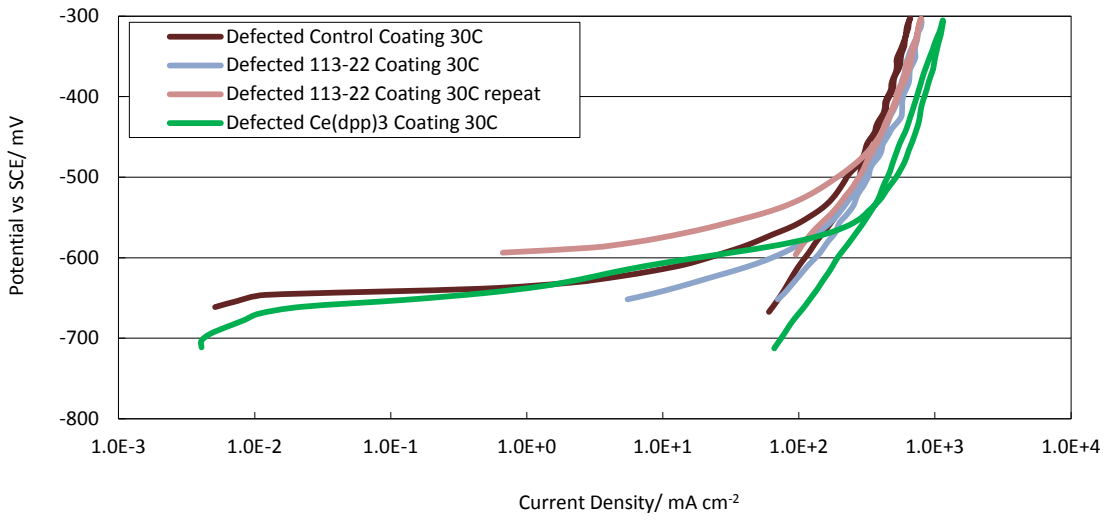

Figure 6.20 – DC Polarisation curves of defected coated AA2024-T3 in 2M NaCl at 30°C

Figure 6.20 shows similar anodic polarisation curves for AA2024-T3 coated with the three different epoxy coatings tested after two days at 30°C, with current-density data area-corrected to the size of the defect, 1mm x 10mm. Both the control and 113-22 coated samples pitted quickly once potential was increased.

However, the rest potential for the 30°C $Ce(dpp)_3$ Epigen coated test starts at -703mV, with the pitting potential difficult to determine at approximately -680mV. This means that there is only a 20mV potential difference at 30°C compared to a 110mV difference seen in the room temperature test. The effectiveness of chromate inhibitors in solution were shown to diminish when the temperature was raised from ambient temperature to 30°C, in chapter 3, and from this test, AA2024-T3 again appears to be a lot more susceptible to pitting corrosion at 30°C and the inhibitive cerium species do not provide as great protection.

Potentiodynamic polarisation tests for the $Ce(dpp)_3$ Epigen coated samples were also performed after one week of immersion to allow more time for the inhibitive ions to interact with the bare alloy surface as before. Direct comparisons with chromate pigment can be made with the polarisation tests in section 5.2.2.1.

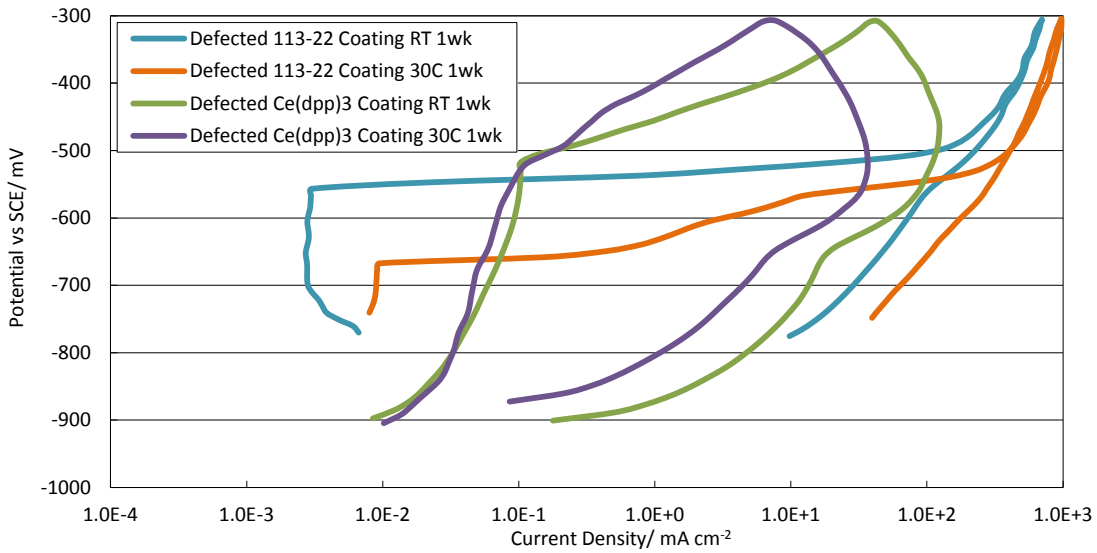

Figure 6.21 – DC Polarisation curves of defected coated AA2024-T3 samples in 2M NaCl

Similar to the 1-week 113-22 coated tests, after immersing the $Ce(dpp)_3$ Epigen coated samples in 2M sodium chloride solution for one week showed significant difference in potentiodynamic corrosion behaviour. The rest potential for the defected 113-22 coated sample at room temperature fell to -760mV while the pitting potential was raised to -556mV, creating a passive potential barrier of almost 200mV. The rest potential for the $Ce(dpp)_3$ Epigen coated sample fell even further to -885mV and the pitting potential was raised to -517mV. A passive potential barrier of 367mV was observed.

For the test at 30°C, it was noted before that the rest potential of the 113-22 coated sample after one week fell to -731mV, but the pitting potential did not change significantly, still being at

-667mV. However, the rest and pitting potentials of the $Ce(dpp)_3$ coated sample at 30°C were similar to the room temperature test, at -892mV and -518mV respectively. Therefore, in this case, the protection provided by the $Ce(dpp)_3$ pigment is much better than the chromate pigment and is maintained even at 30°C.

It can be seen in this section that the $Ce(dpp)_3$ inhibitive species in the Epigen epoxy paint provides significant corrosion inhibition in potentiodynamic polarisation tests. Longer immersion times lowered the free corrosion potential and increased the passive potential range and can be due to inhibitive ions forming complexes over electrode sites, increasing thickness of the oxide layer[75]. Potentiodynamic tests appear to suggest that cerium-based inhibitors are better corrosion protectors than chromate-based inhibitors.

6.6 Scanning Acoustic Microscopy Analysis

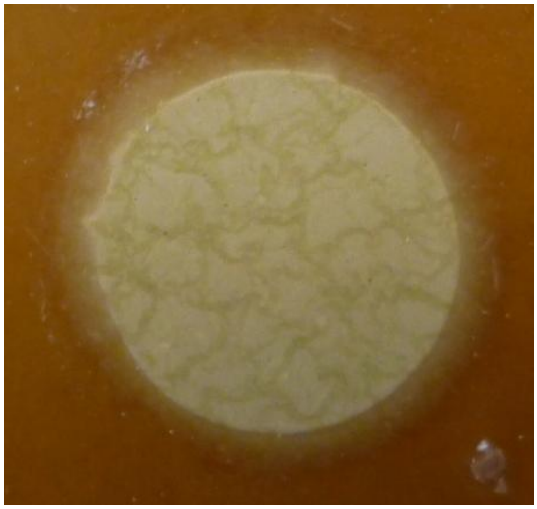

Figure 6.22 – Digital photograph of fully intact $Ce(dpp)_3$ Epigen surface immersed in 2M NaCl

Figure 6.22 shows a photograph of a fully intact $Ce(dpp)_3$ Epigen coated surface after being immersed in 2M sodium chloride solution for four weeks. Direct observation and the digital photograph in figure 6.25, show that the coating loses its light brown colour after immersion. The brown colour has been related to the interaction between the cerium species and amines in the epoxy[86], so the loss of colour suggests the cerium species/pigment is released from the coating when immersed in solution although has not been determined to what degree and what depth.

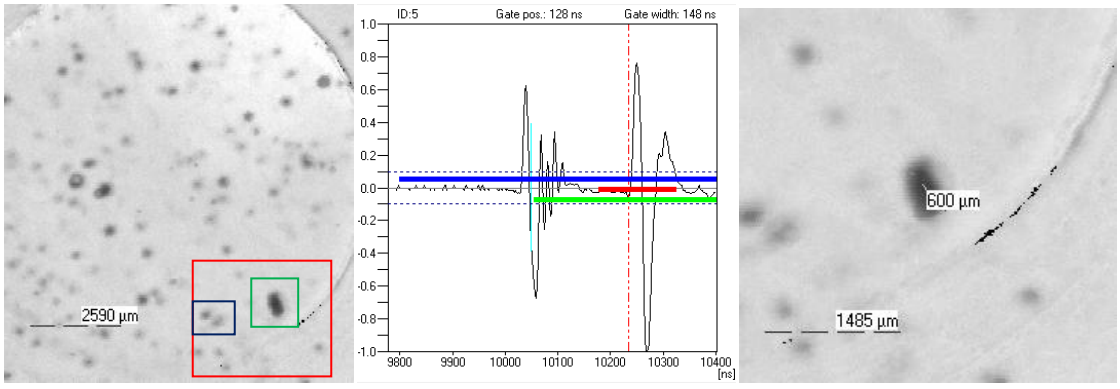

Figures 6.23a-e – a) C-scan, gate set at coating-metal interface, b) A-scan of image 6.23a, c) Close up of red squared-area of image 6.23a, *continued on next page*

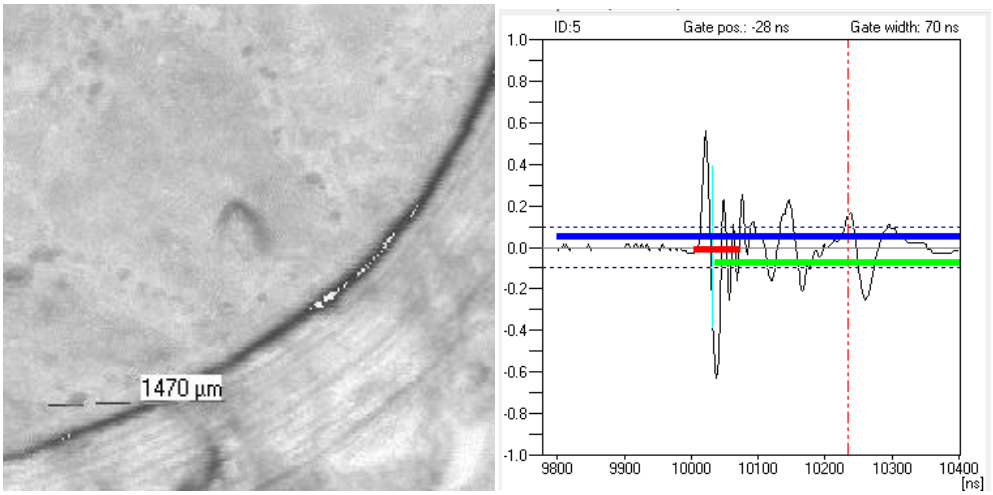

Figures 6.23a-e – a) C-scan, gate set at coating-metal interface, b) A-scan of image 6.23a, c) Close up of red squared-area of image 6.23a, d) C-scan, gate set at coating surface, e) A-scan of image 6.23d

Figure 6.23 shows scanning acoustic micrographs of the tested sample that has been dried for two weeks in figure 6.22. The A-scans were used to determine where the gate for the C-scan is set. They also reveal the time difference as the acoustic wave passes through different interfaces and therefore the approximate speed of the wave in each layer can be calculated.

The average coating thickness has been measured as 250µm and the A-scan reveals the reflected time difference between the top surface of the coating and the interface to be typically 230ns. This time difference is halved to get the time for the wave to travel in one direction.

- Speed of acoustic wave in coating = 250µm/115ns = ~2200ms^{-1}

This value is slightly slower than to typical values of acoustic waves in epoxy resin (2650ms^{-1}).

Figure 6.23a is gated at the coating-metal interface, and an array of black dots can be seen across the sample surface. To interpret these features correctly, we need to examine the A-scan. Here we should find a weak reflection at the dark spots. When a SAM C-scan is gated at the top

surface of the coating, in figure 6.23d, there are no dark spots, confirming that the features in the other image are at the paint-metal interface or within the paint.

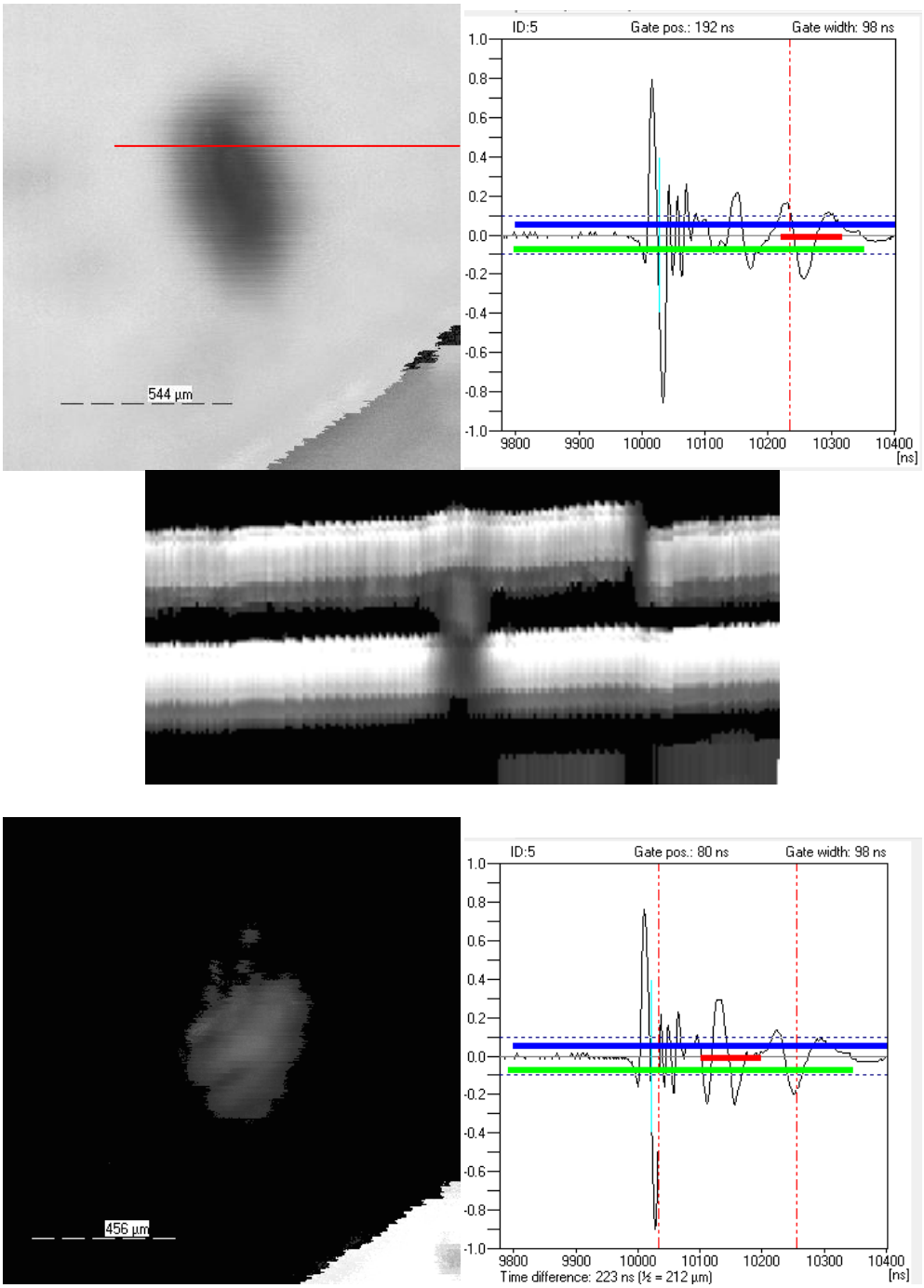

Figures 6.24a-e – a) C-scan of green square in image 6.23a, gate set at coating-metal interface, b) A-scan of image 6.24a, c) B-scan across red line in image 6.24a showing cross-section,d) C-scan, gate set within coating, e) A-scan of image 6.25d

Figure 6.24 shows the SAM examination of one of the spots, highlighted in figure 6.23a by the green square. Figures 6.24a and 6.24b show the C-scan and A-scan taken at the coating-metal interface and a black spot is seen, which strongly suggests a pit. Removal of the metal means that the reflection is no longer at a paint-metal interface, rather at a paint-solution interface. However, a B-scan, shown in figure 6.24c, across the red line in figure 6a reveals that the signal is lost halfway through the coating (the interface reflection is weak, but the phase is not reversed), and the A-scan in figure 6.24b also shows an extra strong acoustic signal in the middle of the coating. Another scan was made, gated at this intermediate signal, as seen in figures 6.24d and 6.24e, an object can be seen. This object lies in the middle on the coating 100-150microns above the coating-metal interface. Therefore, it is suggested that these objects could be holes in the polymer matrix that contain or contained pigment. The difference in the speed of the acoustic waves at these interfaces cause an extra reflection which the A-scan picks up. However, the signal moving from a slower medium to a faster medium, e.g. water to coating, coating to metal, has its phase reversed at the intermediate signals. This means that within the coating, the acoustic waves are passing through a slower medium before reaching the coating metal interface. The object looks like a feature at the interface, but it isn't. As much acoustic energy is reflected back by the object in the middle of the coating, only a weak signal reaches the interface and the reflection is proportionally weaker than the surrounding signals. This could be the wave entering a hole in the polymer matrix filled with water, but it should be noted that no reflection could be discriminated when the wave passes through the other side of the hole back into the polymer before the coating-metal interface signal is observed. However, the second pulse would be weaker – the transmitted beam is less strong and the difference in Z is small as well as being near to the resolution limit of the transducer frequency.

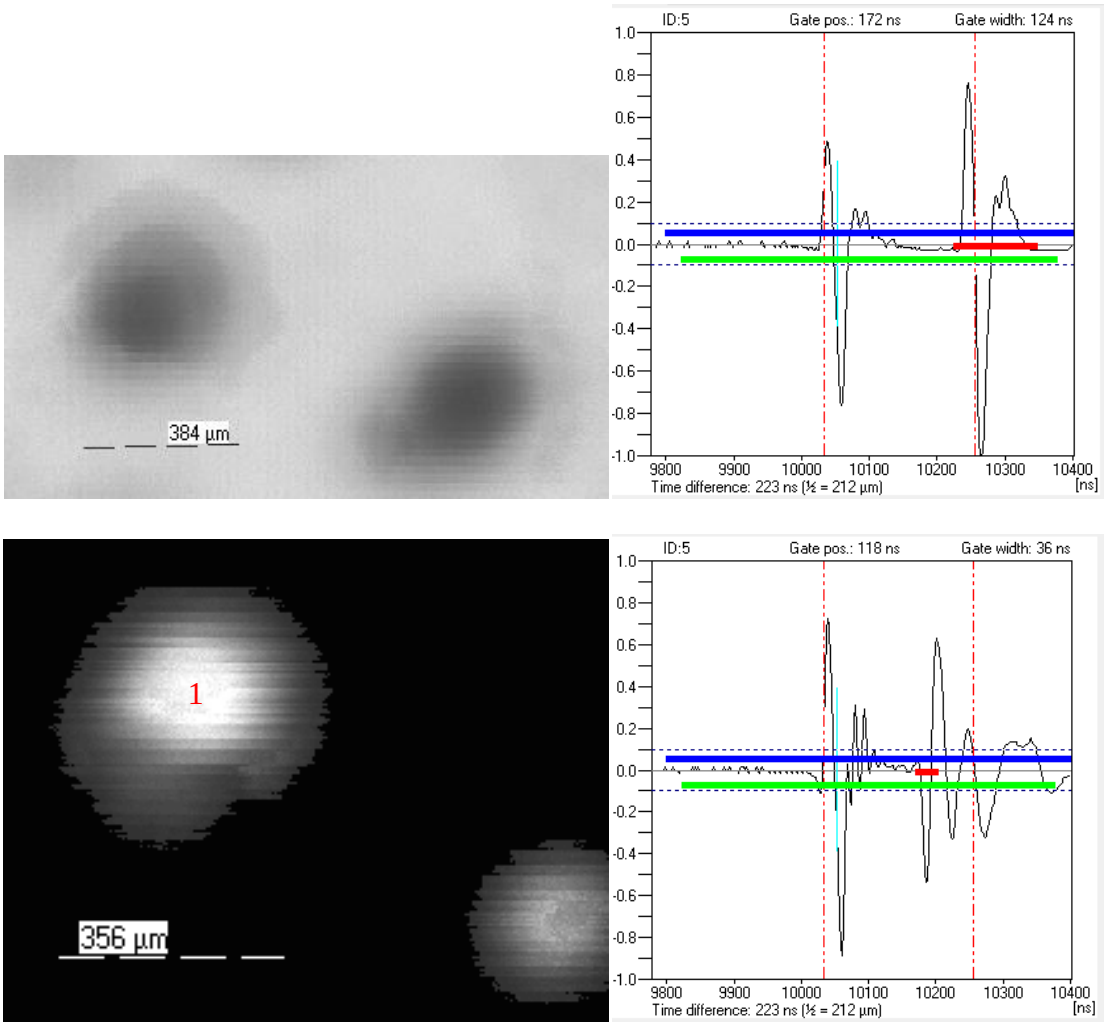

Figures 6.25a-d – a) C-scan of blue square in image 6.23a, gate set at coating-metal interface, b) A-scan of image 6.25a, c) C-scan, gate set within coating, e) A-scan of image 6.25d

Looking at another black spot, the area highlighted by the blue square in figure 6.23a is analysed. Again, when gated on the bulk coating, as in figures 6.25a and 6.25b, the black dots appear in the C-scan for the metal-coating interface micrographs but when the A-scan is focussed on the spot, as in figures 6.25c and 6.25d, extra intermediate signals are observed once again. The phase of the signal is again 'reversed', indicating the acoustic wave is passing into a slower medium. The signal also sits at a different height to the object in figure 6.24, which further supports the theory that the spots arise from object within the coating. This would mean that

the holes, probably caused by pigment, are randomly dispersed at different positions across the whole coating.

Figure 6.26 – Digital photograph of defected $Ce(dpp)_3$ Epigen coating immersed in 2M NaCl for 7 days

Figure 6.26 shows a digital photograph of a defected $Ce(dpp)_3$ Epigen coated sample tested in 2M sodium chloride solution for one week in the small volume cell. There is less fading of colour for the coating surface which suggests that less pigment has been released. The thickness gauge measured the coating thickness to be 150 – 250microns.

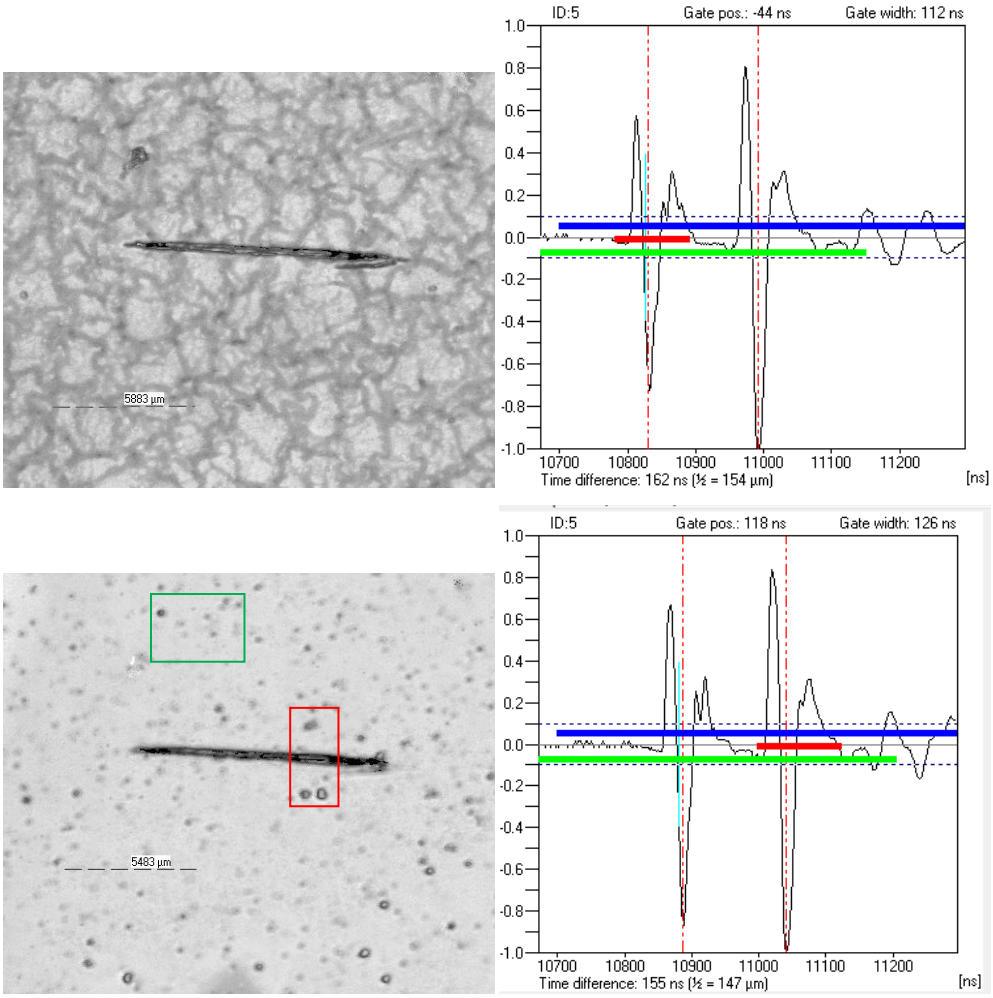

Figures 6.27a-d :

a) C-scan of defected $Ce(dpp)_3$ Epigen coating, gate set at top surface of coating, b) A-scan of image 6.27a, c) C-scan of image 6.27a, gate set at coating-metal interface, d) A-scan of image 6.27c

Figure 6.27 shows the C-scans at the top coating surface and at the coating-metal interface. At the interface, in figure 6.27c, the black spots are again seen dotted across the image. The areas, highlighted by the green and red squares in figure 6.27c, are analysed further.

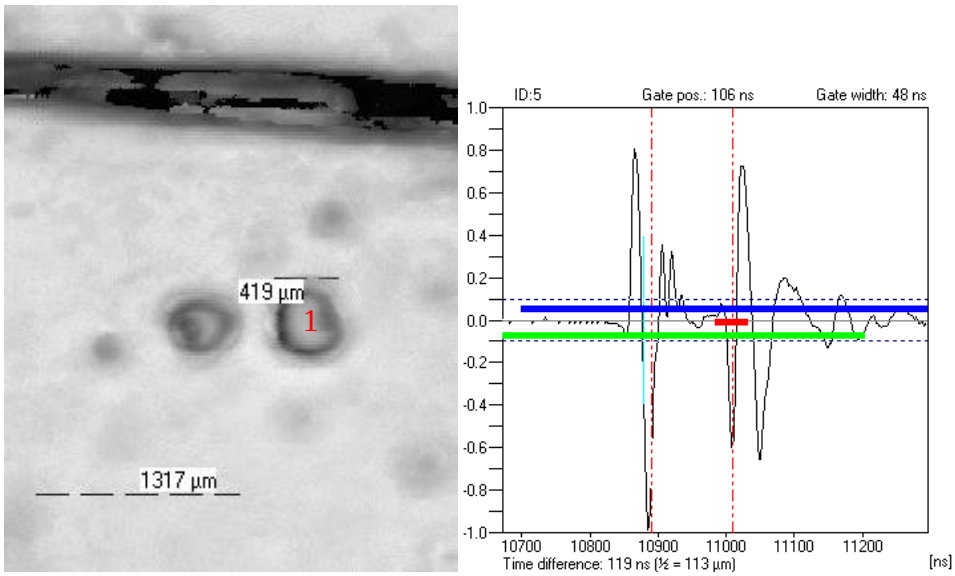

Figures 6.28a-b – a) C-scan of close-up of red square on image 6.27c, gate at coating-metal interface, b) A-scan of image 6.28a, showing depth of article labelled 1 in red on image 6.28a

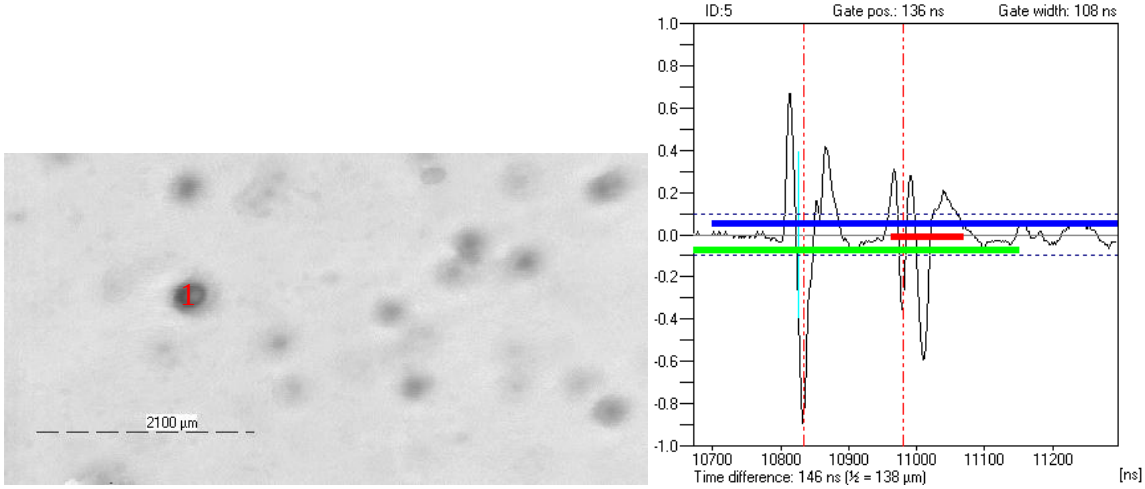

Figures 6.29a-b – a) C-scan of close-up of green square on image 6.27c, gate at coating-metal interface, b) A-scans of image 6.29a, showing depth of article labelled 1 in red on image 6.29a

Figures 6.28 and 6.29 show close-ups of the areas and similar to the previous analyses, intermediate peaks are seen on the A-scan signals when the gate is centred on the spots. The dark spots are therefore expected holes within the coating that cause signal loss below the object.

6.7 Optical Microscopy analysis

6.7.1 Top surface optical microscopy examination

The $Ce(dpp)_3$ Epigen coated samples were examined using a Zeiss Axioskop 2 MAT optical microscope with an Axiocam digital colour camera.

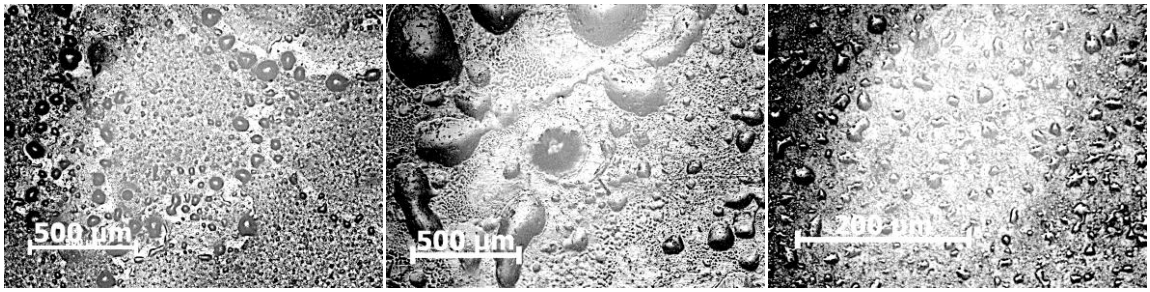

Figures 6.30a-d – Optical micrographs of untested $Ce(dpp)_3$ Epigen surfaces

Figure 6.30 shows images of the $Ce(dpp)_3$ Epigen coating before electrochemical testing and it can be seen that the morphology across the surface is quite uneven. Pores or holes of various sizes are found across the coating surface and range from 10s of microns to greater than 500 microns. It is possible that the holes were formed from poor mixing of paint components. The poor dispersion of the components could cause clusters of various sizes. It is possible that the pigment particles in the wet paint mixture could not be mixed thoroughly and agglomerate into larger clumps. The polymer matrix then form around the pigment particles and the holes across the polymer matrix can be seen. This would mean that the local concentrations at a defect would be heavily dependent on the amount of pigment close to the exposed surface. Tested surfaces (after EIS) were also examined as well as cross-sectional analysis.

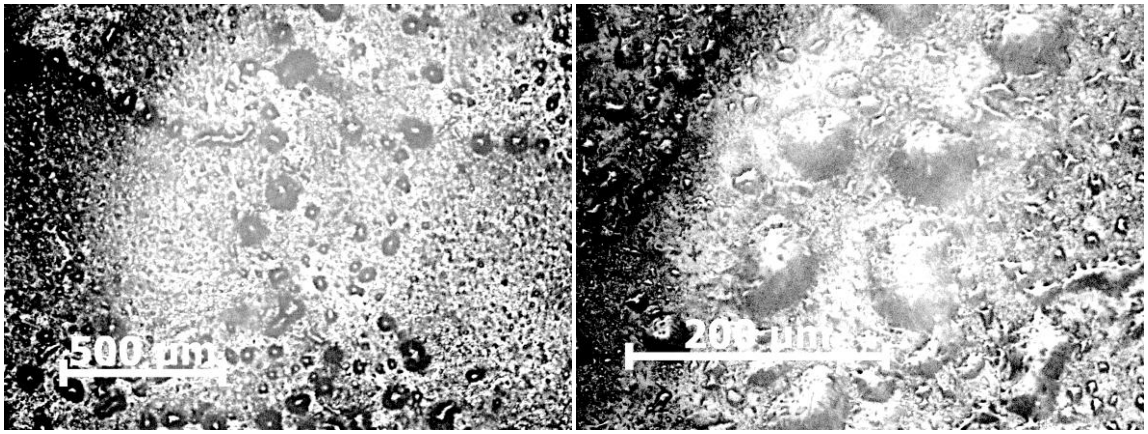

Figures 6.31a-b – Optical micrographs of $Ce(dpp)_3$ Epigen surfaces tested in 2M NaCl

Figure 6.31 shows optical microscope images of the $Ce(dpp)_3$ Epigen coating where the surface has been immersed in 2M sodium chloride solution for four weeks and undergone EIS testing. The morphology of the surface is still similar to the untested surfaces seen in figure 6.30. This indicates that the polymer does not significantly change morphology after water uptake and pigment release.

Figures 6.32a-b – Optical micrographs of $Ce(dpp)_3$ Epigen surfaces close to defect

Again, the same observations are seen when samples were examined close to a defect in figure 6.32. MicroXAM and cross-sectional optical microscopy were then used to investigate further.

6.7.2 Cross-section optical images of $Ce(dpp)_3$ coated AA2024-T3

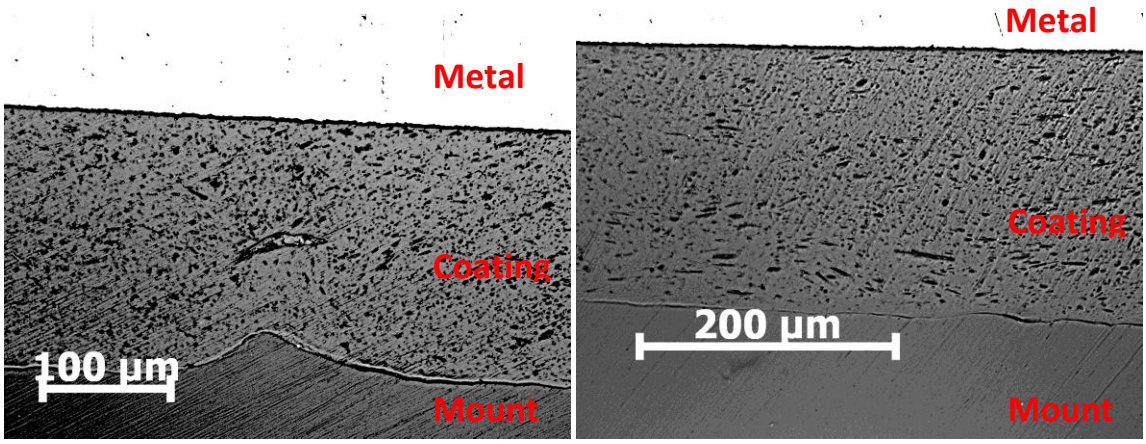

Figure 6.33a,b – Cross-sectional optical image of metal-coating-mount

Figure 6.33 shows the $Ce(dpp)_3$ coating polished down to 1µm diamond solution with the method described in chapter 2. An array of black dots and long black flakes are seen across the whole cross-section. It is likely to be the pigment particles distributed within the paint.

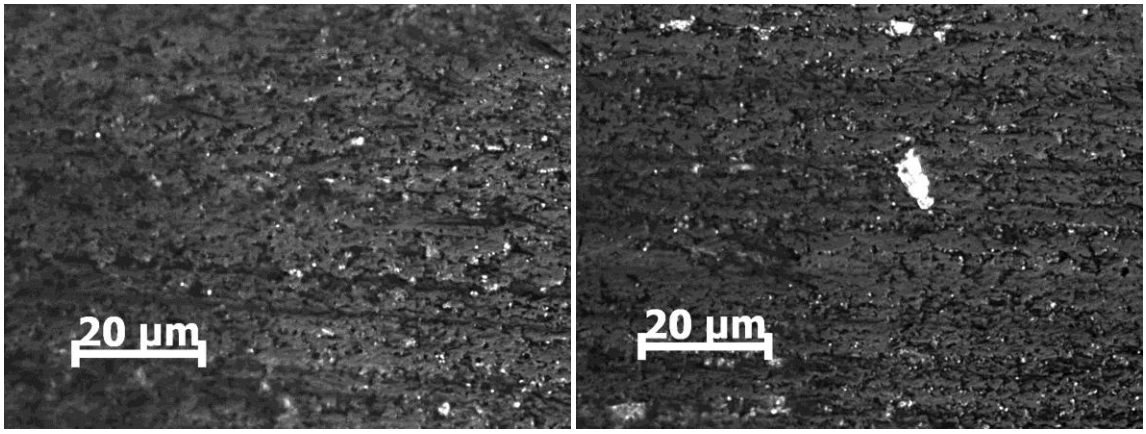

Figure 6.34a, b – Optical images of coating with image 6.34b showing a larger bright object

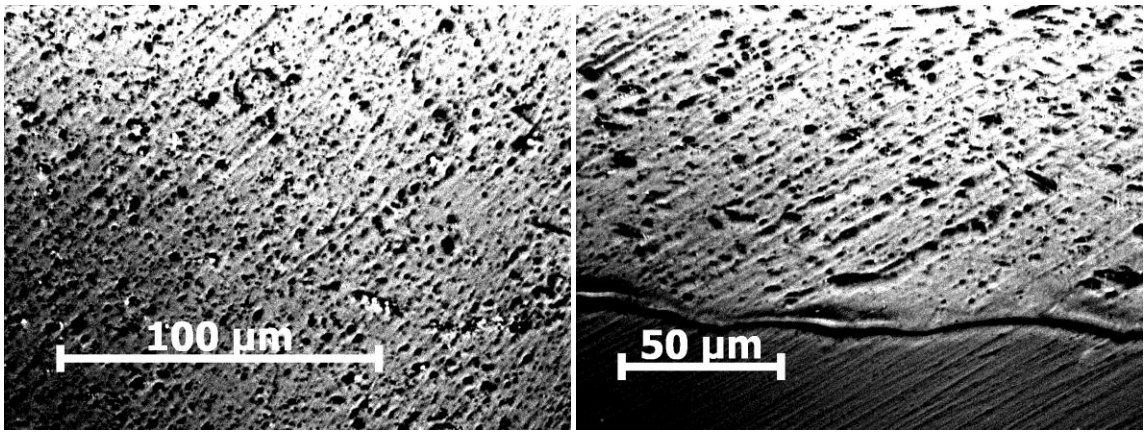

Figure 6.35c, d – Images of epoxy coating after further polishing

Figure 6.34 shows micrographs of the coating at a rougher polish (P1600 grit) during initial polishing. The black dots seen across the surface in figure 6.33 are not seen but white objects are observed instead. The black and white objects are typically less than a micron although figure 6.34b shows areas where a larger object is seen of approximately 10µm in size. The composition of the coating is stated as containing 20%wt cerium diphenylphosphate, and black specks, on figure 6.35, occupy a proportion of surface area that suggests it is due to the pigment. It seems likely that the specks went from white to black when light pigment particles become removed by dissolving or physical removal of the inhibitor during polishing, leaving the holes and areas were the pigments resided within the paint.

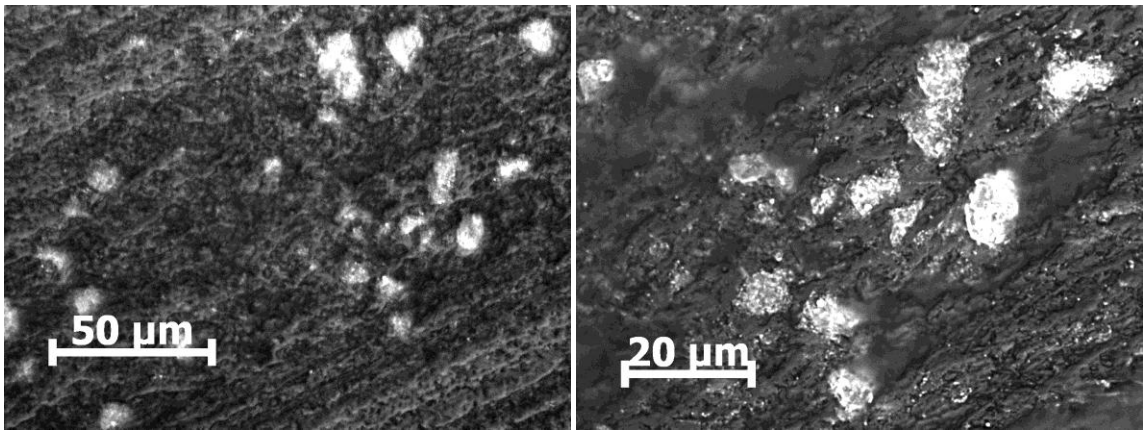

Figure 6.36a, b – Images of rough epoxy coating showing clusters of bright objects

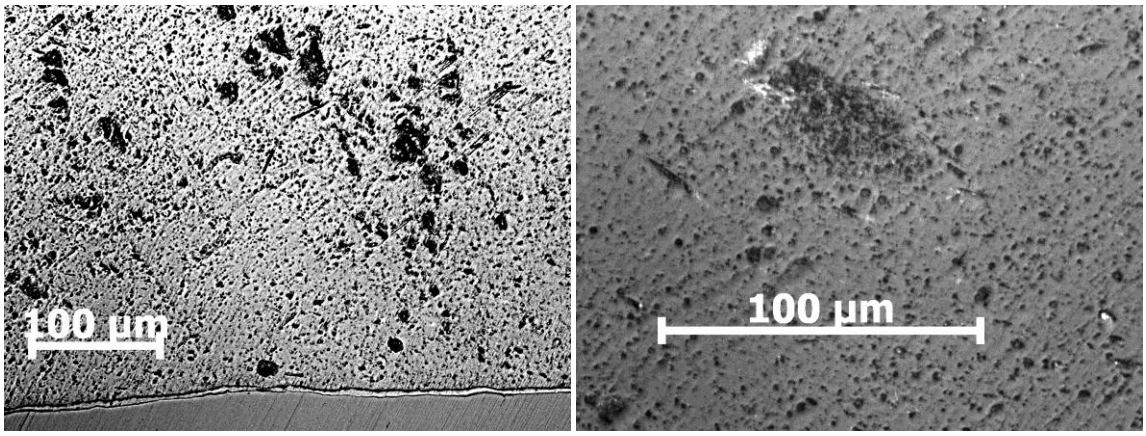

Figure 6.36c, d – Images of smooth coating after further polishing showing clusters of holes

Figures 6.36a and b show images of a cluster of bright features within the coating, with individual artefacts having a side of greater than 20µm in length. Again after further polishing in figures 6.36c and d, the bright specks disappear but clusters of dark holes can still be found.

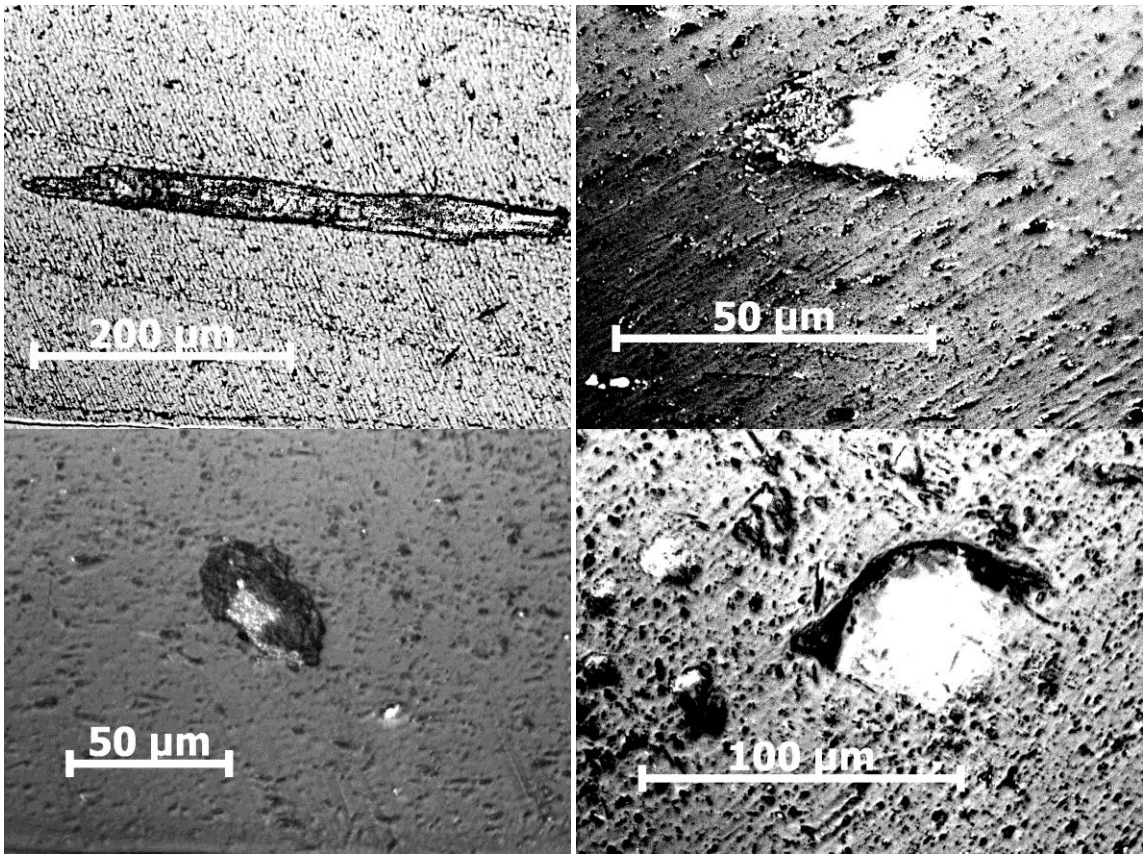

Figure 6.37a-d – Images of epoxy coating showing larger inclusions

The large inclusions seen in the cross-sectional optical images are likely related to the large objects observed in the SAM images (figure 6.23a).

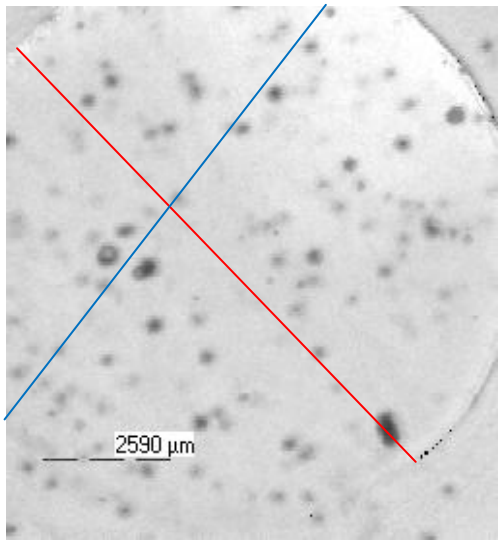

Figure 6.37 – SAM C-scan of $Ce(dpp)_3$ coating (from figure 6.23)

Figure 6.37 shows images of some larger inclusions observed. There were not very frequently observed across the cross-sectional images, but a simple line analysis of the SAM image (drawing lines across image above to see how many objects are intersected) shows that this low frequency isn't unexpected. It is possible that these larger objects are agglomerates of inhibitive pigment, and the dispersion of holes across the whole cross-section show that most of the pigment is more evenly distributed in the coating.

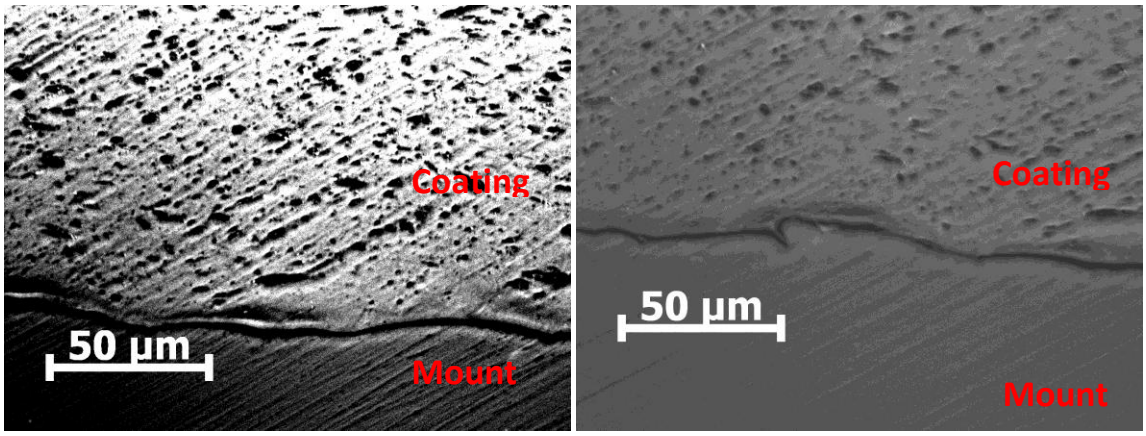

Figure 6.38a, b – Images of coating surface showing curved depressions of various sizes

Figure 6.38 shows the topographical features at the surface of the paint related to the large holes seen across the surface of the coating. The curved depressions do not reveal any large holes or cavities. It is not certain how the coating was applied, but the depressions could be due to air bubbles on the surface of the wet coating or imbalanced evaporation of the solvent.

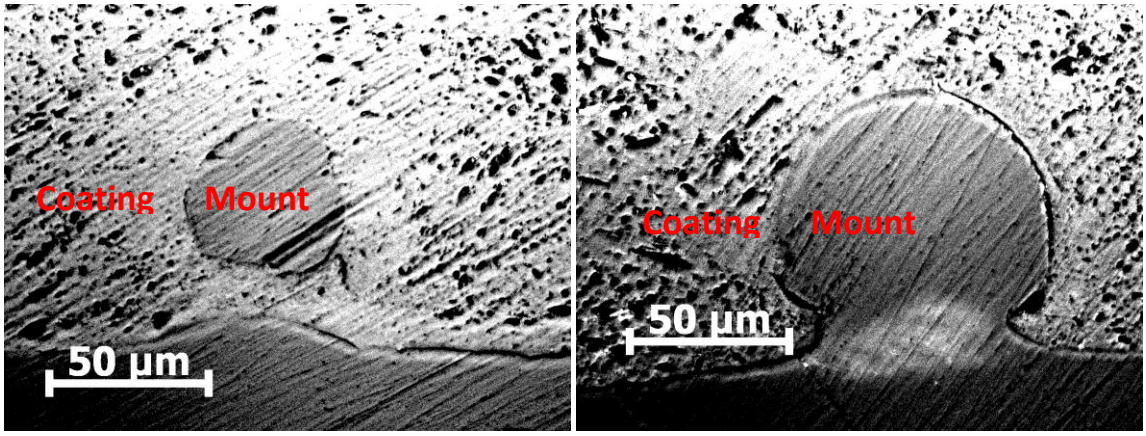

Figure 6.39a, b – Image of coating surface showing a circular cavity

The large holes observed on the surface of the coating using optical microscopy and MicroXAM (in the next section) were occasionally seen in the cross-section images. Figure 6.39 shows large circular holes that appear beneath a smaller depression on the coating surface. A small number of these cavities were found across the samples which suggest that the numerous holes seen on the surface are likely to be air bubbles that were encased by viscous polymer during the coating application. In figure 6.39b, the neck linking the bubble to the surface can be seen, but the connection appears to be out of the plane of section.

6.8 MicroXAM analysis

The $Ce(dpp)_3$ Epigen coated samples were also examined with the MicroXAM to investigate the depths of the depression.

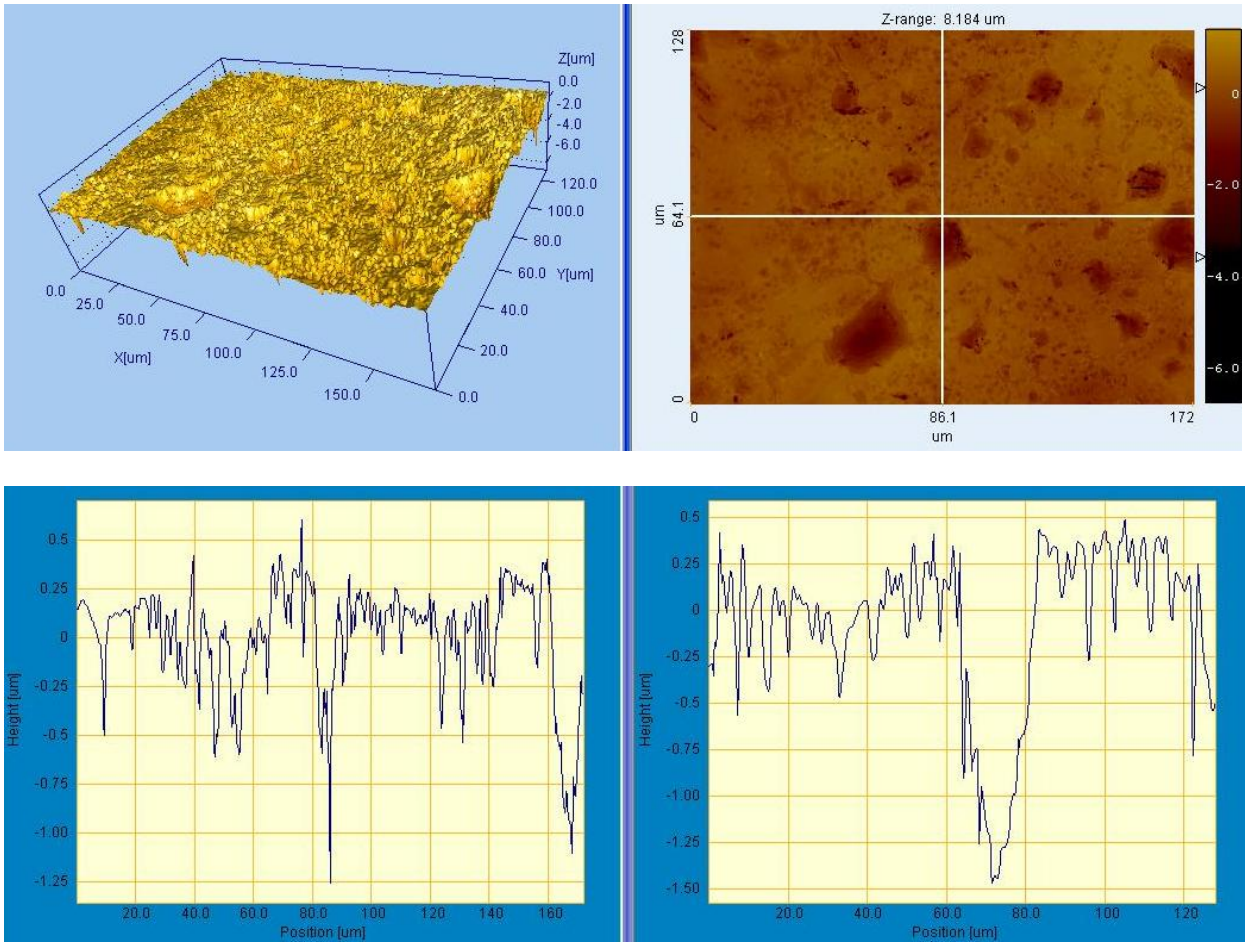

Figure 6.40a-d – a) 3-axis and top-surface MicroXAM images of $Ce(dpp)_3$ coating, b) X and Y-axis height analyses across the c) horizontal and d) vertical lines on figure 6.40b

Figure 6.40 shows images from a MicroXAM analysis across an intact tested surface of the $Ce(dpp)_3$ coating. MicroXAM analysis confirms that the features seen across the surface are holes rather than inflections and the height analysis shows that the inflections are only one micron or less in depth.

6.9 Discussion

The results from the electrochemical impedance spectroscopy and potentiodynamic polarisation tests on cerium diphenylphosphate inhibited epoxy-coated AA2024-T3 were promising. From the limited number of EIS experiments, it was found that the incorporation of $Ce(dpp)_3$ into Epigen did not consistently provide corrosion protection whether the coating was intact or damaged. Fully-intact coated samples still had pits on the alloy surface and defected coated samples exhibited corrosion resistances that were in general lower than the chromate-inhibited coating. However, in the one defected coated test where good corrosion protection was observed, corrosion resistances after a week of testing were greater than those calculated for the defected 113-22 coated tests.

Potential logging and polarisation experiments showed that given sufficient time, the free corrosion potential is greatly lowered and the pitting potential raised to provide both cathodic and anodic protection. It is expected that the cerium ions act as a cathodic inhibitor and diphenylphosphate as an anodic inhibitor. Markley, Forsyth and Hughes[75] tested cerium diphenylphosphate in solution on AA2024-T3 in solution and found that it predominantly protects as a cathodic inhibitor, decreasing the cathodic current density and lowering the rest potential. Cyclic potentiodynamic tests were also performed, with concentrations of 0.2mM $Ce(dpp)_3$ in 0.1M NaCl. The AA2024-T3 coupons were immersed in solution to rest for either 30 minutes or 24 hours before testing. The corrosion potential after 30 minutes, E_{corr}, was -501mV for 0.1M NaCl and adding 0.2mM $Ce(dpp)_3$ lowered it to -651mV. The pitting potential after 30 minutes was -514mV for the uninhibited system and -440mV for the 0.2mM $Ce(dpp)_3$ system. A passive region of 200mV was observed in the polarisation curves after 30 minutes of immersion, which indicate that the inhibitive species quickly adsorb unto the oxide surface, thickening the

oxide layer above the intermetallics (prone to become cathodic sites). After 24 hours of immersion, E_{corr}, was -453mV for 0.1M NaCl and -600mV for 0.1M NaCl with 2mM $Ce(dpp)_3$. No pitting potential information was given for the 24 hour test. It was suggested by Markley et al. that the $Ce(dpp)_3$ deposits itself as a thin protective film across the surface of the alloy. Cerium inhibitive species act as local cathodic inhibitors, suppressing the enrichment of copper-rich regions in the alloy which subsequently inhibits the intermetallic particles from becoming cathodic sites. They used Raman spectroscopy to identify Ce-O and O-P-O shifts and found that the cerium ions appeared to precipitate on the intermetallics, whilst the diphenylphosphates provide anodic inhibition by reacted with the surrounding aluminium matrix or oxide to form a protective film over the entire alloy surface[75].

Optical microscopy revealed holes of various sizes across the surface of the coating, which would also be present in the tested coatings and near defects in the coating. It is thought that the holes are formed when the paint is still wet and the polymer matrix solidifies around air bubbles or clumps of pigment particles. The holes then do not significantly change morphology even if the pigment is dissolved. Scanning acoustic microscopy showed an array of different sized spots across images and A-scans revealed that these features sat at different heights within the thickness of the coating. Therefore, it is expected that the clusters of pigment exist throughout the coating cross-section. Visual observation revealed that samples that were tested in solution for four weeks lost considerable colour compared to the small volume one week test. This shows that pigment release for this paint is time-dependent, and unlike the 113-22 chromate-pigmented coating, will continue to release pigment into the solution for at least one week.

These results could explain the difference between the EIS results of the two different primer coatings with a defect, where small volume one week testing showed one sample performing particularly well and the other two rather poorly. The uneven dispersion of pigment means that a defect or exposed area could be close to clusters of pigment >500µm or at an area where small 10s of microns pigments and lightly dispersed. One week of testing in a non-stirring environment (agar gel and filter paper) would likely reduce pigment release, so that pigment from other areas in the coating may not have sufficient time to reach the exposed area and provide protection. However, the long-term test in a large volume of sodium chloride solution caused blistering at the defect which reduces corrosion protection further or simply increased the exposed area so that it was difficult to determine the active area of the test sample for calculations.

It is possible that potentiodynamic polarisation tests showed good corrosion protection because of the free-stirring environment before testing so that cerium species released from the top surface and other areas in the coating can move to the defect. Therefore, the limited corrosion protection of $Ce(dpp)_3$ Epigen coated AA2024-T3 which varied between tests because of the poorly mixed coating and the environment it was in (non-stirred).

6.10 Conclusions

Chapter 6 investigated the corrosion behaviour of AA2024-T3 coated with an epoxy coating with a rare-earth, $Ce(dpp)_3$, pigment using potentiodynamic polarisation and electrochemical impedance spectroscopy techniques and the coating was studied various microscopy techniques. The samples provided from Monash University were much thicker than the 113-22 coatings and of a different polymer matrix, so a direct comparison could not be easily made between the two inhibitive systems.

$Ce(dpp)_3$ inhibitor exhibited good corrosion protection in potentiodynamic polarisation tests when the pre-exposure time of the samples were increased, similar to the 113-22 samples. Unlike the chromate inhibitor, $Ce(dpp)_3$ Epigen coated samples continued to show a significant passive potential barrier at 30°C.

EIS experiments were unable to provide consistent data and microscopy techniques were used to study the dispersion $Ce(dpp)_3$ pigment in the coating. Scanning acoustic microscopy and optical microscopy showed areas in the coating that contained clusters of pigment whilst other areas in the coating contained smaller, more evenly dispersed pigment. Therefore, it was expected that the inconsistent corrosion protection provided by the $Ce(dpp)_3$ inhibitor was related to the uneven dispersion of pigment within the polymer matrix and the availability of the inhibitor to the exposed metal surface.

Chapter 7 Summary and Future Work

7.1 Conclusions of the Present Work

In this work, the corrosion protection of three primers coated on AA2024-T3 was studied, and for comparison, the electrochemical behaviour of the bare alloy itself. The coated samples were tested as fully-intact coatings and coatings with a 1mm-wide defect or a thin scalpel defect. 2M sodium chloride solution was used for most experiments because direct current potentiodynamic polarisation tests showed that the innate passive behaviour of the alloy is only eliminated at the high chloride concentration. Tests were also performed in 0.5M NaCl solution as a comparison.

7.2 AA2024-T3 Bare Alloy Electrochemical Behaviour

Polarisation of AA2024-T3 after immersion in 0.5M sodium chloride solution for 24 hours showed the pitting potential of the alloy to be approximately -600mV and the bare alloy exhibited a passive region of 80 to 180mV between the free corrosion potential and the pitting potential. Testing the alloy in 2M sodium chloride solution exhibited a pitting potential of the alloy was approximately -680 mV and eliminated the passive region when the alloy was subjected to an anodic bias.

AA2024-T3 was further tested in 2M sodium chloride with varying concentrations of strontium chromate, and it was found that for lower concentrations of strontium chromate (0M to $1x10^{-4}$M), there was no passive region between the rest potential and the pitting potential when the alloy was anodically polarised although higher concentrations of strontium chromate, $1x10^{-3}$M and above, exhibited a clear region of passivity develops where there was little current increase

with increasing potential, up to the the onset of pitting at a higher potential. The potential barrier between the free corrosion potential and the pitting potential was between 100 – 270mV increasing with chromate concentration.

It was found that increasing the test temperature by 10°C greatly affected the electrochemical behaviour of the alloy in solution. Increasing the test temperature lowered the rest potential of the alloy, more than raising the pitting potential. Lowering of the rest potential with additions of chromate was apparent at ambient temperature conditions after prolonged immersion, but when the test temperature was raised by 5 or 10°C, the additions of strontium chromate caused a more rapid lowering of the corrosion potential. Passivity was still exhibited but was greatly reduced, and the pitting potential lies much closer to the rest potential.

Experiments using electrochemical impedance spectroscopy also demonstrated the protective qualities of strontium chromate in aggressive solution, as the charge transfer resistance increases with chromate concentration. As time progressed, the alloy exhibited increased resistances and decreased capacitances. The results suggest that the chromate inhibits corrosion processes by limiting reactions such as oxygen reduction or metal dissolution and the decreasing capacitance supports the theory that chromate ions adsorb unto the oxide layer reducing the active area of the cathode.

7.3 Corrosion Behaviour with Intact Coatings

7.3.1 Electrochemical Behaviour of Intact Coatings on AA2024-T3

Electrochemical impedance spectroscopy was used to test fully-intact coated AA2024-T3 samples. EIS data revealed a two time-constant response which was attributed to the coating response and the polarisation response.

Non-inhibitive control-paint coated samples tested over one week showed that the polarisation resistance, R_{pol}, decreased from approximately 40MΩcm^2 to 10MΩcm^2. The decrease of polarisation resistance indicates that the rate of corrosion attack or the area being attacked increases. This could be due to ions passing through the coating so that the increase of chloride ions at the oxide surface leads to more pitting. The polarisation resistance of the chromate-pigmented 113-22 coated sample decreased slowly over time and was greater than 1GΩcm^2(two orders of magnitude greater than the control coated sample and four orders of magnitude greater than the bare alloy tests). This indicates that the corrosion rate of the 113-22 coated sample is low and that the corrosion processes are inhibited.

The coating resistances for both the control and the 113-22 paints were low, approximately 10kΩcm^2, and as the difference between the composition of the control and 113-22 coatings is the pigment, this suggests that the chromate pigments play the major role in protecting against corrosion. The control paint-coated EIS tests revealed that when water and aggressive ions penetrate the organic coating, the corrosion protection comes mainly from the passive oxide layer on the surface of the metal, but localised corrosion takes place following the ingress of chloride ions through the oxide. Therefore, the chromate pigment in the 113-22 coating is likely preventing the breakdown of passivity at local active sites so that filiform or pitting corrosion does not propagate.

7.3.2 Release of inhibitive pigment

UV-Visible spectroscopy experiments concluded that only a small fraction, 1-6%, of the available inhibitor is actually released into the bulk solution and is likely from surface layers in contact with the bulk solution. The majority of accessible inhibitor was released in the first 2-3 days of immersion, and further immersion, up to one month, did not release much more pigment. Water and aggressive ions can penetrate the polymer matrix to initiate corrosion, but pigment release tests indicate that most of the bulkier inhibitive species, chromate, are locked within the coating. Further inhibitor is therefore only released when fresh surfaces to the bulk solution are formed, such as via physical damage. UV-Vis experiments in the current study also revealed that at 30°C, pigment release was initially faster but did not greatly affect the overall longer term amount. When comparing EIS measurements alongside the UV-Vis experiments, the cyclic behaviour of resistance indicate that the metal alloy is pitting and subsequently repassivating over time and suggests that there was a fresh supply of chromate each time resistance was increased.

7.4 Corrosion Behaviour of Coated Systems with a Defect

7.4.1 Potentiodynamic Polarisation

The anodic polarisation behaviour of control paint-coated samples with a 1x10mm defect, at room temperature and 30°C, is quite similar to the bare metal tests. The rest potential for the room temperature test was -634mV (compared to -636mV for the bare metal test) and the rest potential for the 30°C test was -661mV (-667mV for bare test) and the alloy was sitting at or just below the pitting potential so that when the potential is increased, the corrosion current increases almost at once.

For the chromate-pigmented 113-22 coated samples with a 1x10mm defect, the anodic behaviour was again very similar to the bare metal tests. The presence of inhibitive pigments in the paint did not show any significant improvement in corrosion protection for the potentiodynamic polarisation tests, as the corrosion current increased almost at once when the potential was increased from the rest potential. This result was expected from the results of the bare metal DC polarisation tests in chapter 3 and the pigment release test in chapter 4, because the expected amount of chromate released from the 113-22 paint was calculated to be significantly less than the concentrations of strontium chromate needed to cause anodic inhibition and create a passive region. Tests at 30°C in 2M NaCl solution also did not show a passive region for the alloy.

When $Ce(dpp)_3$ Epigen-coated AA2024-T3 with a 1x10mm defect was anodically polarised, the pitting potential did not change significantly (approximately -670mV) although the rest potential decreased to -778mV, so the alloy exhibited a passive region of 110mV. This indicates that the presence of cerium-based inhibitive pigments is able to provide corrosion protection for the bare metal surface, even for tests in bulk solution. However, when tested at 30°C, only a 20mV potential barrier was observed. Polarisation testing appeared to indicate that AA2024-T3 is a lot more susceptible to pitting corrosion at 30°C than testing at room temperature (20°C).

The corrosion protection provided by inhibitors markedly improved when the pre-exposure time of the 113-22 and $Ce(dpp)_3$ Epigen coated samples in 2M NaCl was increased from 48hours to one week. For the 113-22 coated samples, the rest potential at room temperature after one week decreased to -760mV and the pitting potential was raised to -556mV, creating a passive potential range of almost 200mV. At 30°C, the passive region was considerably smaller of around 60mV, where the rest potential fell to -731mV, and the pitting potential remained

around -670mV. $Ce(dpp)_3$ Epigen coated samples exhibited a passive potential barrier of more than 350mV when the rest potential of the $Ce(dpp)_3$ Epigen coated sample fell to -885mV and the pitting potential was raised to -517mV, and at 30°C the rest and pitting potentials of the $Ce(dpp)_3$ coated sample at 30°C were similar to the room temperature test, at -892mV and -518mV respectively. From these results, potentiodynamic tests appear to suggest that cerium-based inhibitors are better corrosion protectors than chromate-based inhibitors and the protection is maintained even at 30°C.

Corrosion protection by cathodic inhibition of the chromate pigment was tested by comparing the cathodic polarisation curves of 113-22 coated and control-coated samples with a scalpel defect. Because EIS tests (summarised in next section) revealed that the polarisation resistance of a sample is usually highest after 12-24 hours to immersion in the small volume electrochemical cell, samples were cathodically polarised after 18hours of pre-immersion. When samples were cathodically polarised, the anodic current decreased but the cathodic current was strongly inhibited. For the control coated sample tests, any anodic current was rapidly eliminated as the potential was decreased, and the cathodic current increased steadily. Comparing with the 113-22 coated tests, it was clearly seen that the presence of inhibitive pigments greatly limited the cathodic reaction, (oxygen reduction). The cathodic inhibition by chromate also lowered corrosion potential.

7.4.2 Electrochemical Impedance Spectroscopy

Coated AA2024-T3 samples with a scalpel defect were tested using a small electrochemical cell using filter paper and sodium chloride agar as the test solution. EIS data mostly showed a two-

time constant response which was attributed to the oxide response and the interface chemistry response.

For the non-inhibitive control coating, the polarisation resistance of the system typically increased from approximately 10kΩcm^2 by a factor of 2-3 in the first 12-24 hours and then subsequently decreases rapidly back to 10kΩcm^2. This short increase of resistance was related to the presence of chloride ions, decreasing the density of oxygen vacancies in the oxide layer so that the charge transport and corrosion rate is reduced. Another explanation could be the increase in oxide layer thickness due to the exposed metal, i.e. exposing defect sodium chloride solution. The rapid decrease of resistance is likely related to the breakdown of the passive layer and the onset of pitting corrosion.

The polarisation resistance of the 113-22 coated samples exhibited a continuous build up and decay of resistance. The resistance of the 113-22 coated systems would usually start an order of magnitude higher than the control coated systems at approximately 0.1MΩcm^2 and would also increase in the first 12-24 hours. After reaching a peak, varying between 0.3 to 0.90MΩcm^2, the polarisation resistance would fall sharply to values similar to the control coated tests (10kΩcm^2). However, the resistance would build up again and after reaching a subsequent peak would again break down. Results indicated that the inhibitive pigment can prevent the propagation of stable pitting, but cannot provide continuous corrosion protection. Inhibitor protects against corrosion as a reactive response to corrosion rather than a purely preventative process.

Pigment release experiments suggested that the majority of inhibitor released came from the free surfaces of coating in direct contact with the bulk solution. Pre-washed 113-22 samples and

113-22 coated samples with an additional topcoat were prepared and tested to investigate inhibitor protection when the chromate on the top surface is removed or restricted. Both investigations revealed that the corrosion protection provided by released inhibitor at the fresh-cut edges was comparable to the 113-22 coated samples with no further preparation. Similarly, no stable passivity was observed and there was again a cyclic rise and fall of polarisation resistance.

The EIS experiments on the limited number of $Ce(dpp)_3$ Epigen coated AA2024-T3 with a scalpel defect were unable to provide consistent data. One test exhibited corrosion protection that was superior to the chromate-pigment 113-22 tests, although this could not be replicated and repeat tests showed polarisation resistances closer to the un-inhibited control coated samples.

The dispersion of pigment in the $Ce(dpp)_3$ was investigated using scanning acoustic microscopy and optical microscopy and revealed that there were areas in the coating that contained clusters of pigment greater than 500µm and other areas where small 10s of microns pigments were evenly dispersed. Therefore, a week of testing in a non-stirring environment would limit reduce pigment release, whilst a longer term test in a large volume of NaCl solution would allow pigment from other areas in the coating to reach the exposed area and provide protection. Release of inhibitive species for the Epigen coating was time-dependent unlike the 113-22 primer where the chromate pigment was locked in the polymer matrix.

7.4.2.1 Rest potential comparison

The rest potentials of the scalpel-defect coated samples were measured before the EIS tests and compared. The free corrosion potential of the control coated samples decreased steadily over time from around the typical pitting potential (-630mV) to approximately -800mV and remained there. This indicated the onset of stable pitting corrosion (rather than cathodic inhibition) and is

consistent with the calculated low polarisation resistance values from EIS measurements. Chromate and cerium species are known cathodic inhibitors, meaning that the cathodic reaction, e.g. oxygen reduction, is inhibited and the lowering of the rest potential would be related to the suppression of the cathodic reaction so that the corrosion potential is lowered and a passive region is created. The rest potentials for chromate-pigmented 113-22 samples started below the pitting potential, indicating cathodic inhibition, and over time fluctuated above and below the typical pitting potential level. This reflected the polarisation resistances calculated in the EIS measurements as it suggested that there was a continuous process of corrosion initiating on the alloy and inhibitor preventing the stable pitting propagation. The rest potentials of the $Ce(dpp)_3$ started off the even lower than that of the 113-22 primer, indicating rapid cathodic inhibition from the inhibitors. The free corrosion potential increased over time but does not shift above and below the pitting potential. Other than the low free corrosion potential at the start of the tests, the potential of $Ce(dpp)_3$ inhibited systems did not decrease noticeably until the alloy was pitting.

7.4.3 Electrochemical Noise Analysis

Electrochemical noise resistance measurements were consistent with the polarisation resistance values calculated from EIS experiments. This supports the use of ECN for inhibitor studies and suggests that the EIS technique can effectively measure the electrochemical behaviour of systems without seriously affecting the system. A continuous build up and breakdown of resistance was also seen, to a less obvious extent. ECN analysis also showed that inhibitors provide corrosion protection by reducing the frequency of events, where the frequency was higher for the control coating than the 113-22 coating, although ECN indicated that the amount of charge of each event between the two coated samples were similar.

7.5 Future Work

1. Repeat inhibitor studies of cerium diphenylphosphate incorporated into the same binder as the 113-22 coating for a fairer comparison.

2. Investigate other pigments to explore protection mechanism, e.g. ion-exhange

3. Further evaluation of corrosion protection of inhibitive in different test conditions, e.g. variance of temperature (hot climates of 40+°C), pH.

4. The integrity of the commercial 113-22 primer can be tested using weather testing, wet-dry cycles before the corrosion protection qualities are investigated. ECN of scanning Kelvin probe microscopy could be used to evaluate the effectiveness of chromate from atmospheric attack under condensation

References

1. Szklarska-Smialowska, Z., Pitting Corrosion of Metals. NACE International: Houston, 1986.
2. Frankel, G., *Journal of the Electrochemical Society* **1998,** *145* (8), 2970-2970.
3. K. R. Trethewey, J. C., *Corrosion for Science and Engineering*. 2nd ed.; Longman: 1995.
4. Murphy, G.; Pourbaix, M., *Science* **1966,** *154* (3756), 1537-&.
5. Vargel, C., *Corrosion of Aluminium*. 2004.
6. Ghali, E., *Corrosion Resistance of Aluminium and Magnesium Alloys*. 2010.
7. Marcus, P.; Maurice, V., Corrosion and Environmental Degradation. Wiley-VCH: 2000.
8. Lifka, B. W., Corrosion Tests and Standards, Application and Intepretation. 2nd ed.; ASM International.
9. Uhlig, H., *Journal of the Electrochemical Society* **1950,** *97* (11), C215-C220.
10. Sato, N., *Electrochimica Acta* **1971,** *16* (10), 1683-&.
11. Evans, U. R., *J. Electrochem. Soc* **1927**.
12. Weil, K.; Menzel, D., *Zeitschrift Fur Elektrochemie* **1959,** *63* (6), 669-673.
13. Chao, C.; Lin, L.; MacDonald, D., *Journal of the Electrochemical Society* **1981,** *128* (6), 1187-1194.
14. De Micheli, S. M., *Corrosion Science* **1978,** *18* (7).
15. Bohni, H.; Uhlig, H., *Journal of the Electrochemical Society* **1969,** *116* (7).
16. Kaesche, H. In *Pitting Corrosion of Aluminum and Intergranular Corrosion of Al Alloys*, International, N., Ed. 1971.
17. Rudd, W.; Scully, J., *Corrosion Science* **1980,** *20* (5), 611-631.
18. Barr, T., *Journal of Vacuum Science & Technology* **1977,** *14* (1), 660-665.
19. Lee, E.; Pyun, S., *Corrosion Science* **1995,** *37* (1), 157-168.
20. Szkalrska-Smialowska, Z., *Pitting Corrosion of Metals*. NACE International: Houston, 1986.
21. Hoar, T., *Corrosion Science* **1967,** *7* (6), 341-&.
22. Buchheit, R.; Grant, R.; Hlava, P.; Mckenzie, B.; Zender, G., *Journal of the Electrochemical Society* **1997,** *144* (8), 2621-2628.
23. Boag, A.; Hughes, A.; Wilson, N.; Torpy, A.; MacRae, C.; Glenn, A.; Muster, T., *Corrosion Science* **2009,** *51* (8), 1565-1568.
24. Kendig, M.; Buchheit, R., *Corrosion* **2003,** *59* (5), 379-400.
25. Birbilis, N.; Buchheit, R.; Ho, D.; Forsyth, M., *Electrochemical and Solid State Letters* **2005,** *8* (11), C180-C183.
26. Ambat, R.; Davenport, A.; Scamans, G.; Afseth, A., *Corrosion Science* **2006,** *48* (11), 3455-3471.
27. V. Guillaumin, P. S., G.S. Frankel, in: A.C. Hillier, M. Seo In *Localized In-Situ Methods for Investigating Electrochemical Interfaces*, The Electrochemical Society Proceedings Series, Pennington, NJ, (Eds.), S. R. T., Ed. Pennington, NJ, 2000.
28. Zhu, D.; van Ooij, W., *Corrosion Science* **2003,** *45* (10), 2177-2197.
29. Weldon, D. G., *Failure Analysis of Paints and Coatings*. Wiley & Sons: 2002.
30. Funke, W., *Journal of the Oil & Colour Chemists Association* **1979,** *62* (2), 63-67.
31. van den Brand, J.; Van Gils, S.; Terryn, H.; Sivel, V.; de Wit, J., *Progress in Organic Coatings* **2004,** *51* (4), 351-364.
32. Guruviah, S., *Journal of the Oil & Colour Chemists Association* **1970,** *53* (8), 669-&; Funke, W.; Haagen, H., *Industrial & Engineering Chemistry Product Research and Development* **1978,** *17* (1), 50-53.
33. Mayne, J., *Anti-Corrosion Methods and Materials* **1973,** *20* (10), 3-8.

34. Funke, W., *Progress in Organic Coatings* **1981,** *9* (1), 29-46.
35. Schneider, O.; Kelly, R., *Corrosion Science* **2007,** *49* (2), 594-619.
36. Jenkins, A.; Armstrong, R., *Corrosion Science* **1996,** *38* (7), 1147-1157.
37. McMurray, H.; Williams, G.; O'Driscoll, S., *Journal of the Electrochemical Society* **2004,** *151* (7), B406-B414.
38. Bautista, A., *Progress in Organic Coatings* **1996,** *28* (1), 49-58.
39. Grundmeier, G.; Schmidt, W.; Stratmann, M., *Electrochimica Acta* **2000,** *45* (15-16), 2515-2533.
40. Shreir, L. L.; Burstein, G. T.; Jarman, R. A., *Corrosion*. Butterworth-Heinemann: 1994.
41. Sinko, J., *Progress in Organic Coatings* **2001,** *42* (3-4), 267-282.
42. Hinton, B.; Arnott, D.; Ryan, N., *Metals Forum* **1984,** *7* (4), 211-217; Markley, T.; Mardel, J.; Hughes, A.; Hinton, B.; Glenn, A.; Forsyth, M., *Materials and Corrosion-Werkstoffe Und Korrosion* **2011,** *62* (9), 836-840.
43. Hinton, B., *Journal of Alloys and Compounds* **1992,** *180*, 15-25.
44. Aldykiewicz, A.; Davenport, A.; Isaacs, H., *Journal of the Electrochemical Society* **1996,** *143* (1), 147-154.
45. Davenport, A.; Isaacs, H.; Kendig, M., *Corrosion Science* **1991,** *32* (5-6), 653-663.
46. Muster, T.; Sullivan, H.; Lau, D.; Alexander, D.; Sherman, N.; Garcia, S.; Harvey, T.; Markley, T.; Hughes, A.; Corrigan, P.; Glenn, A.; White, P.; Hardin, S.; Mardel, J.; Mol, J., *Electrochimica Acta* **2012,** *67*, 95-103.
47. LaPuma, P.; Fox, J.; Kimmel, E., *Regulatory Toxicology and Pharmacology* **2001,** *33* (3), 343-349.
48. El Abedin, S., *Journal of Applied Electrochemistry* **2001,** *31* (6), 711-718.
49. Pokhmurs'kyi, V.; Kwiatkowski, L.; Zin, I.; Lyon, S.; Bilyi, L.; Ratushna, M., *Materials Science* **2006,** *42* (5), 573-578.
50. LaPuma, P.; Rhodes, B., *Regulatory Toxicology and Pharmacology* **2002,** *36* (3), 318-324.
51. Kondratenko, N. A.; Sherstyuk, V. P., *Theoretical and Experimental Chemistry* **1987,** *22* (6).
52. Kendig, M.; McCreery, R.; Ramsey, J.; Xia, L.; Seo, M.; MacDougall, B.; Takahashi, H.; Kelly, R., *Passivity and Localized Corrosion* **1999,** *99* (27), 239-248; Ramsey, J.; McCreery, R., *Journal of the Electrochemical Society* **1999,** *146* (11), 4076-4081; Xia, L.; McCreery, R., *Journal of the Electrochemical Society* **1998,** *145* (9), 3083-3089.
53. Clark, W.; McCreery, R., *Journal of the Electrochemical Society* **2002,** *149* (9), B379-B386.
54. Ilevbare, G.; Scully, J., *Journal of the Electrochemical Society* **2001,** *148* (5), B196-B207.
55. Zhao, J.; Xia, L.; Sehgal, A.; Lu, D.; McCreery, R.; Frankel, G., *Surface & Coatings Technology* **2001,** *140* (1), 51-57.
56. Kolics, A.; Besing, A.; Wieckowski, A., *Journal of the Electrochemical Society* **2001,** *148* (8), B322-B331.
57. Cartledge, *Journal of the Electrochemical Society* **1966,** *113* (4), 328-&.
58. Buchheit, R., *Journal of the Electrochemical Society* **1995,** *142* (11), 3994-3996; Kolics, A.; Polkinghorne, J.; Thomas, A.; Wieckowski, A., *Chemistry of Materials* **1998,** *10* (3), 812-824.
59. Baghni, I.; Lyon, S.; Ding, B., *Surface & Coatings Technology* **2004,** *185* (2-3), 194-198.
60. Prosek, T.; Thierry, D., *Progress in Organic Coatings* **2004,** *49* (3), 209-217.
61. Jakab, M.; Scully, J., *Nature Materials* **2005,** *4* (9), 667-670.
62. Howard, R.; Zin, I.; Scantlebury, J.; Lyon, S., *Progress in Organic Coatings* **1999,** *37* (1-2), 83-90.

63. J. M. Pommersheim, T. N., K. A. Hartzfeld *Polymeric Materials Science and Engineering* **1996,** *74*; Pommersheim, J.; Nguyen, T.; Hartzfeld, K., *Abstracts of Papers of the American Chemical Society* **1996,** *211*, 25-PMSE.
64. Osborne, J.; Blohowiak, K.; Taylor, S.; Hunter, C.; Bierwagon, G.; Carlson, B.; Bernard, D.; Donley, M., *Progress in Organic Coatings* **2001,** *41* (4), 217-225.
65. Furman, S.; Scholes, F.; Hughes, A.; Lau, D., *Progress in Organic Coatings* **2006,** *56* (1), 33-38.
66. Goldie, B. P. F., *Paint and Resin* **1985,** *1*.
67. Chrisanti, S. The Application of Ion-Exchanged Clay as Corrosion Inhibiting Pigments in Organic Coatings. 2008.
68. Bohm, S.; McMurray, H.; Powell, S.; Worsley, D., *Materials and Corrosion-Werkstoffe Und Korrosion* **2001,** *52* (12), 896-903.
69. Buchheit, R.; Guan, H.; Mahajanam, S.; Wong, F., *Progress in Organic Coatings* **2003,** *47* (3-4), 174-182.
70. Stern, M., *Journal of the Electrochemical Society* **1958,** *105* (11), 638-647.
71. Lorking, K. F.; Mayne, J. E. O., *Journal of Applied Chemistry* **1961,** *11* (5).
72. Iannuzzi, M.; Young, T.; Frankel, G., *Journal of the Electrochemical Society* **2006,** *153* (12), B533-B541.
73. Hinton, B. R. W.; Arnott, D. R.; Ryan, N. E., *Metals Forum* **1984,** *7* (4), 211-217.
74. Smith, C. J. E.; Baldwin, K. R.; Garrett, S. A.; Gibson, M. C.; Hewins, M. A. H.; Lane, P. L., *Progress in the understanding and prevention of corrosion* **1993**.
75. Markley, T.; Forsyth, M.; Hughes, A., *Electrochimica Acta* **2007,** *52* (12), 4024-4031.
76. Guillaumin, V.; Landolt, D., *Corrosion Science* **2002,** *44* (1), 179 - 189.
77. Crossen, J.; Sykes, J.; Zhai, T.; Briggs, G., *Faraday Discussions* **1997,** *107* (0), 417 - 424.
78. Reddy, B.; Doherty, M.; Sykes, J., *Electrochimica acta* **2004,** *49* (17-18), 2965 - 2972.
79. Doherty, M.; Sykes, J., *Corrosion Science* **2004,** *46* (5), 1265 - 1289.
80. Martin, F.; Cheek, G.; O'Grady, W.; Natishan, P., *Corrosion Science* **2005,** *47* (12), 3187-3201.
81. McCafferty, E., *Journal of Applied Electrochemistry* **2010,** *40* (3), 543-549.
82. Raps, D.; Hack, T.; Wehr, J.; Zheludkevich, M.; Bastos, A.; Ferreira, M.; Nuyken, O., *Corrosion Science* **2009,** *51* (5), 1012-1021; Zin, I.; Howard, R.; Badger, S.; Scantlebury, J.; Lyon, S., *Progress in Organic Coatings* **1998,** *33* (3-4), 203-210.
83. Furman, S.; Scholes, F.; Hughes, A.; Jamieson, D.; Macrae, C.; Glenn, A., *Corrosion Science* **2006,** *48* (7), 1827-1847.
84. Cottis, R.; Al-Awadhi, M.; Al-Mazeedi, H.; Turgoose, S., *Electrochimica Acta* **2001,** *46* (24-25), 3665-3674.
85. Al-Mazeedi, H.; Cottis, R., *Electrochimica Acta* **2004,** *49* (17-18), 2787-2793.
86. Mardel, J.; Garcia, S.; Corrigan, P.; Markley, T.; Hughes, A.; Muster, T.; Lau, D.; Harvey, T.; Glenn, A.; White, P.; Hardin, S.; Luo, C.; Zhou, X.; Thompson, G.; Mol, J., *Progress in Organic Coatings* **2011,** *70* (2-3), 91-101.
87. Muster, T.; Lau, D.; Wrubel, H.; Sherman, N.; Hughes, A.; Harvey, T.; Markley, T.; Alexander, D.; Corrigan, P.; White, P.; Hardin, S.; Glenn, M.; Mardel, J.; Garcia, S.; Mol, J., *Surface and Interface Analysis* **2010,** *42* (4), 170-174.